LBNL-42674

ERNEST ORLANDO LAWRENCE
BERKELEY NATIONAL LABORATORY

Dynamic Behavior of Semivolatile Organic Compounds in Indoor Air

Michael Van Loy

Environmental Energy Technologies Division

December 1998

Ph.D. Thesis

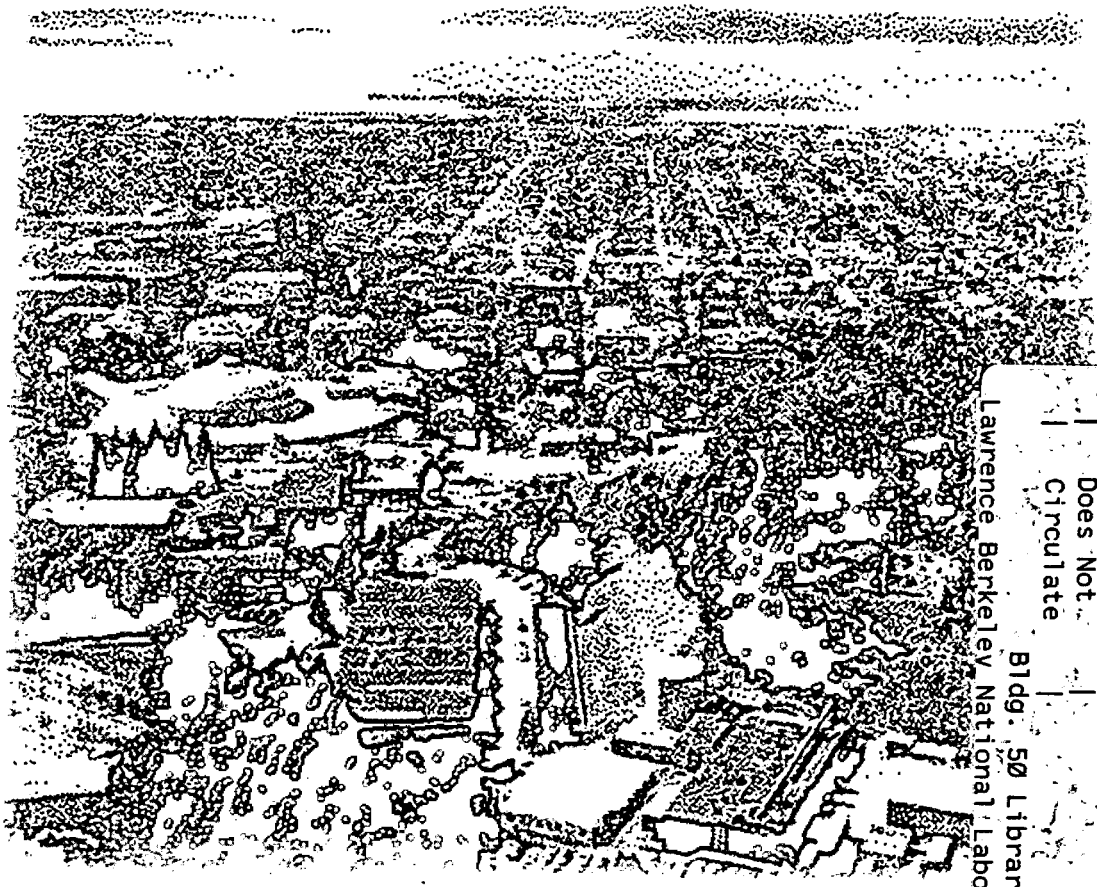

REFERENCE COPY
Does Not
Circulate
Bldg. 50 Library - Ref.
Lawrence Berkeley National Laboratory
Copy 1
LBNL-42674

DISCLAIMER

This document was prepared as an account of work sponsored by the United States Government. While this document is believed to contain correct information, neither the United States Government nor any agency thereof, nor the Regents of the University of California, nor any of their employees, makes any warranty, express or implied, or assumes any legal responsibility for the accuracy, completeness, or usefulness of any information, apparatus, product, or process disclosed, or represents that its use would not infringe privately owned rights. Reference herein to any specific commercial product, process, or service by its trade name, trademark, manufacturer, or otherwise, does not necessarily constitute or imply its endorsement, recommendation, or favoring by the United States Government or any agency thereof, or the Regents of the University of California. The views and opinions of authors expressed herein do not necessarily state or reflect those of the United States Government or any agency thereof or the Regents of the University of California.

LBNL-42674

Dynamic Behavior of Semivolatile Organic Compounds in Indoor Air

By

Michael Van Loy
Ph.D. Thesis

College of Engineering
Civil and Environmental Engineering
University of California, Berkeley

And

Environmental Energy Technologies Division
Lawrence Berkeley National Laboratory
University of California
Berkeley, CA 94720

Fall 1998

This work was supported by the U.S. Environmental Protection Agency Graduate Fellowship, the S.C. Johnson Wax Research and Development Fellowship and the State of California Toxic Substance Research Program. Additional research support was provided by Grant No. R01-HL42490 from the National Heart, Lung and Blood Institute through the U.S. Department of Energy under Contract No. DE-AC03-76SF00098.

Dynamic Behavior of Semivolatile Organic Compounds in Indoor Air

Copyright © 1998

by

Michael Van Loy

The U.S. Department of Energy has the right to use this document
for any purpose whatsoever including the right to reproduce
all or any part thereof.

Abstract

Dynamic Behavior of Semivolatile Organic Compounds in Indoor Air

by

Michael David Van Loy

Doctor of Philosophy in Engineering-Civil and Environmental Engineering

University of California, Berkeley

Professor William W Nazaroff, Chair

Exposures to a wide range of air pollutants are often dominated by those occurring in buildings because of three factors: 1) most people spend a large fraction of their time indoors, 2) many pollutants have strong indoor sources, and 3) the dilution volume in buildings is generally several orders of magnitude smaller than that of an urban airshed. Semivolatile organic compounds (SVOCs) are emitted by numerous indoor sources, including tobacco combustion, cooking, carpets, paints, resins, and glues, so indoor gas-phase concentrations of these compounds are likely to be elevated relative to ambient levels. The rates of uptake and release of reversibly sorbing SVOCs by indoor materials directly affect both peak concentrations and persistence of the pollutants indoors after source elimination. Thus, accurate predictions of SVOC dynamics in indoor air require an understanding of contaminant sorption on surface materials such as carpet and wallboard.

The dynamic behaviors of gas-phase nicotine and phenanthrene were investigated in a 20 m^3 stainless steel chamber containing carpet and painted wallboard. Each compound was studied independently, first in the empty chamber, then with each sorbent individually, and finally with both sorbents in the chamber. The test compounds were emitted into the sealed chamber by flash evaporation of a measured mass of the condensed-phase compound. After emission, the gas-phase concentration was monitored

until a steady-state concentration was achieved. Then, the chamber was flushed with clean, HEPA-filtered air to reduce the airborne concentration of the test compound to zero. Finally, the chamber was resealed to observe reemission of sorbed mass. For the nicotine experiments in the empty chamber, more than 80% of the emitted mass was accounted for at the end of the experiment by thermally desorbing and collecting nicotine sorbed on small, wall-mounted stainless steel panels. More than 99% of the measured nicotine was sorbed to either the tested sorbent(s) or to the chamber surfaces at equilibrium at 25 °C. Similar results were observed for phenanthrene experiments in the empty chamber. In the experiments with real surface materials, the gas-phase decay patterns following emission of each SVOC were qualitatively similar to those observed in the empty chamber. However, the times required to reach equilibrium for both the adsorption and desorption phases of these experiments were more than two orders of magnitude longer, indicating the importance of transport processes within the sorbent material relative to direct adsorption at the presented surface.

The gas-phase data are interpreted using reversible sorption models. A commonly employed model based on linear partitioning between the gas- and sorbed-phases could not be accurately fit to the time-dependent data collected in the empty chamber nicotine experiments, so equilibrium partitioning was measured separately for each sorbent-sorbate pair to test the linear model assumption. Incorporating isotherm parameters into a kinetic, reversible sorption model which assumes a nonlinear, power-law rate of sorbed nicotine reemission and gas-phase deposition provides a significantly better fit to the dynamic data from experiments in the empty stainless steel chamber. Phenanthrene-stainless steel sorption is adequately described by linear partitioning. For carpet and wallboard, a two-box sorption model which also incorporated the nonlinear equilibrium partitioning is successfully employed. In this model, deposition from the gas-phase to the sorbent's air-surface interface occurs on a time scale comparable to that observed for sorption on stainless steel and wallboard. A second sorbed-phase sink (for instance, the

rubber backing of a carpet or the porous gypsum of wallboard) with a larger sorption capacity but slower uptake and release kinetics is coupled to the gas phase through bulk-phase diffusion.

The models developed and validated in this study should be applicable to a broad range of other SVOCs. The developed porous sorbent sorption model is successfully applied to resolve a discrepancy between concentrations of nicotine measured in laboratory and field studies of environmental tobacco smoke (ETS) that has been debated in the literature. Experimentally determined sorption kinetic parameters were used to predict the ratio between gas-phase nicotine and respirable particulate matter (RSP) for different smoking rates and ventilation rates in a typical house and a stainless-steel laboratory chamber. The results indicate that nicotine is a viable marker for RSP (and other ETS constituents with similar indoor air behavior) in environments where habitual smoking occurs if the concentration data are averaged over a period significantly longer than the period between cigarettes. Its utility as a tracer erodes at shorter time scales or in environments where smoking occurs more erratically.

The sorption kinetic parameters obtained experimentally in this study are also incorporated into a comprehensive modeling framework which includes gas-particle partitioning, deposition of particles on indoor surfaces, adsorption and desorption of SVOC on deposited particles, and homogeneous and heterogeneous chemical decay. The resulting set of coupled ordinary differential equations is solved numerically to simulate five scenarios which illustrate the impacts of varying model parameters on indoor SVOC concentrations and persistence.

Dedication

To Michele:

For her love, patience, and support through this long, arduous, and sometimes even painful journey; for providing a voice of reason when nothing seemed to be going right; for knowing when to let me drive myself crazy and when to help me forget about my research for a while; and most of all for being the most wonderful friend and partner for whom I could ever ask.

Table of Contents

Dedication iii

Table of Contents iv

List of Figures vii

List of Tables xvi

List of Symbols xix

Acknowledgements xxvi

Chapter 1. Introduction 1

Background 1

Dissertation Overview 7

Applications 9

Figures 11

Tables 13

Chapter 2. Interactions of Nicotine with the Stainless Steel Surfaces of an Environmental Test Chamber 14

Abstract 14

Introduction 15

Materials and Methods 17

Modeling 27

Results and Discussion 30

Conclusions 34

Figures 35

Tables 41

Chapter 3. Interactions of Nicotine and Phenanthrene with Carpet and Painted Wallboard in a Stainless Steel Test Chamber ..46

Abstract 46

Introduction 47

Methods and Materials 51
Data Analysis 58
Results and Discussion 63
Conclusions 66
Figures 67
Tables 83

Chapter 4. Nicotine as a Marker for Environmental Tobacco Smoke — Implications of Sorption on Indoor Surface Materials 100

Abstract 100
Introduction 101
Modeling Approach 105
Experimental Methods 111
Results and Discussion 113
Conclusions 118
Figures 119
Tables 128

Chapter 5. Modeling Framework to Predict Indoor Air Concentrations of Semivolatile Organic Compounds 138

Abstract 138
Introduction 139
Factors Impacting Indoor SVOC Concentrations 139
Modeling Framework 147
Definitions of Modeled Scenarios 157
Results and Discussion 160
Conclusions 164
Figures 165
Tables 171

Chapter 6. Conclusions 176

Summary 176
Implications and Directions for Future Research 179

Closing Thoughts 181

References 182

Appendices 197

Appendix A: Non-Porous Sorbent Data Analysis Program 197

Appendix B: Porous Sorbent Data Analysis Program 204

Appendix C: ETS Nicotine/RSP Predictor Program 211

Appendix D: SVOC Gas-Particle-Sorption Program 217

List of Figures

Figure 1.1 Comparison of linear and Freundlich isotherms. The linear isotherm is given in equation 1.2 and the Freundlich in equation 1.3 11

Figure 1.2 Comparison of hypothetical modeled indoor concentrations following puff emission of a pollutant. Panel A shows contaminant dynamics in the first 15 hours following emission and panel B shows the first 200 hours for a the reversibly sorbing contaminant. 12

Figure 2.1. Schematic diagram of 20 m^3 stainless steel environmental test chamber configuration used in empty chamber nicotine experiments. The integrated organic vapor-particle sampler system was used only in experiment 2A. The nicotine source was three machine-smoked cigarettes in experiment 2A. Liquid nicotine was flash evaporated from a glass petri dish on a hot plate in experiments 2B and 2C and from a stainless steel tube in an aluminum heater block in experiments 2D and 2E. 35

Figure 2.2. Representative chronology for kinetic nicotine-stainless steel experiments. The nicotine emission method was cigarette smoking which started at t = 0 and continued for 32 minutes in experiment 2A and flash (instantaneous) evaporation of liquid nicotine in experiments 2B and 2C. 36

Figure 2.3. Equilibrium partitioning of nicotine between the gas- and sorbed-phases in the stainless steel environmental chamber. The squares show data from experiments 2D and 2E. The solid line represents the best fit Freundlich isotherm for the experimental data (see Table 2.2). 37

Figure 2.4. Experimental data, estimated errors, and fully nonlinear model predictions for gas-phase concentration and sorbed-phase density for nicotine as a function of time in experiment 2A. The lengths of the solid and dashed horizontal bars and their positions relative to the time axis in panel **A** indicate the duration and timing of IOVPS and XAD-4 sorbent samples, respectively. Experiment 2A gas-phase data are tabulated in Table 2.3. 38

Figure 2.5. Experimental data, estimated errors, and nonlinear model predictions for gas-phase concentration and sorbed-phase density for nicotine as a function of time in experiment 2B. The lengths of the horizontal bars and their positions relative to the time axis in panel **B** indicate the duration and timing of XAD-4 sorbent tube samples. Experiment 2B gas-phase data are tabulated in Table 2.3. 39

Figure 2.6. Experimental data, estimated errors, and nonlinear model predictions for gas-phase concentration and sorbed-phase density for nicotine as a function of time in experiment 2C. The lengths of the horizontal bars and their positions relative to the time axis in panel **B** indicate the duration and timing of XAD-4 sorbent tube samples. Gas-phase sample data for this experiment are listed in Table 2.5 40

Figure 3.1 Schematic diagram of the 20 m^3 stainless steel environmental test chamber used in sorption dynamic studies for nicotine and phenanthrene with carpet and wallboard. 67

Figure 3.2 Experimental data, estimated errors, and diffusion model predictions for gas-phase (**A**) and stainless steel adsorbed and carpet adsorbed and absorbed nicotine (**B**) in experiment 3A.....68

Figure 3.3 Experimental data, estimated errors, and diffusion model predictions for gas-phase (**A**) and stainless steel and carpet sorbed nicotine (**B**) for 200 hours following the first injection of nicotine in experiment 3A. The lengths of the horizontal bars and their positions relative to the time axis in panel **A** indicate the duration and timing of Tenax-TA sorbent samples. 69

Figure 3.4 Experimental data, estimated errors, and diffusion model predictions for gas-phase (**A**) and stainless steel and carpet sorbed nicotine (**B**) for 200 hours following the fifth injection of nicotine in experiment 3A. The lengths of the horizontal bars and their positions relative to the time axis in panel **A** indicate the duration and timing of Tenax-TA sorbent samples. 70

Figure 3.5 Experimental data, estimated errors, and diffusion model predictions for gas-phase (**A**) and stainless steel adsorbed and wallboard adsorbed and absorbed nicotine (**B**) in experiment 3B. 71

Figure 3.6 Experimental data, estimated errors, and diffusion model predictions for gas-phase (**A**) and stainless steel and wallboard sorbed nicotine (**B**) for 200 hours following the first injection of nicotine in experiment 3B. The lengths of the horizontal bars and their positions relative to the time axis in panel **A** indicate the duration and timing of Tenax-TA sorbent samples.....72

Figure 3.7 Experimental data, estimated errors, and diffusion model predictions for gas-phase (**A**) and stainless steel and wallboard sorbed nicotine (**B**) for 200 hours following the second injection of nicotine in experiment 3B. The lengths of the horizontal bars and their positions relative to the time axis in panel **A** indicate the duration and timing of Tenax-TA sorbent samples.....73

Figure 3.8 Experimental data, estimated errors, and surface sorption model predictions for gas-phase (**A**) and stainless steel adsorbed phenanthrene (**B**) in experiment 3C. The lengths of the horizontal bars and their positions relative to the time axis in panel **A** indicate the duration and timing of Tenax-TA sorbent tube samples.....74

Figure 3.9 Experimental data, estimated errors, and diffusion model predictions for gas-phase (**A**) and stainless steel sorbed phenanthrene (**B**) for 10 hours following the first injection of phenanthrene in experiment 3C. The lengths of the horizontal bars and their positions relative to the time axis in panel **A** indicate the duration and timing of Tenax-TA sorbent samples.....75

Figure 3.10 Experimental data, estimated errors, and diffusion model predictions for gas-phase (**A**) and stainless steel sorbed phenanthrene (**B**) for 10 hours following the fourth injection of phenanthrene in experiment 3C. The lengths of the horizontal bars and their positions relative to the time axis in panel **A** indicate the duration and timing of Tenax-TA sorbent samples.....76

Figure 3.11 Experimental data, estimated errors, and diffusion model predictions for gas-phase (**A**) and stainless steel adsorbed and carpet adsorbed and absorbed phenanthrene (**B**) in experiment 3D.....77

Figure 3.12 Experimental data, estimated errors, and diffusion model predictions for gas-phase (**A**) and stainless steel and carpet sorbed nicotine (**B**) for 200 hours following the first injection of phenanthrene in experiment 3D. The lengths of the horizontal bars and their positions relative to the time axis in panel **A** indicate the duration and timing of Tenax-TA samples.....78

Figure 3.13 Experimental data, estimated errors, and diffusion model predictions for gas-phase (**A**) and stainless steel and carpet sorbed phenanthrene (**B**) for 200 hours following the fourth injection of phenanthrene in experiment 3D. The lengths of the horizontal bars and their positions relative to the time axis in panel **A** indicate the duration and timing of Tenax-TA samples.....79

Figure 3.14 Experimental data, estimated errors, and diffusion model predictions for gas-phase (**A**) and stainless steel adsorbed and wallboard adsorbed and absorbed phenanthrene (**B**) in experiment 3E. 80

Figure 3.15 Experimental data, estimated errors, and diffusion model predictions for gas-phase (**A**) and stainless steel and wallboard sorbed phenanthrene (**B**) for 200 hours following the first injection of phenanthrene in experiment 3E. The lengths of the horizontal bars and their positions relative to the time axis in panel **A** indicate the duration and timing of Tenax-TA samples.....81

Figure 3.16 Experimental data, estimated errors, and diffusion model predictions for gas-phase (**A**) and stainless steel and wallboard sorbed phenanthrene (**B**) for 200 hours following the second injection of phenanthrene in experiment 3E. The lengths of the horizontal bars and their positions relative to the time axis in panel **A** indicate the duration and timing of Tenax-TA samples.....82

Figure 4.1 Observed relationship between gas-phase nicotine and RSP concentrations in approximately 100 smokers' houses in two New York counties (from Leaderer and Hammond, 1991).....119

Figure 4.2 Four- to seven-hour average $PM_{2.5}$ concentrations measured in public places vs. corresponding total airborne nicotine concentrations (Miesner *et al.*, 1989). The solid line is the least-squares regression for all of the data and the dashed line is the best fit for all data except the highest concentration point which was collected in a smoking lounge. 120

Figure 4.3 Mean values of 24-hour time weighted average airborne concentrations of RSP and nicotine. These data were collected as part of a personal sampler study of approximately 1000 nonsmokers in 16 U.S. cities (Jenkins *et al.*, 1996b). The eight data points represent mean values for the subjects grouped according to gender and whether they were exposed to ETS at home, at work or in both or neither of these locations.....121

Figure 4.4 Normalized ratio of experimental airborne nicotine and RSP concentrations in a 18 m^3 stainless steel chamber for of chamber air exchange rates (AER) between 0 and 4 h^{-1} and sampling (measurement) times between 30 minutes and 6 hours (from Nelson *et al.*, 1992). 122

Figure 4.5 Reversible surface sorption model predictions for the relationship between 24-h average RSP and nicotine concentrations in a 500 m^3 house with 250 m^2 of carpet and 1000 m^2 of painted wallboard surface area. These calculations simulate the field measurements shown in Figure 4.1 (Leaderer and Hammond, 1991). Model parameters are given in Table 4.1. Each data point represents a different set of smoking and air exchange rates. 123

Figure 4.6 Model predictions for the normalized ratio between nicotine and RSP concentrations for experiments in an 18 m^3 stainless steel chamber. These calculations simulate the experimental results shown in Figure 4.4 (Nelson *et al.*, 1992). In the model, two cigarettes are sequentially smoked for 10 minutes each starting at $t = 0$. The labels next to each curve denote the sampling period in hours. The values are normalized to the ratio calculated for a 30 minute sample at AER = 0 h^{-1} (0.129).....124

Figure 4.8 Measured ratio between RSP and total airborne nicotine concentrations for three experiments in a 20 m^3 stainless steel chamber containing painted wallboard and carpet as a function of measurement period duration starting at $t = 0$. The air exchange rates and smoking conditions for Experiments 4A, 4B, and 4C are listed in Table 4.2 and the data are tabulated in Table 4.3. The first cigarette in each experiment was started at $t = 0$.....126

Figure 4.9. 24-hour average RSP concentrations from Experiments 4A, 4B, and 4C with simulated ETS in a 20 m^3 stainless steel chamber containing painted wallboard and carpet vs. the corresponding 24-h average total airborne nicotine concentrations. Experimental conditions for the three runs are given in Table 4.2.....127

Figure 5.1 Gas-particle adsorption rate constants (k_{ag-p_i}) as a function of accommodation coefficient (γ) and SVOC molecular weight (MW) for different particle diameters, d_{p_i}: 0.05 μm, 0.3 μm, and 3.0 μm. The curves were generated using equation 5.15 and the non-continuum correction factor from equation 5.17.....165

Figure 5.2 Predicted gas and airborne particle phase (**A**) and sorbed and deposited particle phase (**B**) SVOC mass balance for simulation 5A (phenanthrene, slow gas-particle kinetics, low gas-particle equilibrium coefficient).....166

Figure 5.3 Predicted gas and airborne particle phase (**A**) and sorbed and deposited particle phase (**B**) SVOC mass balance for simulation 5B (phenanthrene, medium gas-particle kinetics, low gas-particle equilibrium coefficient).....167

Figure 5.4 Predicted gas and airborne particle phase (**A**) and sorbed and deposited particle phase (**B**) SVOC mass balance for simulation 5C (phenanthrene, fast gas-particle kinetics, low gas-particle equilibrium coefficient).....168

Figure 5.5 Predicted gas and airborne particle phase (**A**) and sorbed and deposited particle phase (**B**) SVOC mass balance for simulation 5D (phenanthrene, medium gas-particle kinetics, high gas-particle equilibrium coefficient).....169

Figure 5.6 Predicted gas and airborne particle phase (**A**) and sorbed and deposited particle phase (**B**) SVOC mass balance for simulation 5E (nicotine, medium gas-particle kinetics, low gas-particle equilibrium coefficient).....170

List of Tables

Table 1.1 Building and sorption parameters used in the comparison of indoor air behaviors of nonsorbing, irreversibly sorbing, and reversibly sorbing contaminants in Figure 1.2 13

Table 2.1. Summary of experimental parameters and kinetic model initial conditions for experiments 2A – 2E 41

Table 2.2. Best fit model parameters for fits of linear and nonlinear reversible sorption models to kinetic data from experiments 2A, 2B, and 2C. 42

Table 2.3 Gas-phase nicotine sample data from experiment 2A (ETS). 43

Table 2.4 Gas-phase nicotine sample data from experiment 2B (12.5 mg of nicotine) 44

Table 2.5 Gas-phase nicotine sample data from experiment 2C (33 mg of nicotine) 45

Table 3.1 Summary of experimental parameters and kinetic model initial conditions for experiments 3A – 3E 83

Table 3.1b SVOC mass emitted in each phase of experiments 3A – 3E 84

Table 3.2 Isotherm parameters for nicotine and phenanthrene sorption on stainless steel, carpet, and painted wallboard. Units are mg m^{-3} for concentration and mg m^{-2} for sorbed mass 86

Table 3.3 Kinetic sorption parameters for nicotine and phenanthrene interactions with stainless steel, carpet, and painted wallboard. 87

Table 3.4 Gas-phase nicotine sample data from experiment 3A (nicotine-carpet). 88

Table 3.5 Gas-phase nicotine sample data from experiment 3B (nicotine-wallboard). 91

Table 3.6 Gas-phase phenanthrene sample data from experiment 3C (phenanthrene-stainless steel). 93

Table 3.7 Gas-phase phenanthrene sample data from experiment 3D (phenanthrene-carpet). 95

Table 3.8 Gas-phase phenanthrene sample data from experiment 3E (phenanthrene-wallboard). 98

Table 4.1 Parameters used in model simulations of nicotine and RSP dynamics. 128

Table 4.2 Chamber operation and smoking parameters for three experiments in a stainless steel chamber containing carpet and painted wallboard. 129

Table 4.3 Gas-phase nicotine concentration sample data from experiments 4A – 4C with ETS in a 20 m^3 stainless steel chamber containing samples of carpet and wallboard as described in Table 4.2. 130

Table 4.4 Particle mass concentration sample data from experiments 4A – 4C with ETS in a 20 m^3 stainless steel chamber containing samples of carpet and wallboard as described in Table 4.2. 133

Table 4.5 Air-exchange rate and cigarette smoking histories for the stainless steel chamber prior to and during experiments 4A – 4C. 135

Table 5.1. Representative values (or ranges of values) and justifications for parameters used in the indoor SVOC dynamics model described in this chapter 171

Table 5.2. SVOC emission rates and outdoor concentrations used in all modeled scenarios 174

Table 5.3. Building operation and sorption dynamics parameters for modeled scenarios. 175

List of Symbols

a = empirical constant in equation 2.8, no units (Chapter 2)

A_F = bisulfate impregnated filter area, m^2 (Chapter 2)

$A_{molecular}$ = interfacial area occupied by a single sorbate molecule, m^2 (Chapter 1)

A_{p_i} = particle surface area per mass for particles of diameter d_{p_i}, m^2 mg^{-1} (Chapter 5)

C = indoor gas-phase concentration, mg m^{-3} (Chapters 1 and 2)

c = empirical constant in equation 2.8, no units (Chapter 2)

C_{ave} = average gas-phase nicotine concentration in the chamber during bisulfate filter sampling, mg m^{-3} (Chapter 2)

$C_{b_{ij}}(t,z)$ = instantaneous sorbent bulk-phase concentration of SVOC i at a distance z away from the air-sorbent interface, mg m^{-3} (Chapter 3)

$C_{b_j}(t,z)$ = instantaneous sorbent bulk-phase SVOC concentration at a distance z away from the air-sorbent interface, mg m^{-3} (Chapter 5)

$C_{b_{nj}}(t,z)$ = instantaneous sorbent bulk-phase concentration of nicotine at a distance z away from the air-sorbent interface, mg m^{-3} (Chapter 4)

C_i = gas-phase concentration of SVOC i in the chamber or building, mg m^{-3} (Chapters 3 and 4)

C_{io} = gas-phase concentration of SVOC i in chamber ventilation supply air, mg m^{-3} (Chapter 3)

C_n = indoor gas-phase nicotine concentration, mg m^{-3} (Chapter 4)

C_o = concentration in chamber ventilation supply air, mg m^{-3} (Chapter 2)

C_p = indoor airborne particle concentration, mg m^{-3} (Chapter 4)

C_{p_i} = indoor concentration of airborne particle-phase SVOC associated with particles of diameter d_{p_i}, mg m^{-3} (Chapter 5)

$C_{p_i o}$ = outdoor particle-phase SVOC concentration for particles of diameter d_{p_i} mg m^{-3} (Chapter 5)

C_{pm_i} = indoor concentration of airborne particles of diameter d_{p_i}, mg m^{-3} (Chapter 5)

$C_{pm_i o}$ = outdoor concentration of airborne particles of diameter d_{p_i} mg m^{-3} (Chapter 5)

C_g = indoor gas-phase SVOC concentration, mg m^{-3} (Chapter 5)

C_{go} = outdoor gas-phase SVOC concentration, mg m^{-3} (Chapter 5)

$C_{g\infty}$ = gas-phase SVOC concentration far from a particle's surface, mg m^{-3} (Chapter 5)

C_{gS} = gas-phase SVOC concentration at a particle's surface, mg m^{-3} (Chapter 5)

C_{pm_i} = airborne mass concentration of particles of diameter d_{p_i}, mg m^{-3} (Chapter 5)

$D_{b_{ij}}$ = diffusion coefficient for SVOC i in the bulk of sorbent j, m^2 h^{-1} (Chapter 3)

D_{b_j} = diffusion coefficient for SVOC molecules in the bulk of sorbent j, m^2 h^{-1} (Chapter 5)

D_g = diffusion coefficient for SVOC molecules in air, m^2 h^{-1} (Chapter 5)

d_{p_i} = aerodynamic diameter of particles in size bin i, m (Chapter 5)

E = nicotine emission rate, mg h^{-1} (Chapter 2)

E_i = gas-phase mass emission rate of SVOC i, mg h^{-1} (Chapter 3)

$E_g(t)$ = instantaneous gas-phase SVOC mass emission rate at time t, h (Chapter 5)

$E_i(t)$ = instantaneous gas-phase mass emission rate of pollutant i at time t, mg h^{-1} (Chapter 4)

$E_n(t)$ = instantaneous gas-phase mass emission rate of nicotine at time t, mg h^{-1} (Chapter 4)

$E_p(t)$ = instantaneous particle mass emission rate at time t, mg h^{-1} (Chapter 4)

$E_{p_i}(t)$ = instantaneous mass emission rate for particle-phase SVOCs associated with particles of diameter d_{p_i} at time t, mg h^{-1} (Chapter 5)

$E_{pm_i}(t)$ = instantaneous mass emission rate for particles of diameter d_{p_i} at time t, mg h^{-1} (Chapter 5)

f_i, = multiplicative correction factor for k_{ag-p_i} from the Fuchs-Sutugin equation (Chapter 5)

g = total number of different sorbent materials in the chamber during an experiment, no units (Chapters 3 and 4)

γ = gas-particle accommodation or sticking coefficient (ratio of the number of molecules adhering to a surface and the number colliding with it, no units (Chapter 5)

i = subscript signifying parameters applying to SVOC i, no units (Chapters 3 and 4) or to particles in size bin i (Chapter 5)

j = subscript signifying parameters applying to sorbent i, no units (Chapters 3, 4 and 5)

J = net nicotine flux to stainless steel chamber surfaces, mg m^{-2} h^{-1}, $J > 0$ for transport to the surface (Chapter 2)

J_{D_i} = net diffusive flux of gas-phase SVOC molecules to the surfaces of particles of diameter d_{p_i}, mg m^{-2} h^{-1} (Chapter 5)

J_{ij} = net flux of SVOC i from the gas phase to the air-sorbent interface of sorbent j, mg m^{-2} h^{-1} (Chapter 3)

J_{p_i} = net adsorptive mass flux of SVOCs to a particle surface, mg m^{-2} h^{-1} (Chapter 5)

J_{S_i} = adsorptive flux of SVOCs at a particle surface, mg m^{-2} h^{-1} (Chapter 5)

k = the Boltzmann constant, 1.38×10^{-23} J K^{-1} (Chapter 5)

K = equilibrium isotherm "constant" — actually a function of temperature, relative humidity, and other environmental factors, m if $n = 1$ as in equation 1.2 or mg^{-n} m^{3n+1} if $n \neq 1$ as in equation 1.3 (Chapters 1 and 2)

k_a = nicotine-stainless steel adsorption rate coefficient, $mg^{1-n_a}\ m^{3n_a-2}\ h^{-1}$ (Chapter 2)

k_{ag-p_i} = gas-particle adsorption rate constant for particles of diameter d_{p_i}, m h^{-1} (Chapter 5)

$k_{ag-dp_{ij}}$ = adsorption rate constant for sorption of gas-phase SVOCs on particles of diameter d_{p_i} deposited on surface material *j*, m h^{-1} (Chapter 5)

k_{ag-s_j} = gas-surface adsorption rate constant for sorbent *j*, m h^{-1} (Chapter 5)

$k_{a_{ij}}$ = adsorption rate coefficient for SVOC *i* on sorbent *j*, m h^{-1} (Chapter 3)

k_{ans} = nicotine-stainless steel adsorption rate coefficient, $mg^{1-n_a}\ m^{3n_a-2}\ h^{-1}$ (Chapter 4)

k_{ap} = particle deposition velocity (deposition rate coefficient), m h^{-1} (Chapter 4)

k_{anj} = nicotine adsorption rate coefficient on sorbent *j*, m h^{-1} (Chapter 4)

k_d = nicotine-stainless steel desorption rate coefficient, $mg^{1-n_d}\ m^{2n_d-2}\ h^{-1}$ (Chapter 2)

k_{dg-p_i} = gas-particle desorption rate constant for particles of diameter d_{p_i}, h^{-1} (Chapter 5)

$k_{dg-dp_{ij}}$ = desorption rate constant for sorption of gas-phase SVOCs on particles of diameter d_{p_i} deposited on surface material *j*, h^{-1} (Chapter 5)

k_{dg-s_j} = gas-surface desorption rate constant for sorbent *j*, h^{-1} (Chapter 5)

$k_{d_{ij}}$ = desorption rate coefficient for SVOC *i* on sorbent *j*, h^{-1} (Chapter 3)

k_{dnj} = nicotine desorption rate coefficient from sorbent *j*, h^{-1} (Chapter 4)

k_{dns} = nicotine-stainless steel desorption rate coefficient, $mg^{1-n_d}\ m^{2n_d-2}\ h^{-1}$ (Chapter 4)

k_{dpm_i} = the particulate matter deposition velocity for particles of diameter d_{p_i}, m h^{-1} (Chapter 5)

K_{ij} = linear isotherm partitioning coefficient for SVOC *i* on sorbent *j*, m (Chapters 3 and 5)

Kn_i = Knudsen number for particles of diameter d_{p_i}, no units (Chapter 5)

K_{ns} = nonlinear isotherm partitioning coefficient for nicotine on stainless steel, m (Chapter 4)

K_p = gas-particle equilibrium partitioning constant, $m^3\ mol^{-1}$ (Chapter 5)

K_p' = gas-particle partitioning equilibrium constant normalized to particle surface area, m (Chapter 5)

k_{rg} = average pseudo-first order chemical decay rate for gas-phase SVOC, h^{-1} (Chapter 5)

k_{rp} = average pseudo-first order chemical decay rate for particle- and deposited particle-phase SVOC, h^{-1} (Chapter 5)

k_{rs_j} = average pseudo-first order chemical decay rate for SVOC sorbed at the air-sorbent interface of surface *j*, h^{-1} (Chapter 5)

λ_v = building, chamber or other indoor environment air exchange rate, h^{-1} (Chapters 1, 3, 4, and 5)

$\lambda_{v,T}$ = total chamber ventilation rate including ventilation due to sampling, h^{-1} (Chapter 2)

M = mass sorbed per unit area of sorbent, mg m^{-2} (Chapters 1 and 2)

M_F = nicotine mass collected on a bisulfate impregnated filter, μg (Chapter 2)

M_{ij} = sorbed mass of SVOC *i* per unit area at the air-surface interface of sorbent *j*, mg m^{-2} (Chapters 3, 4, and 5)

$M_{nj,surface}$ = sorbed mass of nicotine per unit area at the air-surface interface of sorbent *j*, mg m^{-2} (Chapter 4)

M_{ns} = sorbed mass of nicotine per unit area of stainless steel, mg m^{-2} (Chapter 4)

$M_{p_{ij}}$ = SVOC mass associated with particles of diameter d_{p_i} deposited on indoor surface material *j*, mg m^{-2} of surface *j* (Chapter 5)

$M_{pm_{ij}}$ = deposited particle mass of particles of diameter d_{p_i} per unit area of indoor surface material *j*, mg m^{-2} (Chapter 5)

m_s = molecular weight of a single sorbate molecule, kg (Chapter 5)

M_{s_j} = SVOC mass reversibly sorbed at the air-sorbent interface of indoor surface material j, mg m^{-2} (Chapter 5)

m_{air} = molecular weight of a single "average" air molecule, 4.8×10^{-26} kg at 50% *RH* (Chapter 5)

$M_{T_{ij}}$ = total sorbed mass of SVOC i per presented area of sorbent j, mg m^{-2} (Chapter 3)

n = Freundlich isotherm exponential coefficient, no units (Chapters 1 and 2)

n_{ns} = nicotine-stainless steel Freundlich isotherm exponential coefficient, no units (Chapters 4)

$N(Q)$ = frequency of sites with sorption energy Q, no units (Chapter 2)

n_a = adsorption rate exponential coefficient, no units (Chapter 2)

$n_{a_{is}}$ = nicotine-stainless steel adsorption rate exponential coefficient, no units (Chapter 3)

n_{ans} = nicotine-stainless steel adsorption rate exponential coefficient, no units (Chapter 4)

$N_{Avogadro}$ = Avogadro's number, 6.022×10^{23} molecules mol^{-1} (Chapter 1

n_d = nonlinear desorption rate exponential coefficient, no units (Chapter 2)

$n_{d_{is}}$ = nicotine-stainless steel nonlinear desorption rate exponential coefficient, no units (Chapter 3)

n_{dns} = nicotine-stainless steel desorption rate exponential coefficient, no units (Chapter 4)

ω = total number of discrete particle size bins used in modeling analysis, no units (Chapter 5)

P = air pressure, Pa (Chapter 5)

Q_B = building ventilation air flow rate, m^3 h^{-1} (Chapter 1)

R = universal gas constant, 8.3144 J mol^{-1} K^{-1} (Chapter 2)

RH = relative humidity, % (Chapters 2, 3, and 5)

s = subscript denoting stainless steel as the sorbent of interest, no units (Chapter 3)

S = stainless steel chamber internal surface area, m^2 (Chapter 2)

S_j = presented surface area of sorbent j, m^2 (Chapters 3 and 4)

S_S = chamber stainless steel surface area, m^2 (Chapters 3 and 4)

S_{s_j} = total presented surface area available for sorption on sorbent j, m^2 (Chapter 5)

S_T = total presented indoor surface area, m^2 (Chapters 4 and 5)

$\sigma_{a\text{-}s}$ = collision diameter for binary collisions between SVOC and air molecules, m (Chapter 5)

T = temperature, K (Chapters 2 and 5)

t = time, h (Chapters 2, 3, 4, and 5)

t_s, = duration of the bisulfate filter sampling period, h (Chapter 2)

$\langle v \rangle$ = mean molecular speed of SVOC molecules in air, m h^{-1} (Chapter 5)

V = chamber or indoor environment volume, m^3 (Chapters 2, 3, 4, and 5)

V_B = building volume, m^3 (Chapter 1)

v_t = mass transport limited nicotine deposition velocity determined from bisulfate coated filter experiment, m h^{-1} (Chapter 2)

z = distance into the bulk of the sorbent material — $z = 0$ at the sorbent surface, m (Chapters 3, 4, and 5)

Acknowledgements

The work presented in this dissertation would not have been possible without the intellectual prodding and helpful feedback provided by Professor William Nazaroff, my faculty advisor at U.C. Berkeley, and Dr. Joan Daisey, my advisor and supervisor at Lawrence Berkeley National Laboratory. Professor Rob Harley also provided helpful guidance, especially during Bill's sabbatical. Tsair-Fuh Lin and John Little both helped me greatly as mentors during my first two years of graduate school in addition to making things more fun. I would also like to thank Al Hodgson for extensive technical guidance regarding sampling and analysis techniques. Lara Gundel, Rich Sextro, Serena Dong, K. R. R. Mahanama, and Brian Laurenson assisted with many aspects of the laboratory work.

During my tenure as a graduate student at Berkeley, I have been supported by the U. S. Environmental Protection Agency Science to Achieve Results Graduate Fellowship, the S. C. Johnson Wax Research and Development Fellowship, and the State of California Toxic Substances Research Program. Additional research support was provided by Grant No. R01-HL42490 from the National Heart, Lung, and Blood Institute through the U. S. Department of Energy under Contact No. DE-AC03-76SF00098.

Chapter 1. Introduction

BACKGROUND

On average, people spend more than 85% of their time in buildings, cars, or other indoor environments (Wiley *et al.,* 1991). In addition, the concentrations of many toxic air pollutants are higher indoors than outdoors (Brown *et al.*, 1994). Exposures to toxic air contaminants may be calculated as the product of exposure duration and average concentration. The large fraction of time spent indoors and the high pollutant concentrations encountered in many indoor settings cause inhalation of indoor air to dominate overall human exposures to many toxic air contaminants.

Pollutant concentrations encountered in all environmental settings result from the competition among chemical and physical removal and generation mechanisms ("sinks" and "sources," respectively). Sinks generally considered in indoor air quality analyses are ventilation, filtration, and deposition on indoor surfaces. Sources of indoor air pollutants include outdoor air contaminants transported indoors by ventilation, direct emissions from indoor sources, and reemission of reversibly deposited pollutants from indoor sinks. This dissertation focuses on the dynamic, reversible, sorptive interactions of low volatility organic air pollutants with indoor surface materials. This phenomenon is a potentially important, but largely unexplored, topic in indoor air quality.

Semivolatile Organic Compounds. Semivolatile organic compounds (SVOCs), comprise a large and important class of air pollutants. Many VOCs and SVOCs have known health or comfort effects, ranging from irritation to carcinogenicity or teratogenicity (Rothweiler & Schlatter, 1993; Lewtas, 1994). Several researchers have reported evidence of a possible link between indoor VOC concentrations and "sick building syndrome" (SBS) (Mølhave *et al.*, 1986; Morrow, 1992; Gold, 1992; Ten Brinke, 1995; Ten Brinke *et al.*, 1998), although not all of the available evidence supports such a link (Sundell *et al.*, 1993; Mendell, 1994). SVOCs are generally defined as compounds

with vapor pressures between 10^{-6} and 10 Pa at environmental temperatures (Bidleman, 1988) or with boiling points exceeding 250° C at ambient pressure. These physical property ranges are only approximate and should be considered as conveniently measured surrogates for the propensity of a compound to exist in both condensed and vapor phases at environmental temperature and pressure. Because of their low vapor pressures, it is thermodynamically favorable for SVOCs to partition into condensed phases in the environment. Because SVOCs in the environment are usually present at concentrations far below their saturation vapor pressures, they most commonly partition into condensed phases by sorbing to particles or fixed environmental surfaces rather than by forming a pure condensed liquid phase.

Many of the 189 hazardous air pollutants listed in the 1990 U.S. Clean Air Act Amendments are SVOCs. Examples of SVOCs found indoors include nicotine; polycyclic aromatic and nitrated polycyclic aromatic hydrocarbons (PAHs and NPAHs); polychlorinated biphenyls (PCBs); dioxins; pesticides; and a wide variety of polar compounds with molecular weights larger than approximately 130 g mol^{-1} including alcohols, organic acids, carbonyls, and amines. Many of these compounds have known health or comfort effects, ranging from irritation to carcinogenicity or teratogenicity (Rothweiler and Schlatter, 1993, Lewtas, 1994). The research presented in this dissertation investigates the sorptive behavior of nicotine and phenanthrene, two SVOCs with different chemical properties and reactivities, with two common indoor sorbents, carpet and painted wallboard. Nicotine and phenanthrene are commonly encountered indoor air pollutants. Nicotine is the dominant single compound emitted by tobacco combustion. Phenanthrene is also a component of tobacco smoke which is emitted by other incomplete combustion processes as well.

Sorption. A net increase or decrease in a compound's concentration at the interface between two phases relative to that in the bulk of either phase is an important environmental process known as *sorption*. Sorption can occur at the interface between

any two phases, including gas-liquid, gas-solid, liquid-solid, liquid-liquid and even solid-solid contact surfaces. The most commonly considered sorption systems in environmental engineering are those involving a fluid phase, such as gas, water, or some other liquid, and a solid phase, such as soil, activated carbon, or any of the nearly infinite variety of environmental surfaces. The solid phase is known as the *sorbent* and the sorbing compound is referred to as the *sorbate*.

Two commonly reported expressions of sorbate accumulation at the fluid-sorbent interface are the surface excess or superficial density, Γ (mol m^{-2}), and the fractional monolayer surface coverage, θ (no units). The interfacial excess is derived by assuming that the two bulk phases on either side of the interface have uniform concentrations up to an arbitrary plane parallel to the interface. Any accumulation or deficiency (the latter leading to a negative surface excess) of sorbate molecules in the interfacial region relative to the bulk phase concentrations is expressed as Γ at this two dimensional plane. This simplification is not a perfect representation of most real sorption systems which are typically more accurately characterized by a concentration gradient over a finite distance on either side of the interface. For positive values of Γ (net positive sorption at the interface) θ is obtained as follows:

$$\theta = \Gamma N_{Avogadro} A_{molecular} \tag{1.1}$$

where $N_{Avogadro}$ is Avogadro's number (6.022×10^{23} molecules mol^{-1}) and $A_{molecular}$ is the interfacial area occupied by a single sorbate molecule (m^2). Applications of Γ and θ and their thermodynamic derivation are discussed in detail by Adamson (1990, §III-5).

Sorption Equilibrium. Equilibrium partitioning of a compound between a fluid phase (in this work the gas phase) and a stationary sorbed phase is mathematically described with an isotherm equation. The simplest model for equilibrium between the fluid and sorbed phases assumes that the mass sorbed per unit surface area of the sorbent, M (μg m^{-2}) is directly proportional to the fluid phase concentration C (μg m^{-3}):

$$M = KC \tag{1.2}$$

where K is an equilibrium partitioning "constant" which is a function of several parameters: temperature; chemical and physical interactions of the sorbent with the sorbate; and other variables, such as relative humidity, surface roughness or soiling, and the presence of other sorbates, which may alter the thermodynamics of the sorbent-sorbate interaction. This isotherm, which is analogous to Henry's Law for gas-aqueous phase partitioning equilibrium, is generally accepted as a valid representation of sorption equilibrium on homogeneous or nearly homogeneous sorbents when the sorbate concentration in the fluid phase is low and θ is small compared to one (Lin, 1995, Adamson, 1990). At these low concentrations and values of θ, each sorbate molecule on the surface interacts nearly independently with the sorbent surface. As the fluid concentration and θ increase, sorbate-sorbate interactions become more important and the affinity of the surface for additional sorbate molecules changes. For sorbents with heterogeneous surfaces, including those encountered in many environmental applications, the thermodynamics of the sorbate-sorbent interaction may change as coverage of the sorbent surface with sorbate molecules changes. More favorable sorption sites are filled by the initially sorbed sorbate molecules, and the surface's affinity for the sorbate changes as Γ increases. These phenomena are often modeled using the Freundlich isotherm:

$$M = KC^n \tag{1.3}$$

where n is an experimentally determined coefficient that reflects the effects of increasing surface coverage on equilibrium partitioning and K is an equilibrium "constant" whose units depend on n. Freundlich isotherms with $n < 1$ have been reported to fit experimental data for several VOCs on dry environmental soils and activated carbon (Lin, 1995). These isotherms are referred to as *convex*, meaning that when C is plotted on the abscissa and M on the coordinate axis, the isotherm curves back toward the C axis as the concentration increases as shown in Figure 1.1. Physically, this means that less mass is

sorbed for a given increase in concentration at higher values of M than at lower M for the same concentration increase. The effects of Freundlich isotherm partitioning with $n < 1$ are explored in greater detail in Chapter 2.

Sorption Kinetics. In some environmental systems, equilibrium data are sufficient to make accurate predictions of contaminant dynamics. However, for situations in which the time scale of interest is comparable to or smaller than that for attainment of equilibrium, the kinetics of a process must also be considered. The time scale of interest in indoor air quality analyses is typically on the order of the time required to exchange the air inside a building with outdoor air. This period is generally expressed as the reciprocal of the air-exchange rate (AER), λ_v which has units of h^{-1} and is defined as

$$\lambda_v = Q_B / V_B \tag{1.4}$$

where Q_B and V_B are the building ventilation rate ($m^3\ h^{-1}$) and volume (m^3), respectively. A discussion of sorption kinetics requires introduction of two additional terms: the *sorption rate*, which indicates net accumulation at the sorbent-sorbate interface, and the *desorption rate*, denoting a net flux of sorbate molecules away from the interface into the gas phase. The kinetic sorption and desorption processes are also often referred to as *deposition* or *uptake* and *reemission*, respectively. However, deposition often connotes an irreversible process, so its use should be avoided in discussions of reversible sorption to avoid unnecessary confusion. Several studies have investigated sorption and desorption kinetics of volatile organic compounds (VOCs) on indoor surface materials such as carpet, wallboard, and upholstery (Matthews *et al.*, 1987; Tichenor *et al.*, 1991; Jørgensen *et al.*, 1993; Neretnieks *et al.*, 1993; Kjaer *et al.*, 1996). VOCs are a class of air pollutants similar to SVOCs but with vapor pressures greater than 10 Pa at room temperature. As such, they are found more predominantly in the gas phase than SVOCs although they do sorb measurably on indoor materials. Reversible sorption kinetics for VOCs on indoor surface materials have generally been modeled by assuming that

equilibrium obeys a linear isotherm (equation 1.2) and that the adsorption and desorption rates are directly proportional to the gas-phase concentration (C) and sorbed mass density (M), respectively. This model, originally described by Dunn and Tichenor (1988) and Tichenor *et al.* (1991), has been successfully applied to model the sorption and desorption kinetics of compounds such as tetrachloroethylene and ethylbenzene on carpet fibers and other indoor materials (Tichenor *et al.*, 1991). However, no data have been published to demonstrate that this model applies to a broader range of indoor surface materials or to compounds, such as SVOCs, with lower vapor pressures and higher surface affinities. For compounds with these properties, the linear isotherm assumption may fail because of increased surface coverage (θ) at typically encountered gas-phase concentrations. Additionally, most previous studies have not examined sorption kinetics over periods longer than a few weeks. For flat, nonporous materials, this omission is unlikely to introduce many errors. However, carpet, wallboard, and other common indoor materials may have significant sorption capacity which lies a finite distance away from the air-sorbent interface and can only be accessed by diffusion of sorbate molecules through the sorbent bulk. Consideration of this process requires minor redefinition of the terms discussed above. For materials with significant sorption capacity contained in the bulk of the sorbent, *sorption* refers to the total amount of sorbate associated with the sorbent both at the air-sorbent interface and in the sorbent bulk. Sorption is further broken down into two related processes: *adsorption* which refers to accumulation at the air-sorbent interface and *absorption* which indicates accumulation in the bulk of the sorbent. This dissertation extends the existing understanding of organic compound sorption on indoor materials to SVOCs and also investigates the sorption kinetics of porous sorbents over periods of a month or more.

Sorption Effects on Exposures to Indoor Air Contaminants. Reversible sorption on fixed indoor surfaces shifts the evolution of exposures for intermittently emitted indoor air pollutants. For instance, consider the case of an instantaneous puff

emission of three air contaminants, A, B, and C into a ventilated volume. The compounds do not interact with each other and their interactions with the indoor surfaces are as follows: A is inert to surface interactions, B sorbs reversibly to indoor surfaces, and C deposits irreversibly on indoor materials. There are no other important sources or sinks except ventilation for any of the compounds and the same mass of each compound is emitted. Compound A will have the largest peak concentration for any ventilation rate. If the rates of deposition of B and C on indoor surfaces are similar, then their concentrations will decay at approximately the same rate for a short time immediately after emission. However, as time progresses, the concentration of B will remain higher than that of C due to reemission of sorbed mass. Thus, reversible sorption reduces peak pollutant concentrations but increases the time required to eliminate a contaminant from indoor air following elimination of its primary source. This comparison is illustrated in Figure 1.2 using the parameters listed in Table 1.1.

DISSERTATION OVERVIEW

This dissertation describes the results of my study of the dynamics and equilibrium of reversible sorption of SVOCs on surface materials typically found in indoor environments. The investigation consisted of two main phases: experimental investigations of the dynamic behavior of two SVOCs (nicotine and phenanthrene) in a room-sized stainless steel environmental test chamber containing carpet or painted wallboard (Chapters 2 and 3) and computer model predictions of the effects of SVOC gas-surface and gas-particle partitioning on human exposures under various SVOC emission scenarios (Chapters 4 and 5).

Chapter 2 describes what was intended as a preliminary investigation of the interactions of nicotine with the stainless steel walls of the chamber used in the experiments discussed in Chapter 3. Because of the low vapor pressures and affinity for condensed phases typical of SVOCs (even those, such as stainless steel, that are generally

assumed to be inert) it was necessary to quantify gas-surface interactions with the walls of the empty chamber to facilitate accurate interpretation of data collected in the subsequent experiments. This initial study became much more interesting after the discovery that approximately 85% of the nicotine emitted into the sealed, empty chamber could not be accounted for based on gas-phase measurements and solvent extraction of sorbed-phase samples at the end of a 4 hour experiment. After exploring many alternative hypotheses to explain this observation, mass balance closure was achieved through development and application of a thermal desorption technique for recovery of sorbed-phase nicotine. This new method collected approximately 80% of the originally emitted nicotine after the chamber had been sealed for 5 hours. A nonlinear reversible sorption model based on the Freundlich isotherm equation was developed to predict sorptive interactions of nicotine with stainless steel. This modified model produced better model-measurement agreement throughout the kinetic experiments and particularly during and after chamber ventilation.

Chapter 3 applies the experimental and modeling methods developed in Chapter 2 to study nicotine and phenanthrene sorption and desorption on two materials more typically encountered in indoor environments: carpet and painted wallboard. In this study, data from experiments with the two porous sorbents were accurately simulated using a model that couples sorption at the air-sorbent interface (*adsorption*) and diffusion into the bulk of the sorbent (*absorption*). In addition, phenanthrene dynamics in the empty chamber were studied to extend the results of Chapter 2 to another SVOC. Phenanthrene behaved slightly differently than nicotine in the empty chamber — its equilibrium partitioning and sorption and desorption kinetics were accurately simulated with linear models rather than the nonlinear model developed in Chapter 2 for nicotine-stainless steel sorption. The results of the study of carpet and wallboard sorption of nicotine and phenanthrene indicate that these sorbents have very large capacities for SVOCs and that sorption and desorption kinetics are very slow. Diffusion into the

sorbent bulk limits the rate of sorbate uptake and reemission because most of the sorbent's sorption capacity is not immediately accessible to the air-sorbent interface.

Using the data collected in these experiments, numerical models that accurately described the dynamic behavior of the tested SVOCs were developed. To conclude my investigation, I employed the models developed and validated in Chapters 2 and 3 to predict the dynamic behavior of nicotine in real indoor environments to examine its effectiveness as a marker for environmental tobacco smoke. The results of this work indicate that nicotine concentrations can serve as a valid surrogate for the concentrations of other ETS constituents in indoor environments where smoking occurs regularly and are discussed in Chapter 4. Chapter 5 describes another modeling investigation of the effects of interphase mass transfer of SVOCs between the gas phase, surface-sorbed phase, and airborne particle-associated phase and its impacts on concentrations and persistence of SVOCs indoors.

APPLICATIONS

The results of the research presented in this dissertation have a number of important uses. Improved understanding of the factors impacting SVOC gas-phase sorption on indoor surface materials will facilitate more accurate predictions of indoor air concentrations of these potentially important pollutants. The sorption dynamics model frameworks developed in Chapters 2 and 3 are likely applicable to a variety of other reversible sorption systems. Furthermore, the results of the studies described in Chapter 3 indicate that diffusion of surface-sorbed SVOCs into the bulk of a porous sorbent can have a significant impact on their long-term persistence even after the gas-phase concentration has been reduced by elimination of indoor sources. The SVOCs considered in this study are chemically dissimilar. Nicotine has a higher vapor pressure and lower molecular weight than phenanthrene. However, nicotine has fairly reactive functional groups — a tertiary cyclic amine (also known as a pyrrolidine ring) and a substituted

pyridine ring — while phenanthrene is an unsubstituted three-ring PAH. Data on the sorptive behavior of these compounds may be valuable as a tool for predicting the indoor behavior of other SVOCs with similar chemical and physical properties.

In addition to the generalizations to other SVOCs facilitated by these studies, the nicotine data and kinetic parameters obtained in Chapter 3 have more specific applications. Nicotine is commonly used as a tracer compound to estimate indoor concentrations and human exposures to environmental tobacco smoke (ETS). However, its dynamic behavior in indoor air has been poorly understood. The elucidation of nicotine's interactions with indoor surfaces described in Chapter 3 and the application of these results to explain previously reported observations of nicotine in ETS described in Chapter 4 should increase the usefulness of data collected in previous and future studies of ETS dynamics.

Finally, the analysis and model development presented in Chapter 5 provide a valuable framework for considering organic compound behavior in indoor air from a mass balance perspective that is more complete than what has been previously reported in the literature. Incorporation of data from more detailed future studies of indoor chemistry and gas-surface partitioning of SVOCs and other indoor contaminants should eventually lead to development of vastly improved indoor air quality prediction capabilities. This progress will be invaluable in identifying and mitigating those sources and reversible sinks which have the largest negative impacts on indoor air quality.

FIGURES

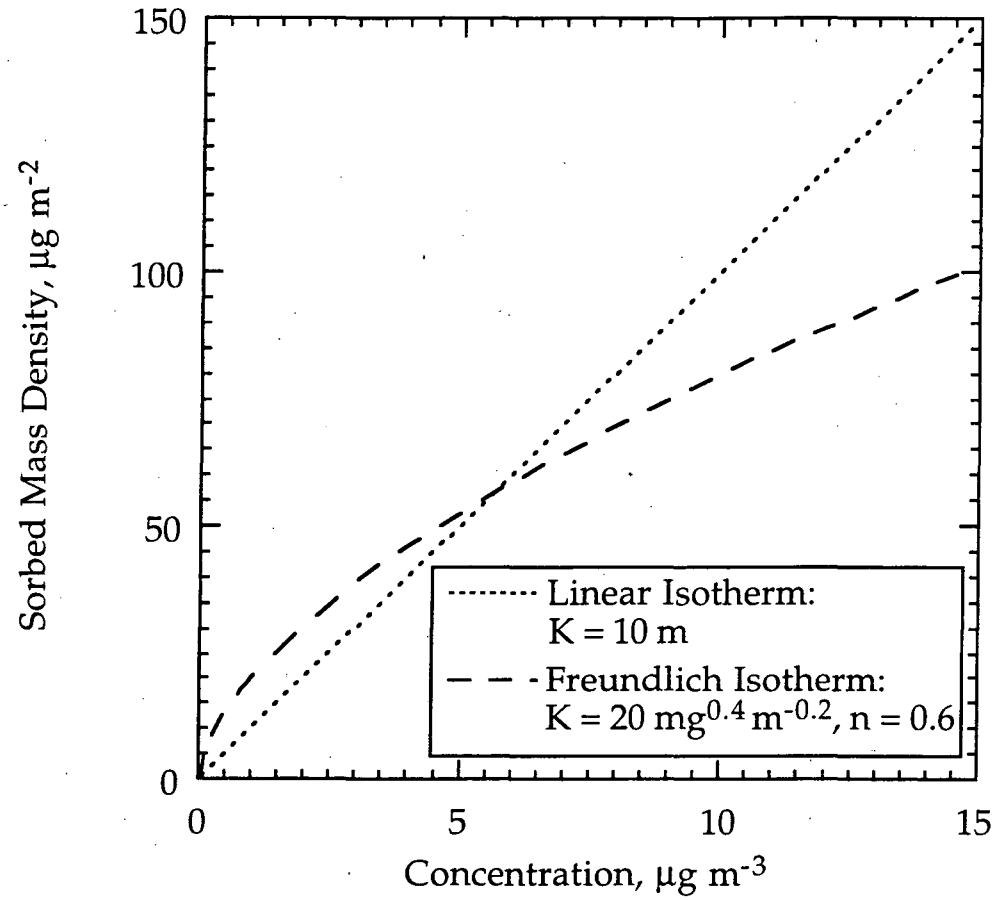

Figure 1.1 Comparison of linear and Freundlich isotherms. The linear isotherm is given in equation 1.2 and the Freundlich in equation 1.3.

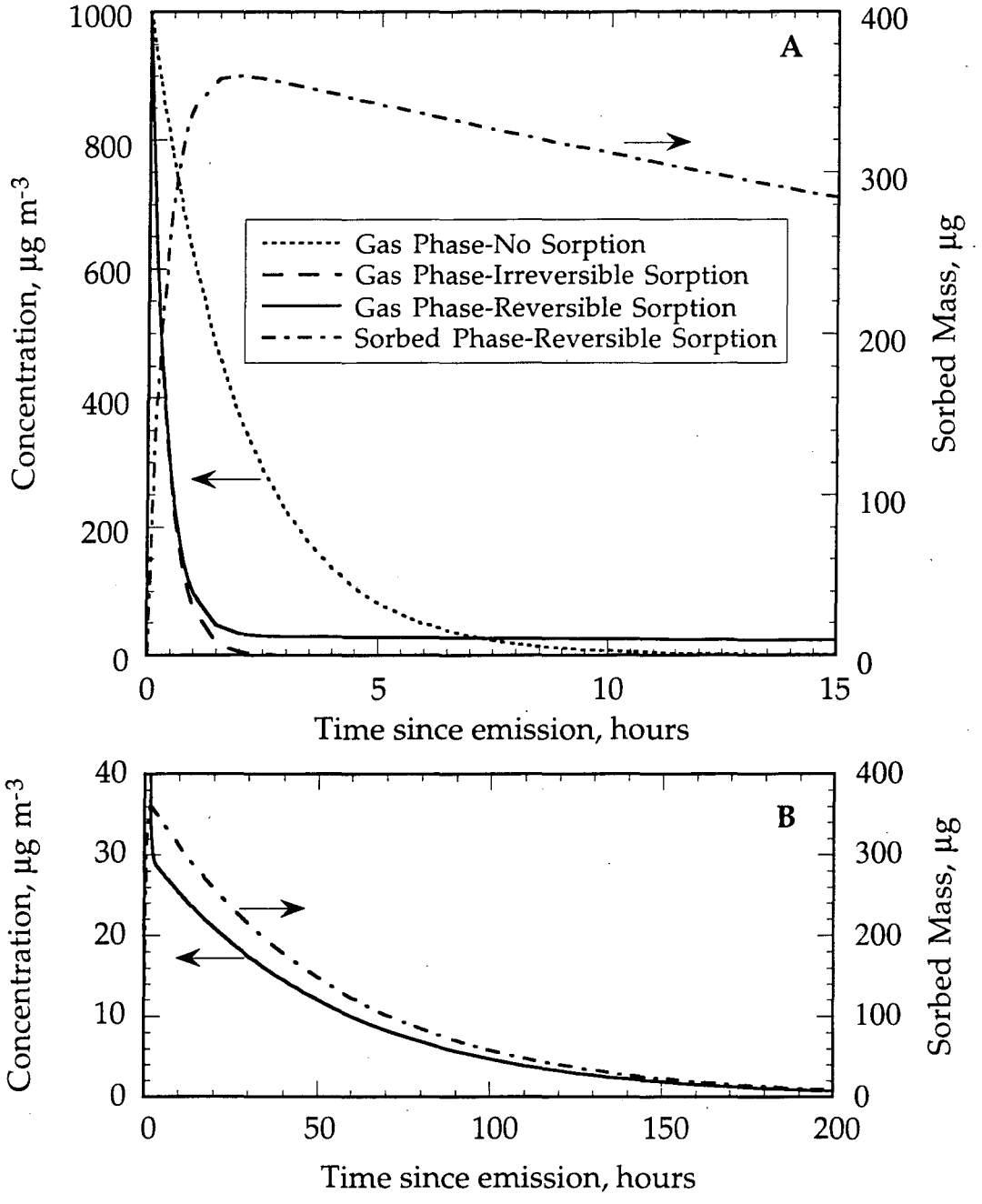

Figure 1.2 Comparison of hypothetical modeled indoor concentrations following puff emission of a pollutant. Panel A shows contaminant dynamics in the first 15 hours following emission and panel B shows the first 200 hours for a the reversibly sorbing contaminant.

TABLES

Table 1.1 Building and sorption parameters used in the comparison of indoor air behaviors of nonsorbing, irreversibly sorbing, and reversibly sorbing contaminants in Figure 1.2.

Parameter	Nonsorbing Contaminant	Irreversibly Sorbing Contaminant	Reversibly Sorbing Contaminant
Building Volume (m^3)	200	200	200
Building Surface Area (m^2)	450	450	450
Building Ventilation Rate (h^{-1})	0.5	0.5	0.5
Mass of Contaminant Released at t = 0 (mg)	200	200	200
Adsorption/Deposition Rate Constant (m h^{-1})	0	1.0	1.0
Desorption Rate Constant (h^{-1})	0	0	0.1

Chapter 2. Interactions of Nicotine with the Stainless Steel Surfaces of an Environmental Test Chamber*

ABSTRACT

The dynamic behavior of gaseous nicotine was studied in a 20 m^3 stainless steel chamber. Nicotine (10-40 mg) was emitted into the sealed chamber by cigarette combustion or flash evaporation of pure liquid. After three hours, during which the airborne concentration was monitored, the chamber was ventilated for two hours and then resealed to investigate reemission of sorbed nicotine. Gas-phase, airborne particle-phase, and wall-sorbed nicotine were measured to achieve mass-balance closure. More than 80% of the nicotine in the chamber was accounted for by thermally desorbing and collecting sorbed-phase nicotine. More than 99% of the measured nicotine was sorbed to chamber surfaces at equilibrium at 25 °C.

The gas-phase data were interpreted using reversible sorption models. A model based on linear partitioning between the gas- and sorbed-phases could not be accurately fit to the time-dependent data, so equilibrium partitioning was measured separately to test the linear model assumption. The equilibrium data are well described by a nonlinear Freundlich isotherm. Incorporating isotherm parameters into a kinetic, reversible sorption model which assumes a nonlinear, power-law rate of sorbed nicotine reemission and gas-phase deposition provided a significantly better fit to the dynamic data, especially during reemission after chamber ventilation.

---

* This chapter is based on a paper published elsewhere as Van Loy M.D., Lee V.C., Gundel L.A., Sextro R.G., Daisey J.M., and Nazaroff W.W. Dynamic behavior of semivolatile organic compounds in indoor air: 1. Nicotine in a stainless steel chamber, *Environmental Science and Technology*, **1997**, *31*, 2554-2561.

INTRODUCTION

Nicotine ($C_{10}H_{14}N_2$) is an important SVOC constituent of environmental tobacco smoke (ETS) whose emission rate is larger than that of any other compound in ETS. Environmental tobacco smoke is a complex, dynamic mixture of exhaled mainstream smoke (that which is inhaled by the smoker through the unburned end of a cigarette, cigar or pipe) and sidestream smoke (that emitted directly from the smoldering end of a cigarette). Nicotine's vapor pressure at room temperature is approximately 2 Pa (Jordan, 1954; Lencka *et al.,* 1984), and it is present in airborne ETS almost entirely in the gas-phase (Hammond *et al.,* 1987; Eatough *et al.,* 1989a; Caka *et al.,* 1990). Nicotine has been widely used as a marker of ETS exposure because 1) combustion of tobacco products is its only significant source in indoor air, 2) it is easy to detect (Eatough, 1993), and 3) it has similar emission rates for different types of cigarettes (Leaderer and Hammond, 1991; Daisey *et al.,* 1994, 1998, Martin *et al.*, 1997). However, the suitability of nicotine as a marker for ETS has been questioned by some researchers because gas-phase nicotine exhibits different indoor behavior patterns than do many other ETS constituents (Löfroth *et al.,* 1989; Löfroth, 1993a; Nelson *et al.,* 1990; Nelson *et al.,* 1992). Nevertheless, Leaderer and Hammond (1991) found high correlations between nicotine and respirable suspended particulate matter concentrations measured in residences. The debate over nicotine's utility as a marker remains unresolved. Elucidation of the factors affecting nicotine concentrations in indoor environments would improve the basis for using nicotine to assess ETS exposures.

In a study of emissions of organic compounds in ETS by Daisey *et al.* (1994, 1998) a significant discrepancy was observed between the apparent emissions of nicotine from sidestream smoke and from ETS. Sidestream smoke was collected from the air and the walls of a 125 cm^3 glass sampling chamber. ETS was sampled from the gas- and airborne particle-phases, but not the surfaces, of a 20 m^3 stainless steel environmental test chamber. The nicotine emission factor obtained from the sidestream measurement

was more than a factor of three greater than that obtained from the ETS measurement, suggesting that a large fraction of the emitted nicotine quickly deposited on the stainless steel surfaces of the environmental chamber.

Other investigators who have studied ETS in metal chambers (Leaderer and Hammond, 1991; Nelson *et al.,* 1990; Nelson *et al.,* 1992) have reported emissions factors for nicotine in ETS comparable to those reported by Daisey *et al.* (1994, 1998). These other studies also noted that the gas-phase nicotine concentration in indoor air decreases at a faster rate than can be attributed to ventilation alone. The decrease in the gas-phase concentrations of several other ETS components has been shown in laboratory chamber studies to be approximately first-order in the component's concentration (Nelson *et al.,* 1992; Baker *et al.,* 1988). In contrast, nicotine's concentration decreases rapidly for the first 30-45 minutes following its emission before achieving a very slowly decaying plateau (Baker and Proctor, 1990). This behavior more closely resembles a second order reaction.

The present investigation originated as an effort to resolve the disagreement between nicotine emission factors calculated for ETS and undiluted sidestream smoke (Daisey *et al.,* 1994, 1998) and evolved into a consideration of the impact of sorption on the dynamic behavior of SVOCs in indoor air. Experiments were designed and conducted to investigate the time-dependent concentration and fate of nicotine in a stainless steel chamber. Gas-phase, particulate-phase, and sorbed-phase measurements were made to complete a mass balance on nicotine emitted into the chamber. Sorption dynamic models were applied to the gas-phase data and refined to give better representations of the observed trends. Equilibrium partitioning between the gas and sorbed phases was measured in independent experiments. The resulting isotherm parameters were incorporated into a nonlinear, reversible sorption model to reduce the number of fitted model parameters to no more than two. The results of this study provide information relevant to the use of nicotine as an ETS marker compound and contribute to our general understanding of the dynamic behavior of SVOCs in indoor air.

MATERIALS AND METHODS

Stainless Steel Test Chamber. Five experiments were conducted in an environmental test chamber with a volume of 20 m^3 and an internal surface area of 45.2 m^2 (see Figure 2.1). All of the chamber's internal surfaces were clad with Type 304 stainless steel and the walls, floor, and ceiling were insulated with a 10-cm-thick layer of high density polyurethane foam. The door and interior seams were sealed with low-VOC-emitting silicone gasket material. Six 8-cm-diameter wall-mounted fans, aligned with their axes parallel to the floor but at a 45° angle to the wall surface, circulated the air during the experiments. The temperature and relative humidity (RH) inside the chamber were uncontrolled, but fairly constant for all five experiments, at 23 ± 3 °C and 55 ± 10%, respectively. Ventilation air, when provided, was passed through HEPA and granular activated carbon (GAC) filters.

The chamber door was left open for at least 90 days prior to each experiment to allow reemission and natural ventilation through the door to eliminate any previously sorbed nicotine. Several days prior to each experiment, the chamber interior was washed with a 2% by volume aqueous solution of potassium hydroxide detergent (Kart-Klenz, Calgon, City of Industry, CA). The detergent solution was applied with a sponge and removed with a rubber window wiper. Then, the surfaces were rinsed twice, with tap water and deionized water. Rinse water was removed with the window wiper, a wet-dry vacuum, and clean cotton or paper towels. The chamber was then ventilated continuously for at least two days, at approximately four air changes per hour, to allow equilibration with the humidity in outdoor air. The alkaline detergent was intended to decrease sorption of nicotine on the stainless steel surfaces by consuming acidic functional groups that might react with nicotine's basic moiety.

Experimental Protocol. Table 2.1 summarizes the five environmental chamber experiments conducted in this study. The first three experiments were designed to investigate the dynamic behavior of nicotine in the stainless steel chamber, and each

consisted of three stages. Figure 2.2 illustrates the approximate sequence of events that occurred in these experiments. In the first stage, nicotine was pulse-injected into the unventilated chamber and its concentration monitored. Before this stage, the ventilation ducts and chamber door were sealed with duct tape to minimize infiltration. Approximately three hours after nicotine emission began, the chamber was reentered for approximately two minutes to remove the seals from the ducts and half of the stainless steel foils from the walls for analysis. For the second stage, the chamber was then resealed and ventilated with HEPA- and GAC-filtered air having a negligible particle and VOC concentration at 68 $m^3\ h^{-1}$ for approximately two hours. During this period, the gas-phase was sampled to determine the nicotine mass removed by ventilation. Finally, to begin the third stage, the chamber was reentered for two minutes to reseal the ducts; then another two hours elapsed at the original low ventilation rate. The high ventilation rate during the second stage cleared the room air of nicotine, so any nicotine detected during the third stage would be due to reemission from chamber surfaces. The remaining wall-mounted stainless steel foils were removed from the chamber for analysis at the end of the third stage.

The sealed-chamber infiltration rate was determined prior to the experiments by tracer gas decay to be 0.15 $m^3\ h^{-1}$. In the smoking experiment (2A), ventilation caused by sampling was 0.23 $m^3\ h^{-1}$. Thus, Q_T, the total effective chamber ventilation rate was 0.38 $m^3\ h^{-1}$ during the first and third periods for the first run. For the second and third experiments, ventilation due to sampling was 0.12 $m^3\ h^{-1}$, so during the sealed stages, Q_T = 0.27 $m^3\ h^{-1}$. In experiments 2D and 2E, ventilation due to sampling was 0.006 $m^3\ h^{-1}$, so Q_T = 0.16 $m^3\ h^{-1}$.

Equilibrium partitioning of nicotine between the gas-phase and the stainless steel sorbed-phase was measured in the experiments 2D and 2E. After being ventilated and washed, the chamber was sealed as described above for the duration of experiment 2D. Once a day for four days, 10 mg of liquid nicotine was evaporated in the chamber as

described below. After each addition of nicotine, the gas-phase concentration was monitored for 6-8 hours, until an effective equilibrium concentration was achieved. The measured concentration changed by less than 3% over a two-hour period within 5 hours after emission. The sorbed mass in equilibrium with the measured concentration was determined by subtracting the gas-phase mass and the estimated cumulative mass removed by ventilation from the total mass injected.

Experiment 2E was conducted to verify recovery of sorbed nicotine from the walls of the 20 m^3 stainless steel chamber. The chamber was again ventilated, washed and sealed as in the previous runs. Then 20 mg of nicotine was evaporated in the chamber and allowed to equilibrate for 14 hours. After a gas-phase sample was collected to determine the airborne mass, the chamber was entered and one of several wall-mounted stainless steel plates was removed and thermally desorbed as described below. The chamber was resealed and allowed to equilibrate for another ten hours and then the gas- and sorbed-phase were sampled again to check for reproducibility.

Nicotine emission methods. In experiment 2A, three cigarettes (Marlboro Class A Filtered) were sequentially smoked using a cigarette smoking machine (Arthur D. Little, Cambridge, MA). Sidestream smoke was emitted into the chamber while the mainstream smoke was vented to a fume hood outside of the room. Prior to smoking, the cigarettes were conditioned at 60% relative humidity for more than 72 hours over a saturated aqueous solution of NaBr. Each cigarette burned for approximately 11 minutes starting at 0, 12, and 22 minutes, respectively, relative to the beginning of the experiment. The smoking machine drew one 35 cm^3 puff every 60 seconds. The chamber was entered for about thirty seconds after each cigarette to position the next cigarette to be smoked.

For experiments 2B and 2C pure liquid nicotine in a clean glass petri dish was placed on a preheated hot plate on the floor of the chamber. The masses used in each experiment are listed in Table 2.1. The petri dish was prewashed with ethanolic potassium hydroxide, rinsed with ethyl acetate containing 0.01% triethylamine by volume

(EA/TEA) to reduce sorption of nicotine to the glass (Ogden *et al.*, 1989), and dried under a clean nitrogen gas stream. Nicotine visibly evaporated from the glass surface within two minutes of the start of heating, and the electric current to the hot plate was shut off after 10 minutes. Heat emitted from the hot plate caused the chamber temperature to increase slowly from 20 to 24 °C during the first phase of the experiment. After the experiment, the petri dish was extracted with EA/TEA to estimate the mass of nicotine remaining on the glass. Approximately 20% (3 or 8 mg out of approximately 15 or 40 mg initially placed in the dish)) of the mass of nicotine placed on the petri dishes remained after each experiment. The unvolatilized fraction was excluded from the emitted mass in the kinetic model and mass balance calculations for experiments 2B and 2C. The emitted mass values reported in Table 2.1 reflect this correction.

In the two equilibrium experiments (2D and 2E), nicotine was also flash evaporated. However, to avoid the need to repeatedly enter the chamber to inject additional nicotine, a special evaporator unit was employed. This apparatus consisted of a 0.53 cm inner diameter, 10-cm-long stainless steel tube mounted in a small aluminum block heated by an electrical resistance cartridge heater (Chromalux). One end of the tube was open to the chamber, and the other end was connected to a small fan which pushed chamber air through the tube at approximately 25 cm^3 min^{-1}. The entire unit was mounted on the end of a 0.95 cm outer diameter stainless steel tube which extended approximately 75 cm into the chamber through a wall port. Immediately prior to each nicotine injection, the unit was withdrawn from the chamber, loaded with nicotine at the open end from an Eppendorf pipette, and quickly reinserted into the chamber. As this process took less than one minute, evaporative losses of nicotine outside the chamber are expected to be negligible. Once the evaporator unit was properly positioned, the current to the heater cartridge and fan was turned on. Within five minutes the temperature of the heater unit reached approximately 175 °C (as measured by a thermocouple) and remained fairly steady until the heater current was shut off after approximately 15 minutes. The

fan remained on until the unit was removed to prepare for the next injection. At the end of the experiment, the stainless steel tube which held the liquid nicotine was thermally desorbed at 275 °C while being flushed with dry helium at 100 cm^3 min^{-1} for one hour. The desorbed nicotine was collected on a multisorbent tube and analyzed by gas chromatography-mass spectrometry. Less than 0.5 μg (out of a total of 40 mg injected) was recovered.

Gas-Phase Sampling. Gas- and particulate-phase nicotine concentrations were measured as a function of time in experiment 2A (ETS) using the newly-developed annular denuder-based IOVPS system (Gundel *et al.,* 1995). This apparatus consists of two serial denuders coated with ground XAD-4 resin for the collection of gas-phase nicotine followed by two 47-mm-diameter Teflon-coated glass fiber filters to collect particle-phase nicotine. The second denuder in the sample chain was used to check for gas-phase breakthrough and determine the collection efficiency of the denuders. The second filter was coated with sodium bisulfate (Hammond *et al.,* 1987) to collect nicotine volatilized from filter-collected ETS particles. Only the gas-phase data were considered in this study since less than 5% of the airborne nicotine mass was found in the particle-phase. Additionally, previously published studies (Eatough *et al.,* 1989a; Hammond *et al.,* 1987; Caka *et al.,* 1990) have indicated that approximately 95% of the airborne nicotine mass in ETS exists in the gas-phase. The airborne particle-phase nicotine concentration changed much more slowly than the gas-phase. A more thorough investigation of dynamic partitioning of nicotine and other SVOCs between the gas- and particle-phases is warranted but beyond the scope of the current study.

After sampling, the IOVPS system was disassembled. Each denuder section was filled with approximately 20 cm^3 of EA/TEA, spiked with 27 μg of quinoline, and sonicated in a 40 °C water bath. The EA/TEA extract was filtered, and the denuder was extracted and filtered a second time with another volume of solvent. The EA/TEA extracts were concentrated using a rotary evaporator (Brinkmann Rotavapor-R) and a 42

°C water bath. Final sample volumes ranged from 150 to 700 μL. The concentrates were stored at -15 °C until they were analyzed. All samples from each experiment were processed and analyzed within nine days of collection. Blanks were analyzed concurrently with the chamber samples, and the results used to correct the corresponding experimental measurements.

In each of the kinetic experiments (2A-2C), gas-phase nicotine was collected by XAD-4 (Alltech Associates, Inc., Deerfield, IL) resin sorbent tube samplers (SKC West Inc., Fullerton, CA). In the ETS experiment (2A), the sorbent samplers followed an open-face filter pack containing a 47 mm Teflon-coated glass fiber filter for the collection of particle-phase nicotine. Filter packs were not used in the sampler chain for the pure liquid nicotine experiments because the chamber was flushed prior to the experiment with HEPA filtered air, and so the airborne particle concentration was expected to be nearly zero. The sorbent tubes were placed in a freezer immediately after removal from the chamber. To recover the sorbed nicotine, each tube was broken and its contents emptied into a storage vial. The vial was spiked with 27 μg of quinoline, and the inside surfaces of the tube were rinsed into the vial with 2 cm^3 of EA/TEA. The vials were capped and sonicated for 15 minutes. After sonication, the vials were stored at -15 °C until the extracts were analyzed with a gas chromatograph equipped with a nitrogen-phosphorus detector.

To determine whether nicotine in the stainless steel chamber decayed by heterogeneous reaction, samples in experiments 2D and 2E were analyzed by gas chromatography-mass spectrometry. Nicotine samples were collected on reusable, commercially available multisorbent samplers (Part # ST032, Envirochem Inc.). These sample tubes were packed with glass beads at the inlet followed by Tenax-TA, Ambersorb XE-340, and activated charcoal, in series (Hodgson and Girman, 1989). Before each use, the samplers were cleaned and conditioned by heating them to 300 °C for 30 minutes with a helium purge flowing at 100 cm^3 min^{-1} in the reverse direction of

sample collection. During sample collection, the tubes were mounted on the end of a 45 cm stainless steel tube which could be retracted from the chamber through a port in the wall to exchange clean sample tubes for exposed ones. The stainless steel tube was connected to a peristaltic pump outside of the chamber which sampled at 90-100 cm^3 min^{-1}.

Measurement of the Mass-Transport-Limited Deposition Rate. Bisulfate-coated filter sheets mounted on the chamber walls were used to determine the mass-transfer-limited deposition rate of nicotine. Four 400 cm^2 Teflon-coated glass fiber filter sheets (Pallflex Products Corporation, Putnam, CT) were cleaned with ethyl acetate, coated with an aqueous 4% $NaHSO_4$ solution, and air dried. These coated sheets were framed with aluminum foil and mounted flat on the center of each chamber wall where they passively collected nicotine by acid-base reaction to simulate irreversible wall deposition losses. The coated filters were only used during experiment 2A (ETS). However, since the air flow conditions were virtually identical in the all of the experiments, these data are also applicable to the other runs. Nicotine collected on these sheets was protonated and thus not highly soluble in ethyl acetate. The filter sheets were extracted with ethanol and aqueous 10N NaOH using a method similar to that outlined by Hammond *et al.* (1987).

Measurement of Nicotine Sorbed to Stainless Steel. To definitively close the mass balance for nicotine in the chamber, it was necessary to measure the mass sorbed on stainless-steel surfaces. A solvent extraction method using EA/TEA extraction of stainless steel foils mounted in the chamber during experiments 2A-2C recovered only 20% of the expected sorbed nicotine mass. Consequently, a second method was developed in which sorbed nicotine was captured following thermal desorption of stainless steel surfaces. This technique was applied to experiments conducted in both a 67 L stainless steel chamber and in the 20 m^3 chamber. The smaller chamber permitted us to test the hypothesis that sorbed nicotine could be thermally desorbed and recovered,

thereby achieving mass balance closure, while controlling system variables more easily than in the full-sized chamber.

The 67 L chamber was cylindrical with a 1.0 m^2 surface area and was constructed of Type 304 stainless steel. One end of the cylinder could be removed to access the interior. During operation, this lid was secured by a circular bracket which compressed a low-VOC-emitting silicone rubber gasket to provide an airtight seal. The gasket was wrapped in aluminum foil and recessed in a groove on the lid so that the total gasket area exposed to the chamber interior was less than 1 cm^2. The chamber was operated inside a wooden cabinet maintained at 25 ± 1 °C by circulating water from a constant temperature bath through copper tubing mounted inside the cabinet. A relative humidity of 50 ± 5% was maintained at the chamber inlet by passing one half of the flow of nitrogen from a compressed gas cylinder through a water bubbler immersed in the constant temperature bath. Four 100-W electrical resistance cartridge heaters (Chromalux) were mounted in heating blocks attached to the outer surface of the chamber. The cartridge heaters were controlled by an electrical contact thermostat (Thermoswitch model 17000, Fenwal). This heating system permitted elevating the chamber temperature to 100 ± 15 °C.

For thermal desorption experiments in the small chamber, the chamber was preconditioned by flushing it with at least 30 chamber volumes of nitrogen gas at 25 °C and 50% RH. Then 1 mg of liquid nicotine was injected with a syringe through a port into the chamber and allowed to equilibrate at 25 °C. After four hours, a gas-phase sample was collected on a multisorbent tube at 100 cm^3 min^{-1} for 20 minutes. During sampling, the chamber inlet valve was open so that gas removed by the sample pump was replaced with 50% RH nitrogen gas from the stream flowing past the inlet, and the chamber pressure remained constant at approximately 1 atm. The inlet and sample ports were positioned on opposite ends of the chamber to reduce sample dilution due to incomplete mixing. After sample collection, the chamber was heated to 100 °C and flushed with clean, dry nitrogen gas at 5 L min^{-1} for 3 to 5 hours. A multisorbent tube

sampled at approximately 3 cm^3 min^{-1} from this flushing flow at the chamber outlet throughout the heating and flushing procedure to quantify the nicotine mass remaining in the chamber. The product of the mass collected on this sample tube and the ratio of the flushing volume to the sample volume minus the product of the chamber volume and the gas-phase concentration at 25 °C gave the total mass collected from the sorbed-phase.

In experiment 2E in the 20 m^3 chamber, sorbed-phase samples were collected on 15 cm × 15 cm plates of 304 stainless steel mounted on the chamber walls with adhesive tape. These samplers were thermally desorbed using a custom designed apparatus. The desorber consisted of a 15 cm square × 2.5 cm thick aluminum heater block which had a 13 cm × 13 cm × 1 cm-deep depression in one face. To recover sorbed-phase nicotine, a plate was clamped between a piece of plywood and the aluminum heater block with the exposed plate surface facing the depression on the heater unit. Two layers of Teflon™ tape applied along the contact edges of the heater block ensured an airtight seal. The block was heated with two electrical resistance cartridge heaters (Chromalux) and its temperature was controlled to 130 ± 5 °C with an electrical contact thermostat (Thermoswitch model 17000, Fenwal). The sample plate was heated indirectly by contact with the heater block. A sample port in the center of the heater block allowed sampling of the volume enclosed by the heater block and sample plate. This volume was swept with clean dry nitrogen gas from Tedlar bags connected to gas inlet ports at each corner of the aluminum block by Teflon™ tubing. The sample was collected on a multisorbent tube through the center port with a peristaltic pump at approximately 30 cm^3 min^{-1} for approximately 5 hours. In this manner, the volume of the thermal desorption apparatus was flushed more than 50 times. For samples expected to have more than 600 ng of nicotine, another pump withdrew gas and discarded it from a second port in the center of the heater to prevent the sample size from exceeding the capacity of the analysis system. The sorbed mass was calculated as the product of the collected mass and the ratio of the total volume removed by the pumps to the sample volume.

Sample Analysis. Ethyl acetate sample extracts of the gas- and sorbed- phase samples collected in experiments 2A-2C were analyzed using a gas chromatograph (GC) (Shimadzu Corporation, Kyoto, Japan) equipped with a thermionic nitrogen-phosphorous detector (Detector Engineering Technology, Walnut Creek, CA). Signal peaks were plotted and integrated on a Shimadzu Chromatopac C-R3A data processor. Nicotine and quinoline peak area responses were calibrated using standards prepared in EA/TEA. External nicotine and quinoline standards were injected periodically between samples to obtain a drift correction for the nicotine and quinoline response factors. A linear regression analysis of the response factors was performed for each day of analysis and factored into nicotine and quinoline mass calculations for all injected samples. The calculated mass of nicotine recovered from each solvent extracted sample was corrected for losses in the extraction and sample handling process by scaling the determined mass by the inverse of the fractional quinoline recovery for that sample. For all samples, this correction factor was in the range 0.8-1.25.

The analytical procedures for organic compounds collected on multisorbent samplers have previously been described (Hodgson and Girman, 1989). In brief, a sample with an added internal standard is thermally desorbed from a sampler, concentrated and introduced into a capillary GC with a sample concentrating and inletting system (UNACON Model 810) and a thermal desorption system (Model 8916 Multiple Tube Desorber, Envirochem, Inc.). This instrument concentrates the sample using dual sequential traps. Sample components are resolved with a GC (Model 5890 Series II, Hewlett Packard Co.) equipped with liquid nitrogen subambient cooling and a 30 m × 0.25 mm ID × 1.0-μm thick film fused-silica capillary column (Rtx-5, Restek Corp.). The GC is connected via a direct capillary interface to a mass selective detector (MSD Series 5970B, Hewlett Packard Co.) equipped with peak analysis and identification software (MS ChemStation software, Hewlett Packard Co.). The MSD is mass tuned using perfluorotributylamine. It was operated to scan an ion mass/charge range (m/z) from 33

to 300. For nicotine, the two dominant mass ions (84 and 133) were chosen as quantitative ions. The peak areas of these target mass ions were integrated using the MSD software. Calibration regression lines were generated by analyzing Tenax TA cartridges spiked with known volumes of nicotine in methanol containing 0.01% TEA. The calibration curve was linear up to approximately 450 ng total injected mass. However, the regression line had a negative intercept indicating a possible loss of approximately 30 ng of nicotine per sample in the desorption system.

MODELING

Reversible Sorption "2-Box" Model. Dynamic sorption systems in which a single sink interacts with the gas-phase under well-mixed conditions in a fixed-volume chamber can be described generically with the following mass balance equations:

gas-phase:
$$\frac{dC}{dt} = \frac{E}{V} + \lambda_{v,T}\left(C_o - C\right) - \frac{S}{V}J \tag{2.1}$$

sorbed-phase:
$$\frac{dM}{dt} = J \tag{2.2}$$

where C is the gas-phase concentration in the chamber (mg m^{-3}), V is the chamber volume (m^3), t is time (h), E is the pollutant emission rate (mg h^{-1}), $\lambda_{v,T}$ is the total chamber air exchange rate (h^{-1}), C_o is the concentration in the ventilation air (mg m^{-3}), S is the chamber internal surface area (m^2), J is the net flux to chamber surfaces (mg m^{-2} h^{-1}, $J > 0$ for transport to the surface), and M is the sorbed mass density (mg m^{-2}). The kinetics of the deposition and reemission processes are defined by the specific functional form used for J. At equilibrium there is no net flux to the surface, so $J = 0$. This relationship permits the use of equilibrium data to reduce the number of independent kinetic parameters as shown below.

Nonlinear Reversible Sorption Models. Nonlinear equilibrium partitioning between the gas- and sorbed- phases has been observed previously for interactions of

some VOCs with indoor surfaces (Borrazzo *et al.,* 1993). For sorption systems in which equilibrium is described by a nonlinear isotherm, nonlinearity must also be exhibited in the kinetics of adsorption and/or desorption. Assuming that the adsorption and desorption rates take a power-law functional form, the net flux to the surface becomes

$$J = k_a C^{n_a} - k_d M^{n_d} \tag{2.3}$$

where k_a and k_d are adsorption and desorption rate constants ($\mathrm{mg}^{1-n_a}\ \mathrm{m}^{3n_a-2}\ \mathrm{h}^{-1}$ and $\mathrm{mg}^{1-n_d}\ \mathrm{m}^{2n_d-2}\ \mathrm{h}^{-1}$, respectively) and n_a and n_d are dimensionless constants. By incorporating equation 2.3 into equations 2.1 and 2.2, the governing equations for this model become

$$\frac{dC}{dt} = \frac{E}{V} + \lambda_{v,T}\left(C_o - C\right) - \frac{S}{V}\left(k_a C^{n_a} - k_d M^{n_d}\right) \tag{2.4}$$

$$\frac{dM}{dt} = k_a C^{n_a} - k_d M^{n_d} \tag{2.5}$$

Tichenor *et al.* (1991) achieved a very good fit to data from an experiment with VOC emissions from wood stain in an indoor air quality test house using this model with a linear adsorption rate ($n_a = 1$). However, there is no clear basis on which to establish $n_a = 1$ *a priori*. The current study applies this model both with $n_a = 1$ and with n_a as an adjustable parameter. The equilibrium isotherm for this model is derived by setting $J = 0$ in equation 2.3:

$$M = KC^n \tag{2.6}$$

where

$$n = {}^{n_a}\!/_{n_d} \text{ and } K = \left({}^{k_a}\!/_{k_d}\right)^{1/n_d} \tag{2.7}$$

K and n are determined empirically from independent equilibrium experiments and then used to reduce the number of adjustable parameters in the kinetic model.

Tichenor *et al.* (1991), while noting the excellent fit that this model gives for their data (with $n_a = 1$), state that it is not as well based in theory because the Freundlich isotherm (equation 2.6) is an empirical equation. However, the Freundlich isotherm does have a theoretical foundation if the surface sites are assumed to have an exponential distribution of sorption energies:

$$N(Q) = a\left[e^{(Q/RT)} - 1\right]^{-c} \tag{2.8}$$

where $N(Q)$ is the frequency of sites with sorption energy Q, R and T are the gas constant and Kelvin temperature, and a and c are constants (Cooney, 1990). The Freundlich isotherm is widely used to describe sorption equilibrium in environmental systems with heterogeneous surfaces (Lin *et al.*, 1996). Although stainless steel is superficially a homogeneous material, significant heterogeneity likely exists at the atomic scale. Also, over time, stainless steel slowly oxidizes which may further contribute to surface heterogeneity.

Initial Conditions and Model Fitting Protocol. The initial conditions differed slightly among experiments due to differences in the nicotine emission method. These values and those for the other constant parameters used in the models are presented in Table 2.1. For each of the experiments, the chamber was assumed to be completely free of nicotine at the beginning of the run. In the ETS experiment (2A), nicotine was modeled as being emitted continuously during the first 32 minutes at a constant rate calculated from the sidestream emission factor for nicotine from cigarettes (Daisey *et al.,* 1994, 1998). The results of the liquid nicotine flash evaporation experiments (2B and 2C) were modeled by assuming that all of the emitted nicotine was instantly vaporized and well mixed throughout the chamber. Using the parameters in Table 2.1, equations 2.4 and 2.5 were integrated using a fourth-order Runge-Kutta scheme described by Press *et al.* (1986). The best fit model parameters and simulations discussed in the following section were

obtained by minimizing the sum of the absolute values of the relative error between model predictions and experimental concentration data individually for each kinetic experiment (2A, 2B, and 2C).

RESULTS AND DISCUSSION

The equilibrium data from experiments 2D and 2E are shown in Figure 2.3. As the figure shows, the equilibrium partitioning is nonlinear, and the Freundlich isotherm (equation 2.6) fits the data well. Table 2.2 (note a) lists the Freundlich isotherm parameters for these data. The results of the three kinetic experiments (2A-2C), which were all qualitatively similar, are shown in Figures 2.4–2.6. The data from these runs are tabulated in Tables 2.3–2.5. Figure 2.4 includes the best fit fully nonlinear sorption model predictions for gas- and sorbed-phase nicotine from the ETS experiment. Figures 2.5 and 2.6 show best fit model predictions for both nonlinear reversible sorption models described above (equations 2.4 and 2.5). The model parameters for the best fits to the data from experiments 2A-2C are listed in Table 2.2.

In experiments 2B and 2C (Figures 2.5 and 2.6), the gas-phase nicotine concentration rapidly decayed from its maximum to a plateau within approximately 45 minutes. Measurable nicotine was still detected after the chamber was flushed at 3.4 air changes per hour for two hours, although at a significantly lower concentration than that measured prior to chamber ventilation. The initial gas-phase concentration decay shown in Figures 2.4 experiments 2A with ETS is somewhat slower. The slower gas-phase concentration decay in the ETS experiment is likely due to competitive sorption of other ETS constituents on the stainless steel chamber surfaces. The best-fit kinetic parameters listed in Table 2.2 support this hypothesis. The value for k_a calculated from the nonlinear desorption model fit to the experiment 2A data is almost a factor of 3 smaller than the values for experiments 2B and 2C. The observed trends in gas-phase nicotine

decay rates in these chamber experiments are qualitatively similar to chamber experiment data discussed in a recent review of ETS exposure studies (Eatough, 1993).

As Figures 2.5 and 2.6 show, the fully nonlinear model generates a good fit to the gas-phase data collected during the first three hours of the clean chamber-liquid nicotine experiments with the chamber operated in low air-exchange rate mode. The nonlinear adsorption model fits the data for the first 30 to 50 minutes of each experiment, but underpredicts the concentration for the remainder of the runs. The fully nonlinear model performed comparably in the ETS experiment (2A). After the high air-exchange rate phase of the experiments, both nonlinear models performed reasonably well in the clean chamber experiments. However, during the ventilation phase, both models underpredict the gas-phase concentration. This discrepancy may be caused by a fraction of the stainless steel-sorbed nicotine being held less tightly than the rest of the sorbed mass. This loosely sorbed mass may be reemitted more quickly than the model predicts, leading to an elevated measured concentration during ventilation. If this hypothesis were true, a longer ventilation phase would allow the labile sorbed mass to be removed, and the measured gas-phase concentration might more closely agree with the predicted values. Also note that the concentration axes in Figures 2.4-2.6 use log coordinates which tend to emphasize relative model-measurement discrepancies. The absolute disagreement between the model and measurements during the high air-exchange rate periods is very small compared to the peak concentration in the chamber.

Development of the Investigation. In the initial phase of this research, we struggled to understand the large discrepancy between nicotine emission factors for sidestream smoke and ETS. Our initial attempts to quantitatively close the nicotine material balance with ETS in experiment 2A were unsuccessful. This fact, combined with the failure of a linear reversible sorption model (Tichenor *et al.,* 1991) to accurately predict the nicotine concentration in the chamber after it was ventilated, led us to simplify the system in subsequent experiments by eliminating other ETS constituents to reduce

the availability of reactants that might consume emitted nicotine. Additionally, we standardized the chamber surface pretreatment protocol to allow better characterization of the chamber initial conditions. Repetition of experiment 2A with nicotine emission by flash evaporation instead of cigarette combustion in experiments 2B and 2C gave qualitatively similar results. In all three experiments, solvent extraction of wall-mounted stainless steel foils failed to yield mass closure. Approximately 80% of the nicotine that should have been sorbed to the walls was not detected.

Several possible explanations were considered for these results. The solvent extraction procedure for the stainless steel foils was tested by spiking foils with nicotine in an EA/TEA standard solution. These tests indicated that better than 85% recovery was possible using solvent extraction. However, this test may have been flawed because of the presence of TEA which could have hindered sorption of nicotine to the foils in the same way it reduces nicotine loss from solution to glass surfaces. Alternative models for nicotine interactions with the stainless steel surfaces were hypothesized and applied to the data. The proposed mechanisms, described in detail elsewhere (Van Loy *et al.,* 1996), included irreversible sorption with first-order, second-order, and Langmuir kinetics and a surface-catalyzed reaction coupled to nonlinear sorption.

None of these potential explanations adequately resolved the differences between model predictions and experimental observations. Gas- and sorbed-phase samples from experiments 2D and 2E were analyzed by GC-MS to check for products of degradation of nicotine by heterogeneous or homogeneous reactions. No significant masses of nitrogen containing compounds other than nicotine were observed.

Mass Balance. After failing to account for the missing nicotine through several experimental and modeling tests, we returned to the hypothesis that our chemical extraction procedure was inadequate to quantitatively remove sorbed nicotine from the foils. Substantial loss of nicotine from the foils during the time between their removal from the chamber and the beginning of the extraction procedure is improbable. The foils

were exposed to air for less than 15 minutes before immersion in EA/TEA, and our model predictions indicate that less than 5% of the sorbed nicotine would have been lost during this period. Three possible explanations for the failure of our solvent extraction method are 1) the free energy of the nicotine-stainless steel surface complex is more favorable than that of nicotine solvated in TEA/EA, 2) the activation energy for desorption of sorbed nicotine into solution is prohibitively high, or 3) the stainless steel foils did not accurately represent the chamber surfaces due to oxidation of the aged chamber surfaces relative to the newer foils.

Experiments conducted in the small stainless steel chamber indicated that thermal desorption held greater promise of high nicotine recoveries than did solvent extraction. In two thermal desorption experiments, more than 850 μg of an initial 1 mg injection was recovered after 4 hours of heating to 100 °C while flushing the small chamber with dry nitrogen. Based on our success at recovering nicotine from the small chamber, sorbed nicotine in the 20 m^3 chamber was recovered from wall mounted stainless steel plates using the thermal desorption apparatus. In this manner, approximately 80% of the mass calculated to be sorbed to the exposed plate area in experiment 2E was recovered, a significant improvement over the 15% recovery obtained for extraction of the wall mounted foils with EA/TEA in experiments 2A-2C. The isotherm nonlinearity might explain the remaining 15 to 20% of the originally emitted nicotine unrecovered by thermal desorption in experiment 2E. For a Freundlich isotherm with n less than 1, the free energy of adsorption increases as surface coverage decreases. Thus, the final fraction of nicotine to desorb from the stainless steel is held very tightly. Perhaps heating the surface to a higher temperature or for a longer period might liberate this last fraction of sorbed nicotine. Alternatively, the unaccounted mass may have been sorbed on extremely labile sites on the stainless steel. Because sampling during the chamber ventilation phase did not start until 60 minutes after the start of ventilation, this mass could have been

released as an undetected pulse of relatively high concentration in the period immediately following the start of the high air-exchange rate phase.

Mass-Transport-Limited Deposition. Data from the $NaHSO_4$-treated filter sheets collected during the ETS run (experiment 2A) were used to determine the mass-transport-limited deposition velocity (v_t) using the approach described by Nazaroff *et al.* (1993a). This parameter was computed from the experimental data using the expression

$$v_t = M_F / A_F t_s C_{ave} \tag{2.9}$$

where M_F, A_F, t_s, and C_{ave} are the nicotine mass collected on the filter (μg), the filter area (m^2), the duration of the sampling period (h), and the average gas-phase concentration (μg m^{-3}), respectively. The calculated value, $v_t = 4.0$ m h^{-1}, is similar to reported values for mass-transport-limited deposition of gases indoors (Cano-Ruiz *et al.,* 1993). The acid-base chemistry involved in the reaction of nicotine with the $NaHSO_4$ coated filters is fast and irreversible. Thus, the rate at which air motion delivered nicotine to the filter surface determined the rate of uptake, and v_t is an upper bound on v_d, the rate at which nicotine deposits from the gas-phase onto chamber surfaces.

CONCLUSIONS

Previous investigators have shown that the linear reversible sorption model described by Tichenor *et al.* (1991) correctly captures the dynamics of VOC sorption on indoor materials. However, that model failed in the current study when it was applied to a less volatile compound and when the gas-phase concentration was varied over a large range. An improved dynamic model of indoor pollutant-surface interactions incorporates nonlinear equilibrium partitioning as described by the Freundlich isotherm. Despite the extra adjustable parameters introduced by such a model, the number of free variables was reduced by independently measuring the isotherm and incorporating these data into the model fit. It may be useful to study SVOC-surface interactions in small-scale

experiments to determine the equilibrium partitioning parameters independently before conducting full-scale dynamic studies.

FIGURES

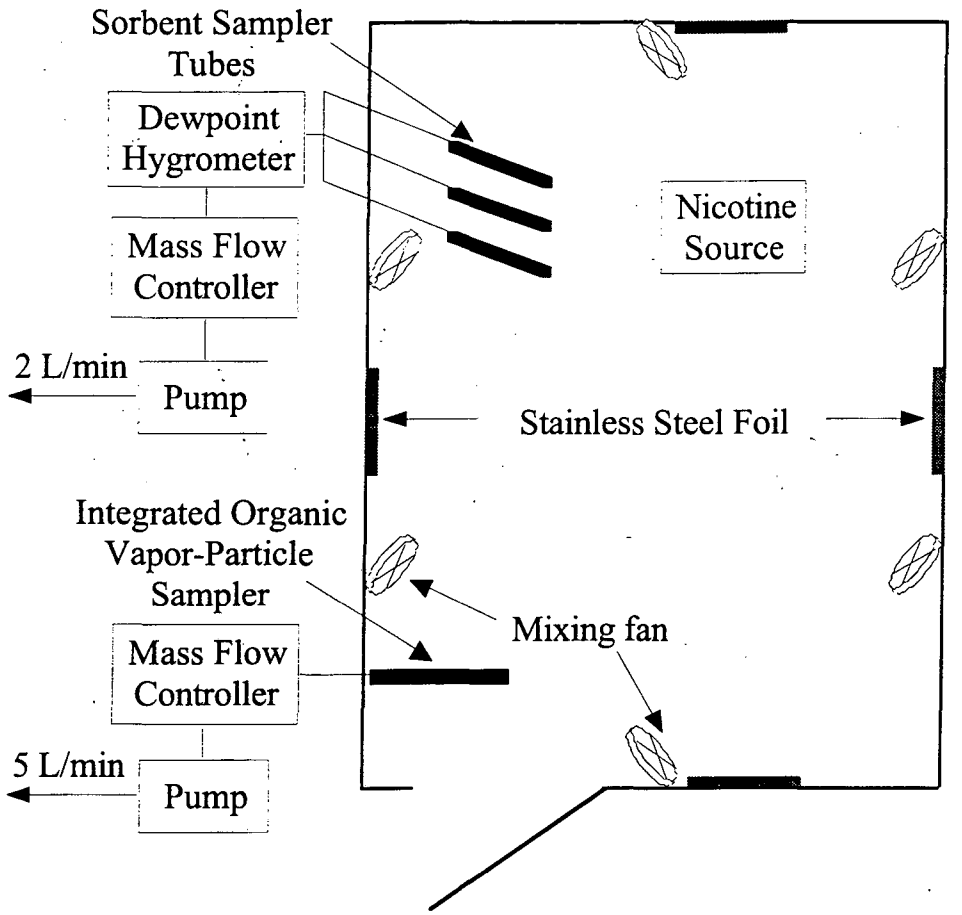

Figure 2.1. Schematic diagram of 20 m^3 stainless steel environmental test chamber configuration used in empty chamber nicotine experiments. The integrated organic vapor-particle sampler system was used only in experiment 2A. The nicotine source was three machine-smoked cigarettes in experiment 2A. Liquid nicotine was flash evaporated from a glass petri dish on a hot plate in experiments 2B and 2C and from a stainless steel tube in an aluminum heater block in experiments 2D and 2E.

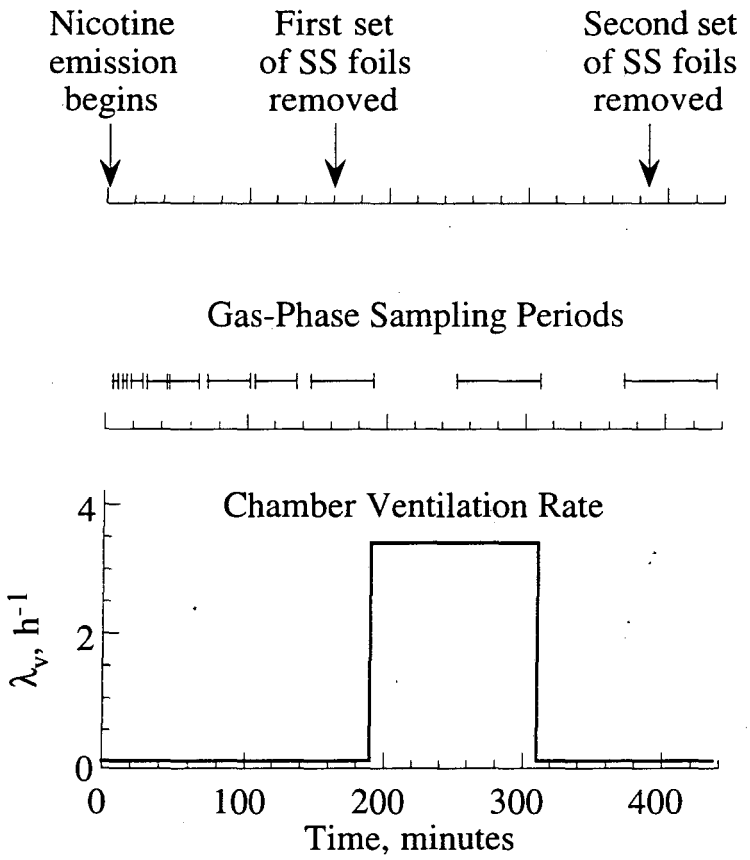

Figure 2.2. Representative chronology for kinetic nicotine-stainless steel experiments. The nicotine emission method was cigarette smoking which started at t = 0 and continued for 32 minutes in experiment 2A and flash (instantaneous) evaporation of liquid nicotine in experiments 2B and 2C.

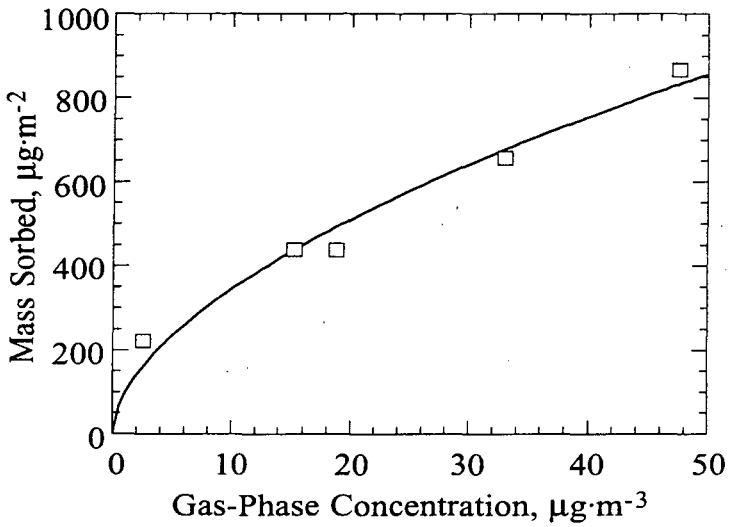

Figure 2.3. Equilibrium partitioning of nicotine between the gas- and sorbed-phases in the stainless steel environmental chamber. The squares show data from experiments 2D and 2E. The solid line represents the best fit Freundlich isotherm for the experimental data (see Table 2.2).

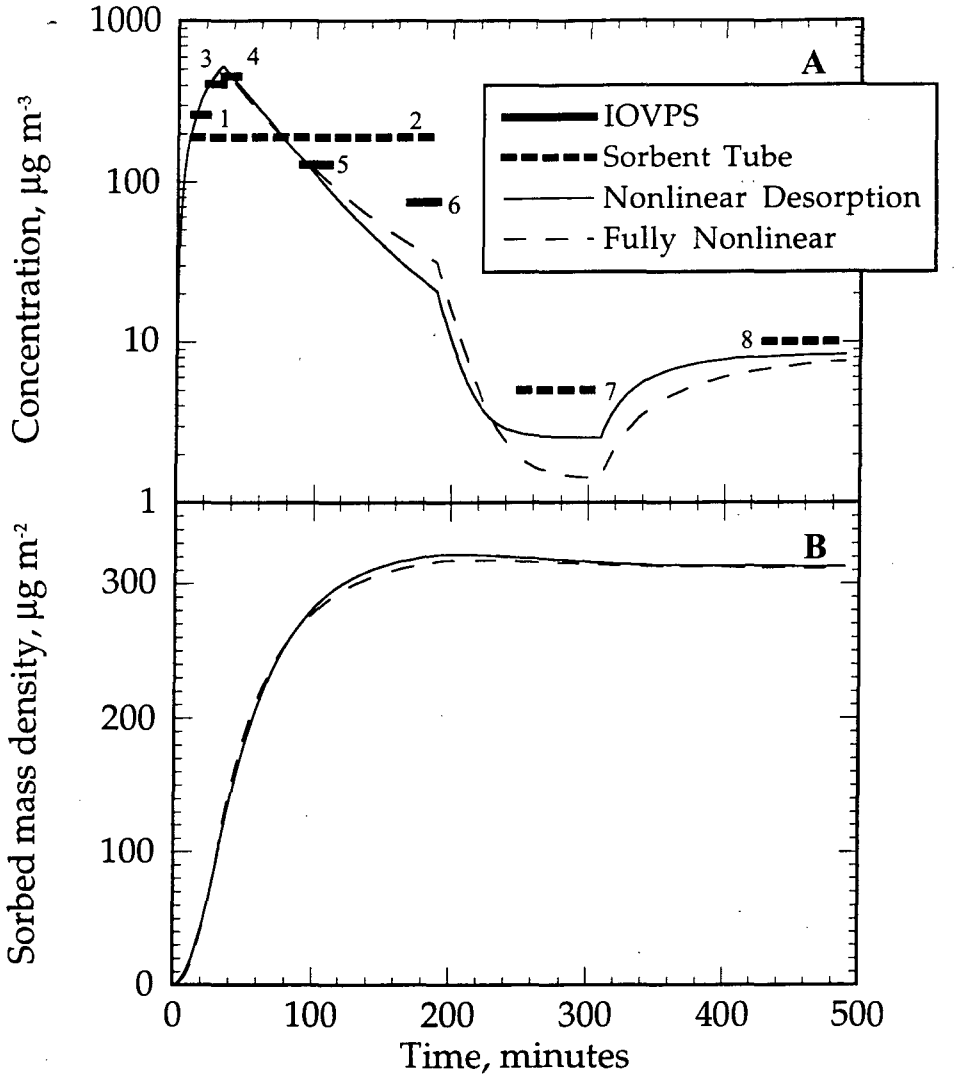

Figure 2.4. Experimental data, estimated errors, and fully nonlinear model predictions for gas-phase concentration and sorbed-phase density for nicotine as a function of time in experiment 2A. The lengths of the solid and dashed horizontal bars and their positions relative to the time axis in panel **A** indicate the duration and timing of IOVPS and XAD-4 sorbent samples, respectively. Experiment 2A gas-phase data are tabulated in Table 2.3.

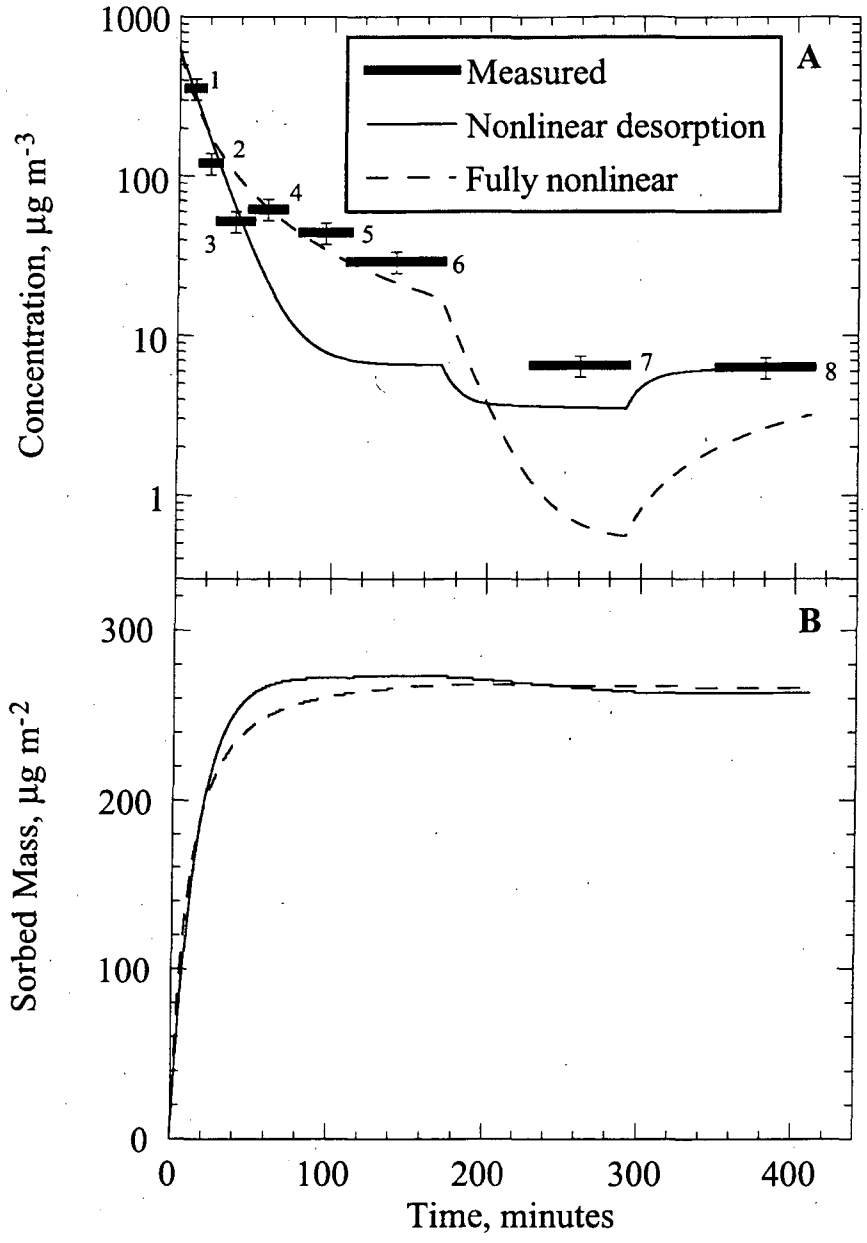

Figure 2.5. Experimental data, estimated errors, and nonlinear model predictions for gas-phase concentration and sorbed-phase density for nicotine as a function of time in experiment 2B. The lengths of the horizontal bars and their positions relative to the time axis in panel **B** indicate the duration and timing of XAD-4 sorbent tube samples. Experiment 2B gas-phase data are tabulated in Table 2.3.

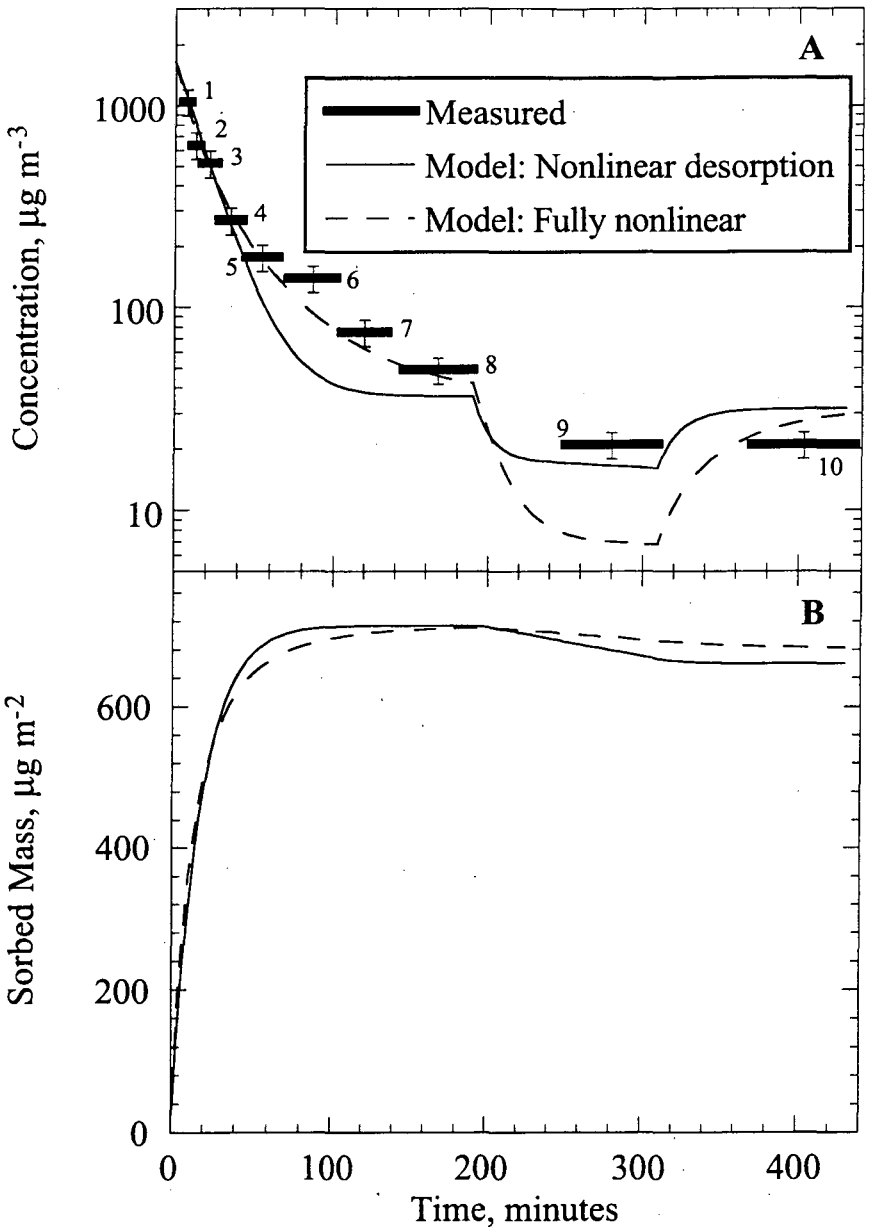

Figure 2.6. Experimental data, estimated errors, and nonlinear model predictions for gas-phase concentration and sorbed-phase density for nicotine as a function of time in experiment 2C. The lengths of the horizontal bars and their positions relative to the time axis in panel **B** indicate the duration and timing of XAD-4 sorbent tube samples. Gas-phase sample data for this experiment are listed in Table 2.5.

TABLES

Table 2.1. Summary of experimental parameters and kinetic model initial conditions for experiments 2A-2E

	Nicotine emission method				
	Three cigarettes	Liquid Evap.	Liquid Evap.	Liquid Evap.	Liquid Evap.
Experiment number	2A	2B	2C	2D	2E
Sealed flow rate (Q_T), $m^3\ h^{-1}$	0.38	0.27	0.27	0.16	0.16
Nicotine mass emitted, mg	~15	12.5	33	40[a]	20
Duration of emission, min.	32	0[b]	0[b]	0[b]	0[b]
Kinetic model initial conditions					
C_{init}, $mg\ m^{-3}$	0	0.62	1.65		
M_{init}, $mg\ m^{-2}$	0	0	0		

[a] Nicotine was injected in 10 mg increments once a day for 4 days during experiment 2D.

[b] Emission occurred by flash evaporation, so emission duration was very short (< 1 min.)

Table 2.2. Best fit model parameters for fits of linear and nonlinear reversible sorption models[a] to kinetic data from experiments 2A, 2B, and 2C.

Experiment number	2A	2B	2C
Linear Deposition/Nonlinear Reemission[b]			
n_d (-)	1.76	1.76	1.76
k_a (m h^{-1})	0.62	1.67	1.45
k_d (mg$^{1-n_d}$ m$^{2n_d-1}$ h^{-1})	0.041	0.11	0.095
Nonlinear Deposition and Reemission[c]			
n_a (no units)	1.22	1.68	1.47
n_d (no units)	2.15	2.96	2.59
k_a (mg$^{1-n_a}$ m$^{3n_a-2}$ h^{-1})	0.81	3.50	2.52
k_d (mg$^{1-n_d}$ m$^{2n_d-2}$ h^{-1})	0.029	0.035	0.029

a Nonlinear model fits are based on the Freundlich isotherm determined in experiments 2D and 2E: $M = 4.69\ C^{0.57}$ where M is mass sorbed per surface area (mg m^{-2}) and C is gas-phase concentration (mg m^{-3}).

b Defined by equations 2.4 and 2.5 with $n_a = 1$. The Freundlich isotherm parameters were obtained independently in experiments 2D and 2E, so only one adjustable parameter was used in the model fits. See Appendix A for discussion of how the model parameters were obtained from the experimental data.

c Defined by equations 2.4 and 2.5 with both n_a and n_d adjustable. The Freundlich isotherm parameters were obtained independently in experiments 2D and 2E, so two adjustable parameters were used in the model fits. See Appendix A for discussion of how the model parameters were obtained from the experimental data.

Table 2.3 Gas-phase nicotine sample data from experiment 2A (ETS).

Sample Number[a]	Sample Start Time, minutes	Sample End Time, minutes	Measured Concentration[b], $\mu g\ m^{-3}$	Modeled Concentration, $\mu g\ m^{-3}$
1	11	21	261	315
2	11	189	190	177
3	22	32	407	466
4	33	43	455	448
5	90	110	128	119
6	169	189	74	36
7	250	310	5.0	1.5
8	430	490	10	7.1

[a] Sample numbers correspond to the data labels in Figure 2.4.

[b] Errors in measured concentrations are approximately 15% of the reported values.

Table 2.4 Gas-phase nicotine sample data from experiment 2B (12.5 mg of nicotine).

Sample Number[a]	Sample Start Time, minutes	Sample End Time, minutes	Measured Concentration[b], $\mu g\ m^{-3}$	Modeled Concentration[c], $\mu g\ m^{-3}$
1	6	15	354	296
2	16	26	120	178
3	27	47	52	105
4	48	68	62	63
5	80	110	44	35
6	111	170	29	22
7	230	290	6.5	0.72
8	350	410	6.3	2.6

a Sample numbers correspond to the data labels in Figure 2.5.

b Errors in measured concentrations are approximately 15% of the reported values.

c Model predictions are based on the best fit to the data with fully nonlinear model (equation 2.4 and 2.5 using the parameters listed in Table 2.2.

Table 2.5 Gas-phase nicotine sample data from experiment 2C (33 mg of nicotine).

Sample Number[a]	Sample Start Time, minutes	Sample End Time, minutes	Measured Concentration[b], $\mu g\ m^{-3}$	Modeled Concentration[c], $\mu g\ m^{-3}$
1	5	10	1040	1008
2	11	16	636	725
3	17	27	515	494
4	28	43	269	301
5	45	65	177	175
6	71	101.5	139	96
7	105	135	75	63
8	145	190	49	46
9	250	310	21	7.0
10	370	436	21	24

a Sample numbers correspond to the data labels in Figure 2.6.

b Errors in measured concentrations are approximately 15% of the reported values.

c Model predictions are based on the best fit to the data with fully nonlinear model (equation 2.4 and 2.5 using the parameters listed in Table 2.2.

Chapter 3. Interactions of Nicotine and Phenanthrene with Carpet and Painted Wallboard in a Stainless Steel Test Chamber

ABSTRACT

To better understand factors affecting the fate of gas-phase semivolatile organic compounds (SVOCs) in indoor environments, the surface interactions of nicotine and phenanthrene with carpet and painted wallboard were investigated in a room-sized stainless steel environmental test chamber. Nicotine is a major component of environmental tobacco smoke (ETS) and is widely used as a marker to estimate human exposures to ETS. Phenanthrene is a polycyclic aromatic hydrocarbon (PAH) commonly found in both the gas and condensed phases in the atmosphere and typically emitted by incomplete combustion processes. Little is known about the gas-phase interactions of SVOCs with indoor surface materials. In this study, a known mass of each tested SVOC was individually flash evaporated into a sealed 20 m^3 chamber containing a sample of one of the tested sorbents. The gas-phase concentration was monitored until the rate of gas-phase concentration decrease was less than 0.5% day^{-1}. This process was repeated several times for each sorbate-sorbent pair to characterize sorption kinetics under varying initial conditions. Then, the chamber was alternately ventilated and resealed to monitor reemission of sorbed SVOC from the sorbent material.

The experimental results were analyzed using a model coupling surface sorption kinetics with diffusion into the bulk of the sorbent. The sorption capacities of wallboard and carpet for the two SVOCs were from 2 to 4 orders of magnitude larger than those for stainless steel. Both sorbents had a stronger affinity for nicotine than for phenanthrene. The results of this study will facilitate more accurate assessment of indoor SVOC concentrations under transient or noncontinuous emission conditions.

INTRODUCTION

Organic compounds are an important class of indoor air pollutants. As such, a significant body of research has focused on factors affecting concentrations and persistence of these contaminants in indoor environments. However, much of the existing indoor air research has been directed at low molecular weight organic contaminants commonly known as volatile organic compounds or VOCs. Higher molecular weight organic compounds with vapor pressures between 10^{-6} and 10 Pa at ambient temperatures are generally classified as semivolatile organic compounds (SVOCs) (Bidleman, 1988). Relatively few studies have focused on these pollutants in indoor air, probably because of the difficulties associated with sampling and analysis of lower-volatility compounds. Low vapor pressures strongly favor condensed phases, so SVOCs are expected to interact strongly with surfaces, readily sorbing on many materials found inside buildings. The importance of this phenomenon has been demonstrated for a range of more volatile compounds such as benzene, trichloroethylene, and ethanol (Matthews *et al.,* 1987; Tichenor *et al.,* 1991; Borrazzo *et al.,* 1993; Colombo *et al.,* 1993; Jørgensen *et al.,* 1993; Neretnieks *et al.,* 1993; De Bortoli *et al.,* 1996; Kjaer *et al.,* 1996). Sorption and desorption may have an even greater impact for SVOCs because of their greater affinity for condensed phases. Most buildings have a large surface area-to-volume ratio, so surface interactions can significantly affect the dynamic behavior of sorbing contaminants (Seifert and Schmahl, 1987). Additionally, because reversibly sorbed compounds slowly reenter the gas-phase through desorption from surfaces (Jørgensen *et al.,* 1993), occupant exposures to these contaminants may occur long after elimination of sources. Thus, accurate knowledge about the dynamic behavior and surface interactions of SVOCs indoors is important for assessing and mitigating health risks from inhalation of indoor air, as well as for improving occupant comfort (Guo *et al.,* 1990; Guo, 1993; Sparks *et al.,* 1993).

Nicotine ($C_{10}H_{14}N_2$, molecular weight = 162.24 g mol^{-1}) is the most prevalent constituent of environmental tobacco smoke (ETS). Its vapor pressure at room temperature is approximately 2 Pa (Jordan, 1954; Lencka, 1984), and it is present in ETS almost entirely in the gas-phase (Eatough *et al.*, 1989a; Eatough *et al.*, 1989b; Hammond *et al.*, 1987). ETS includes exhaled mainstream smoke and diluted sidestream smoke from the burning tip of a cigarette. Approximately 300 to 400 individual compounds have been identified and measured in ETS (Eatough *et al.*, 1989b; Baker and Proctor, 1990). Mainstream smoke is known to contain over 4000 compounds, variably distributed between the gas- and particulate-phases (Eatough *et al.*, 1989b; Leaderer and Hammond, 1991; Daisey *et al.*, 1994, 1998). ETS has been identified as a human carcinogen (USEPA, 1992; California EPA, 1997), and there is now evidence that it is also a cause of heart disease (Steenland, 1992; Glantz and Parmley, 1995; California EPA, 1997). Because of the complexity of ETS and its adverse health effects (IARC, 1985; NRC, 1986), it would be convenient to have marker compounds that could be used for measuring human exposure to ETS (Eatough *et al.*, 1989b).

Nicotine has been widely used as a marker of ETS because it is specific to and a major constituent of ETS, it is easy to detect (Eatough, 1993), and it has similar emission rates for different types of cigarettes (Leaderer and Hammond, 1991; Daisey *et al.,* 1994, 1998). However, the suitability of nicotine as a marker for ETS has been questioned by some researchers because gas-phase nicotine exhibits different indoor dynamic behavior than do many other ETS constituents (Löfroth *et al.,* 1989; Nelson *et al.,* 1990; Nelson *et al.,* 1992; Löfroth, 1993a; Ogden, 1996). Nevertheless, Leaderer and Hammond (1991) found high correlations between nicotine and respirable suspended particulate matter concentrations measured in residences, and Hammond *et al.* (1987) showed a close relationship between the enforcement of smoking restrictions in work places and nicotine concentrations. The debate over nicotine's utility as a marker remains unresolved. Elucidation of the factors affecting nicotine concentrations in indoor environments would

improve the basis for using nicotine to assess ETS exposures. Additionally, because of nicotine's polar functional groups, it may be a useful surrogate for other SVOCs with similar moieties, such as amines, carbonyls, and organic acids, which generally have lower odor and irritation thresholds than nonpolar compounds (Zhang *et al.,* 1996).

Phenanthrene ($C_{14}H_{10}$, molecular weight = 178.24 g mol^{-1}) is a 3-ring polycyclic aromatic hydrocarbon (PAH) with a vapor pressure of approximately 0.1 Pa at 300 K (Jordan, 1954). It is present in ETS as a relatively minor constituent and in emissions from other incomplete combustion sources. Phenanthrene is not a known human carcinogen, but its behavior is representative of other condensible, potentially carcinogenic PAHs and other nonpolar SVOCs. Additionally, phenanthrene is relatively stable to chemical decay in indoor environments, so its long-term behavior may be representative of other non-PAH SVOCs with high molecular weights, such as polychlorinated biphenyls (PCBs); pesticides; and dioxins, whose interactions with surfaces may depend more on physical sorption than on chemical interactions.

Chapter 2 describes the interactions of nicotine with the interior surfaces of the stainless steel chamber used in the current study. The results of that investigation indicate that nicotine interacts strongly with stainless steel, with greater than 85% of the emitted mass sorbed to the internal surfaces of a 20 m^3 stainless steel chamber at equilibrium at 20° C. In these experiments 15 to 45 mg of nicotine were emitted into the chamber. Because of the nonlinearity of the nicotine-stainless steel isotherm, the fraction of the mass sorbed to the walls depends on the total mass emitted. Gas-phase and sorbed-phase measurements were made to complete a mass balance on nicotine emitted in the chamber. Sorption dynamic models were applied to the gas-phase data and refined to give better representations of the observed time-dependent behavior. Equilibrium partitioning between the gas and sorbed phases was measured in independent experiments. The resulting isotherm parameters were incorporated into a nonlinear, reversible sorption model to reduce the number of fitted model parameters to no more

than two. This model has also been applied to phenanthrene-stainless steel sorption data collected in the current investigation to facilitate correction for sorbate interactions with the chamber surfaces during experiments on the other tested sorbents.

Several mathematical models have been proposed to describe the mechanisms of gas-phase volatile organic compound sorption on indoor materials (Dunn and Tichenor, 1988; Colombo *et al.*, 1993; Axley and Lorenzetti, 1993; Dunn and Chen, 1993; Sollinger *et al.,* 1993; Sollinger *et al.,* 1994; Little *et al.,* 1994; Little and Hodgson, 1996; Sparks *et al.,* 1996). While smooth, nonporous materials such as stainless steel require consideration only of sorption processes occurring at the air-sorbent interface, most indoor surface materials are not as simple as stainless steel. Materials such as carpet, wallboard, upholstery fabric, draperies, and pillow and cushion filling are far more complex. For these materials, a preponderance of the available sorption capacity likely resides some distance from the air-sorbent interface where it is accessible only by diffusion through a finite thickness of the bulk sorbent. To accurately model these systems, the impact of diffusion into the sorbent material must be considered in addition to the mass transport limitation for gas-phase diffusion across the air-surface boundary layer and any chemical activation barrier to adsorption at the surface.

In this chapter, the experimental approach described in Chapter 2 for nicotine sorption on stainless steel was applied in five sets of experiments to investigate the sorption dynamics for each of the following sorbent-sorbate pairs: nicotine-carpet, nicotine-painted wallboard, phenanthrene-stainless steel, phenanthrene-carpet, and phenanthrene-painted wallboard. The dynamic behavior of each tested SVOC with each sorbent was measured in a sealed environmental chamber with a very low air-exchange rate for a period of 16–155 days. The gas-phase concentration was monitored during and following several flash evaporations of the tested compound. After several cycles of SVOC emission and uptake by the materials in the chamber, the chamber was ventilated at a high air-exchange rate for a few days to reduce the gas-phase SVOC concentration.

Finally, the chamber was resealed to observe reemission of sorbed mass. The gas-phase data were analyzed with a sorption dynamics model that couples surface sorption kinetics with bulk-phase diffusion through a homogeneous polymer slab.

METHODS AND MATERIALS

Adsorbents and Reagents. Reagent grade nicotine and phenanthrene (CAS # 54-11-5 and #85-01-8, Aldrich Chemicals) were used in this study. Standard solutions used for calibration of analytical instruments and sample internal standards were prepared with High Performance Liquid Chromatography grade methanol (Burdick and James) in glassware washed with a saturated solution of potassium hydroxide in ethanol and rinsed with deionized water. To prevent loss of nicotine onto glassware, all nicotine standard solutions were prepared with methanol modified with 0.01% v/v triethylamine (TEA) (Ogden *et al.,* 1989). This treatment was not used in phenanthrene solutions.

The carpet used in this study was purchased from a carpet dealer in Richmond, California with a large inventory of older but unused new carpet. The tested carpet was obtained from a roll which had been manufactured approximately three years prior to the commencement of this study. It had been stored in the dealer's showroom tightly rolled but unwrapped for most of the intervening time. It had nylon fibers with an approximately 1-cm-deep pile. The backing is typical of that found most residential carpets, consisting of a coarse polypropylene mesh bonded to the primary backing with styrene-butadiene rubber (SBR) latex adhesive layer. The backing layer is approximately 0.24 ± 0.03 cm thick. No stain resistance or other treatment was applied to the carpet.

Gypsum wallboard used in this study was purchased at a hardware store in Emeryville, California. The outside face of each $1.2\ \text{m} \times 2.4\ \text{m} \times 1 \pm 0.1$ cm panel was covered with approximately 700 mL of flat white indoor latex paint (Sherwin Williams Classic 99) applied with a 30 cm felt roller. The average thickness of the applied paint layer was 0.02 cm based on wet volume. After the panels were painted, they were stored

in a warehouse for approximately 180 days. During this time, a significant mass of dust and dirt accumulated on the panel surfaces. Before the panels were used in sorption dynamics experiments, the dirt was removed with a very dilute solution of dishwashing detergent in water applied with a hand sponge. After washing, each panel was given a finishing coat of paint diluted 1:1 with deionized water applied with the roller. Each panel received less than 150 mL of additional paint in this step which increased the surface layer by less than 0.005 cm. Following application of the finishing coat, each panel was allowed to air dry in a clean, well-ventilated laboratory for 3 weeks prior to use in sorption dynamics experiments.

Stainless Steel Test Chamber. Experiments were conducted in the environmental test chamber described in Chapter 2 (volume = 20 m^3; internal surface area = 45.2 m^2; all internal surfaces clad with Type 304 stainless steel; walls, floor, and ceiling insulated with a 10-cm-thick layer of high density polyurethane foam; door and interior seams sealed with low-VOC-emitting silicone gasket material). A schematic diagram of the chamber configuration used in the current study is shown in Figure 3.1. As in the earlier nicotine-stainless steel experiments, six 8-cm diameter wall-mounted fans, aligned with the blade axes at a 45° angle to the wall surface and parallel to the floor, circulated the air in a clockwise direction and created well mixed conditions during the experiments. For experiments with carpet, a sample measuring approximately 3.6 m × 2.1 m covered most of the chamber floor. Pairs of painted wallboard panels were bolted together back-to-back with the painted sides facing outward. The edges of each panel pair was sealed with aluminized furnace tape so that each bolted set of panels had an exposed painted wallboard surface area of approximately 5.7 m^2. In each wallboard experiment, two pairs (four panels with 11.4 m^2 of exposed, painted surface area) were arranged in a parallel, vertical configuration with approximately 1 m separating the pairs as shown in Figure 3.1. The panels were supported by a wood frame covered with aluminum foil to stand with a 2.4 m edge on the chamber floor. The total exposed area of aluminum (tape and foil) in

the wallboard experiments was approximately 0.015 m^2 (compared to 45 m^2 of stainless steel and 11.4 m^2 of wallboard). Sorption on the aluminum surfaces was assumed to be negligible in the model simulations.

The temperature and relative humidity inside the chamber were uncontrolled, but fairly consistent during the initial sealed chamber phase of each experiment, at 23 ± 4 °C and 55 ± 12%, respectively, for all four experiments. The sealed-chamber infiltration rate was determined periodically during the experiments by tracer gas decay to be 0.15 $m^3\ h^{-1}$. Ventilation due to sampling was 0.01 $m^3\ h^{-1}$, so the total sealed chamber ventilation rate (Q_S) was 0.16 $m^3\ h^{-1}$. Because the chamber remained sealed with a very low air-exchange rate for most of each experiment, the temperature and relative humidity did not vary by more than 2 °C and 6%, respectively during the sealed chamber period of each run. However, these parameters did vary more substantially during the ventilation phases of the nicotine-carpet and nicotine-wallboard experiments which were conducted in January during cold, dry weather conditions. The temperature and relative humidity inside the chamber dropped to approximately 14 ± 5 °C and 25 ± 15%, respectively during the ventilation phases of these experiments. After the chamber was resealed, the temperature and relative humidity stabilized at approximately 20 ± 3 °C and 35 ± 5%, respectively during the reemission phase. Temperature and relative humidity variations during the ventilation phases of the phenanthrene experiments were substantially smaller because these experiments were conducted during more mild weather in April and September. Changes in the chamber temperature and humidity may have altered the equilibrium gas-sorbed phase partitioning by as much as a factor of 2. However, the gas-phase concentrations measured during these phases of the experiments were very small, so the errors introduced by changing the temperature and relative humidity are likely to be similar to the uncertainty in the concentration measurements during these phases of the experiments.

Prior to each experiment described in this chapter, the chamber interior surfaces were washed with a phosphoric acid-based detergent (Heavy Duty LC-30, EcoLab), followed by an alkaline detergent (Kart-Klenz) to remove residual sorbate from the stainless steel surfaces and provide a consistent starting condition. After each detergent application, the walls were rinsed thoroughly with tap water which was removed from the surfaces with a rubber window wiper and cleaned up with a wet-dry vacuum cleaner. As a final washing step, the chamber was rinsed with deionized water and then dried with the window wiper and vacuum followed by clean paper towels to remove remaining water. Finally, the chamber was closed and ventilated at 40 $m^3 \cdot h^{-1}$ for two days with HEPA and granulated activated carbon filtered outdoor air to allow equilibration with the humidity in ambient air. After two days, the chamber was reentered to install the sorbent to be tested and then resealed and ventilated for five more days to condition the sorbent.

Experimental Protocol. The five experiments conducted in this study are summarized in Tables 3.1a and 3.1b which include information on chamber ventilation rates, SVOC mass emitted, and number of emission events. During each experiment, 20-100 mg of the tested sorbate was vaporized in the sealed chamber on each of 2 to 5 occasions. Except for experiment 3C with phenanthrene in the empty chamber, the gas-phase concentration was monitored for at least a week following each SVOC emission. In experiment 3C, the equilibration period following each emission was curtailed to one to two days because equilibrium was not expected to be slowed by diffusion through stainless steel. Following the final sorbate emission and concentration decay period in each experiment, the chamber was ventilated at the vented flow rate to remove gas-phase SVOC and then resealed to monitor reemission from the sorbed phase.

SVOC Emission Methods. Nicotine and phenanthrene were flash evaporated in the chamber using the custom designed evaporator unit described in Chapter 2 with a few minor modifications. The 0.53-cm-inner diameter, 10-cm-long stainless steel tube was loosely packed with clean glass wool to prevent nicotine or the phenanthrene solution

described below from flowing out of the tube during loading. As in experiments 2D and 2E in Chapter 2, one end of the tube was open to the chamber. However, the small electrical fan was replaced by a 20 cm^3 min^{-1} flow of clean, dry nitrogen from a compressed gas cylinder located outside of the chamber and connected to the back end of the emission tube by clean, 0.2-cm-inner diameter copper tubing. Immediately prior to each SVOC emission, the unit was pulled out of the chamber through its port, loaded through the front end with nicotine or the phenanthrene solution from a clean syringe, and quickly reinserted into the chamber. For phenanthrene, a solid at room temperature, the SVOC emission procedure was modified slightly. An aliquot of a saturated solution of phenanthrene in methanol was loaded into the open end of the evaporator apparatus with a clean syringe. The loading process took less than one minute, so evaporative losses of the SVOC outside the chamber were minimal. Once the evaporator unit was properly positioned, the current to the heater cartridge and nitrogen gas flow were initiated. The temperature of the heater unit was monitored with a thermocouple but not directly controlled. Within 10 minutes the temperature reached approximately 300 °C and remained fairly steady at that temperature until the heater current was shut off after approximately 30 minutes. The nitrogen gas flushing flow remained on until the evaporator unit cooled to less than 35 °C.

At the end of each experiment, the stainless steel tube was removed from the SVOC evaporator and thermally desorbed at 300° C while being flushed with dry helium at 100 cm^3 min^{-1} for one hour. The desorbed nicotine or phenanthrene was collected on a Tenax sorbent tube and analyzed by gas chromatography with flame ionization detection as described below. Less than 0.5 μg of SVOC (out of a total of 40-250 mg injected in all of the phases in each experiment) was recovered in this manner. Thus, the evaporator unit quantitatively delivered the SVOC into the chamber gas-phase. In fitting the experimental data, the evaporated mass was assumed to be emitted in an instantaneous pulse when heating of the evaporator unit began.

Gas-Phase Sampling. Gas-phase SVOC samples were collected on reusable, commercially available sorbent samplers (Part # ST032, Envirochem Inc.) packed with Tenax-TA (Aldrich Chemicals). Before each use, the samplers were cleaned and conditioned by heating them to 300° C for 30 minutes with a helium purge flowing at 100 $cm^3 \cdot min^{-1}$ in the reverse direction of sample collection gas flow. During collection of chamber gas-phase samples, the sample tubes were mounted on the end of a 45 cm stainless steel tube which could be retracted from the chamber through a port in the wall to exchange exposed sample tubes for clean ones. The stainless steel tube was connected to a peristaltic pump outside of the chamber which sampled at a flow rate of 90-110 $cm^3 \cdot min^{-1}$. The sample flowrate was measured during each sample with a soap bubble flowmeter. Several duplicate samples were collected over the course of the experiment to verify measurement reproducibility. The lower limit of detection for this method was approximately 0.1 $\mu g\ m^{-3}$ with a limit of quantification (LOQ) of 0.5 $\mu g\ m^{-3}$. Below these limits, interference by the background VOC concentration prevented accurate quantification of the collected SVOC mass. For samples which exceeded the LOQ by more than a factor of three, the variability between duplicate samples was generally less than 15%.

Sorbed-Phase Samples. Several attempts were made to employ the sorbent thermal desorption system described in Chapter 2 in this study to measure nicotine and phenanthrene sorbed to carpet and wallboard samples and phenanthrene sorbed to stainless steel. However, the collected thermal desorption samples proved to be usable only for phenanthrene on stainless steel. The large mass of organic compounds emitted during heating of carpet and wallboard samples prevented quantification of sorbed nicotine or phenanthrene with the analysis system used in this study. Nicotine and phenanthrene peaks were observed on the chromatograms obtained from these samples, but the high VOC background made accurate calculation of the nicotine and phenanthrene masses impossible.

Sample Analysis. The analytical procedures for organic compounds collected on sorbent samplers have previously been described (Thompson *et al.,* 1989; Hodgson and Girman, 1989). In brief, a sample is thermally desorbed from a sampler, concentrated and introduced into a capillary GC with a UNACON 810 sample concentrator. This instrument passes the sample through dual sequential traps to concentrate it before it is introduced to the GC. Sample components are resolved with a GC (5890 Series II, Hewlett Packard Co.) equipped with a 15-m x 0.53 mm ID fused-silica capillary column with a film thickness of 1.65 μm (Hewlett Packard Co.). The GC is connected via a direct capillary interface to a flame ionization detector (FID). Calibration regression lines were generated by analyzing Tenax TA cartridges spiked with known volumes of solutions of nicotine in methanol containing 0.01% TEA (MeOH/TEA) or phenanthrene in methanol. The calibration curves for nicotine and phenanthrene were linear from 0 to greater than 1 μg total injected mass. However, both regression lines had negative intercepts indicating a possible loss of approximately 30 ng of nicotine and 40 ng of phenanthrene per sample in the sampler desorption system. For nicotine, the lost mass increased as the concentrator unit's valve and plumbing temperature setpoints were increased indicating that nicotine might be decomposing in the concentrator system. A decrease in the FID response to nicotine standards was also observed at lower concentrator temperatures and was probably due to adsorption of nicotine in the system. Experimentation with different temperatures allowed optimization of the FID response at a system temperature of approximately 150 °C. For phenanthrene, sample losses decreased with increasing concentrator temperatures up to 270 °C (the maximum operating temperature). Even at this elevated temperature, system blanks immediately after phenanthrene samples exhibited non-zero phenanthrene response. To avoid contamination of sequential samples, the concentrator was cycled twice after each phenanthrene standard or sample run. This procedure kept the phenanthrene background smaller than 1 ng as measured by system blanks.

Reagent grade quinoline (CAS # 91-22-5, Aldrich), added to each nicotine sample tube as a 1 μL aliquot of a 109 ng μL^{-1} solution prepared in MeOH/TEA, was used as an internal standard in this study. No internal standard was used in analysis of the phenanthrene samples to reduce the risks of sample contamination during the addition of the standard. Prior to analysis (and after application of the internal standard for nicotine samples), each sorbent sample tube was conditioned to remove methanol and water collected during sampling by purging with clean, dry nitrogen flowing at 100 $cm^3 \cdot min^{-1}$ in the direction of sample collection gas flow for 20 minutes. Loss of collected SVOC during this procedure could be neglected as demonstrated by the reproducible recovery of nicotine and phenanthrene from tubes spiked with standard solutions and conditioned for periods varying from 0 to more than 30 minutes. A nicotine calibration standard was run at least once per analysis day during nicotine experiments. Response of the FID to nicotine remained nearly constant over time. Some variability in the FID response to phenanthrene was observed. To correct for this, calibration standards were run approximately every three phenanthrene samples and a time-dependent response factor was calculated for each phenanthrene sample.

DATA ANALYSIS

Modeling Framework. Reversible sorption in the environmental chamber was represented mathematically by the following generalized system of coupled differential equations :

$$\frac{dC_i}{dt} = \frac{E_i}{V} + \lambda_{v,T}\left(C_{io} - C_i\right) - \frac{1}{V}\sum_{j=1}^{g} S_j J_{ij} \tag{3.1}$$

$$\frac{dM_{ij}}{dt} = J_{ij} \tag{3.2}$$

where the subscripts i and j specify parameters applicable to a given SVOC and sorbent, respectively; C_i and C_{io} are the gas-phase concentrations in the chamber and in the

ventilation supply air, respectively (mg m^{-3}); t is time (h), E_i is the mass emission rate (mg h^{-1}); V is the indoor volume (m^3); λ_v is the chamber air exchange rate (h^{-1}); g is the total number of different sorbent materials (-); S_j is the sorbent surface area (m^2); J_{ij} is the net SVOC flux from the gas phase to the air-sorbent interface (mg m^{-2} h^{-1}); and M_{ij} is the sorbed mass of compound i per unit area of at the air-surface interface of sorbent j (mg m^{-2}). In words, the rate of change in the gas-phase SVOC concentration is equal to its mass emission rate per chamber volume minus losses due to ventilation and the net of its sorptive interactions with all of the available sorbents in the system (equation 3.1). Similarly, the accumulation rate of SVOC mass at the air-sorbent interface due to deposition is equal and opposite to the rate of the sorbate's loss from the gas-phase onto that sorbent (equation 3.2). In Chapter 2, the single sorbent form of equation 3.2 was used to generate the equilibrium isotherm by inserting an appropriate mathematical expression for the adsorption and desorption rates and setting the left side of the equation to zero (the equilibrium condition). This approach was used to reduce the number of independent model parameters for nicotine sorption on stainless steel using equilibrium data obtained separately from the kinetic experiments. This simplification was not feasible in the current study because the tested sorbents equilibrated much more slowly than stainless steel and sorption equilibrium was probably never reached.

To extract sorption kinetics parameters for a multiple sorbent system, it is necessary to determine the equilibrium partitioning for all but one of the sorbents present during the test individually. Then, the unknown sorbent's sorption parameters can be obtained by first subtracting out the effects of all of the other sorbents. In this study, sorption of nicotine on the chamber surfaces is corrected for by incorporating equilibrium and kinetic data from Chapter 2. In the current study, that model was also applied to determine sorption kinetics of phenanthrene on the stainless steel surfaces of the test chamber. For porous sorbents such as carpet and wallboard, the model described in Chapter 2 is unlikely to accurately simulate sorption dynamics.

Surface-Sorption/Bulk Diffusion Model. The nonlinear surface sorption model described in Chapter 2 fails when applied to porous sorbents (Van Loy *et al.* 1997a). Most of the sorption capacity of these materials lies a finite distance away from the air-sorbent interface accessible only by diffusion through the bulk sorbent. The nonlinear surface sorption model and a model in which the rates of sorption and desorption depend only on diffusion through the bulk have been previously applied to the data presented here for nicotine sorption on carpet with unsatisfactory results (Van Loy *et al.*, 1997a). A diffusion-only model was originally developed to predict emissions of organic compounds from new carpet (Little *et al.,* 1994) or other finite mass slab sources (Dunn and Tichenor, 1988), and its potential utility in modeling source-sink effects for materials which can be represented as a homogeneous polymer slab was also recently described (Little and Hodgson, 1996). An improved model incorporating reversible sorption at the air-sorbent interface and bulk diffusion through the sorbent is developed and presented here. The gas phase mass balance for this model remains identical to equation 3.1. However, a mass balance for the porous sorbent requires the following two partial differential equations, the first to account for mass accumulation at the air-sorbent interface and the second for mass diffusion through the sorbent bulk:

$$\frac{\partial M_{ij}}{\partial t} = k_{a_{ij}} C_i - k_{d_{ij}} M_{ij} + D_{b_{ij}} \left(\frac{\partial C_{b_{ij}}(t,z)}{\partial z} \right)_{z=0} \tag{3.3}$$

$$\left(\frac{\partial C_{b_{ij}}(t,z)}{\partial t} \right) = D_{b_{ij}} \left(\frac{\partial^2 C_{b_{ij}}(t,z)}{\partial z^2} \right) \tag{3.4}$$

where $k_{a_{ij}}$ and $k_{d_{ij}}$ are the adsorption (m h^{-1}) and desorption (h^{-1}) rate constants, respectively, describing gas-phase sorption kinetics at the air-sorbent interface; $D_{b_{ij}}$ is the diffusion coefficient in the sorbent bulk (m^2 h^{-1}); $C_{b_{ij}}(t,z)$ is the instantaneous sorbent bulk-phase concentration (mg m^{-3}) at a distance z away from the air-sorbent

interface, and z is the distance into the bulk of the sorbent material, with $z = 0$ at the sorbent surface (m). Equations 3.3 and 3.4 are based on two implicit assumptions: 1) partitioning between the gas and surface-adsorbed phases is linear, and 2) sorbate does not accumulate at the air-sorbent interface relative to the bulk of the sorbent. To analyze data collected during the experiments described above, equation 3.1 is substituted with the appropriate terms to describe the net flux of SVOCs to the stainless steel chamber surfaces and the sorbent to be tested. The other equations introduced in Chapter 2 are repeated here for clarity:

$$\frac{dC_i}{dt} = \frac{E_i}{V} + \lambda_{v,T}\left(C_{io} - C_i\right) - \frac{S_s}{V}\left(k_{a_{is}} C_i^{n_{a_{is}}} - k_{d_{is}} M_{is}^{n_{d_{is}}}\right) - \frac{S_j}{V}\left(k_{a_{ij}} C_i^{n_{a_{ij}}} - k_{d_{ij}} M_{ij}^{n_{d_{ij}}}\right) \quad (3.5)$$

$$\frac{dM_{is}}{dt} = k_{a_{is}} C_i^{n_{a_{is}}} - k_{d_{is}} M_{is}^{n_{d_{is}}} \quad (3.6)$$

where the subscript s denotes stainless steel kinetic parameters. The coefficients $n_{a_{is}}$ and $n_{d_{is}}$ are included in equation 3.5 to reflect the nonlinear sorption rates for nicotine sorption on stainless steel described in Chapter 2. As discussed in the following section, phenanthrene sorption on stainless steel was found to be well described by linear sorption kinetics. Thus, the power law rate coefficients for phenanthrene ($n_{a_{ps}}$ and $n_{d_{ps}}$) are 1.

For experiment 3C with phenanthrene in the empty chamber, equation 3.5 with the porous sorbent parameters $k_{a_{ij}}$ and $k_{d_{ij}}$ set to zero is simultaneously integrated with equation 3.6 with the stainless steel exponential rate coefficients $n_{a_{ps}}$ and $n_{d_{ps}}$ set to unity. An analytical solution for this problem has been previously reported (Dunn and Tichenor, 1988). For the porous sorbent experiments (3A, 3B, 3D, 3E), equations 3.3 – 3.6 are solved simultaneously to obtain the best fit to the data using the code listed in Appendix A. Sets of nonlinear coupled ordinary differential equations such as those in equations 3.5 and 3.6 are integrated using a fourth-order Runge-Kutta method described by Press *et al.* (1992). A modified version of this method is used to solve the coupled

ordinary and partial differential equations describing the porous sorbent experiments. The sorbent bulk diffusion equation (3.4) is converted into a set of 10 coupled ordinary differential equations using a finite difference approximation with 10 equally spaced nodes along the z axis. Boundary conditions for this set of equations are given by equation 3.3 at the air-sorbent interface node and a no-flux condition at the deepest node. The code for these calculations is listed in Appendix B.

Determination of Equilibrium Isotherms. In Chapter 2, the number of independent kinetic parameters was reduced from 4 to 2 using separately obtained equilibrium partitioning data and equations 2.6 and 2.7. In the current study, this simplification was possible only in experiment 3C with phenanthrene in the empty chamber. Reasonable estimates of the diffusion coefficient for organic compounds in porous building materials like carpet (Little *et al.*, 1994; Little and Hodgson, 1996) indicate that full equilibrium between the gas and sorbed phases would be achieved only after more than a year. Thus, the kinetic best fit parameters for the porous sorbents tested in this study were not constrained by equilibrium data. An estimate of the equilibrium sorption capacity of these sorbents assuming linear gas-sorbed phase partitioning was calculated using the following equation:

$$K_{ij} = {k_{a_{ij}}}/{k_{d_{ij}}} \tag{3.7}$$

where K_{ij} is the linear isotherm partitioning coefficient (m):

$$M_{T_{ij}} = K_{ij} C_i \tag{3.8}$$

in which $M_{T_{ij}}$ is the total sorbed mass of i per presented area of sorbent j (mg m^{-2}). Equation 3.8 is analogous to Henry's Law for gas-water partitioning.

RESULTS AND DISCUSSION

Equilibrium Partitioning. Table 3.2 list isotherm parameters obtained from experiments described in this chapter along with the nicotine-stainless steel isotherm parameters from Chapter 2. As stated in the previous subsection, only the stainless steel sorption equilibria were measured directly. The isotherm parameters for the porous sorbents were calculated using kinetic data and equation 3.7. In general, the results show that carpet and wallboard have a substantially greater sorption capacity per unit presented area than stainless steel. This is true for all sorbate-sorbent pairs except phenanthrene and wallboard which has a lower partitioning coefficient than phenanthrene and stainless steel. This unexpected result might be explained by the chemical characteristics of phenanthrene and wallboard. Phenanthrene is a high molecular weight, nonpolar, hydrophobic organic molecule. In contrast, the core of a sheet of wallboard contains packed gypsum ($CaSO_4$) which occurs most commonly in a dihydrate form. The physicochemical microenvironment inside a wallboard panel may be less thermodynamically favorable for phenanthrene than close packing of many sorbed molecules on the surface of a piece of stainless steel. This phenomenon does not occur in carpet which may be more chemically similar to hydrophobic organic compounds like phenanthrene.

Sorption Dynamics. The concentration vs. time data collected in experiments 3A to 3E are shown in Figures 3.2 to 3.16 along with predictions based on the best fit parameters to the data for the coupled sorption-diffusion model (equations 3.3 to 3.6) in Figures 3.2 – 3.7 and 3.11 – 3.16 and the linear surface sorption model (equations 3.5 and 3.6) for Figures 3.8 – 3.10. The resulting model parameters are listed in Table 3.3 along with the kinetic parameters for nicotine on stainless steel from Chapter 2. These data are also tabulated in Tables 3.4 – 3.8. As Figures 3.2 – 3.7 and 3.11 – 3.16 show, the sorption-diffusion model gives a good overall fit to the gas-phase data collected in experiments 3A, 3B, 3D, and 3E. The surface sorption model accurately simulates

experiment 3C. Despite the good overall fit of the model predictions to the data, there are some discrepancies. The largest relative errors occur during the high air-exchange rate phases of the experiments. During these periods, the model tends to underpredict the gas phase concentration, often by several orders of magnitude. This disagreement is likely due to the reduced measurement accuracy of the analytical method at low gas-phase concentrations. The lower limits of detection for nicotine and phenanthrene mass in the gas chromatograph system were approximately 30 and 40 ng, respectively. For many of the samples collected during ventilation of the chamber, this threshold was not reached.

Careful inspection of the porous sorption data reveals two distinct timescales. The majority of the gas-phase concentration decrease occurs within the 5-6 hours immediately following release of each SVOC pulse into the chamber. Then, for the next several days, the concentration slowly decreased in a nearly linear fashion. These observations suggest that at least two sinks are at work in the system: one rapid and surface dominated, and the other much slower and controlled by diffusion through a bulk layer. Additional fine-tuning of the model may be attained by including additional surface or diffusion sinks. For carpet, which is a combination of several different materials, a more complex approach may better represent the dynamic behavior of an SVOC in contact with the sorbent. The same may be true for painted wallboard, whose cross section consists of a paint layer on top an approximately 1 mm-thick layer of cardboard encasing the gypsum core.

Comparison of the best-fit parameters with literature data is useful in substantiating the model predictions. In the study of nicotine in the empty chamber presented in Chapter 2, the mass-transport-limited deposition velocity for nicotine under chamber airflow conditions was measured using large sheets of filter paper coated with a bisulfate salt which irreversibly reacts with deposited nicotine through acid-base chemistry. This experiment provided an upper bound of 4 m h^{-1} on the rate at which nicotine should be able to deposit in the chamber. This value is approximately half of the

deposition velocity obtained for nicotine-carpet sorption and 80% of the phenanthrene-carpet value listed in Table 3.3. This discrepancy likely results from the effects of surface roughness or the use of the carpet's presented surface area instead of a measured value of the real surface area of the fibers. Despite the range of sorbate and sorbent properties examined in this study and in Chapter 2, the best fit values for the deposition rate constant k_a for all of the sorbate-sorbent pairs are of similar magnitude.

The diffusion coefficients obtained from the diffusion-limited model are consistent with those reported elsewhere as well. Little and Hodgson (1996) reported a diffusion coefficient of 4.3×10^{-9} m^2 h^{-1} for phenylcyclohexane (PCH) in SBR carpet backing. PCH has a molecular weight of 160.26 g mol^{-1} which is close to that of nicotine. The nicotine and phenanthrene diffusion coefficients in the carpet tested in this study were approximately an order of magnitude smaller. The smaller diffusion rates are likely due to nicotine's chemical properties and phenanthrene's greater molecular weight. No data for organic compound diffusion through gypsum wallboard is available in the literature. However, comparison of the values obtained here for nicotine and phenanthrene reveals a two order of magnitude difference. This difference may be due to the chemical differences between the two tested sorbates. Nicotine is much more hydrophilic than phenanthrene, so its diffusion through the hydrated calcium sulfate core of a wallboard panel may be slowed by sorptive retardation. Wallboard has a much lower sorption capacity for phenanthrene, so sorptive retardation is expected to be less significant. This phenomenon is less likely to impact diffusion through carpet backing because the styrene-butadiene rubber backing is chemically similar to the hydrophobic parts of both the phenanthrene and nicotine molecules.

The sorption capacities measured in this study are very large relative to those previously reported for more volatile organic sorbates on indoor materials. Typical values for the ratio of sorbed mass to vapor phase mass for VOCs on carpet and other indoor sorbents are on the order of 10 to 20 (Tichenor *et al.*, 1991; Kjaer *et al.*, 1996;

Borrazzo *et al.*, 1993). The gas-surface partitioning parameters in Table 3.2 indicate that the sorbed mass to gas-phase mass ratio for SVOCs may be three to four orders of magnitude larger. Additionally, the reemission rate constants reported for VOCs are generally on the order of 0.1 h^{-1}. This reemission rate leads to desorption of more than 80% of the sorbed mass after one day of ventilation with VOC-free air. In contrast, desorption of SVOCs from the porous materials tested in this study depends on the rate of diffusion of absorbed mass from within the sorbent bulk to the air-sorbent interface. This process can be extremely slow — the characteristic time for desorption of nicotine or phenanthrene sorbed to carpet is on the order of 1000 days while that for nicotine sorbed to wallboard is more than 35 years. Phenanthrene desorption from wallboard is slightly faster (on the order of 3000 hours), but still several orders of magnitude slower than VOC sorption kinetics. Thus, SVOC sorption and desorption processes are likely to have a substantial impact on long term persistence of these pollutants in indoor air.

CONCLUSIONS

Porous building materials such as carpet and wallboard have very large sorption capacities for SVOCs. The uptake kinetics at the air-sorbent interface are rapid enough to cause these sorbents to be the dominant sink for gas-phase SVOCs during periods of high indoor air concentrations. Because the sorptive interactions are reversible, the beneficial effects of these materials on indoor air quality during high pollutant concentration periods is offset by their contribution to persistence of SVOC contamination in the indoor environment long after removal of the primary source. The analyses presented here consider only gas-surface partitioning. However, the same properties that cause SVOCs to readily sorb to indoor surfaces may also lead to gas-particle partitioning in indoor air. Chapter 5 presents a model-based analysis of this issue.

FIGURES

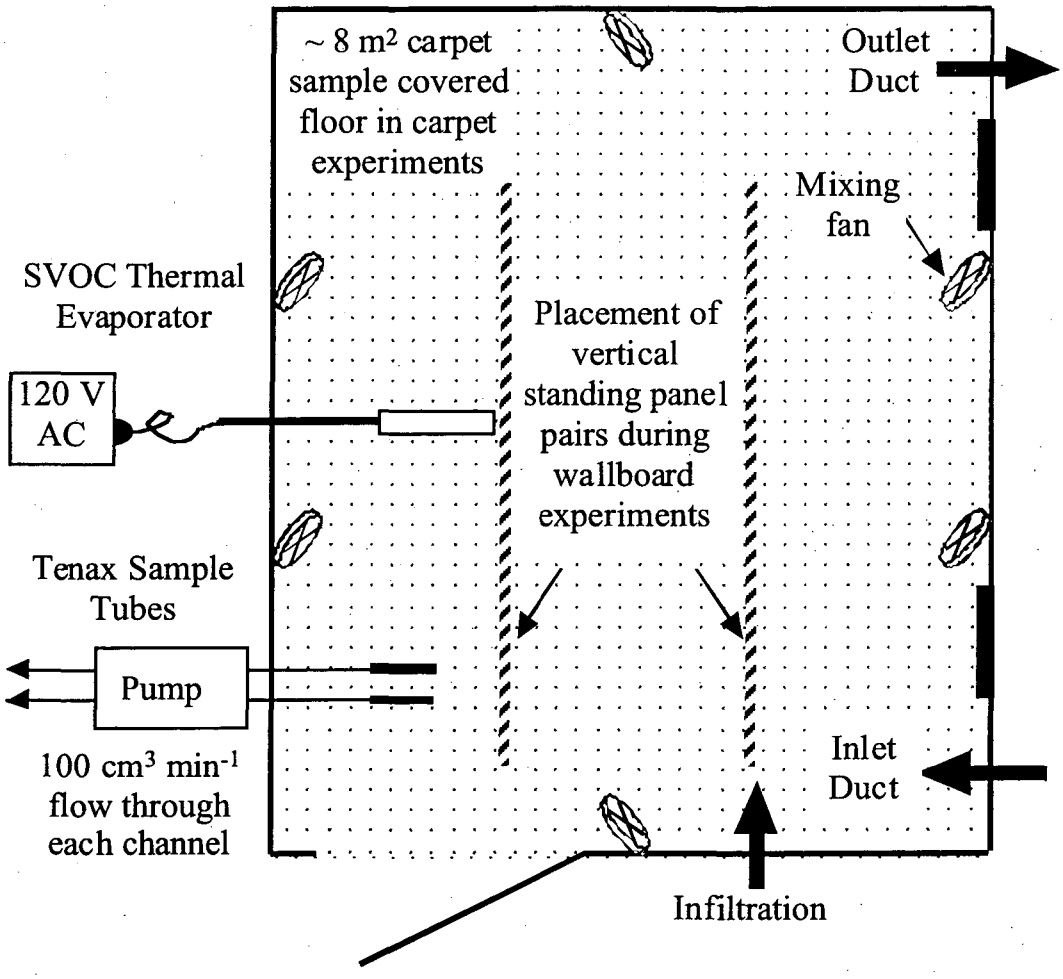

Figure 3.1 Schematic diagram of the 20 m^3 stainless steel environmental test chamber used in sorption dynamic studies for nicotine and phenanthrene with carpet and wallboard.

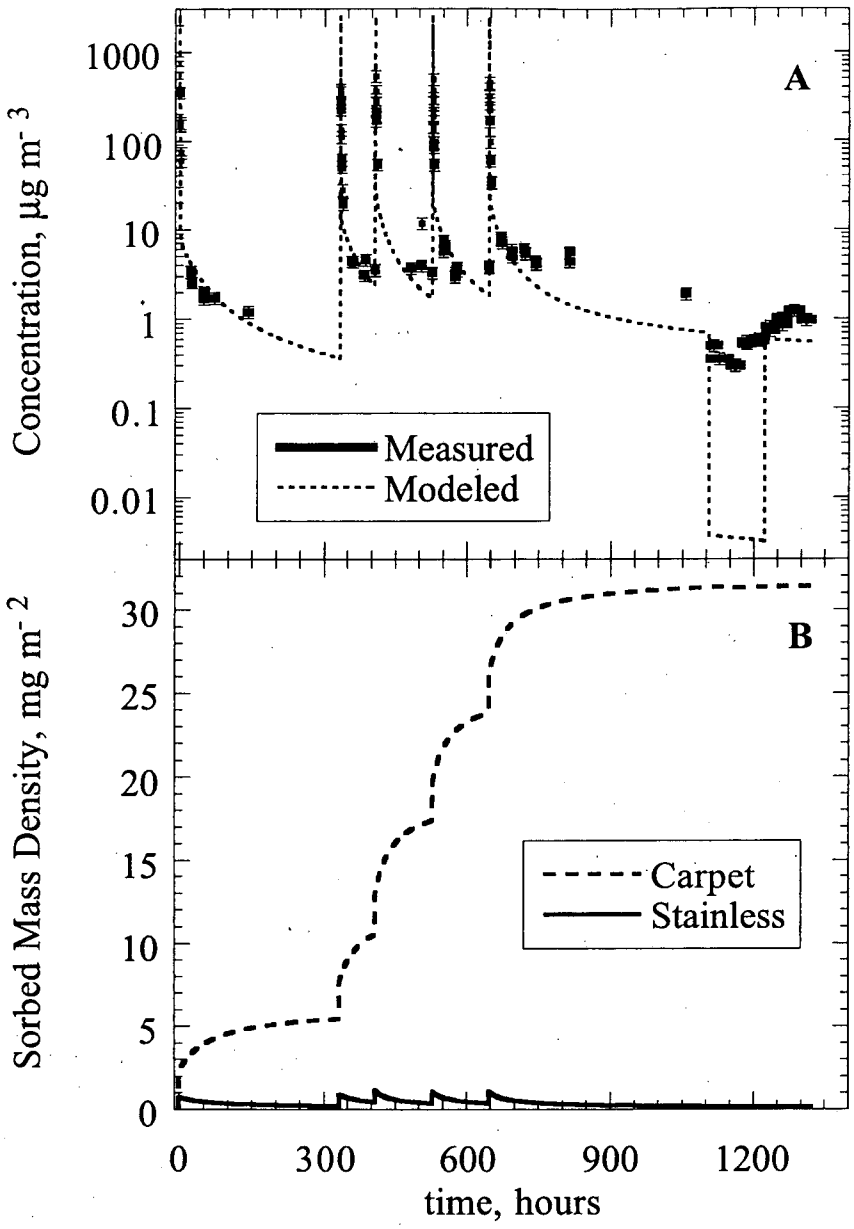

Figure 3.2 Experimental data, estimated errors, and diffusion model predictions for gas-phase (**A**) and stainless steel adsorbed and carpet adsorbed and absorbed nicotine (**B**) in experiment 3A.

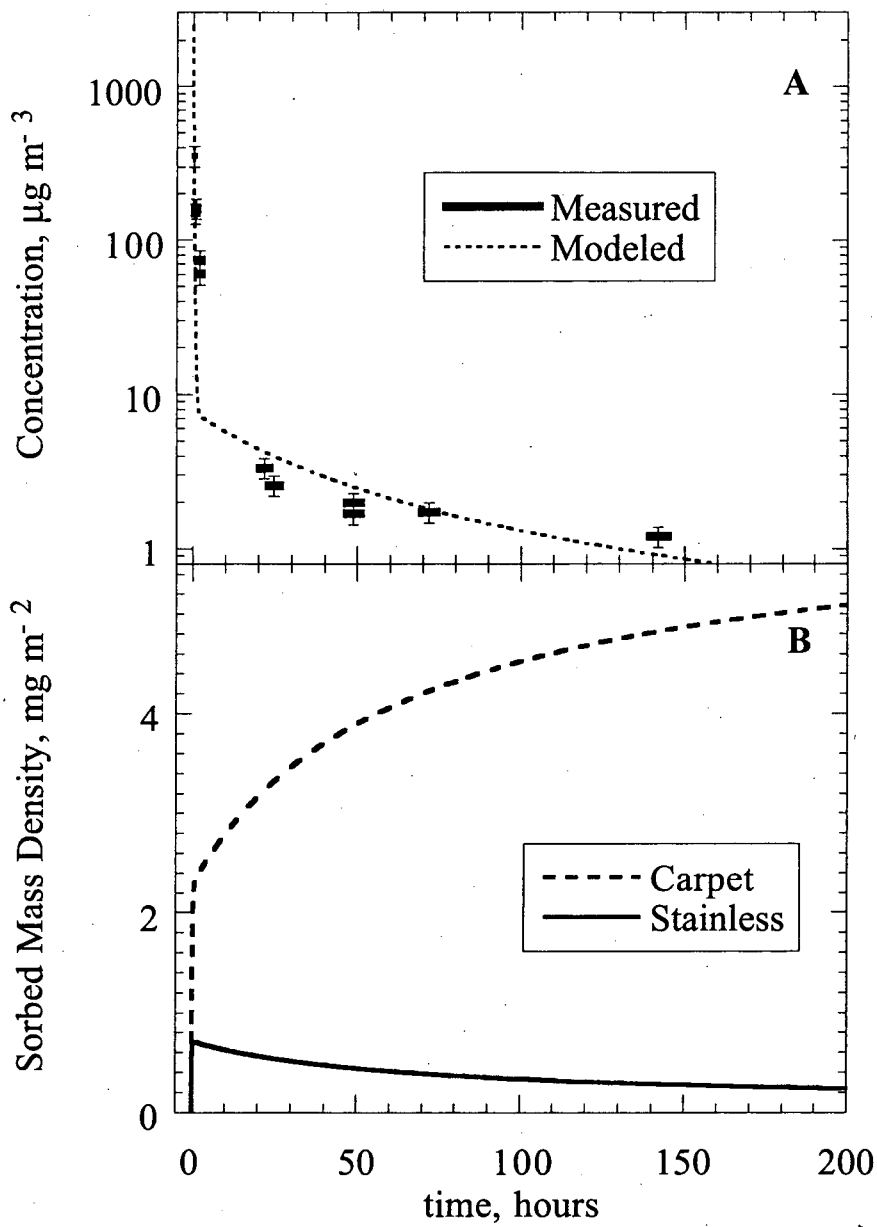

Figure 3.3 Experimental data, estimated errors, and diffusion model predictions for gas-phase (**A**) and stainless steel and carpet sorbed nicotine (**B**) for 200 hours following the first injection of nicotine in experiment 3A. The lengths of the horizontal bars and their positions relative to the time axis in panel **A** indicate the duration and timing of Tenax-TA sorbent samples.

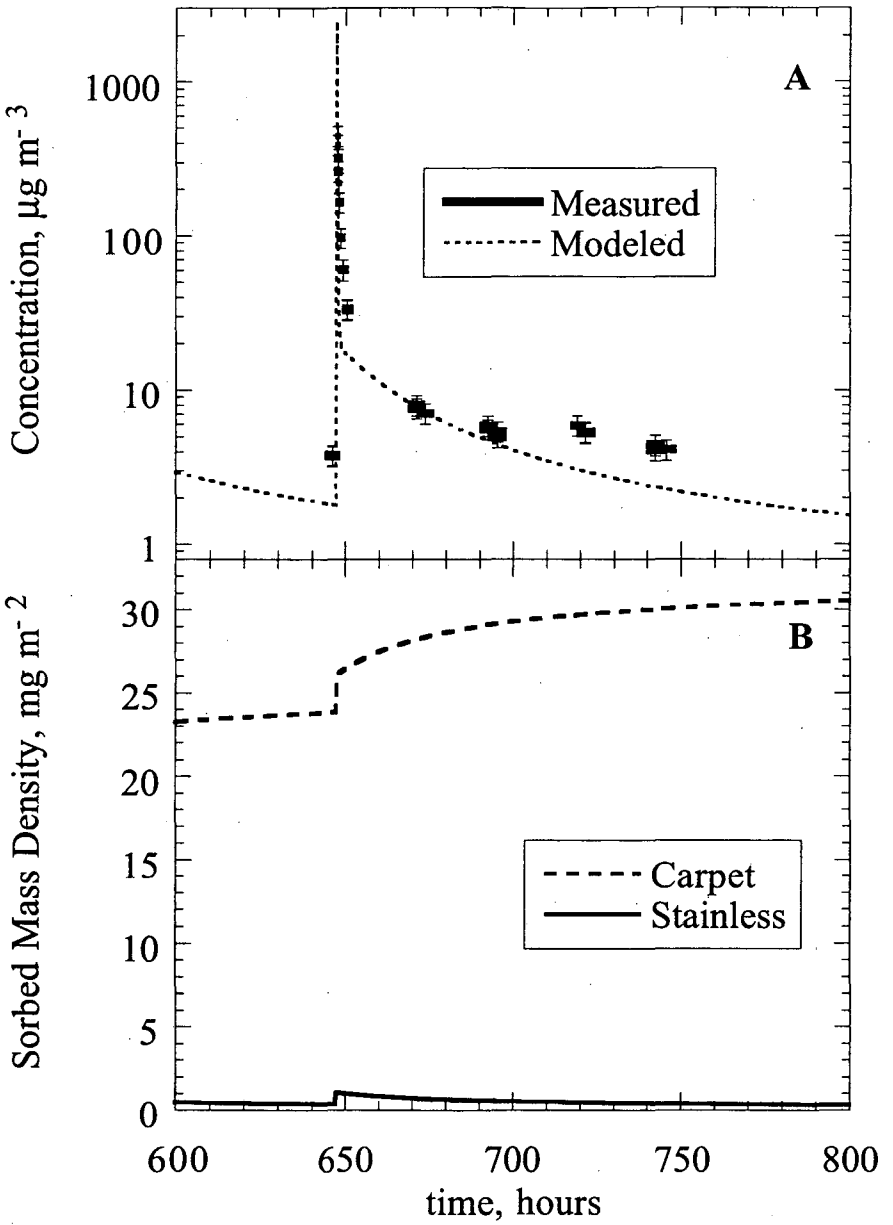

Figure 3.4 Experimental data, estimated errors, and diffusion model predictions for gas-phase (**A**) and stainless steel and carpet sorbed nicotine (**B**) for 200 hours following the fifth injection of nicotine in experiment 3A. The lengths of the horizontal bars and their positions relative to the time axis in panel **A** indicate the duration and timing of Tenax-TA sorbent samples.

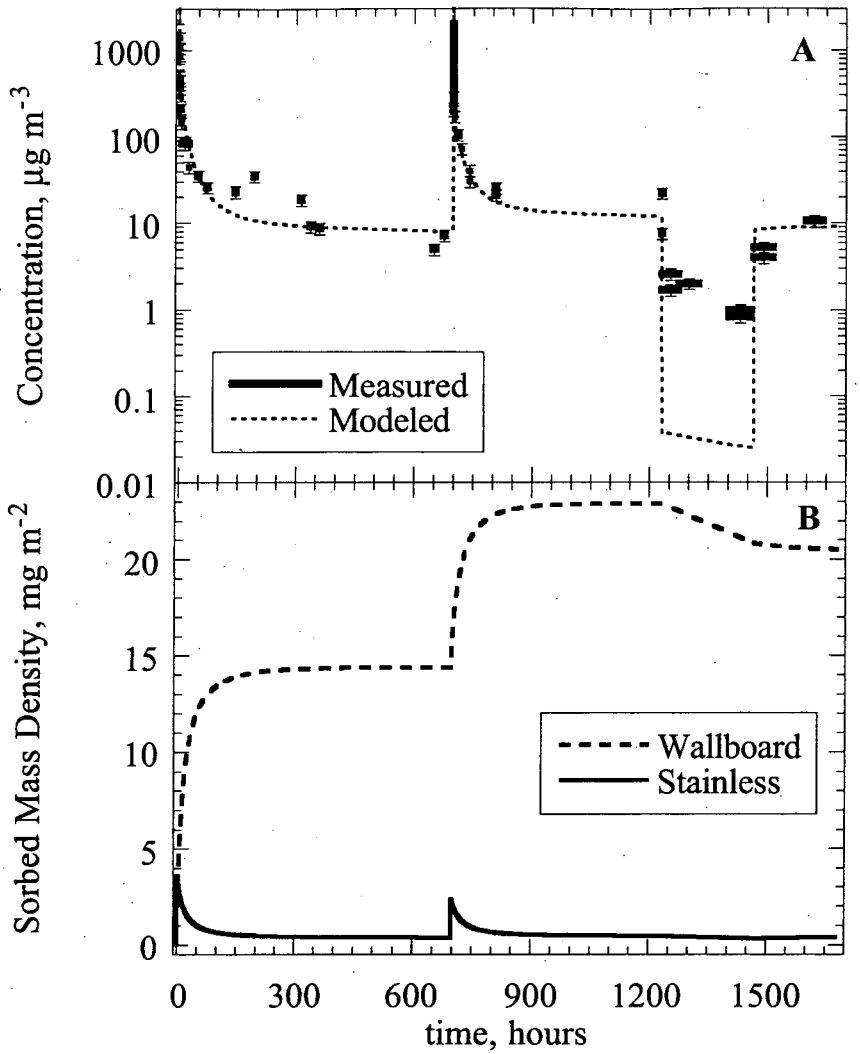

Figure 3.5 Experimental data, estimated errors, and diffusion model predictions for gas-phase (**A**) and stainless steel adsorbed and wallboard adsorbed and absorbed nicotine (**B**) in experiment 3B.

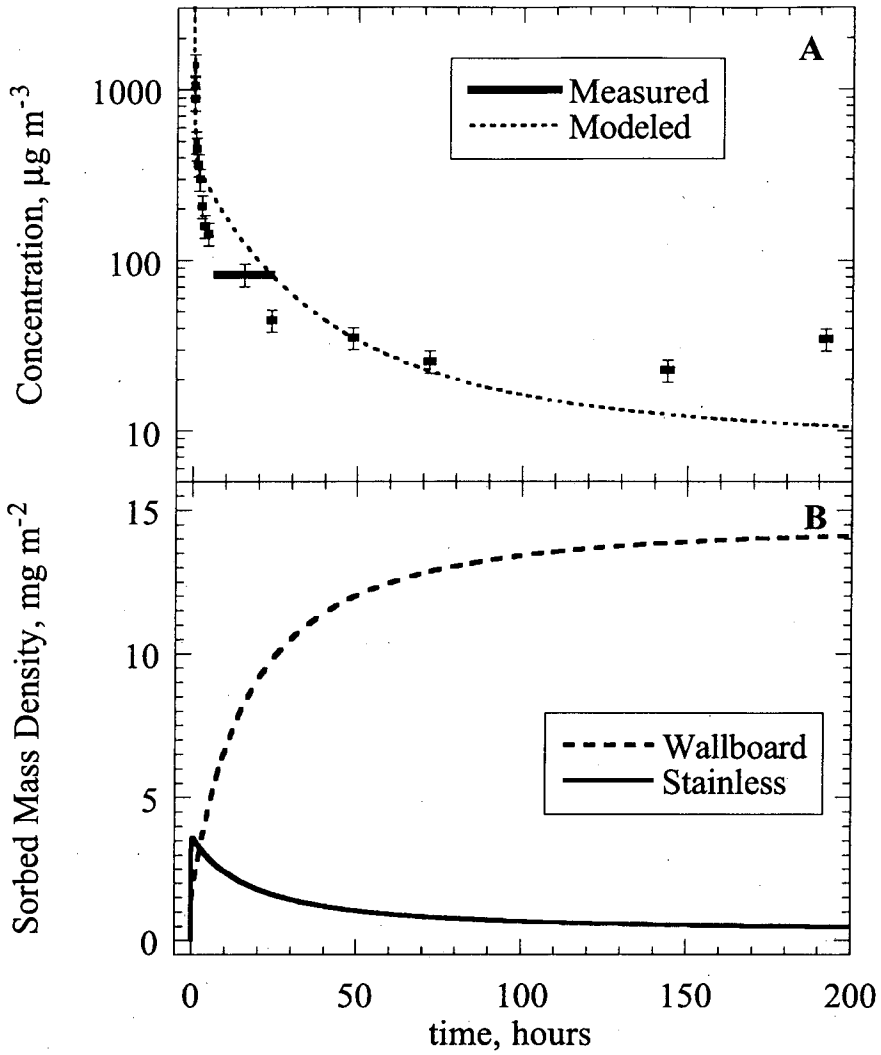

Figure 3.6 Experimental data, estimated errors, and diffusion model predictions for gas-phase (**A**) and stainless steel and wallboard sorbed nicotine (**B**) for 200 hours following the first injection of nicotine in experiment 3B. The lengths of the horizontal bars and their positions relative to the time axis in panel **A** indicate the duration and timing of Tenax-TA sorbent samples.

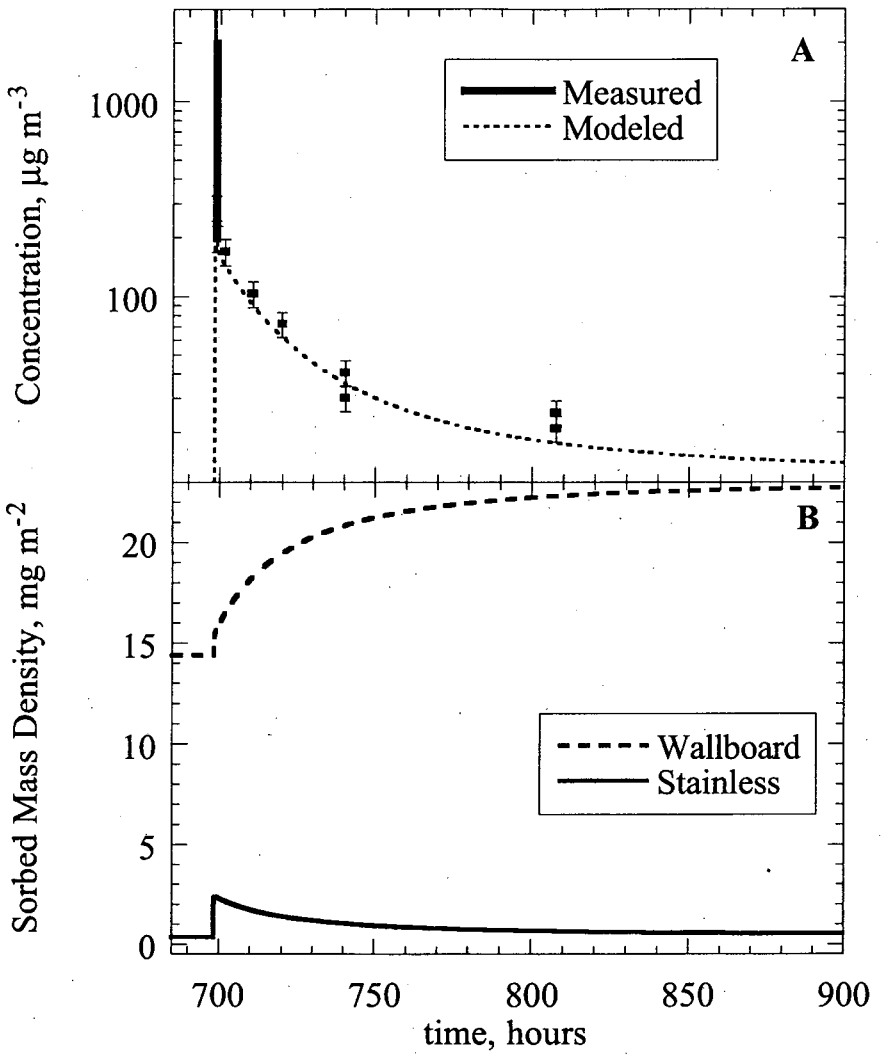

Figure 3.7 Experimental data, estimated errors, and diffusion model predictions for gas-phase (**A**) and stainless steel and wallboard sorbed nicotine (**B**) for 200 hours following the second injection of nicotine in experiment 3B. The lengths of the horizontal bars and their positions relative to the time axis in panel **A** indicate the duration and timing of Tenax-TA sorbent samples.

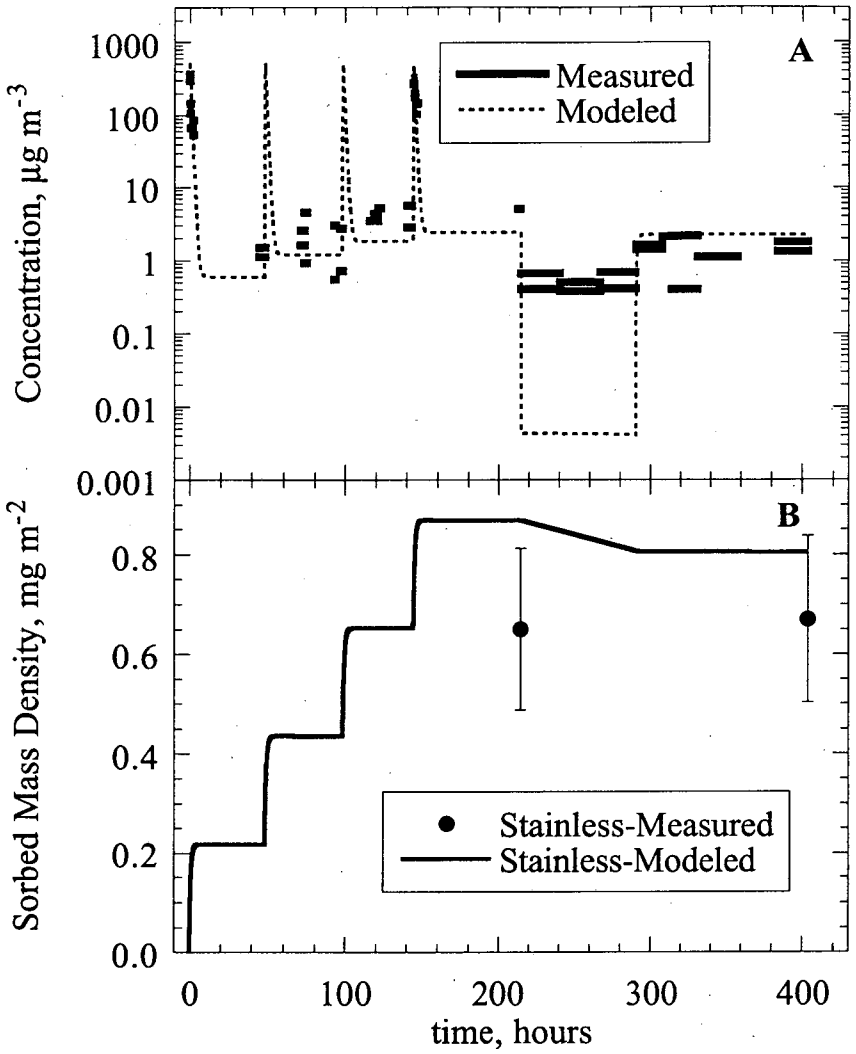

Figure 3.8 Experimental data, estimated errors, and surface sorption model predictions for gas-phase (**A**) and stainless steel adsorbed phenanthrene (**B**) in experiment 3C. The lengths of the horizontal bars and their positions relative to the time axis in panel **A** indicate the duration and timing of Tenax-TA sorbent tube samples.

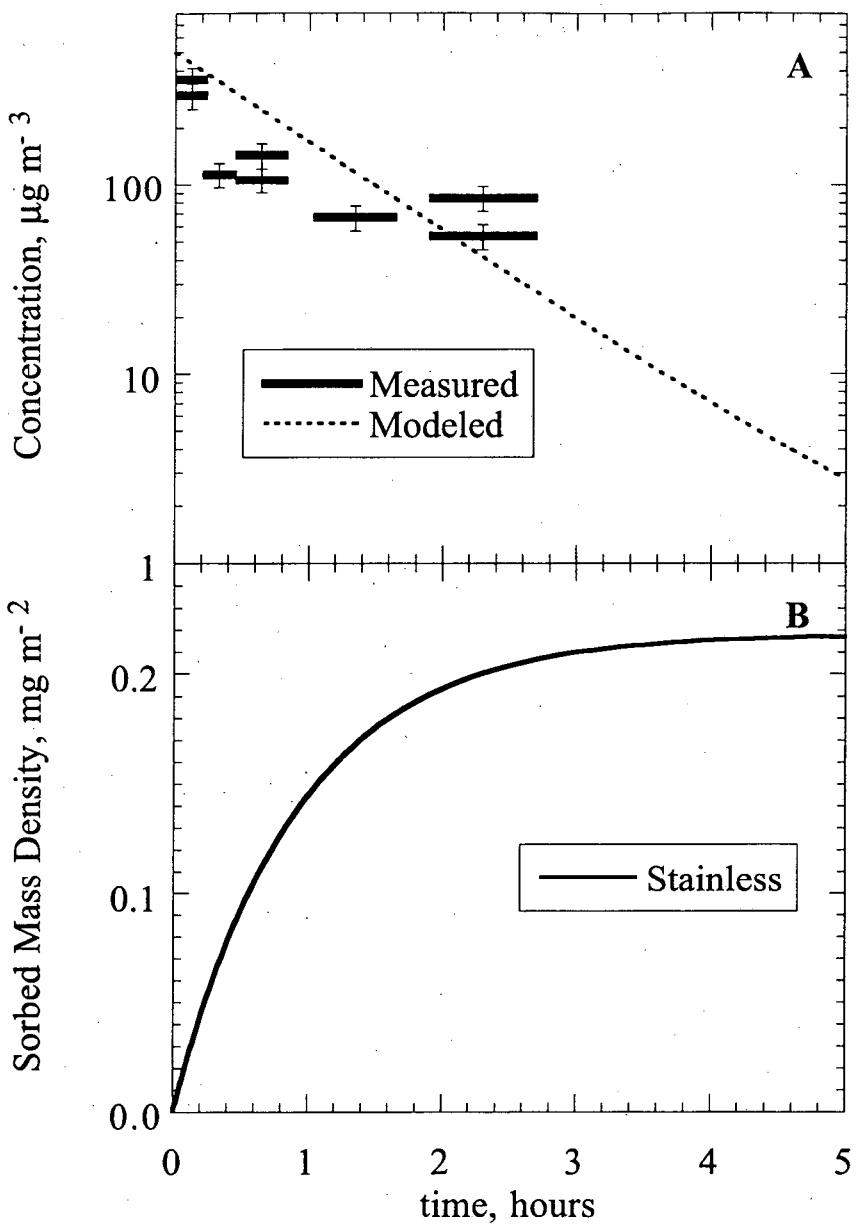

Figure 3.9 Experimental data, estimated errors, and diffusion model predictions for gas-phase (**A**) and stainless steel sorbed phenanthrene (**B**) for 10 hours following the first injection of phenanthrene in experiment 3C. The lengths of the horizontal bars and their positions relative to the time axis in panel **A** indicate the duration and timing of Tenax-TA sorbent samples.

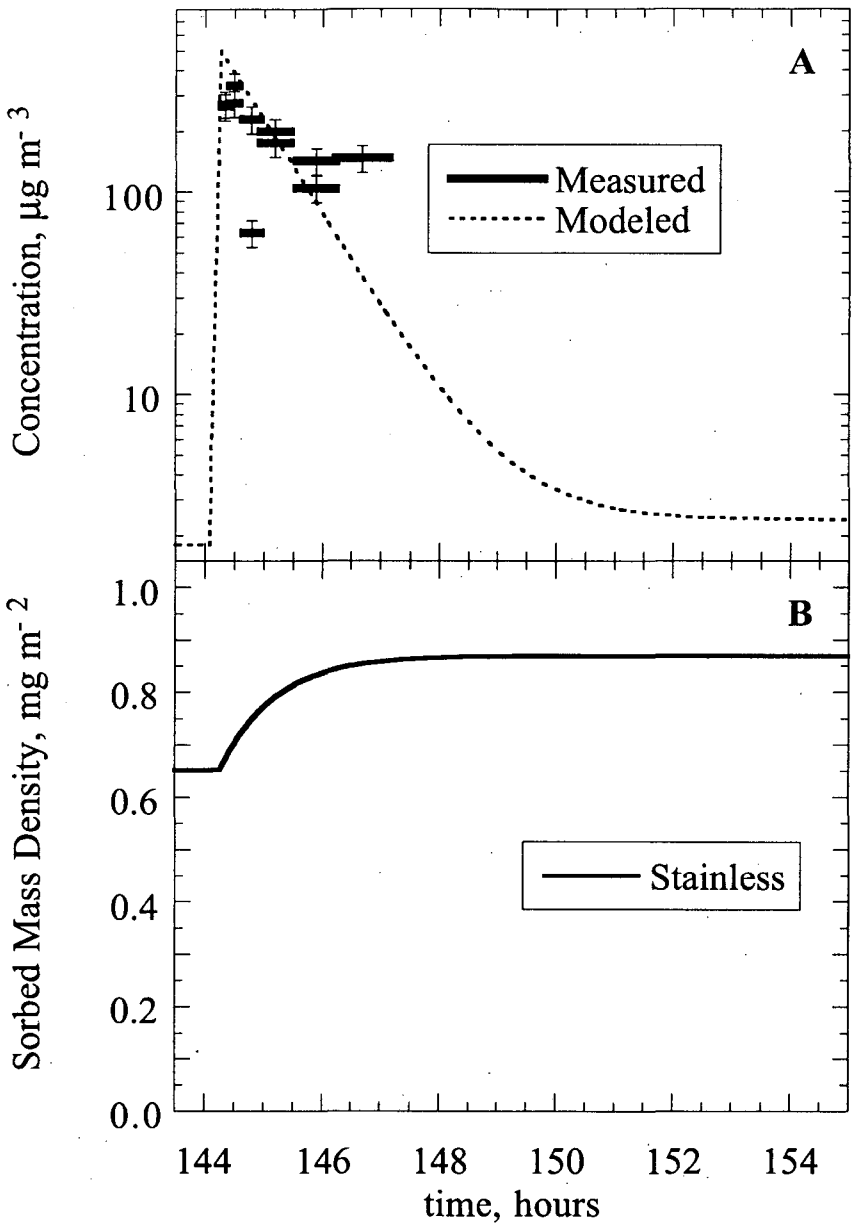

Figure 3.10 Experimental data, estimated errors, and diffusion model predictions for gas-phase (**A**) and stainless steel sorbed phenanthrene (**B**) for 10 hours following the fourth injection of phenanthrene in experiment 3C. The lengths of the horizontal bars and their positions relative to the time axis in panel **A** indicate the duration and timing of Tenax-TA sorbent samples.

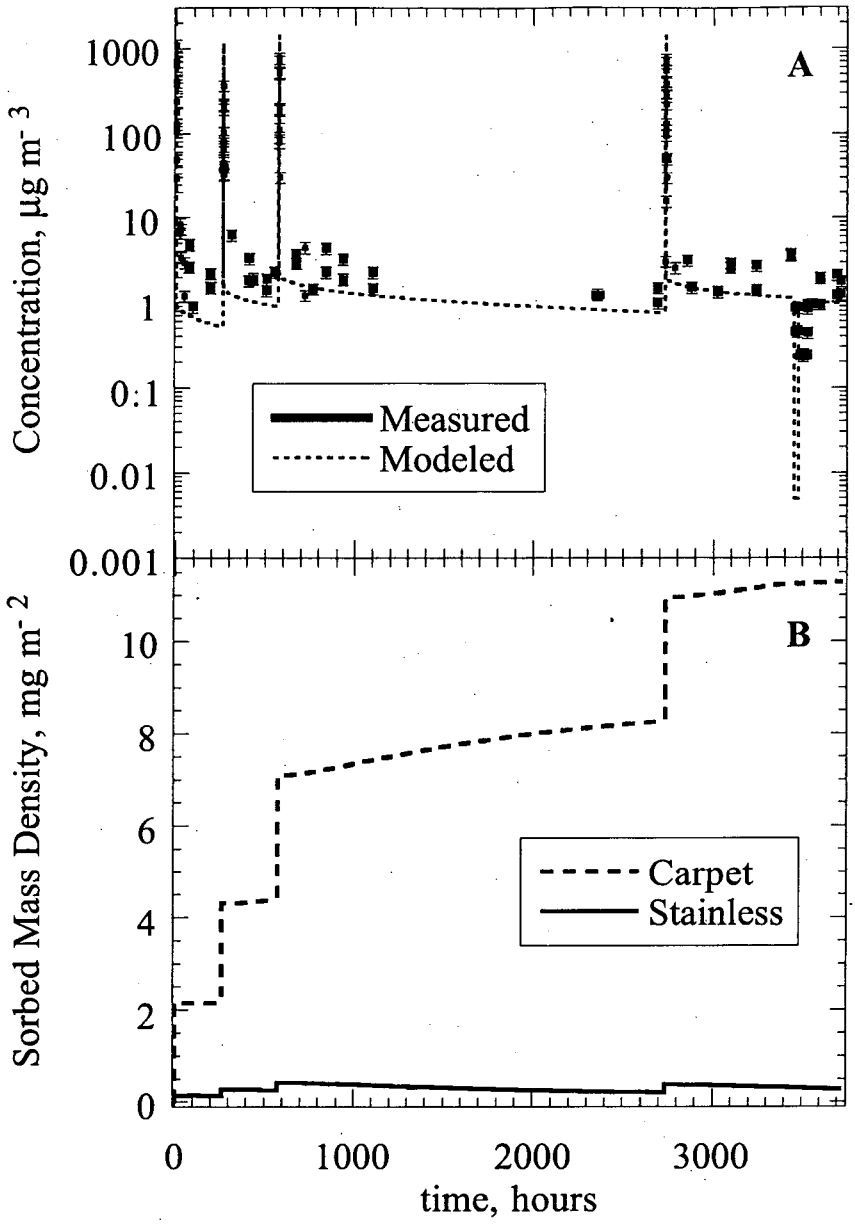

Figure 3.11 Experimental data, estimated errors, and diffusion model predictions for gas-phase (**A**) and stainless steel adsorbed and carpet adsorbed and absorbed phenanthrene (**B**) in experiment 3D.

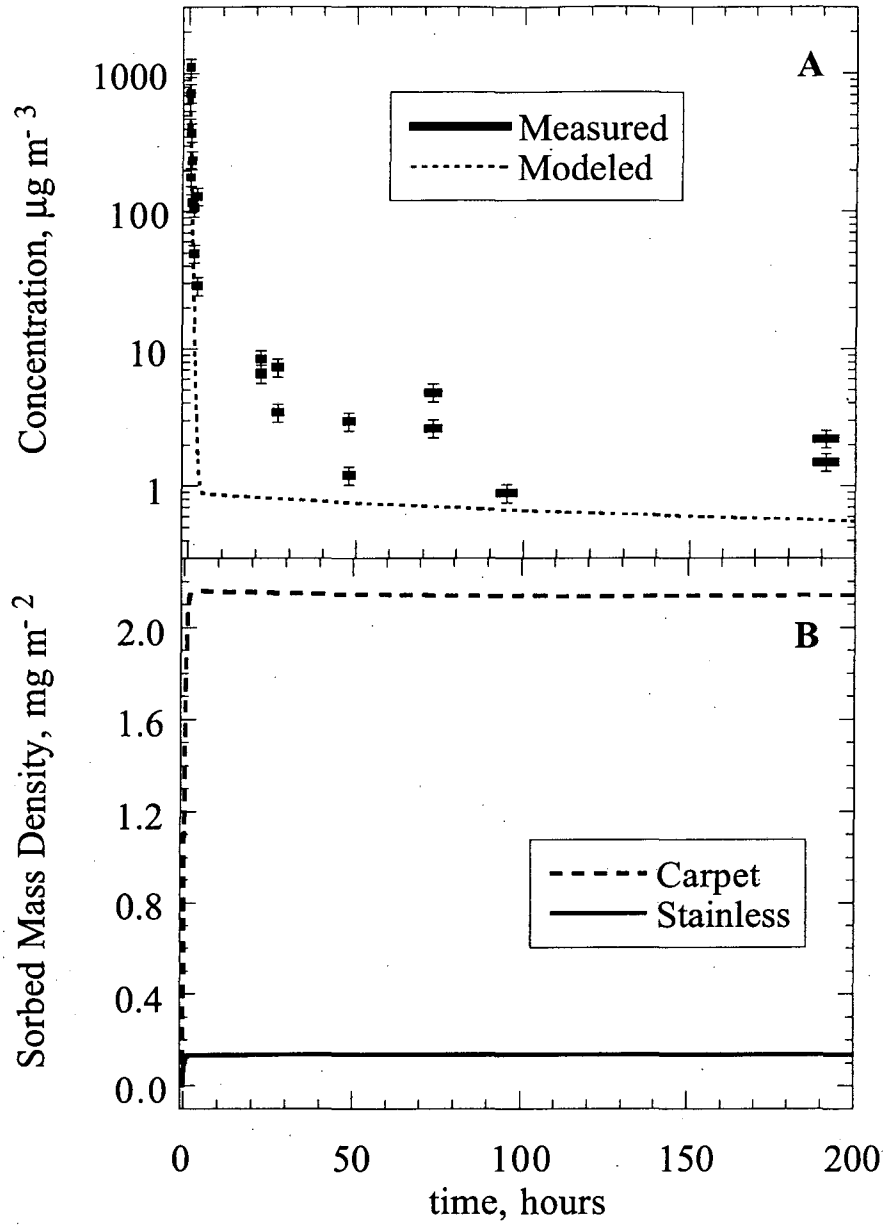

Figure 3.12 Experimental data, estimated errors, and diffusion model predictions for gas-phase (**A**) and stainless steel and carpet sorbed nicotine (**B**) for 200 hours following the first injection of phenanthrene in experiment 3D. The lengths of the horizontal bars and their positions relative to the time axis in panel **A** indicate the duration and timing of Tenax-TA samples.

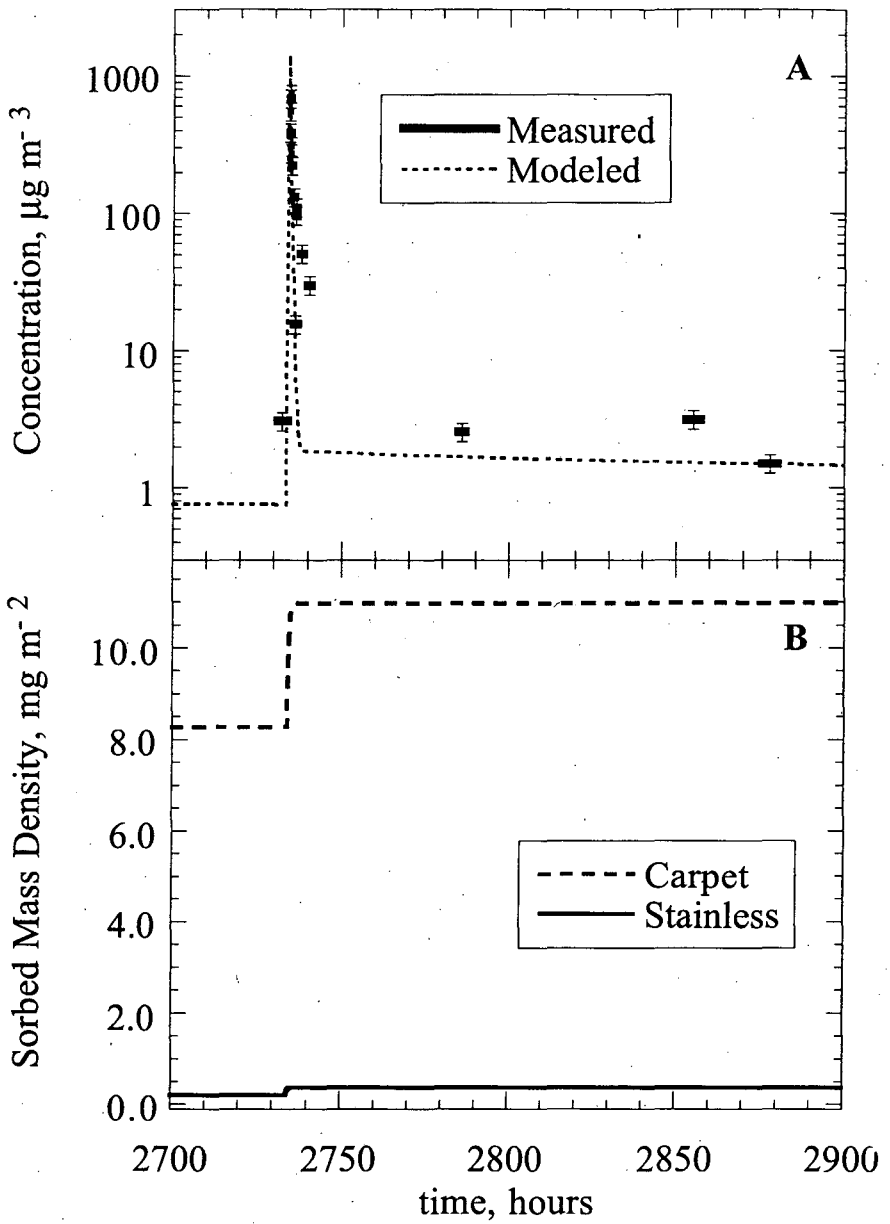

Figure 3.13 Experimental data, estimated errors, and diffusion model predictions for gas-phase (**A**) and stainless steel and carpet sorbed phenanthrene (**B**) for 200 hours following the fourth injection of phenanthrene in experiment 3D. The lengths of the horizontal bars and their positions relative to the time axis in panel **A** indicate the duration and timing of Tenax-TA samples.

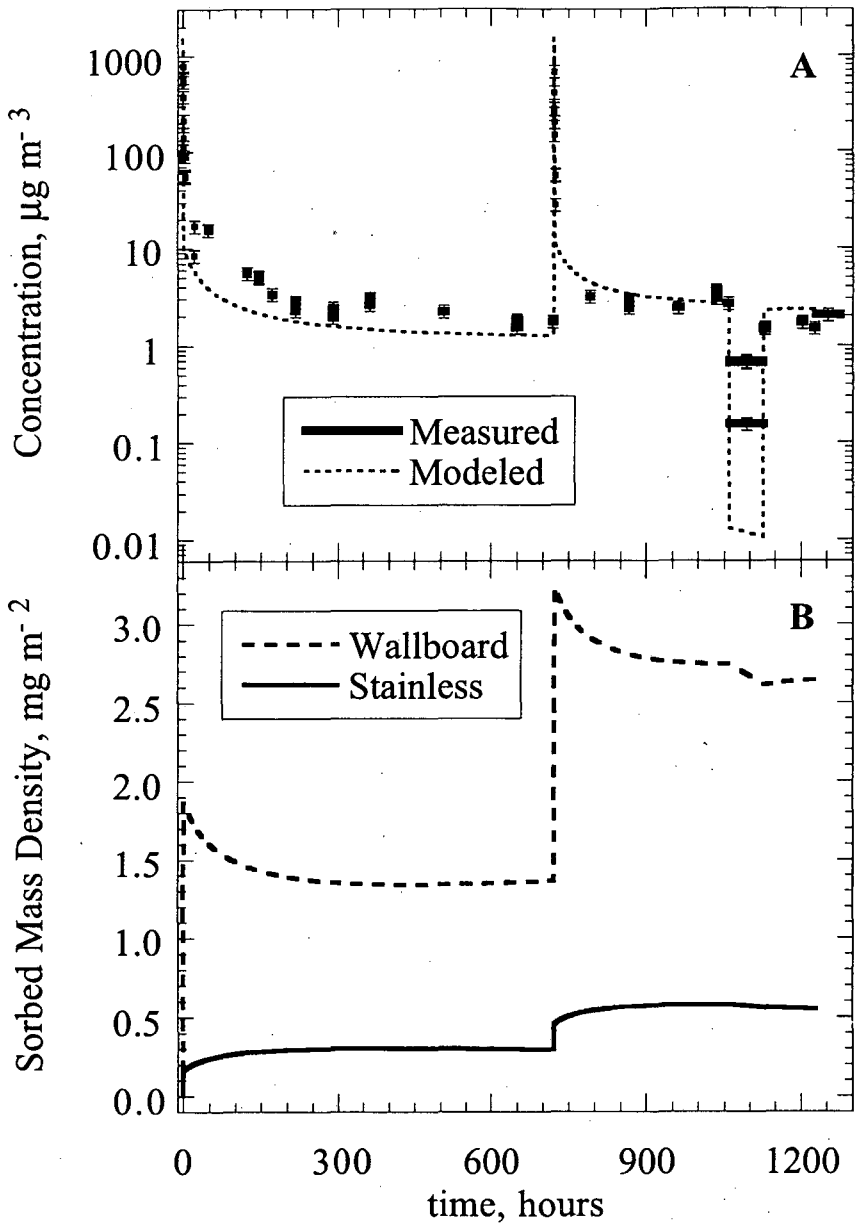

Figure 3.14 Experimental data, estimated errors, and diffusion model predictions for gas-phase (**A**) and stainless steel adsorbed and wallboard adsorbed and absorbed phenanthrene (**B**) in experiment 3E.

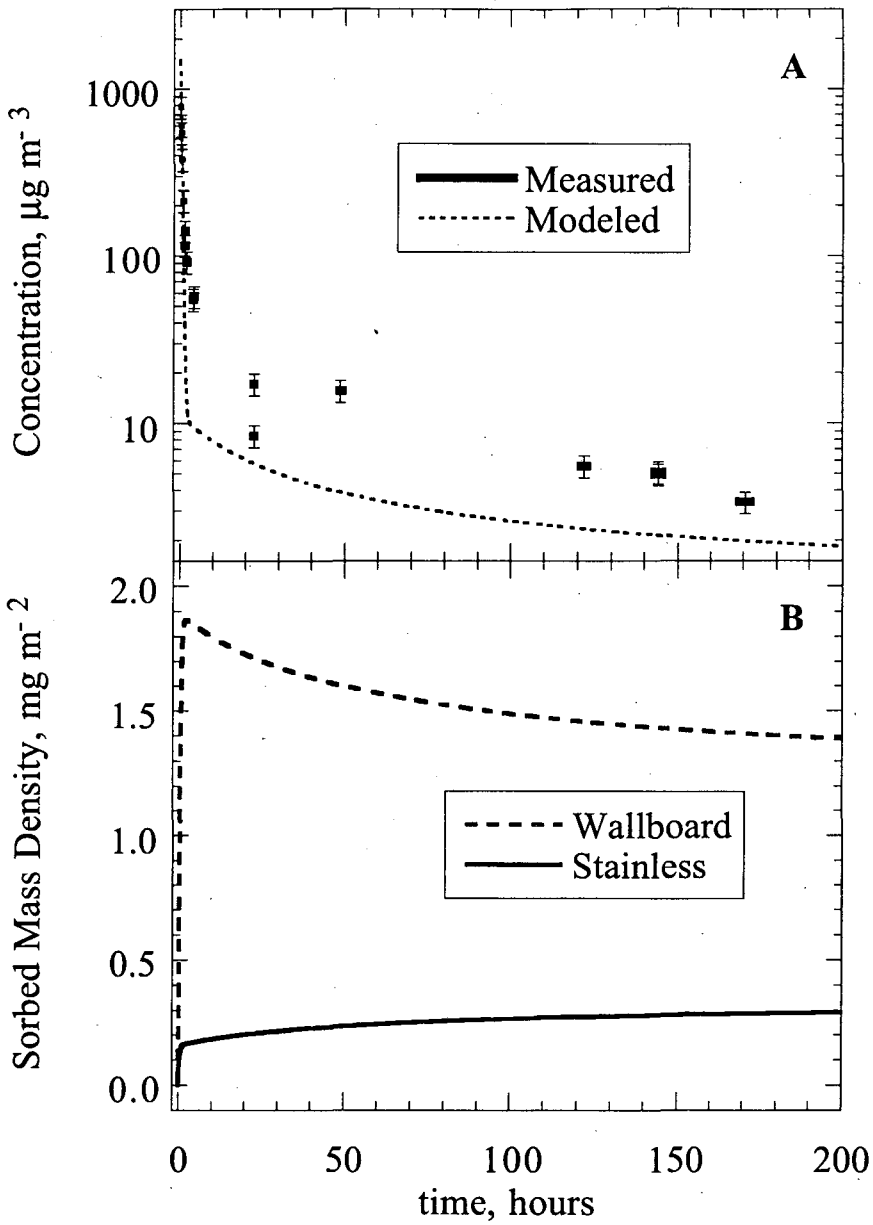

Figure 3.15 Experimental data, estimated errors, and diffusion model predictions for gas-phase (**A**) and stainless steel and wallboard sorbed phenanthrene (**B**) for 200 hours following the first injection of phenanthrene in experiment 3E. The lengths of the horizontal bars and their positions relative to the time axis in panel **A** indicate the duration and timing of Tenax-TA samples.

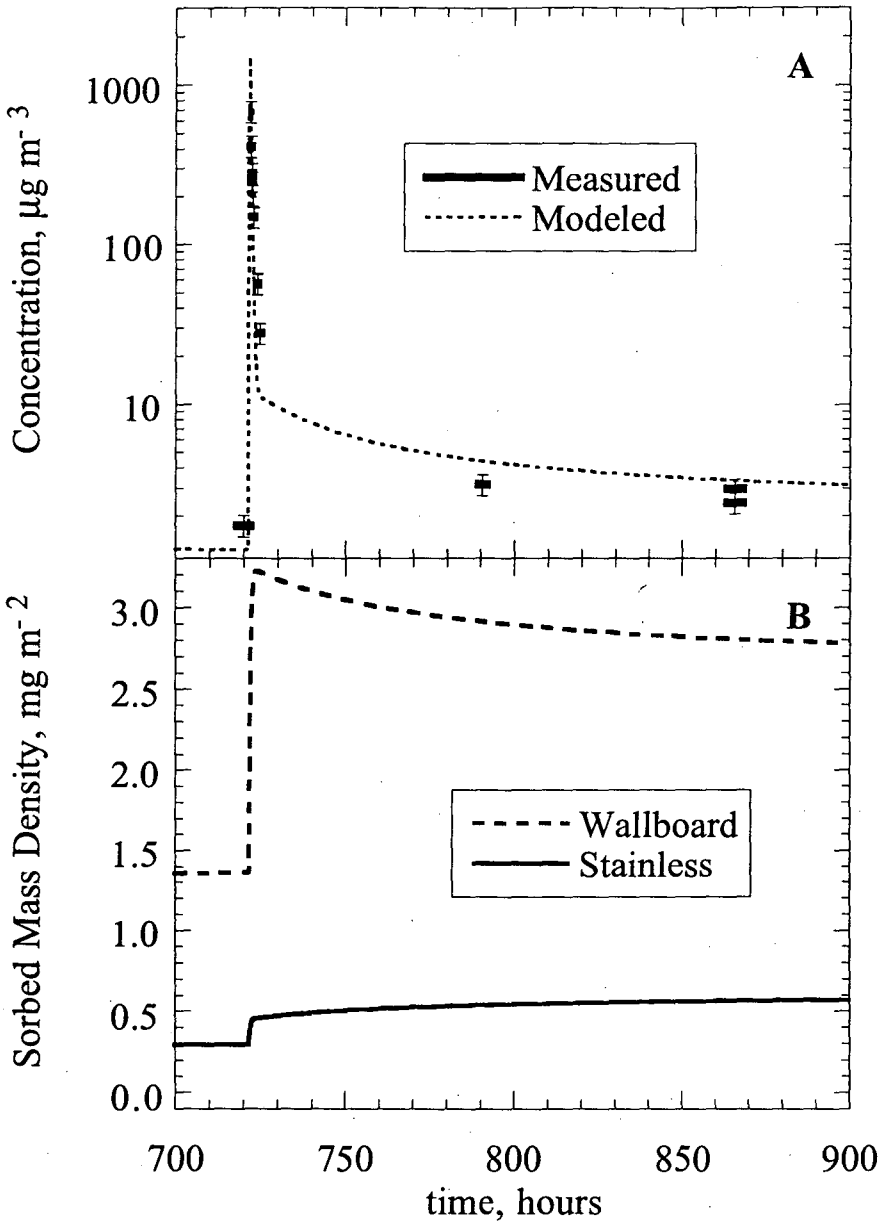

Figure 3.16 Experimental data, estimated errors, and diffusion model predictions for gas-phase (**A**) and stainless steel and wallboard sorbed phenanthrene (**B**) for 200 hours following the second injection of phenanthrene in experiment 3E. The lengths of the horizontal bars and their positions relative to the time axis in panel **A** indicate the duration and timing of Tenax-TA samples.

TABLES

Table 3.1 Summary of experimental parameters and kinetic model initial conditions for experiments 3A-3E.

	Sorbate-Sorbent				
	Nicotine		Phenanthrene		
	Carpet	Wallboard	Stainless Steel	Carpet	Wallboard
Experiment number	3A	3B	3C	3D	3E
Sealed flow rate (Q_T), $m^3\ h^{-1}$	0.34	0.34	0.3	0.34	0.34
Vented flow rate (Q_T), $m^3\ h^{-1}$	20	20	60	20	20
Total SVOC mass emitted, mg	250	301	40	102	60
Number of discrete emission events	5	2	4	4	2
Total experiment duration, days	56	70	16	155	54
Number of fitted parameters in sorption dynamics model	3	3	1	3	3

Table 3.1b SVOC mass emitted in each phase of experiments 3A – 3E

Experiment (SVOC, sorbent)	Stage	Emitted Mass (mg)	Phase Start Time (h)	Air-Exchange Rate During Phase (h^{-1})
3A	1	50	0.00	0.017
(nicotine, carpet)	2	50	333.55	0.017
	3	50	407.55	0.017
	4	50	528.00	0.017
	5	50	647.23	0.017
	6	0	1106.50	1
	7	0	1172.77	0.17
	8	0	1222.97	0.017
3B	1	192	0.00	0.017
(nicotine, wallboard)	2	109	698.37	0.017
	3	0	1231.95	1
	4	0	1466.72	0.017
3C	1	10	0.00	0
(phenanthrene, stainless steel)	2	10	48.44	0.015
	3	10	98.86	0.015
	4	10	144.27	0
	5	0	214.89	3
	6	0	290.61	0.015

Table 3.1b (Continued)

Experiment (SVOC, sorbent)	Stage	Emitted Mass (mg)	Phase Start Time (h)	Air-Exchange Rate During Phase (h^{-1})
3D	1	23	0.00	0.02
(phenanthrene, carpet)	2	23	262.15	0.017
	3	28	574.07	0.017
	4	28	2734.15	0.017
	5	0	3452.65	1
	6	0	3477.27	0.17
3E	1	30	0.00	0.017
(phenanthrene, wallboard)	2	30	721.72	0.017
	3	0	1060.55	1
	4	0	1126.52	0.017

Table 3.2 Isotherm parameters for nicotine and phenanthrene sorption on stainless steel, carpet, and painted wallboard. Units are mg m^{-3} for concentration and mg m^{-2} for sorbed mass.

Sorbate and Sorbent	Equation
Nicotine:	
Stainless Steel[a]	$M = 4.69\ C^{0.57}$
Carpet[b]	$M = 19400\ C$
Painted Wallboard[b]	$M = 1500\ C$
Phenanthrene:	
Stainless Steel	$M = 360\ C$
Carpet[b]	$M = 2180\ C$
Painted Wallboard[b]	$M = 136\ C$

[a] Nicotine-stainless steel equilibrium data were obtained in Chapter 2

[b] Equilibrium parameters for SVOC sorption on carpet and painted wallboard are estimated as the ratio of the adsorption and desorption rate constants for sorption the air-sorbent interface. Equilibrium was not achieved in experiments with these materials.

Table 3.3 Kinetic sorption parameters for nicotine and phenanthrene interactions with stainless steel, carpet, and painted wallboard.

SVOC/Sorbent	Parameter	Best Fit Value
Nicotine:		
Stainless Steel[a]:	$n_{a_{ns}}$, no units	1.47
	$n_{d_{ns}}$, no units	2.59
	$k_{a_{ns}}$, $\mathrm{mg}^{1-n_{a_{ns}}}\,\mathrm{m}^{3n_{a_{ns}}-2}\,\mathrm{h}^{-1}$	2.52
	$k_{d_{ns}}$, $\mathrm{mg}^{1-n_{d_{ns}}}\,\mathrm{m}^{2n_{d_{ns}}-2}\,\mathrm{h}^{-1}$	0.029
Carpet:	$k_{a_{nc}}$, $\mathrm{m\,h^{-1}}$	7.8
	$k_{d_{nc}}$, $\mathrm{h^{-1}}$	0.00040
	$D_{b_{nc}}$, $\mathrm{m^2\,h^{-1}}$	2.5×10^{-10}
Wallboard:	$k_{a_{nw}}$ $\mathrm{m\,h^{-1}}$	1.98
	$k_{d_{nw}}$, $\mathrm{h^{-1}}$	0.0013
	$D_{b_{nw}}$, $\mathrm{m^2\,h^{-1}}$	2.9×10^{-10}
Phenanthrene:		
Stainless Steel:	$n_{a_{ps}}$, no units	1
	$n_{d_{ps}}$, no units	1
	$k_{a_{ps}}$, $\mathrm{h^{-1}}$	0.47
	$k_{d_{ps}}$, $\mathrm{h^{-1}}$	0.0013
Carpet:	$k_{a_{pc}}$, $\mathrm{m\,h^{-1}}$	4.98
	$k_{d_{pc}}$, $\mathrm{h^{-1}}$	0.0023
	$D_{b_{pc}}$, $\mathrm{m^2\,h^{-1}}$	2.7×10^{-10}
Wallboard:	$k_{a_{pw}}$ $\mathrm{m\,h^{-1}}$	3.66
	$k_{d_{pw}}$, $\mathrm{h^{-1}}$	0.027
	$D_{b_{pw}}$, $\mathrm{m^2\,h^{-1}}$	3.0×10^{-8}

- Sorbent thicknesses used in model predictions are 0.0025 m for carpet and 0.0095 m for wallboard. These values are based on the thickness of the backing layer in the tested carpet samples and the full thickness of the tested wallboard samples.

[a] Based on fully nonlinear model applied to experiment 2C (Table 2.2)

Table 3.4 Gas-phase nicotine sample data from experiment 3A (nicotine-carpet).

Sample Number	Sample Start Time, hours	Sample End Time, hours	Measured Concentration, $\mu g\ m^{-3}$	Modeled Concentration*, $\mu g\ m^{-3}$
1	0.18	0.35	353	298
2	0.47	0.82	150	52
3	0.47	1.13	161	35
4	1.42	2.43	60	7.7
5	1.42	2.43	75	7.7
6	20.42	22.98	3.3	4.2
7	23.02	26.37	2.6	4.0
8	46.78	50.82	1.7	2.5
9	46.78	50.82	2.0	2.5
10	69.65	73.95	1.7	1.8
11	139.33	144.50	1.2	0.9
12	333.73	333.83	376	356
13	333.73	333.87	350	326
14	333.90	334.10	275	113
15	333.90	334.17	224	100
16	334.40	334.73	133	20
17	334.40	334.90	111	19
18	335.30	335.72	62	12
19	335.30	336.05	52	12
20	336.57	337.42	28	11
21	337.43	338.85	19	11
22	356.05	359.37	4.4	5.8
23	359.38	362.43	4.4	5.3
24	381.83	385.80	3.1	3.3
25	385.83	387.12	4.6	3.1
26	404.95	407.10	3.5	2.3
27	407.72	407.80	536	417
28	407.72	407.83	362	380
29	407.92	408.08	293	117
30	407.92	408.17	272	101
31	408.33	408.63	215	31
32	408.33	408.70	168	30
33	408.92	409.42	184	21
34	410.71	411.27	54	19
35	480.13	483.25	3.7	2.8
36	502.48	504.47	3.9	2.1
37	504.48	505.28	12	2.1

Table 3.4 (Continued)

Sample Number	Sample Start Time, hours	Sample End Time, hours	Measured Concentration, μg m^{-3}	Modeled Concentration*, μg m^{-3}
38	524.92	527.87	3.3	1.7
39	528.13	528.20	492	558
40	528.13	528.23	364	502
41	528.27	528.35	304	228
42	528.27	528.40	278	202
43	528.50	528.67	224	67
44	528.50	528.73	188	61
45	528.92	529.18	131	25
46	528.92	529.18	144	25
47	529.42	529.83	95	19
48	529.42	530.00	84	19
49	530.17	531.05	54	17
50	549.23	551.55	5.7	8.0
51	549.23	551.55	7.5	8.0
52	551.57	555.18	6.6	7.4
53	551.57	555.18	6.1	7.4
54	573.08	576.17	3.2	4.4
55	573.08	576.17	2.9	4.4
56	576.22	578.88	3.7	4.2
57	576.22	578.88	3.4	4.2
58	644.93	647.18	3.8	1.8
59	644.93	647.18	3.7	1.8
60	647.40	647.45	445	475
61	647.40	647.45	388	475
62	647.48	647.58	317	244
63	647.48	647.58	262	244
64	647.67	647.78	221	96
65	647.90	648.07	165	41
66	648.33	648.70	97	21
67	649.07	649.58	60	18
68	650.23	651.08	34	17
69	650.23	651.08	33	17
70	669.85	672.35	7.6	7.8
71	669.85	672.35	8.0	7.8
72	672.38	675.20	7.1	7.2
73	691.27	693.72	5.9	4.7
74	691.27	693.72	5.5	4.7

Table 3.4 (Continued)

Sample Number	Sample Start Time, hours	Sample End Time, hours	Measured Concentration, μg m^{-3}	Modeled Concentration*, μg m^{-3}
75	693.77	696.90	5.4	4.4
76	693.77	696.90	5.0	4.4
77	718.17	720.03	5.9	3.1
78	720.07	723.13	5.4	3.0
79	720.07	723.13	5.3	3.0
80	740.97	743.90	4.4	2.4
81	740.97	743.90	4.1	2.4
82	743.93	747.45	4.1	2.3
83	812.55	815.85	5.5	1.4
84	812.55	815.85	4.4	1.4
85	1054.65	1058.57	4.4	0.7
86	1106.52	1124.75	0.5	0.5
87	1106.52	1148.30	0.4	0.5
88	1148.35	1172.73	0.3	0.5
89	1148.35	1172.73	0.3	0.5
90	1172.77	1196.67	0.5	0.6
91	1172.77	1196.67	0.5	0.6
92	1196.72	1222.92	0.6	0.6
93	1196.72	1222.92	0.6	0.6
94	1222.97	1246.00	0.7	0.6
95	1222.97	1246.00	0.8	0.6
96	1246.05	1271.22	0.8	0.6
97	1246.05	1271.22	1.0	0.6
98	1271.25	1297.73	1.2	0.6
99	1271.25	1297.73	1.2	0.6
100	1297.77	1322.28	1.0	0.5

- Model predictions are based on the best fit to the measured data with the porous sorbent sorption model (equation 3.3–3.6 using the parameters listed in Table 3.3).

Table 3.5 Gas-phase nicotine sample data from experiment 3B (nicotine-wallboard).

Sample Number	Sample Start Time, hours	Sample End Time, hours	Measured Concentration, $\mu g\ m^{-3}$	Modeled Concentration*, $\mu g\ m^{-3}$
1	0.08	0.15	4865	2283
2	0.18	0.25	1392	1097
3	0.30	0.42	1055	614
4	0.30	0.42	882	614
5	0.57	0.70	493	409
6	0.87	1.00	451	372
7	1.25	1.38	364	355
8	1.78	1.93	299	337
9	2.45	2.68	208	316
10	3.17	3.72	159	292
11	4.30	4.74	143	267
12	7.26	23.30	83	133
13	23.30	24.10	44	81
14	48.10	49.20	35	35
15	71.20	72.60	26	22
16	142.80	144.70	23	13
17	190.90	192.90	35	11
18	311.70	313.50	18	9.7
19	336.70	338.50	0.9	9.6
20	359.00	361.10	0.9	9.5
21	648.80	652.70	0.5	9.2
22	673.80	677.70	0.7	9.2
23	698.80	698.90	285	299
24	699.00	699.10	199	215
25	701.30	701.90	170	149
26	710.00	711.00	104	93
27	719.70	720.00	72	64
28	740.00	740.60	30	37
29	740.00	740.60	41	37
30	807.00	808.00	25	19
31	807.00	808.00	21	19
32	1230.00	1232.00	22	14
33	1230.00	1232.00	7.5	9.3
34	1233.00	1273.00	2.5	0.04
35	1233.00	1273.00	1.7	0.04
36	1275.00	1325.00	2.0	0.03

Table 3.5 (Continued)

Sample Number	Sample Start Time, hours	Sample End Time, hours	Measured Concentration, $\mu g\ m^{-3}$	Modeled Concentration*, $\mu g\ m^{-3}$
37	1403	1459	1.0	0.03
38	1403	1459	0.8	0.03
39	1467	1513	5.2	8.4
40	1467	1513	4.0	8.4
41	1600	1640	10	9.0

* Model predictions are based on the best fit to the measured data with the porous sorbent sorption model (equation 3.3–3.6 using the parameters listed in Table 3.3).

Table 3.6 Gas-phase phenanthrene sample data from experiment 3C (phenanthrene-stainless steel).

Sample Number	Sample Start Time, hours	Sample End Time, hours	Measured Concentration, $\mu g\ m^{-3}$	Modeled Concentration*, $\mu g\ m^{-3}$
1	0.04	0.21	297	438
2	0.04	0.21	360	438
3	0.23	0.43	114	352
4	0.48	0.81	106	252
5	0.48	0.81	144	252
6	1.06	1.63	67	120
7	1.93	2.68	53	44
8	1.93	2.68	85	44
9	44.89	48.34	1.1	0.6
10	44.89	48.34	1.5	0.6
11	70.91	73.54	3.5	1.2
12	70.91	73.54	7.6	1.2
13	73.57	75.14	14	1.2
14	73.57	75.14	4.5	1.2
15	92.40	94.46	2.6	1.2
16	92.40	94.46	4.0	1.2
17	96.50	98.81	2.7	1.2
18	96.50	98.81	4.7	1.2
19	115.89	118.71	6.4	1.8
20	118.72	121.18	6.2	1.8
21	118.72	121.18	16	1.8
22	121.18	123.13	5.1	1.8
23	140.44	143.09	5.5	1.8
24	140.44	143.09	5.8	1.8
25	144.28	144.41	265	474
26	144.28	144.41	273	474
27	144.41	144.58	276	402
28	144.41	144.58	337	402
29	144.64	144.92	229	291
30	144.93	145.43	175	190
31	144.93	145.43	200	190
32	145.54	146.21	104	91
33	145.54	146.21	142	91
34	146.21	147.13	148	41

Table 3.6 (Continued)

Sample Number	Sample Start Time, hours	Sample End Time, hours	Measured Concentration, $\mu g\ m^{-3}$	Modeled Concentration*, $\mu g\ m^{-3}$
35	213.06	214.76	6.9	2.4
36	213.06	214.76	7.0	2.4
37	214.89	240.26	0.4	0.6
38	214.89	240.26	0.7	0.6
39	240.28	266.89	0.4	0.6
40	240.28	266.89	0.5	0.6
41	266.91	289.99	0.7	0.6
42	266.91	290.61	0.4	0.6
44	290.63	307.88	1.6	2.1
45	307.90	314.43	2.1	2.2
46	314.43	331.31	2.1	2.2
47	331.41	357.84	1.1	2.2
48	384.13	403.49	1.3	2.2
49	384.13	403.49	1.8	2.2

- Model predictions are based on the best fit to the measured data with the nonporous sorbent sorption model (equation 2.4 and 2.5 using the parameters listed in Table 3.3 with n_a and n_d = 1).

Table 3.7 Gas-phase phenanthrene sample data from experiment 3D (phenanthrene-carpet).

Sample Number	Sample Start Time, hours	Sample End Time, hours	Measured Concentration, μg m^{-3}	Modeled Concentration*, μg m^{-3}
1	0.23	0.33	723	553
2	0.23	0.33	1110	553
3	0.38	0.57	179	333
4	0.38	0.57	378	333
5	0.63	0.89	115	161
6	0.63	0.89	237	161
7	1.26	1.72	49	31
8	1.26	1.72	107	31
9	2.05	2.68	29	9.7
10	2.05	2.68	129	9.7
11	21.05	21.83	8.4	6.1
12	21.05	21.83	22	6.1
13	25.84	26.97	7.3	5.8
14	25.84	26.97	15	5.8
15	46.97	48.43	3.0	4.9
16	46.97	48.43	8.2	4.9
17	71.47	74.31	4.6	4.0
18	71.47	74.31	4.8	4.0
19	93.08	96.88	0.9	3.5
20	188.15	193.82	2.2	2.2
21	188.15	193.82	4.5	2.2
22	262.38	262.51	223	531
23	262.53	262.68	193	348
24	262.74	262.96	104	189
25	262.74	262.96	213	189
26	263.05	263.48	367	72
27	263.79	264.39	45	16
28	264.48	265.14	32	10
29	264.48	265.14	71	10
30	265.15	266.14	40	9.2
31	266.23	267.02	33	9.0
32	310.61	312.11	6.2	6.5
33	404.83	408.83	1.8	4.2
34	428.83	432.83	1.9	3.9

Table 3.7 (Continued)

Sample Number	Sample Start Time, hours	Sample End Time, hours	Measured Concentration, $\mu g\ m^{-3}$	Modeled Concentration*, $\mu g\ m^{-3}$
35	503.97	507.02	1.4	3.4
36	503.97	507.02	1.9	3.4
37	550.23	554.40	2.3	3.2
38	574.22	574.33	704	844
39	574.22	574.33	778	844
40	574.38	574.50	515	543
41	574.60	574.75	187	298
42	574.95	575.12	114	123
43	575.39	575.68	197	42
44	576.00	576.38	90	18
45	576.88	577.38	79	13
46	577.88	578.80	30	12
47	670.10	672.10	2.9	7.2
48	670.10	672.10	3.6	7.2
49	719.44	722.75	4.4	6.1
50	719.44	722.75	6.2	6.1
51	763.88	767.95	31	5.6
52	838.82	841.90	4.3	5.0
53	838.82	841.90	14	5.0
54	932.25	936.42	3.2	4.7
55	932.25	936.42	8.9	4.7
56	1099.03	1105.03	2.3	4.4
57	1099.03	1105.03	4.5	4.4
58	1341.08	1346.25	6.2	4.3
59	2687.50	2691.03	1.0	3.7
60	2687.50	2691.03	1.5	3.7
61	2730.92	2733.82	3.1	3.7
62	2734.52	2734.60	745	477
63	2734.72	2734.82	277	286
64	2734.72	2734.82	309	286
65	2734.98	2735.12	224	142
66	2735.38	2735.65	131	51
67	2735.98	2736.39	96	20
68	2735.98	2736.39	110	20
69	2737.61	2738.43	50	13
70	2739.69	2740.68	30	12
71	2759.62	2760.73	16	11

Table 3.7 (Continued)

Sample Number	Sample Start Time, hours	Sample End Time, hours	Measured Concentration, μg m^{-3}	Modeled Concentration*, μg m^{-3}
72	2784.81	2786.83	2.6	9.5
73	2853.12	2857.05	3.1	7.3
74	2875.72	2880.12	1.5	6.9
75	3021.43	3026.73	1.3	5.8
76	3093.18	3098.00	2.6	5.6
77	3093.18	3098.00	2.9	5.6
78	3237.02	3241.42	1.4	5.3
79	3237.02	3241.42	2.7	5.3
80	3430.17	3434.00	3.7	5.2
81	3430.17	3434.00	4.6	5.2
82	3452.65	3480.43	0.5	3.6
83	3452.65	3480.43	0.9	3.6
84	3480.46	3525.14	0.2	4.4
85	3480.46	3525.14	0.2	4.4
86	3525.27	3529.97	0.4	4.3
87	3525.27	3529.97	0.9	4.3
88	3549.69	3554.98	0.9	4.3
89	3596.28	3601.24	0.9	4.3
90	3596.28	3601.24	1.9	4.3
91	3691.98	3696.98	1.2	4.2
92	3691.98	3696.98	2.1	4.2
93	3715.87	3719.42	1.3	4.2
94	3715.87	3719.42	1.8	4.2

- Model predictions are based on the best fit to the measured data with the porous sorbent sorption model (equation 3.3–3.6 using the parameters listed in Table 3.3).

Table 3.8 Gas-phase phenanthrene sample data from experiment 3E (phenanthrene-wallboard).

Sample Number	Sample Start Time, hours	Sample End Time, hours	Measured Concentration, $\mu g\ m^{-3}$	Modeled Concentration*, $\mu g\ m^{-3}$
1	0.19	0.23	778	824
2	0.29	0.34	546	604
3	0.29	0.34	605	604
4	0.46	0.53	378	366
5	0.64	0.73	214	215
6	0.86	0.96	214	117
7	1.25	1.38	115	43
8	1.25	1.38	141	43
9	1.79	1.96	92	18
10	3.71	3.99	55	9.5
11	3.99	4.29	57	9.4
12	22.38	22.66	8.4	5.8
13	22.38	22.66	17	5.8
14	48.43	49.18	16	3.9
15	121.1	122.9	5.6	2.3
16	143.3	145.6	5.0	2.1
17	143.3	145.6	5.1	2.1
18	168.8	172.1	3.4	2.0
19	214.1	217.7	2.3	1.8
20	214.1	217.7	2.8	1.8
21	286.7	292.2	2.0	1.6
22	286.7	292.2	2.4	1.6
23	359.6	363.7	2.6	1.5
24	359.6	363.7	3.0	1.5
25	503.3	509.6	2.2	1.3
26	646.3	653.2	1.5	1.3
27	646.3	653.2	1.8	1.3
28	718.0	721.7	1.8	1.2
29	721.9	721.9	680	884
30	722.0	722.0	414	648
31	722.2	722.2	248	380
32	722.2	722.2	280	380
33	722.4	722.5	204	198
34	722.8	722.8	148	78

Table 3.8 (Continued)

Sample Number	Sample Start Time, hours	Sample End Time, hours	Measured Concentration, $\mu g\ m^{-3}$	Modeled Concentration*, $\mu g\ m^{-3}$
35	723.9	724.0	56	14
36	723.9	724.0	57	14
37	724.4	724.7	28	12
38	789.5	791.7	3.2	4.4
39	863.7	868.2	2.4	3.3
40	863.7	868.2	3.0	3.3
41	958.0	964.5	2.4	2.9
42	1032	1038	3.0	2.7
43	1032	1038	3.6	2.7
44	1055	1060	2.7	2.7
45	1061	1127	0.7	1.8
46	1061	1127	0.7	1.8
47	1127	1132	1.5	2.1
48	1127	1132	1.5	2.1
49	1199	1205	1.7	2.3
50	1224	1228	1.5	2.3

- Model predictions are based on the best fit to the measured data with the porous sorbent sorption model (equation 3.3–3.6 using the parameters listed in Table 3.3).

Chapter 4. Nicotine as a Marker for Environmental Tobacco Smoke — Implications of Sorption on Indoor Surface Materials*

ABSTRACT

Recently developed models and data describing the interactions of gas-phase semivolatile organic compounds with indoor surfaces are employed to examine the effects of sorption on nicotine's suitability as an environmental tobacco smoke (ETS) marker. Using parameters from our studies of nicotine sorption on carpet, painted wallboard, and stainless steel and previously published data on ETS particle deposition, the dynamic behavior of nicotine was modeled in two different indoor environments: a house and a stainless steel chamber. The results show that apparently contradictory observations of nicotine's behavior in indoor air can be understood by considering the effects of sorption under different experimental conditions. In indoor environments in which smoking has occurred regularly for an extended period, the sorbed mass of nicotine is very large relative to the mass emitted by a single cigarette. The importance of nicotine adsorption relative to ventilation as a gas-phase removal mechanism is reduced. Where smoking occurs less regularly or the indoor surfaces are cleaned prior to smoking (as in a laboratory chamber), nicotine deposition is more significant. Nicotine concentrations closely track the levels of other ETS constituents in environments with habitual smoking if the data are averaged over a period significantly longer than the period between cigarette combustion episodes. However, nicotine is not a suitable tracer for predicting ETS exposures at fine time scales or in settings where smoking occurs infrequently and irregularly.

---

* This chapter is based on a paper published elsewhere as Van Loy M.D., Daisey J.M., and Nazaroff W.W. Nicotine as a marker for environmental tobacco smoke: Implications of sorption on indoor surface materials, *Journal of the Air and Waste Management Association* **1998**, *48*, 959-968.

INTRODUCTION

Environmental tobacco smoke (ETS), a complex mixture of gases and particles generated by combustion of tobacco products indoors, consists of a diluted and aged mixture of sidestream smoke emitted from a burning cigarette plus mainstream smoke exhaled by the smoker. Sidestream smoke is estimated to contribute approximately 90% of the airborne ETS mass (Eatough, 1993).. ETS is a major source of both particle and gas-phase indoor air contamination (Eatough, 1993) and has been implicated as a causal factor in many adverse health effects, including lung cancer, heart disease, childhood asthma, and other respiratory diseases (Aviado, 1990; Wynder and Kabat, 1990; USEPA, 1992; Steenland, 1992; Glantz and Parmley, 1995). ETS is a dynamic mixture of hundreds to thousands of compounds that are variably distributed between the gas and particle phases. The composition of ETS in an indoor environment may evolve because of exchange between the gas and particle phases, dilution, ventilation, and deposition onto and re-emission from indoor surface materials (Eatough, 1993; Pritchard *et al.*, 1988; Baker *et al.*, 1988; Eatough *et al.*, 1989a; Baker and Proctor, 1990; Nelson and Conrad, 1997.).

To accurately assess the risks associated with ETS exposure, it is necessary to develop a method to quantify ETS concentrations in indoor air. Because of the large number of ETS constituents and the lack of adequate information about the specific health risks associated with individual species, a common approach for ETS exposure assessment involves the measurement of one or more marker species. The National Research Council (1986) has defined the desirable attributes of an ETS marker. It should be unique to tobacco smoke and be emitted at similar rates for different types and brands of tobacco products. Also, cigarettes must emit sufficient mass of the marker to allow accurate quantification of its concentrations at low smoking rates, and the marker must be emitted in consistent proportions to other compounds of interest for a range of tobacco products under various combustion conditions. Researchers subsequently defined

another valuable characteristic: the marker's dynamic behavior in indoor air must be similar to that of the compounds for which it serves as a surrogate (Eatough, 1993; Baker *et al.*, 1988; Eatough *et al.*, 1989bc; Nelson *et al.*, 1990; Nelson *et al.*, 1992, Daisey *et al.*, 1998).

The most common marker for ETS is nicotine ($C_{10}H_{14}N_2$, molecular weight = 162.2 g mol^{-1}), a naturally occurring alkaloid found in tobacco leaves. During tobacco combustion, some of the nicotine in a cigarette volatilizes into the mainstream and sidestream smoke while the remainder pyrolyzes to form other nitrogenated products such as ethenyl pyridine, pyridine, and pyrrole (Baker, 1981; Baker and Proctor, 1990). The nicotine emission rate in sidestream smoke is approximately 5.0 ± 0.8 mg per cigarette (Daisey *et al.*, 1994, 1998). Nicotine in mainstream smoke and sidestream smoke captured in small combustion chambers is predominantly present in the particle phase (Eatough *et al.*, 1989a; Baker, 1981) In contrast, more than 95% of ETS nicotine exists in the vapor phase (Eatough, 1993; Eatough *et al.*, 1989abc; Baker and Proctor, 1990). This difference is likely a result of two factors: alkalinity of sidestream smoke particles reduces nicotine protonation and decreases its aqueous solubility; and dilution of the smoke plume as it mixes with cleaner indoor air reduces the partial pressure of the semivolatile nicotine causing net transport from the particle phase to the gas phase (Eatough, 1993; Eatough *et al.*, 1989a; Baker and Proctor, 1990).

Another widely used marker for ETS is respirable suspended particles (RSP), particles with aerodynamic diameters smaller than 10 μm which can penetrate into the human respiratory system. Cigarettes and other combustion sources of airborne particulate matter typically produce particles much smaller than 10 μm. Thus, $PM_{2.5}$, the airborne mass concentration of particles with aerodynamic diameters below 2.5 μm, is commonly measured and taken as a reasonable approximation for RSP from ETS. Two cigarette emission rates for $PM_{2.5}$ in ETS have been recently reported. Daisey *et al.* (1994, 1998) reported an emission rate of 8.1 ± 2.0 mg per cigarette for simulated ETS

generated by emitting sidestream smoke (but not mainstream smoke) from machine smoked cigarettes into a 20 m^3 stainless steel chamber. Martin *et al.* (1997) reported 13.7 mg per cigarette for RSP from cigarettes smoked by human subjects and including exhaled mainstream smoke. As described above for nicotine, there is a significant difference in mass emission rates of RSP (and $PM_{2.5}$) for sidestream smoke captured in small combustion chambers and ETS measured after dilution of the smoke plume into a room volume. Daisey *et al.* (1994, 1998) measured emission factors nearly a factor of four larger for sidestream smoke in small chambers. This difference is attributable to evaporation of volatile smoke components as the plume is diluted with cleaner air. Unlike nicotine, RSP and $PM_{2.5}$ have a variety of indoor and outdoor sources other than cigarette combustion. Field measurements of indoor RSP concentrations include both ETS-generated particles and particles from other sources. The models presented in this chapter consider only RSP from ETS.

The results of field studies support nicotine's utility as a marker for ETS particle exposures by showing a linear relationship between the concentrations of nicotine and RSP in homes (Coultas *et al.*, 1990; Leaderer and Hammond, 1991) and workplaces (Miesner *et al.*, 1989; Turner *et al.*, 1992; Hammond *et al.*, 1995; Hammond, 1996). Similar findings have also been reported in personal monitoring studies of RSP and nicotine exposure (Jenkins *et al.*, 1996b). Leaderer and Hammond (1991) found a strong correlation ($C_{rsp} = 22.9\ \mu g\ m^{-3} + 9.8 \cdot C_{nic}$, $R^2 = 0.64$) between one-week average RSP and nicotine concentrations in 47 smoker's homes in two New York counties. Their data are reproduced here as Figure 4.1. Coultas *et al.* (1990) found a slightly weaker but similar correlation (Spearman correlation coefficient = 0.54) between daily average nicotine and RSP concentrations for 99 measurements in ten smokers' homes. Another study of ETS in workplaces, whose results are shown in Figure 4.2, yielded a similar relationship between RSP and nicotine (Miesner *et al.*, 1989). This study used shorter sampling times (4 to 7 hours) and included a diverse set of indoor smoking environments ranging from the

office of a nonsmoking worker in a building where smoking was allowed to a designated smoking area in a building in which smoking was banned in other areas. Despite the differences between this study and the residential investigation, the regression lines for the two data sets are similar. In fact, exclusion of the highest concentration datum (obtained in a smoking lounge) from the regression for the workplace measurements gives a best fit line that closely resembles that from Leaderer and Hammond's (1991) study of ETS in residences. A recent personal exposure monitoring study calculated time weighted 24-h average RSP and nicotine concentrations for approximately 1000 nonsmokers (Jenkins *et al.*, 1996b). The results of this study are summarized in Figure 4.3. The tested subjects performed their daily activities as usual and moved from location to location during the sampling period. As in the studies discussed previously, these results showed a strong correlation ($R^2 = 0.88$) between RSP and nicotine concentrations and produced a regression line similar to those in Figures 4.1 and 4.2.

Despite nicotine's widespread use as an ETS marker, exposure estimates based on measured nicotine concentrations have been criticized, mainly by the tobacco industry and in tobacco industry funded studies. Nicotine's vapor pressure is low — approximately 2 Pa at environmental temperatures (Lencka *et al.*, 1984) — and the nicotine molecule includes a pyridine ring and a cyclic tertiary amine group, both of which can participate in acid-base chemistry (Eatough *et al.*, 1989b; Baker, 1981). Thus, nicotine should interact more strongly with indoor surfaces than many other ETS compounds and therefore exhibit different dynamic behavior. Several studies (Baker *et al.*, 1988; Eatough *et al.*, 1989a; Eatough *et al.*, 1989c; Nelson *et al.*, 1990; Nelson *et al.*, 1992) have shown marked differences in the concentration decay patterns of nicotine as compared with other ETS contaminants in laboratory chambers. In one such study conducted in an 18 m^3 stainless steel environmental test chamber, the effects of air exchange rate (AER) and sampling time on the ratio of nicotine to RSP were measured for 6 hours immediately following combustion of two cigarettes (Nelson *et al.*, 1992). The

ratio of nicotine to RSP varied by a factor of approximately 4 for AERs between 0 and 4 h^{-1} and sampling times between 30 and 360 minutes. Based on these measurements, Nelson *et al.* (1992) concluded that "the sole use of nicotine as an ETS marker may lead to significant errors in ETS exposure assessments." Figure 3 from the paper by Nelson *et al.* is reproduced here for comparison as Figure 4.4

In the current study, the coupled surface sorption/bulk diffusion model and a surface sorption dynamics model developed in Chapters 2 and 3 are applied to simulate the experimental studies described above. By accounting for nicotine sorption and desorption and for differences in the time history of smoking in the simulations, the apparently contradictory results of these studies are largely reconciled. As a further test of the model predictions, a series of laboratory experiments were conducted in a stainless steel chamber containing wallboard and carpet in which the ratio of nicotine to RSP concentrations from simulated ETS was measured as a function of time for 24-hour periods.

MODELING APPROACH

For pollutants that interact with indoor surfaces, the following differential equation describes a time-dependent mass balance on the gas-phase species, assuming well mixed conditions prevail and the outdoor concentrations of ETS constituents are negligible:

$$\frac{dC_i}{dt} = \frac{E_i(t)}{V} - \lambda_v C_i - \frac{1}{V}\sum_{j=1}^{g} S_j \frac{dM_{ij}}{dt} \tag{4.1}$$

where subscripts i and j denote distinct airborne contaminants and indoor surfaces, respectively, g is the total number of distinct surfaces on which sorption may occur, C_i is the indoor airborne concentration of species i (mg m^{-3}); V is the indoor volume (m^3); t is time (h); $E_i(t)$ is the instantaneous emission rate of compound i at time = t (mg h^{-1}); λ_v is

the air exchange rate (h^{-1}), S_j is the presented surface area of surface j (m^2), and M_{ij} is the mass of compound i deposited or sorbed on surface j (mg m^{-2}).

The summation term in equation 4.1 accounts for the net rate of uptake of compound i on each of the indoor surfaces j, where the specific form of each dM_{ij}/dt depends on the nature of the interaction. For reversible sorption on nonporous materials, such as stainless steel, sorption is expected to be purely a surface phenomenon. The rate of mass uptake by such surfaces depends only on gas-phase mass transfer and surface kinetics which are well represented by a modified version of a two-box reversible sorption model (Dunn and Tichenor, 1988; Tichenor *et al.*, 1991). To model sorption dynamics with sorbents into which species may diffuse, such as carpet and wallboard, the two-box model is modified to include Fickian diffusion into the bulk of the material. The following sections detail the mathematical expressions employed in the current study for two cases: a stainless steel chamber, and a typical indoor environment in which the dominant sorbing surfaces are assumed to be carpet and wallboard. The model treatment of airborne particles in ETS is also described.

Governing Equations: Nicotine in a Stainless Steel Chamber. Equilibrium partitioning of nicotine between stainless steel surfaces and air in a 20 m^3 environmental test chamber is accurately described by the nonlinear Freundlich isotherm (Chapter 2):

$$M_{ns} = K_{ns} C_n^{n_{ns}} \tag{4.2}$$

where M_{ns} is the mass of nicotine sorbed per area of stainless steel (mg m^{-2}) and K_{ns} and n_{ns} are experimentally determined isotherm parameters. A modified version of a two-box, reversible sorption model (Dunn and Tichenor, 1988; Tichenor *et al.*, 1991) expresses the net rate of adsorption on the surface as the difference between a power-law deposition rate and a power-law reemission rate. Mass balances on the gas and sorbed phases yield a pair of coupled nonlinear ordinary differential equations which are solved by Runge-Kutta integration (Press *et al.*, 1992):

$$\frac{dC_n}{dt} = \frac{E_n(t)}{V} + \lambda_v C_n - \frac{S_s}{V}\left(k_{ans} C_n^{n_{ans}} - k_{dns} M_{ns}^{n_{dns}}\right) \tag{4.3}$$

$$\frac{dM_{ns}}{dt} = k_{ans} C_n^{n_{ans}} - k_{dns} M_{ns}^{n_{dns}} \tag{4.4}$$

where the subscripts n and s denote nicotine and stainless steel, respectively; S_s is the stainless steel surface area (m^2); k_{ans} and k_{dns} are the rate constants for adsorption ($mg^{1-n_{ans}}\ m^{3n_{ans}-2}\ h^{-1}$) and desorption ($mg^{1-n_{dns}}\ m^{2n_{dns}-2}\ h^{-1}$), respectively; and n_{ans} and n_{dns} are the adsorption and desorption rate exponential coefficients for nicotine on stainless steel (no units). The rate constants and exponential coefficients in this model are related to the isotherm parameters as follows:

$$K_{ns} = \left(k_{ans}/k_{dns}\right)^{1/n_{dns}} \tag{4.5}$$

$$n_{ns} = n_{ans}/n_{dns} \tag{4.6}$$

The sorption rate parameters used to model nicotine sorption are listed in Table 4.1 along with the nicotine mass emission rate per cigarette, $E_n(t)$. This value for $E_n(t)$ represents an average over six different cigarette brands obtained by solvent extraction of sidestream smoke captured on a sorbent sampler and deposited on the walls of small glass sidestream collection apparatus. The standard deviation of these measurements was approximately 15% (Daisey *et al.*, 1994, 1998).

Governing Equations: Nicotine in a Typical Indoor Environment. The surface sorption model described above for stainless steel does not adequately capture the kinetics of adsorption and desorption of nicotine on porous/absorbing materials such as carpet and wallboard. Experiments show that in addition to the net rate of sorption at the surface, the rate of mass transfer into the material through bulk diffusion governed by Fick's Law must be considered (Chapter 3). In the presence of carpet and wallboard as the only sorbing surfaces, the gas-phase mass balance equation is identical to equation 4.3

except that equilibrium gas-surface partitioning is assumed to be linear and the rates of deposition and reemission are first order in both concentration and the sorbed mass density at the sorbent surface, $M_{nj,surface}$:

$$\frac{dC_n}{dt} = \frac{E_n(t)}{V} - \lambda_v C_n - \sum_{j=c,w} \frac{S_j}{V}\left(k_{anj} C_n - k_{dnj} M_{nj,surface}\right) \tag{4.7}$$

where c and w denote carpet and wallboard and k_{anj} and k_{dnj} are the sorbent-specific adsorption and desorption rate constants for nicotine (m h^{-1} and h^{-1}, respectively). The material balance equation for mass sorbed at the surface differs from equation 4.4 by inclusion of a term accounting for diffusive flux of nicotine into the bulk material:

$$\frac{\partial M_{nj,surface}}{\partial t} = k_{anj} C_n - k_{dnj} M_{nj,surface} + D_{nj}\left(\frac{\partial C_{bnj}(t,z)}{\partial z}\right)_{z=0} \tag{4.8}$$

where D_{nj} is the diffusion coefficient for nicotine in the bulk of sorbent j (m^2 h^{-1}), z is the vertical distance into the sorbent (m), and $C_{bnj}(t,z)$ is the local concentration of nicotine within the sorbent j (mg m^{-3}). As equation 4.8 is written, $z > 0$ within the sorbent and $z = 0$ at the surface. For $z > 0$, $C_{bnj}(t,z)$ is governed by Fick's Second Law:

$$\left(\frac{\partial C_{bnj}(t,z)}{\partial t}\right) = D_{nj}\left(\frac{\partial^2 C_{bnj}(t,z)}{\partial z^2}\right) \tag{4.9}$$

The model calculations assumed a no-flux boundary at the back (not directly exposed to indoor air) side of each sorbent. The other boundary condition in equation 4.9 is determined by matching the sorbed mass at the sorbent surface given by equation 4.8. As discussed earlier for equation 3.4, equation 4.9 assumes that no accumulation occurs at the air-sorbent interface relative to the bulk of the sorbent material. Initial conditions required for this model include the species concentration both in the gas phase and at every point within each sorbent. For an initially ETS-free indoor environment, all of these values are zero. The solution to equations 4.7-4.9 is obtained numerically by Runge-Kutta integration of a set of $N + 1$ linear ordinary differential equations (over time) generated by

a finite-difference approximation (in space) of equation 4.9 with N nodes. The model predictions discussed below were generated using $N = 15$ and a constant integration time step of 15 seconds.

Governing Equations: ETS Particles. RSP concentrations were modeled by assuming that airborne particles are removed from indoor air by ventilation and by first-order irreversible deposition on internal surfaces. With this assumption, $dM_{pj}/dt = k_{apj}C_p$. Because ETS particles occur mainly in the accumulation mode, centered at ~ 0.3 μm, deposition is a minor removal mechanism compared with typical ventilation rates (Nazaroff *et al.*, 1993a; Xu *et al.*, 1994). Therefore, it is reasonable to model particle deposition with a single average rate coefficient, k_{ap} (m h^{-1}) averaged over all surfaces j. Equation 4.1 simplifies to a single linear ordinary differential equation:

$$\frac{dC_p}{dt} = \frac{E_p(t)}{V} - \left(\lambda_v C_p + k_{ap}\frac{S_T}{V}C_p\right) \tag{4.10}$$

where S_T is the total presented indoor surface area (m^2). Values for $E_p(t)$ and k_{ap} were obtained from previous studies of ETS particles in indoor air (Xu *et al.*, 1994; Martin *et al.*, 1997) and are listed in Table 4.1.

Modeling Residential Concentrations. To simulate the field measurements of Leaderer and Hammond (1991) in smokers' homes, the kinetic models for reversible nicotine sorption on carpet and wallboard (equations 4.7 - 4.9) and irreversible deposition of airborne particles (equation 4.10) were used with the kinetic parameters reported in Table 4.1 to predict 24-hour average nicotine and RSP concentrations in a 500 m^3 house in which smoking occurs regularly for 16 hours per day at a constant smoking rate. The modeled building was assumed to have a 250 m^2 floor covered with carpet and 1000 m^2 of painted wallboard surface. Emission rates of nicotine and particles were assumed to be 0.5 mg min^{-1} and 1.37 mg min^{-1} with a 10 min duration for each cigarette, and zero between cigarettes. The model was used to calculate the 24-hour average nicotine and

RSP concentrations resulting from all combinations of a 4 × 12 matrix of air-exchange rates (0.3, 0.5, 1.0, and 3.0 h^{-1}) and smoking rates (1, 3, 6, 9, 12, 16, 20, 24, 30, 36, 42, and 48 cigarettes d^{-1}). Because the daily smoking pattern was held constant for each model run, the calculated 24-h average concentrations are equivalent to those that would result for a 7-d period.

Prior to calculating the 24-h average concentrations for each AER/smoking rate combination, the model simulated the loading of indoor surfaces with nicotine by modeling the indoor concentrations and sorbed masses continuously over time. In this manner, the model represents the loading of indoor surfaces with sorbed nicotine that occurs from a steady emission pattern. After approximately 2000 days with a constant smoking pattern and AER, the sum of the relative variations between the nicotine concentration in all of the sorbent finite difference nodes and the gas-phase at the beginning of successive days was less than 1%. In contrast, the total relative variation between successive days was approximately 580% for a 30-d exposure to a constant AER and smoking pattern and 14% for a 365-d exposure. The particle deposition model assumed no resuspension and no indoor or outdoor sources, so RSP concentrations decayed to nearly zero during the eight hours of each 24-h period during.which no cigarettes were smoked. Thus, a steady diurnal pattern for particles was achieved quickly — less than 1% variation between the starting concentrations for successive days was reached within 4 or 5 days, depending on the smoking pattern and AER.

Modeling Concentrations in an Environmental Chamber. To model the nicotine/RSP ratio from ETS in a stainless-steel chamber with no previously sorbed nicotine, equations 4.3, 4.4, and 4.10 were used to predict RSP and nicotine concentrations in an 18 m^3 stainless steel chamber with 45 m^2 of internal surface area. The chamber is assumed to be initially free of cigarette smoke. In the model run, two cigarettes are sequentially smoked, for 10 min each, starting at $t = 0$, and emissions were zero for all times after 20 minutes. The air-exchange rate was varied between 0 and 4 h^{-1},

and sampling times (averaging time immediately following the start of combustion) between 30 minutes and 360 minutes were considered. The parameters used for nicotine-stainless steel sorption kinetics and particle deposition are listed in Table 4.1. The code for these simulations is listed in Appendix C. These model conditions closely mimic the experiments used to investigate the effects of ventilation rate and sampling duration on the observed nicotine/RSP ratio (Nelson *et al.*, 1990; Nelson *et al.*, 1992).

EXPERIMENTAL METHODS

To substantiate the results of the modeling analysis described above, a series of experiments was conducted with simulated ETS in a 20 m^3 stainless-steel chamber containing four 2.4 m × 1.2 m × 0.0095 m panels (for a total of 11.9 m^2 of presented area) of the painted wallboard and a 7.7 m^2 sample of the carpet used in the study described in Chapter 3. The chamber operation, cigarette combustion, and gas-phase nicotine sampling procedures employed in the current study are described in detail in Chapters 2 and 3, and briefly summarized here.

A total of 16 cigarettes (Marlboro Class A Filtered) were smoked in the chamber over the course of several weeks using a cigarette smoking machine (Arthur D. Little, Cambridge, MA) while the chamber was ventilated at a low air exchange rate (approximately 0.1 h^{-1}). Mainstream smoke was vented to a fume hood, so only sidestream smoke was emitted inside the chamber. The machine was set to take one 2-second, 35-mL puff per minute and took between 9 and 10 minutes to smoke each cigarette. The initial smoking sequence with very low ventilation was designed to simulate sorbent loading in real indoor environments where regular smoking occurs. Afterward, three sequential experiments were conducted in which the chamber was ventilated at air exchange rates more typical of indoor environments while several cigarettes were mechanically smoked over a three-hour period. In each experiment, the gas-phase nicotine and airborne particle concentrations were monitored as functions of

time for 24 hours beginning with the ignition of the first cigarette of each run. Nicotine and RSP samples were collected continuously. Collection of a new sample was started approximately every 20 to 30 minutes during and for two hours following cigarette combustion and then less frequently during the remainder of the 24-h experiment. Each cigarette burned for approximately ten minutes under the smoking machine parameters described above for the surface loading procedure. The cigarettes smoked during each 24 hour experiment were burned sequentially at evenly spaced intervals during the first three hours of the run. The smoking machine was designed to automatically ignite each cigarette, extinguish it after a preset smoking period, and then repeat the cycle after a programmed delay. However, the automated features of the machine often failed to perform properly. In these cases, the chamber was entered briefly to manually ignite and snuff each cigarette at the proper time. The chamber door was opened for less than 30 seconds each time this procedure was required. The air-exchange rate for each run was determined by monitoring the concentration decay of sulfur hexafluoride, injected shortly before ignition of the first cigarette, with a photoacoustic infrared multigas monitor (Type 1302, Brüel and Kjaer, Nærum, Denmark). The chamber operation and smoking parameters for each run are listed in Table 4.2. We deliberately varied the air exchange rate and smoking rate to examine the sensitivity of the nicotine-RSP ratio to changes in these parameters in a system containing real indoor materials previously exposed to ETS. The chamber temperature and relative humidity were monitored but not controlled, so these parameters also varied slightly from run to run as shown in Table 4.2.

Gas-phase nicotine samples were collected on reusable, commercially available glass sample tubes (Part # ST032, Envirochem Inc.) packed with glass beads at the inlet followed by Tenax-TA. Before each use, the samplers were cleaned and conditioned by heating them to 300 °C for 30 minutes with a helium purge flowing at 100 cm^3 min^{-1} in the reverse direction of sample collection. During sample collection, the tubes were mounted on the end of a 30 cm stainless steel tube which could be retracted from the

chamber through a port in the wall to exchange clean sample tubes for exposed ones. The stainless steel tube was connected to a peristaltic pump outside of the chamber which sampled at 100-120 cm^3 min^{-1}. Each sample was thermally desorbed at 275 °C for 5 minutes, concentrated and introduced into a capillary GC with a sample concentrating and inletting system (UNACON Model 810) and a thermal desorption system (Model 8916 Multiple Tube Desorber, Envirochem, Inc.). This instrument concentrates the sample using dual sequential traps. Sample components are resolved with a GC (Model 5890 Series II, Hewlett Packard Co.) equipped with a 30 m × 0.53 mm ID × 1.0-μm thick film fused-silica capillary column (Rtx-5, Restek Corp.). The GC is connected via a direct capillary interface to a flame ionization detector (FID). Calibration regression lines were generated by analyzing Tenax TA cartridges spiked with known volumes of nicotine in methanol containing 0.01% triethylamine. The triethylamine was added to reduce sorptive losses from the solutions to glassware surfaces (Odgen *et al.*, 1989). The calibration curve was linear up to approximately 1000 ng total injected mass. However, the regression line had a negative intercept indicating a possible loss of approximately 50 ng of nicotine per sample in the desorption system compared to a typical sample size of 400 to 600 ng. At least one standard run was performed on each analysis day to verify that the variability over time of the FID response to nicotine was small.

Airborne particle samples were collected at 15 to 20 L min^{-1} on pre-extracted (in methanol followed by dichloromethane), air-dried 47-mm-diameter Teflon-coated glass fiber filters. The particle mass collected was determined gravimetrically using an automatic microgram electrobalance (Model 25, Cahn/Ventron, Inc. Cerritos, CA).

RESULTS AND DISCUSSION

Modeling Results. Figure 4.5 shows the results of model calculations of 24-h average nicotine and RSP concentrations in a prototypical house with carpeted floors and painted wallboard walls. The effects of variations in the house AER between 0.3 and 3.0

h^{-1} are shown by the different symbols. Variation of the daily smoking rate between 1 and 48 d^{-1} resulted in the range of RSP and nicotine concentrations shown in the plot. Each AER tested in the model produced a nearly straight line with an RSP concentration axis intercept of approximately zero. The zero intercepts in Figure 4.5 result from the model's omission of non-ETS particle sources. In realistic indoor environments, non-ETS contributions to the accumulation mode particle mass burden are likely to be poorly correlated with ETS emissions. Thus, non-ETS particle sources should affect the particle concentration axis intercept and the scatter in the data, but not the slope (RSP/nicotine concentration ratio) in Figure 4.5. The slopes of the regression lines vary from 23.7 for AER = 0.3 h^{-1} to 5.0 for 3.0 h^{-1}. The larger slope for the lower AER cases is a result of the increased effect of surface interactions relative to ventilation as a removal mechanism for airborne pollutants. The 0.5 h^{-1} and 1.0 h^{-1} predictions are representative of typical AER conditions for houses in the United States (Murray and Burmaster, 1995).

The slope (9.1) of the AER = 1.0 h^{-1} data in Figure 4.3 is nearly identical (agreement to within 10%) to that shown in Figure 4.1 (Figure 6 in Leaderer and Hammond, 1991) for a study of 47 smokers' homes (9.8). The 0.5 h^{-1} line has a larger slope (15.4), and the data shown in Figures 4.2 and 4.3 have similar slopes (6.9, 14.8, and 8.7). These minor discrepancies may arise from the presence of other sorbents such as upholstery, furnishings, and clothing in indoor environments that were not included in our model calculations. Preliminary model calculations that included carpet but not wallboard resulted in regression line slopes almost two times greater than those reported in this study (Van Loy *et al.*, 1997b). Addition of more sorbent surfaces in the model should result in a further decrease of the slope and a diminished dependence on the AER. Greater indoor surface area increases the rate of RSP deposition but may not significantly reduce the 24-h average nicotine concentration once the mass sorbed on the indoor surfaces is in steady state with the diurnal smoking pattern and the AER because of increased reemission of deposited nicotine during nonsmoking periods.

Results of the modeling simulation corresponding to the experimental results shown in Figure 4.4 (Figure 3 in Nelson *et al.*, 1992) are displayed in Figure 4.6. This figure shows similar trends to the previously reported experimental results: the chamber AER has a significant effect on the nicotine/RSP concentration, but the effect is not as large as the impact of different sampling times. There are some discrepancies between Figures 4.4 and 4.6 , but the agreement is good overall. At longer measurement times, the nicotine/RSP concentration ratio is smaller than at shorter measurement times. This effect is most pronounced for the low AER cases in which surface interactions are the dominant sink for RSP and nicotine. Unlike in the house simulations in which sorbent surfaces are loaded with nicotine, the chamber surfaces are clean at the start of each run. Thus, the available sorption capacity of the sorbents for nicotine is large and nicotine sorption is more significant than RSP deposition. For AER = 4.0 h^{-1}, the ratio varies much less with changes in measurement time because ventilation is the dominant removal mechanism for both pollutants. This effect can also be seen in the house modeling results shown in Figure 4.3. The difference between the predicted slopes for AER = 1.0 and 3.0 h^{-1} is smaller than that between 0.3 and 0.5 h^{-1}.

The differences between the model predictions shown in Figure 4.6 and the data from Nelson *et al.* (1992) in Figure 4.4 may be due to different surface pretreatment protocols in the Nelson *et al.* experiments relative to those used in the study described in Chapter 2, from which the sorption parameters were obtained. Nelson *et al.* do not explicitly describe how or even if their chamber was cleaned between experiments. In the chamber studies described in Chapter 2, the stainless steel walls were washed twice between experiments: once with an acidic detergent intended to increase the solubility of nicotine so that it could be more readily removed and once with an alkaline solution to repassivate the surface to nicotine deposition. The chamber was rinsed with tap and deionized water and dried prior to the beginning of each experiment, but alkaline residue which should retard nicotine adsorption probably remained on the chamber surfaces.

Other differences between the model and experimental data could be introduced by differences in the age of the stainless steel surfaces in the test chambers. Stainless steel is relatively inert to environmental attack, but it is known to oxidize at a finite rate. The data presented in Chapter 2 indicate that differences in the age of stainless steel samples may alter the sorption capacity and lability of sorbed nicotine.

Experimental Results. Figure 4.7 shows measured and modeled nicotine and RSP concentrations in the stainless steel environmental chamber containing carpet and painted wallboard samples as a function of time for experiment 4A in which 12 cigarettes were smoked during the first three hours of the run and the chamber was ventilated at an AER of 0.53 h^{-1} for 24 hours. Tables 4.3 and 4.4 list the sample start and end times and measured RSP and nicotine concentrations for each sample collected prior to and during this series of experiments. The model predictions for the gas-phase nicotine and RSP concentrations were obtained using the model parameters in Table 4.1 and the known time series of cigarette combustion events in the chamber both prior to and during the experiment (tabulated in Table 4.5). The cigarette combustion history in the chamber prior to the start of the experiments was modeled to account for the initial conditions which included some nicotine sorbed to surfaces in the chamber. The ETS RSP emission factor of 8.1 mg cig^{-1} reported by Daisey *et al.* (1994, 1998) was used in the model predictions instead of the 13.7 mg cig^{-1} value reported by Martin *et al.* (1997). The Daisey *et al.* (1994, 1998) value was obtained from experiments with simulated ETS (no mainstream smoke) which more closely approximates the experimental conditions. The model-measurement agreement is fairly good — the RSP calculations agree closely with the measured values while the measured nicotine concentrations are underpredicted by approximately a factor of 2. The nicotine disagreement may be due to the effect of other ETS constituents on the sorption dynamics of nicotine with carpet and wallboard. The model parameters from Table 4.1 for these phenomena were obtained from experiments in which pure nicotine was flash evaporated in a chamber containing the sorbent to be

tested. Both the model and measurements show that the nicotine concentration decays quickly following cessation of smoking but achieves a nearly steady concentration for the last 19 hours of the experiment while the RSP concentration continues to decrease and actually becomes less than the nicotine concentration during the overnight sample period (between 5 and 20 h). Indoor surface loading with nicotine was crudely simulated in these three runs by smoking 16 cigarettes in the chamber during a short period before the start of the experiments with the chamber operated at a low air-exchange rate. A more realistic loading protocol would require ventilating the chamber at the AER to be tested for many weeks, months, or years prior to the start of the experiment while repeating the tested smoking cycle every day. In such an experiment, it is expected that the variation in the nicotine/RSP concentration ratio with time would be even more pronounced.

Figures 4.8 and 4.9 illustrate an important point. Figure 4.8 shows the variation in the nicotine/RSP concentration ratio as a function of sampling times from 0.5 to 5 hours and then for 24 hours. At short sampling times, the ratio varies markedly, but for the 24-hour averages, it is nearly constant for all three runs despite the different ventilation conditions and smoking rates. Figure 4.9 shows the nearly linear relationship between the 24-hour average RSP and nicotine concentrations for the experiments 4A, 4B, and 4C. The best fit slope for the 24-h average data is smaller than those reported by Leaderer and Hammond (1991), Miesner *et al.* (1989), and Jenkins *et al.* (1996b) and also smaller than that predicted by our model probably because of the large stainless steel surface area in the chamber. While particles deposit at approximately the same rate on different surfaces, the nicotine deposition rate on stainless steel that has been previously exposed to ETS is much smaller than that on carpet or wallboard because of the much greater sorption capacity of the more porous surface materials.

CONCLUSIONS

Previously developed models describing nicotine's interactions with indoor surfaces were combined with ETS nicotine and RSP emission factors and ETS particle deposition rates obtained from the literature to predict RSP/nicotine concentration ratios in indoor environments. By accounting for reversible sorption of nicotine, previous discrepancies in reports of nicotine's utility as an ETS marker were reconciled. For long-term (on the order of 24-h) average measurements in environments whose indoor surfaces have been routinely exposed to ETS, nicotine is a valid indicator (or "marker") of RSP concentrations due to ETS. This is true despite significant differences in the transient decay patterns of nicotine and RSP in indoor air. When the sorbed mass of nicotine on indoor surfaces is in steady or near-steady state with the daily indoor smoking rate and the building AER, reversible sorption depresses the indoor nicotine concentration during periods of smoking, but maintains it at a non-zero plateau after smoking stops. Because reversible sorption more significantly affects the transient behavior of nicotine, nicotine is a less effective marker for short-term ETS exposure studies.

This study demonstrates the impact of reversible sorption on human exposures to compounds that are emitted intermittently (as by periodic cigarette combustion) and that interact strongly with surfaces. Additional research is merited to investigate the effects of other common indoor sorbents, such as upholstery, furniture cushions, and clothing, on indoor concentrations of nicotine and other semivolatile organic compounds (e.g. pesticides) whose low vapor pressures or other physicochemical properties give them a high affinity for surfaces.

FIGURES

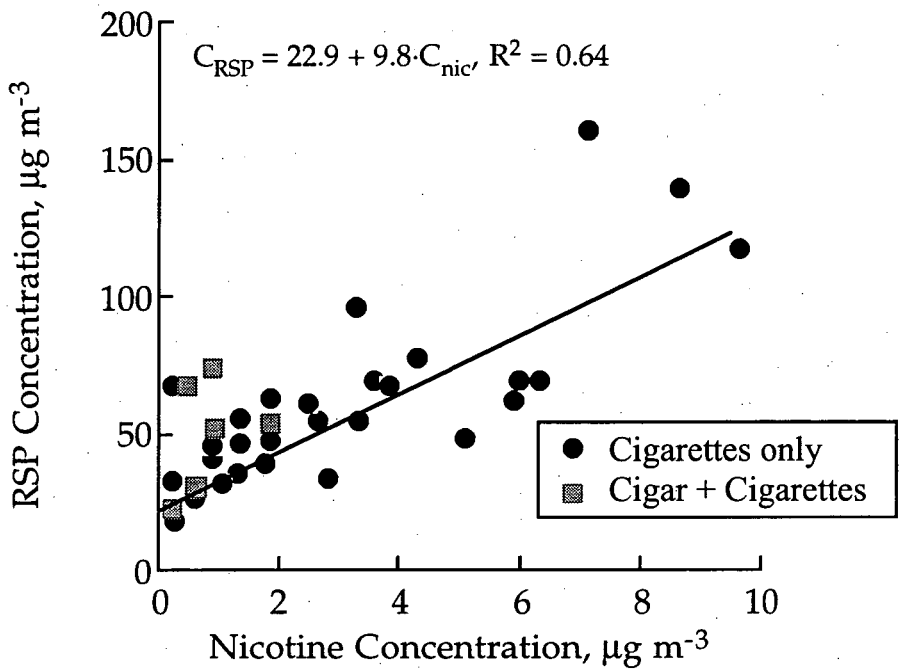

Figure 4.1 Observed relationship between gas-phase nicotine and RSP concentrations in approximately 100 smokers' houses in two New York counties (from Leaderer and Hammond, 1991).

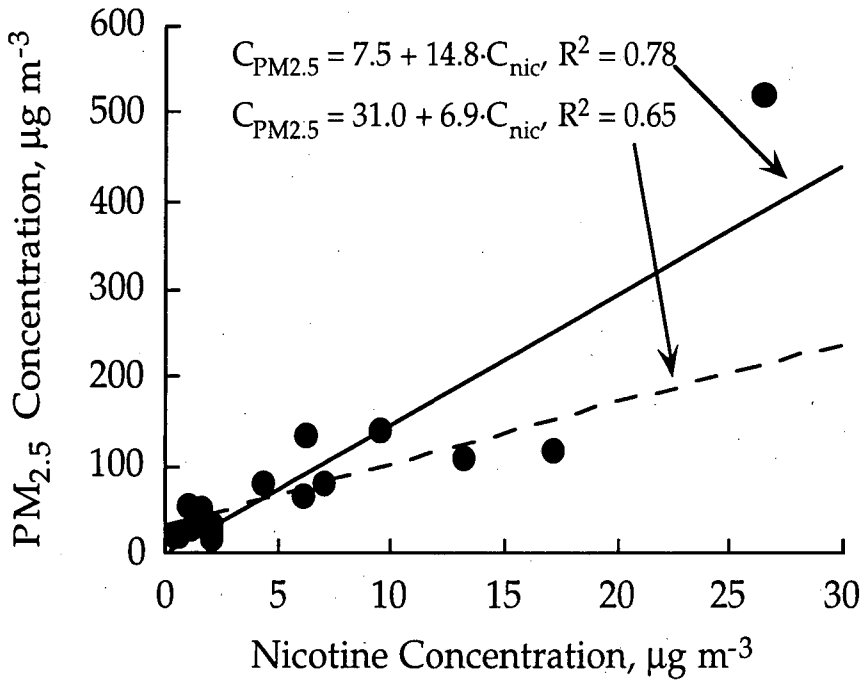

Figure 4.2 Four- to seven-hour average $PM_{2.5}$ concentrations measured in public places vs. corresponding total airborne nicotine concentrations (Miesner *et al.*, 1989). The solid line is the least-squares regression for all of the data and the dashed line is the best fit for all data except the highest concentration point which was collected in a smoking lounge.

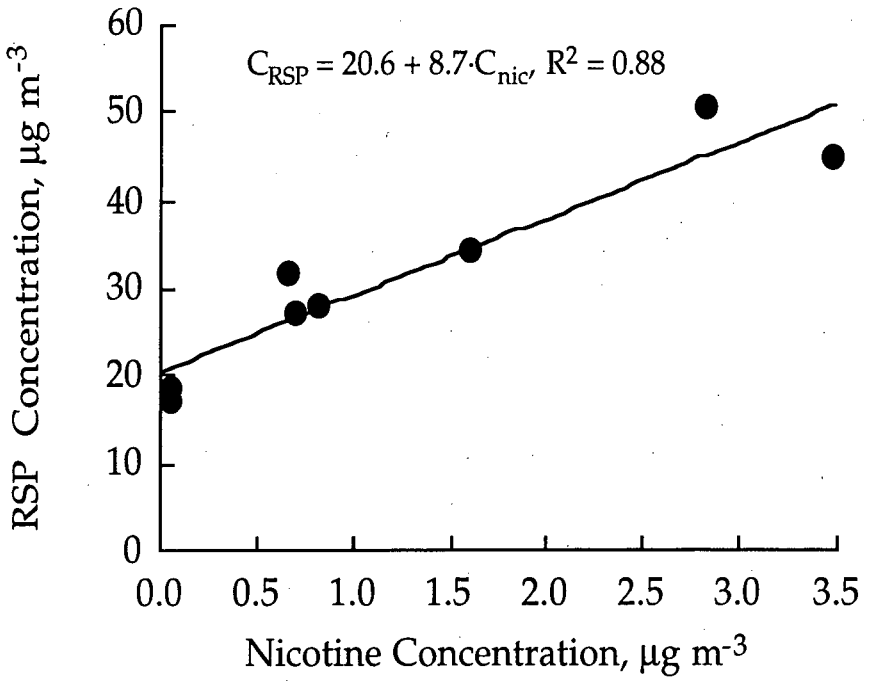

Figure 4.3 Mean values of 24-hour time weighted average airborne concentrations of RSP and nicotine. These data were collected as part of a personal sampler study of approximately 1000 nonsmokers in 16 U.S. cities (Jenkins *et al.*, 1996b). The eight data points represent mean values for the subjects grouped according to gender and whether they were exposed to ETS at home, at work or in both or neither of these locations.

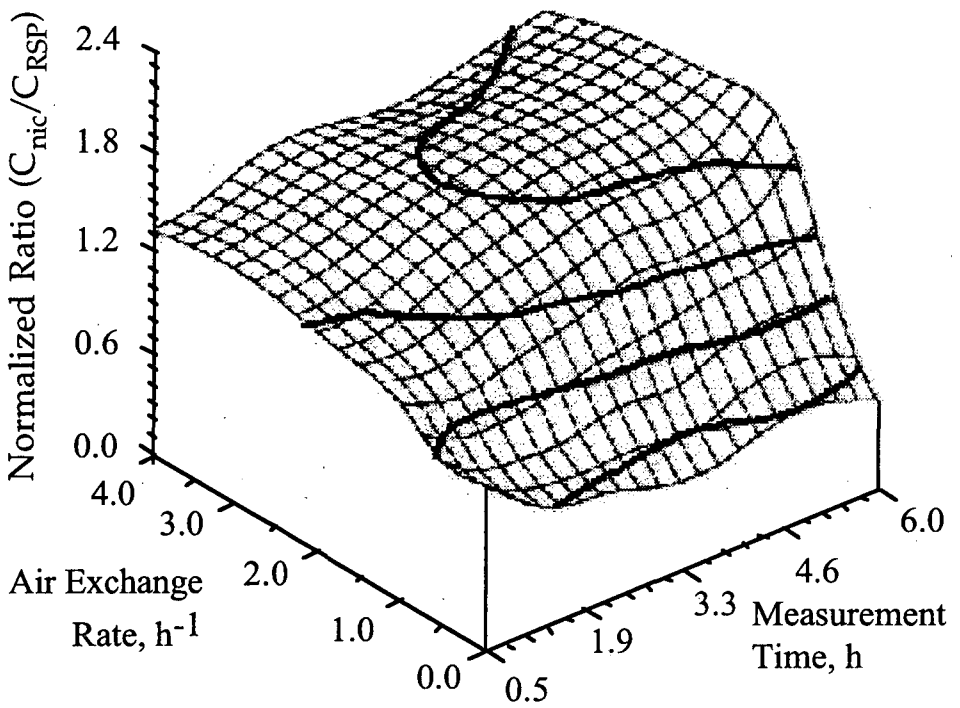

Figure 4.4 Normalized ratio of experimental airborne nicotine and RSP concentrations in a 18 m^3 stainless steel chamber for of chamber air exchange rates (AER) between 0 and 4 h^{-1} and sampling (measurement) times between 30 minutes and 6 hours (from Nelson *et al.*, 1992).

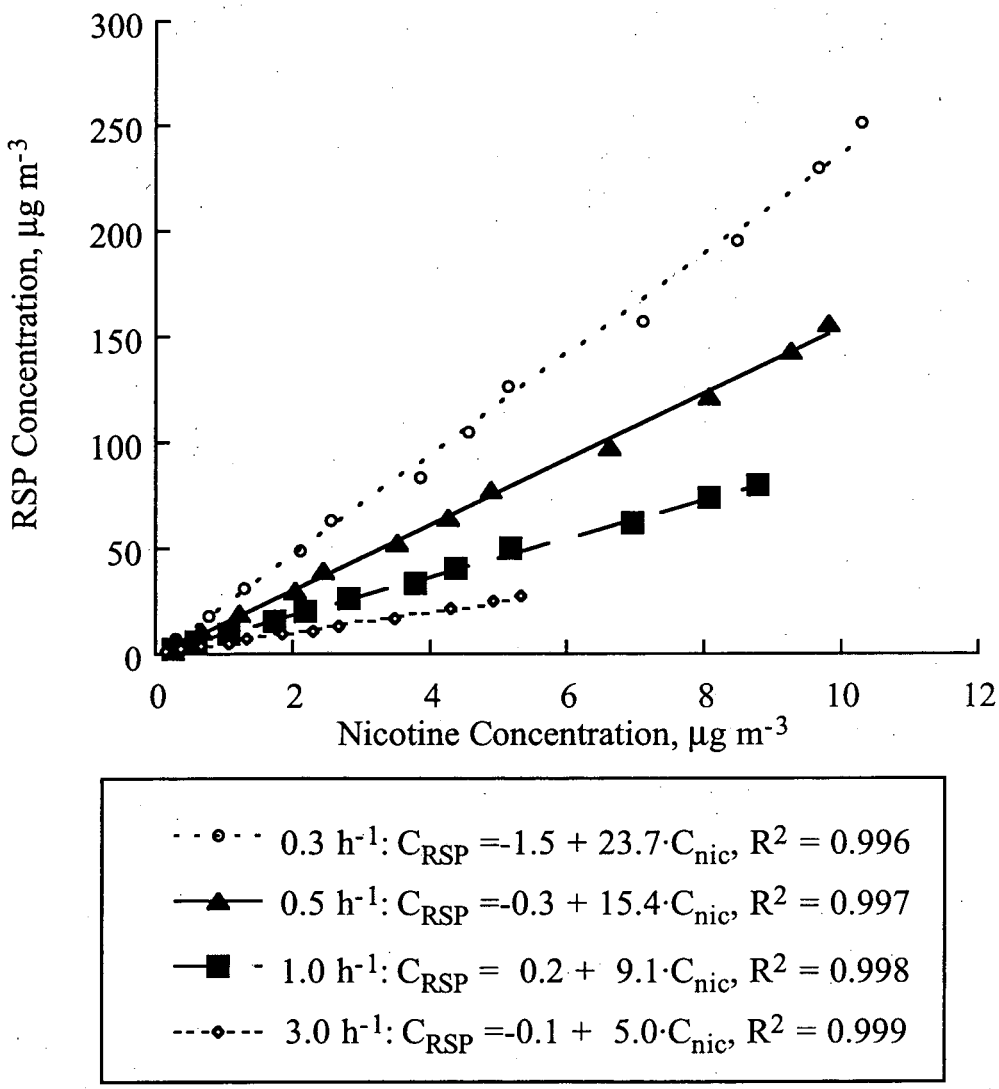

Figure 4.5 Reversible surface sorption model predictions for the relationship between 24-h average RSP and nicotine concentrations in a 500 m^3 house with 250 m^2 of carpet and 1000 m^2 of painted wallboard surface area. These calculations simulate field measurements shown in Figure 4.1 (Leaderer and Hammond, 1991). Model parameters are given in Table 4.1. Each data point represents a different set of smoking and air exchange rates.

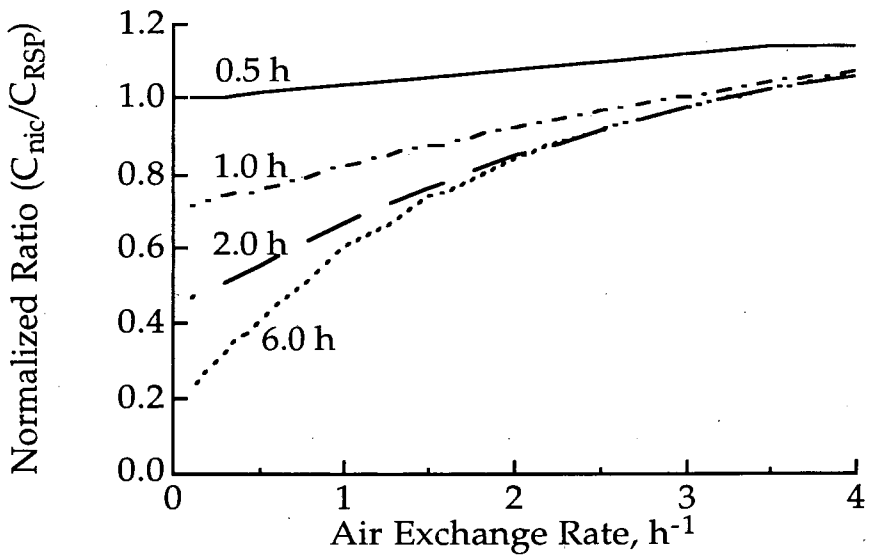

Figure 4.6 Model predictions for the normalized ratio between nicotine and RSP concentrations for experiments in an 18 m^3 stainless steel chamber. These calculations simulate the experimental results shown in Figure 4.4 (Nelson *et al.*, 1992). In the model, two cigarettes are sequentially smoked for 10 minutes each starting at $t = 0$. The labels next to each curve denote the sampling period in hours. The values are normalized to the ratio calculated for a 30 minute sample at AER = 0 h^{-1} (0.129).

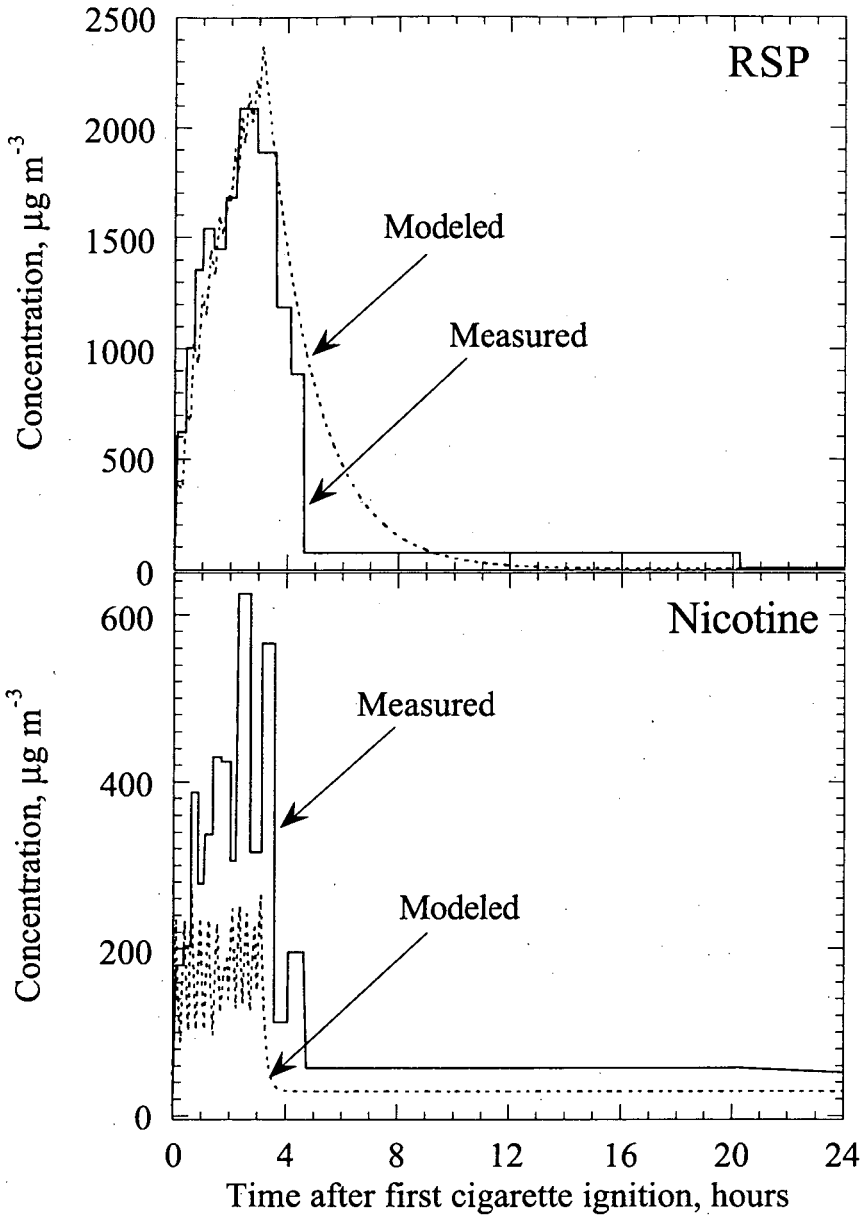

Figure 4.7 Measured total airborne nicotine and RSP concentrations and corresponding model predictions as a function of time in Experiment 4A

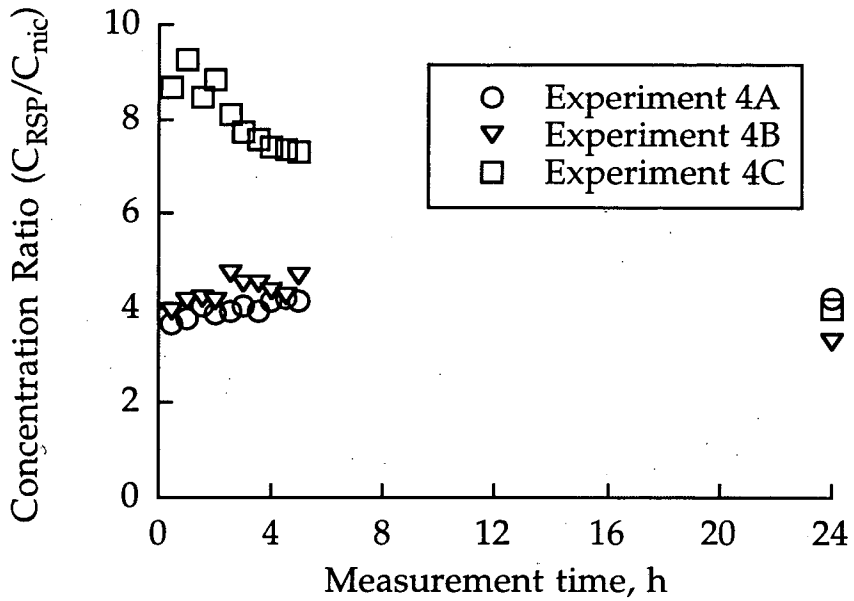

Figure 4.8 Measured ratio between RSP and total airborne nicotine concentrations for three experiments in a 20 m^3 stainless steel chamber containing painted wallboard and carpet as a function of measurement period duration starting at $t = 0$. The air exchange rates and smoking conditions for Experiments 4A, 4B, and 4C are listed in Table 4.2 and the data are tabulated in Table 4.3. The first cigarette in each experiment was started at $t = 0$.

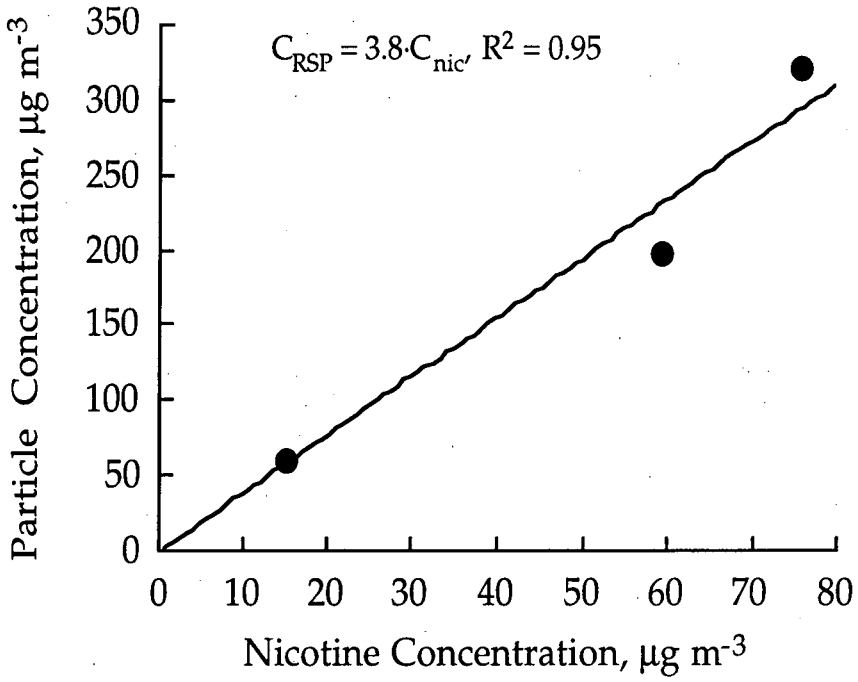

Figure 4.9. 24-hour average RSP concentrations from Experiments 4A, 4B, and 4C with simulated ETS in a 20 m^3 stainless steel chamber containing painted wallboard and carpet vs. the corresponding 24-h average total airborne nicotine concentrations. Experimental conditions for the three runs are given in Table 4.2.

TABLES

Table 4.1 Parameters used in model simulations of nicotine and RSP dynamics.

Parameter	Value	Source
Pollutant Emission Rates During Cigarette Combustion*		
Nicotine ($E_n(t)$), mg h^{-1}	30	Daisey *et al.*, 1994, 1998
RSP ($E_p(t)$), mg h^{-1}	82	Martin *et al.*, 1997
Particle Deposition Parameters		
Deposition velocity (k_{ap}), m h^{-1}	0.011	Xu *et al.*, 1994
Nicotine-Stainless Steel Kinetic Parameters†		
Adsorption rate constant (k_{ans}), $mg^{1-n_{ans}}\ m^{3n_{ans}-2}\ h^{-1}$	0.81	Chapter 2
Adsorption exponential coefficient (n_{ans})	1.22	Chapter 2
Desorption rate constant (k_{dns}), $mg^{1-n_{dns}}\ m^{2n_{dns}-2}\ h^{-1}$	0.029	Chapter 2
Desorption exponential coefficient (n_{dns})	2.15	Chapter 2
Nicotine-Carpet Kinetic Parameters		
Adsorption rate constant (k_{anc}), m h^{-1}	7.8	Chapter 3
Desorption rate constant (k_{dnc}), h^{-1}	4.0×10^{-4}	Chapter 3
Bulk diffusion coefficient (D_{nc}), $m^2\ h^{-1}$	2.5×10^{-10}	Chapter 3
Sorbent thickness, m	0.0024	
Nicotine-Wallboard Kinetic Parameters		
Adsorption rate constant (k_{anw}), m h^{-1}	2.0	Chapter 3
Desorption rate constant (k_{dnw}), h^{-1}	1.3×10^{-3}	Chapter 3
Bulk diffusion coefficient (D_{nw}), $m^2\ h^{-1}$	2.9×10^{-10}	Chapter 3
Sorbent thickness, m	0.0095	

* The models assume that the pollutant emission rates are equal to those given during each 10 minute cigarette burn period and equal to zero at all other times; thus the emission rates correspond to emission factors of 5 mg cig^{-1} for nicotine and 13.7 mg cig^{-1} for RSP. The nicotine emission factor is based on sidestream measurements; measured ETS emission factors are lower because of losses on surfaces.

† Chapter 2 lists three sets of nicotine-stainless steel sorption parameters. The values listed here are from experiment 2A in which simulated ETS was studied in a stainless steel chamber.

Table 4.2 Chamber operation and smoking parameters for three experiments in a stainless steel chamber containing carpet and painted wallboard.

Parameter	Exp. 4A	Exp. 4B	Exp. 4C
Carpet area, m^2	7.7	7.7	7.7
Wallboard area, m^2	11.9	11.9	11.9
Stainless steel area, m^2	37.3	37.3	37.3
Cumulative cigarettes smoked prior to run	16	28	40
Cigarettes smoked during run	12	12	3
Time to smoke 1 cigarette, h	0.17	0.17	0.17
Period between cigarette ignitions, h*	0.25	0.25	1.0
Air exchange rate (λ_v), h^{-1}	0.53	1.15	0.65
Temperature in chamber, °C	25	26	23
Relative humidity in chamber, %	47	55	41

* All cigarettes for each run were burned at the specified intervals during the first three hours of the run.

Table 4.3 Gas-phase nicotine concentration sample data from experiments 4A – 4C with ETS in a 20 m^3 stainless steel chamber containing samples of carpet and wallboard as described in Table 4.2.

Sample Number	Sample Start Time, hours	Sample End Time, hours	Measured Concentration, $\mu g\ m^{-3}$
Preconditioning			
1	0.09	0.28	186
2	0.33	0.59	62
3	0.75	1.08	39
4	1.34	1.85	30
5	2.34	3.01	20
6	8.10	9.43	20
7	12.94	13.66	24
8	13.72	14.60	19
9	13.72	14.60	20
10	14.87	15.10	203
11	15.12	15.37	69
12	15.54	15.84	54
13	15.92	16.59	33
14	16.82	17.82	24
15	32.12	34.22	19
16	105.52	110.19	7
17	175.78	182.27	15
18	302.25	302.53	333
19	302.65	302.89	506
20	302.90	303.10	913
21	303.13	303.30	53
22	303.34	303.54	242
23	319.09	320.10	22
24	344.18	345.95	35
25	367.70	368.02	284
26	368.11	368.35	459
27	368.39	368.67	635
28	368.69	368.96	639
29	369.04	369.33	347
30	371.37	372.05	95
31	373.37	374.07	59
32	439.22	441.29	12

Table 4.3 Continued

Sample Number	Sample Start Time, hours	Sample End Time, hours	Measured Concentration, μg m^{-3}
Experiment 4A			
33	466.61	466.89	180
34	466.89	467.13	202
35	467.15	467.39	387
36	467.39	467.59	277
37	467.64	467.90	337
38	467.90	468.20	430
39	468.21	468.54	424
40	468.54	468.72	305
41	468.82	469.25	625
42	469.25	469.64	316
43	469.65	470.10	566
44	470.10	470.58	112
45	470.60	471.15	196
46	471.25	486.85	57
47	511.63	514.03	17
48	535.92	538.86	11
49	609.36	614.43	8
Experiment 4B			
50	634.38	634.63	104
51	634.65	634.82	282
52	634.85	635.09	82
53	635.11	635.34	353
54	635.38	635.67	366
55	635.68	636.04	151
56	636.05	636.37	444
57	636.44	636.75	114
58	636.75	637.04	130
59	637.10	637.32	555
60	637.35	637.61	203
61	637.67	637.94	103
62	638.12	638.47	166
63	638.60	639.23	29
64	639.24	639.94	73
65	640.00	656.13	23
66	656.15	659.57	11
67	679.75	685.11	3

Table 4.3 Continued

Sample Number	Sample Start Time, hours	Sample End Time, hours	Measured Concentration, μg m^{-3}
68	776.07	782.83	2
69	799.43	803.23	2
70	801.37	803.23	5
Experiment 4C			
71	803.40	803.90	40
72	803.92	804.33	25
73	804.33	804.68	75
74	804.72	805.05	38
75	805.07	805.42	40
76	805.42	805.68	82
77	805.70	806.25	55
78	806.25	806.67	38
79	806.67	807.17	35
80	807.18	824.57	11
81	824.59	831.24	5
82	846.90	853.25	2
83	871.08	875.57	4

Note: samples numbered 1 – 32 (prior to the start of Experiment 4A) were collected during the chamber pretreatment procedures. The complete air-exchange rate and smoking histories for the chamber prior to and during experiments 4A – 4C are given in Table 4.5.

Table 4.4 Particle mass concentration sample data from experiments 4A – 4C with ETS in a 20 m^3 stainless steel chamber containing samples of carpet and wallboard as described in Table 4.2.

Sample Number	Sample Start Time, hours	Sample End Time, hours	Measured Concentration, $\mu g\ m^{-3}$
Preconditioning			
1	302.17	302.42	276.1
2	302.43	302.77	1402.7
3	302.78	303.10	2075.2
4	303.18	303.48	1764.1
5	319.09	320.87	51.1
6	344.23	351.12	17.5
7	367.65	368.02	581.6
8	368.10	368.35	1855.2
9	368.39	368.68	2828.9
10	368.74	369.01	3478.3
11	369.05	369.30	2978.0
12	371.37	372.06	1460.9
13	373.37	374.09	681.8
14	439.22	446.81	6.7
Experiment 4A			
15	466.62	466.91	621.1
16	466.93	467.22	1001.8
17	467.23	467.50	1354.2
18	467.53	467.88	1537.5
19	467.92	468.29	1447.0
20	468.31	468.68	1678.7
21	468.78	469.42	2084.0
22	469.44	470.10	1885.4
23	470.13	470.63	1184.4
24	470.65	471.10	883.1
25	471.12	486.73	71.3
26	486.76	490.96	4.4

Table 4.4 Continued

Sample Number	Sample Start Time, hours	Sample End Time, hours	Measured Concentration, μg m^{-3}
Experiment 4B			
27	634.37	634.70	585.8
28	634.72	635.05	921.1
29	635.07	635.43	944.1
30	635.45	635.77	1328.7
31	635.78	636.10	1288.0
32	636.12	636.46	1387.3
33	636.47	636.88	1307.7
34	636.89	637.28	1442.4
35	637.31	637.70	902.6
36	637.72	638.22	443.2
37	638.24	639.83	124.1
38	639.84	656.08	3.8
39	656.11	659.58	0.7
Experiment 4C			
40	803.41	804.08	346.1
41	804.10	804.45	303.2
42	804.47	804.82	511.4
43	804.83	805.18	320.5
44	805.20	805.56	492.5
45	805.58	805.99	410.8
46	806.01	806.64	268.0
47	806.66	807.23	168.5
48	807.25	824.68	8.5
49	824.70	831.25	3.9

Note: samples numbered 1 – 14 (prior to the start of Experiment 4A) were collected during the chamber pretreatment procedures. The complete air-exchange rate and smoking histories for the chamber prior to and during experiments 4A – 4C are given in Table 4.5.

Table 4.5 Air-exchange rate and cigarette smoking histories for the stainless steel chamber prior to and during experiments 4A – 4C.

Period Start Time, hours	Period End Time, hours	Number of Cigarettes Smoked	Chamber Air-Exchange Rate h^{-1}
Preconditioning			
0.00	0.17	1	0.03
0.17	11.39	0	0.03
11.39	11.56	1	0.03
11.56	14.78	0	0.03
14.78	14.95	1	0.03
14.95	35.67	0	0.03
35.68	35.85	1	0.03
35.85	302.19	0	0.03
302.19	303.18	6	0.03
303.18	367.66	0	0.03
367.66	368.85	6	0.03
368.85	463.95	0	0.03
463.95	466.61	0	0.53
Experiment 4A			
466.61	466.72	1	0.53
466.72	466.89	0	0.53
466.89	467.04	1	0.53
467.04	467.18	0	0.53
467.18	467.28	1	0.53
467.28	467.45	0	0.53
467.45	467.60	1	0.53
467.60	467.74	0	0.53
467.74	467.89	1	0.53
467.89	468.05	0	0.53
468.05	468.20	1	0.53
468.20	468.31	0	0.53
468.31	468.55	1	0.53
468.55	468.60	0	0.53
468.60	468.75	1	0.53
468.75	468.85	0	0.53

Table 4.5 Continued

Period Start Time, hours	Period End Time, hours	Number of Cigarettes Smoked	Chamber Air-Exchange Rate h^{-1}
468.85	469.00	1	0.53
469.00	469.10	0	0.53
469.10	469.25	1	0.53
469.25	469.36	0	0.53
469.36	469.53	1	0.53
469.53	469.60	0	0.53
469.60	469.74	1	0.53
469.74	631.75	0	0.53
Experiment 4B			
631.75	634.36	0	1.15
634.36	634.52	1	1.15
634.52	634.61	0	1.15
634.61	634.79	1	1.15
634.79	634.87	0	1.15
634.87	635.04	1	1.15
635.04	635.12	0	1.15
635.12	635.30	1	1.15
635.30	635.36	0	1.15
635.36	635.55	1	1.15
635.55	635.61	0	1.15
635.61	635.82	1	1.15
635.82	635.86	0	1.15
635.86	636.08	1	1.15
636.08	636.11	0	1.15
636.11	636.30	1	1.15
636.30	636.37	0	1.15
636.37	636.55	1	1.15
636.55	636.62	0	1.15
636.62	636.80	1	1.15
636.80	636.89	0	1.15
636.89	637.06	1	1.15
637.06	637.12	0	1.15
637.12	637.32	1	1.15
637.32	799.28	0	1.15

Table 4.5 Continued

Period Start Time, hours	Period End Time, hours	Number of Cigarettes Smoked	Chamber Air-Exchange Rate h^{-1}
Experiment 4C			
799.28	803.40	0	0.65
803.40	803.59	1	0.65
803.59	804.37	0	0.65
804.37	804.55	1	0.65
804.55	805.39	0	0.65
805.39	805.58	1	0.65
805.57	875.61	0	0.65

Each cigarette was smoked in 10 ± 2 minutes. For periods in which more than one cigarette was smoked, the number of cigarettes listed for that period were started at evenly spaced times during the period.

The listed air-exchange rate was maintained for the entire period listed on each line of the table.

Chapter 5. Modeling Framework to Predict Indoor Air Concentrations of Semivolatile Organic Compounds

ABSTRACT

Semivolatile organic compounds (SVOCs) are an important but largely unstudied class of indoor air pollutants. SVOCs have been investigated as outdoor air pollutants, but much less effort has been focused on understanding the factors affecting their concentrations in indoor air. Because of these compounds' low vapor pressures, they readily partition into condensed phases from the gas phase. In outdoor air, this phenomenon is important as a source of secondary organic aerosol and as a mechanism for long range transport and persistence of SVOCs in the atmosphere as particle-phase species. In addition to airborne particles, indoor environments include large amounts of other surfaces per unit air volume including carpet, wallboard, upholstery, ceiling tiles, linoleum, etc. Adsorption to these materials has a strong and markedly different effect on indoor contaminant concentrations because the condensed phase is stationary. Unlike the airborne particle phase, for which ventilation is a significant removal mechanism, the only significant pathway for removal of reversibly sorbed pollutants from the indoor environment is desorption into the gas phase followed by ventilation. Because buildings have a large ratio of surface area to gas-phase volume, the net removal of SVOCs from the indoor environment via this mechanism can be very slow. Compounds re-emitted from one surface may quickly resorb on another. This chapter presents an analysis of factors affecting indoor concentrations of SVOCs including ventilation, gas-particle partitioning, gas-phase sorption on indoor surfaces, particle deposition, and oxidative radical chemistry and estimates their relative importance to facilitate simplification of numerical simulations of indoor pollutant concentrations.

INTRODUCTION

Comprehensive investigations of semivolatile organic compounds (SVOCs) in indoor air have not yet been reported. However, synthesis of data from studies of related topics will facilitate design of studies. Those studies published to date have focused mainly on measurement of concentrations and identification of sources of SVOCs indoors rather than on the factors affecting their dynamic behavior and persistence in the indoor environment. This paper reviews the scientific literature on ventilation, reversible sorption to surfaces, gas-particle partitioning, indoor chemistry, and other processes which impact indoor concentrations of SVOCs. Results from previous studies of the dynamic and equilibrium behavior of organic compounds in indoor and outdoor air are incorporated to demonstrate the relative importance of primary emission sources, reversible sinks, and homogeneous chemical reactions on SVOC concentrations under different building operation and pollutant emission conditions. This information is synthesized within a mathematical framework based on the dynamic processes affecting the fate and persistence of organic compounds in indoor air to assess potential human exposures in four indoor pollution scenarios.

FACTORS IMPACTING INDOOR SVOC CONCENTRATIONS

Sorption on Aerosol Particles and Stationary Indoor Surfaces. A substantial body of research has been published on equilibrium and dynamic partitioning of SVOCs with ambient air aerosols and outdoor environmental surfaces such as vegetation. These studies have demonstrated that three dominant factors influence organic vapor sorption on environmental surfaces: 1) temperature; 2) relative humidity or coverage of the sorbent surfaces by sorbed water; and 3) the surface or bulk phase sorbent chemical composition and physical properties (Bidleman, 1988; Pankow, 1994; Allen *et al.*, 1997; Storey *et al.*, 1995; Lee and Tsay, 1994; Lee and Nicholson, 1994; Falconer and Bidleman, 1994; Foreman and Bidleman, 1990; Gustafson and Dickhut, 1997; Hornbuckle and Eisenreich,

1996; Jang *et al.*, 1997; Jenkins *et al.*, 1996a; Kamens *et al.*, 1995; Kaupp *et al.*, 1994; Kaupp and Umlauf, 1992; Odum *et al.*, 1996; Odum *et al.*, 1994; Pankow and Bidleman, 1992; Pankow *et al.*, 1993; Simonich and Hites, 1994; Subramanyan *et al.*, 1994; Thibodeaux *et al.*, 1991; Umlauf *et al.*, 1994; Westerholm *et al.*, 1991). Sorption in indoor environments has not received as much attention to date, but understanding of this important process is improving.

Physical adsorption processes on environmental surfaces are often assumed to occur analogously to the following reversible chemical reaction (Axley, 1991; Axley and Lorenzetti, 1993):

$$A_g + S \rightleftarrows S - A + \Delta H_{sorption} \tag{5.1}$$

where A_g is a reversibly sorbing contaminant in the gas phase, S is an unoccupied surface sorption site, S-A is an occupied sorption site (formed by adsorption of a molecule of A on a site S), and $\Delta H_{sorption}$ is the heat of adsorption (kJ mol^{-1}). This "reaction" can be applied to reversible sorption on both fixed and airborne particle surfaces. A correction to this conceptual model is required for dynamic analyses of partitioning processes which incorporate effects of transport in the bulk phase of the sorbent. Equation 5.1 can be used to derive an equilibrium relationship for gas-particle partitioning:

$$K_p = \frac{[S-A]}{[A_g][S]} \tag{5.2}$$

where K_p is the equilibrium constant (m^3 mol^{-1}), "[ ]" denotes the "concentration" of one of the reactants or products (S-A, A_g, or S) in air (mol m^{-3}). The concentrations on the right side of equation 5.2 have different meanings for gas-particle and gas-surface partitioning. The meaning of $[A_g]$ is the same in both cases, but the expressions for the concentrations of occupied ($[S\text{-}A]$) and unoccupied ($[S]$) surface sites in air are not defined

in the same manner for fixed surfaces as for particle surfaces. This topic is discussed in further detail in succeeding sections of this chapter.

Gas-Particle Partitioning Equilibrium and Kinetics. Equilibrium partitioning between the gas and particle-sorbed phases in the atmosphere is most often modeled using the linear portion of the Langmuir adsorption equation (Pankow, 1987; Allen *et al.*, 1997; Odum *et al.*, 1996). Other mathematical expressions for equilibrium partitioning have been applied by some researchers, but these equations also reduce to a linear partitioning relationship at low surface coverages (Bidleman, 1988). This simplification has been demonstrated for single compounds at low concentrations, but it may require correction for sorption of many different compounds each sorbed at low levels (Allen *et al.*, 1996). Equation 5.2 can be converted to a linear-Langmuir expression by incorporating the product of the mass concentration of airborne particles, C_{pm_i} (mg m^{-3}), and a proportionality factor to link particle mass to surface, A_{p_i} (m^2 mg^{-1}). Modifying equation 5.2 in this way and rearranging slightly yields

$$C_{p_i} = K_p' C_g A_{p_i} C_{pm_i} \tag{5.3}$$

where C_{p_i} and C_g are the particle-phase and gas-phase SVOC concentrations, respectively (mg m^{-3} of air) and K_p' is the gas-particle partitioning equilibrium constant (m). The subscript i refers to particles with aerodynamic diameter d_{p_i} (m). For spherical particles of diameter d_{p_i} and unit density,

$$A_{p_i} = \left(6 \times 10^{-9}\ \mathrm{m}^3\ \mathrm{mg}^{-1}\right) \Big/ d_{p_i}. \tag{5.4}$$

Equation 5.3 is the most commonly reported equilibrium relationship for partitioning of SVOCs between the gas and airborne particle phases (Bidleman, 1988; Pankow, 1987; Pankow, 1994; Allen *et al.*, 1997; Storey *et al.*, 1995; Hornbuckle and Eisenreich, 1996). In this study, it is assumed that particle sorption capacity is proportional to the airborne particle surface area as expressed in equation 5.3

The temperature dependence of K_p' in equation 5.3 is obtained from a semi-empirical fit to the Clausius-Clayperon equation. Linear regressions to data sets from several studies of SVOC gas-particle partitioning have indicated an inverse proportionality between absolute temperature, T (K) and $\log\left(K_p'/A_{p_i}\right)$ (Pankow, 1994; Jenkins *et al.*, 1996a; Pankow *et al.*, 1993). The effects of varying relative humidity, *RH* (%), can be accounted for in a similar manner using a simple linear regression to data reported by Pankow *et al.* (1993) who found slopes ranging from -0.004 to -0.009 for plots of $\log\left(K_p'/A_{p_i}\right)$ vs. *RH*. These results are similar to those reported in several studies of nonpolar VOC adsorption on soil mineral surfaces (Goss and Eisenreich, 1996) and on gas-surface partitioning in a peat bog (Hornbuckle and Eisenreich, 1996). Combining the effects of T and *RH* on gas-particle partitioning into a single equation produces

$$\log\left(\frac{K_p'}{A_{p_i}}\right) = \frac{\alpha_p}{T} + \beta_p + \varepsilon_p RH + \psi_p \tag{5.5}$$

where T is the temperature (K); α_p is the slope obtained from a linear regression fit to $\log\left(K_p'/A_{p_i}\right)$ vs. $1/T$ data, ε_p is the slope obtained from a linear regression fit to $\log\left(K_p'/A_{p_i}\right)$ vs. *RH* data, and β_p and ψ_p are obtained from the intercepts of these regressions. In addition to the work discussed above on SVOC adsorption on particle surfaces, there has been some study of a parallel process: absorption of SVOCs by the bulk of the particle. This absorption mechanism has been suggested as the dominant gas-particle partitioning mechanism for SVOCs with secondary organic aerosol, which contains a large fraction of organic carbon (Odum *et al.*, 1996; Liang *et al.*, 1997; Liang and Pankow, 1996). Under these conditions, the partitioning coefficient for SVOCs is inversely related to the subcooled liquid vapor pressure (p_L°). This model gives excellent fits to data collected for partitioning of SVOCs onto laboratory generated dioctylphthalate, ambient smog, ammonium sulfate, and environmental tobacco smoke

particles in addition to synthetic secondary organic aerosol particles generated from whole gasoline vapor (Liang *et al.*, 1997). Incorporation of a correction for activity in the sorbed phase is necessary to accurately predict partitioning of polar SVOCs in nonpolar organic phases (Jang *et al.*, 1997).

The equilibrium relationships between the gas and particle phases for SVOCs in outdoor air have been fairly thoroughly elucidated. In contrast, the kinetics of the SVOC-particle adsorption-desorption-absorption process are not as well understood. Though there have been several reports of observed variations in gas-particle SVOC concentration ratios, a predictive model describing the dynamics of this phase transfer has not yet been reported. Those studies that have been published on this subject indicate that the partitioning dynamics between gas and sorbed phases may occur on the order of a day or less. A study of SVOCs in a peat bog reported measurable diurnal variations in the gas phase concentration which the authors attributed to changes in the partitioning coefficient with temperature (Hornbuckle and Eisenreich, 1996). Gustafson and Dickhut (1997) reported that rates of desorption from particles in the atmosphere were comparable to the rate of homogeneous-phase photolysis reactions with characteristic times on the order of a day or two. The rate of gas-urban aerosol reequilibration for PAH and oxygenated PAH in response to a temperature or relative humidity change is strongly dependent on the molecular weight (and consequently the vapor pressure) of the SVOC. Higher molecular weight (lower vapor pressure) compounds repartitioned much more slowly than more volatile species (Allen *et al.*, 1997).

Gas-Surface Partitioning. Adsorption onto stationary surfaces in indoor environments is generally the dominant mechanism impacting long-term exposures to SVOCs and other reversibly sorbing contaminants. Many investigators have studied adsorption of organic compounds on sorbent materials including carpet, painted and unpainted gypsum wallboard, furniture coverings and upholstery, hardwood flooring, and stainless steel (Chapter 2; Chapter 3; De Bortoli *et al.*, 1996; Kjaer *et al.*, 1996; Borrazzo

et al., 1993; Colombo *et al.*, 1993; Jørgensen *et al.*, 1993; Tichenor *et al.*, 1991; Borrazzo *et al.*, 1990; Matthews *et al.*, 1987; Seifert and Schmahl, 1987). In contrast to SVOC gas-particle partitioning, for which most published studies have focused on equilibrium issues, indoor gas-surface sorption has been examined more thoroughly from a kinetic perspective. Equilibrium partitioning in indoor environments has been mostly neglected. In general, the characteristic time scale for indoor air exchange with outdoor air is much shorter than that for sorption equilibrium. Additionally, the intrasorbent diffusion transport distance (and the characteristic time to reach equilibrium) is generally much shorter for particles than for indoor building materials such as carpet and wallboard.

Pollutants whose indoor source strengths vary with time are most significantly affected by surface sorption phenomena (Axley, 1991; Axley and Lorenzetti, 1993). Peak concentrations are depressed while indoor lifetimes are extended. Due to reversible sorption, surfaces serve both as sinks that reduce gas-phase concentrations and as secondary sources that result in elevated indoor concentrations after removal of the primary sources. If the air concentration in contact with a surface is greater than the concentration in equilibrium with the sorbed mass on that surface, a net flux from the gas phase to the sorbed phase results and the surface behaves as a sink. For systems in which the equilibrium concentration exceeds the actual gas-phase concentration, net desorption occurs and the surface acts as a secondary source.

Sorption kinetics and equilibrium depend strongly on the properties of the sorbate compound as well as the nature of the sorbent material. Very few studies have directly considered the importance of gas-surface interactions of SVOCs in indoor air. Gebefugi and Korte (1988) showed that various types of fibrous materials have different affinities for semivolatile organic sorbates. Seifert and Schmahl (1987) showed that reversible sorption has a significant effect on the concentration vs. time behavior of several organic compounds, including many VOCs and a few SVOCs, in contact with plywood and nylon and wool carpeting. They reported that the removal rate of the less volatile compounds,

such as lindane, α-pinene, and d-limonene, from the chamber ceased to depend on the air-exchange rate within a few hours after a pulse injection of the compounds. Instead, the concentration decay was governed by sorption phenomena. A study of PCB concentrations in the downwind plume near a harbor dredging site revealed larger concentrations indoors than outdoors, even for homes directly adjacent to the active dredging site (Vorhees *et al.*, 1997). The authors attributed this observation to two factors: indoor emissions from primary sources such as sealants and fluorescent light ballasts, and continuous slow re-emission of PCBs deposited during earlier periods with higher outdoor (and indoor) concentrations. The second hypothesis is supported by the predominance of heavier PCB congeners in indoor samples relative to simultaneously collected outdoor samples. Other studies, such as those conducted by Borrazzo *et al.* (1990, 1993) have focused on the interactions of more volatile compounds such as ethanol and trichloroethylene with fleecy materials such as carpet fibers and pillow stuffing. They found that the sorbed phase is more favored for compounds with lower volatilities. Tichenor *et al.* (1991) monitored the total VOC concentration in a test house following application of a wood stain. They found that the concentration decay rate was much slower than that due to ventilation alone. Adsorption rates depended much less strongly on the strength of the sorptive interaction than desorption rates, probably because of the interference of other factors such as bulk-phase transport.

Decay by Chemical Reaction. Indoor homogeneous gas-phase chemistry is often neglected because of the drastically smaller actinic flux available to drive photolysis reactions relative to that encountered outdoors during daylight hours (Nazaroff and Cass, 1986). However, although photodegradation reactions are likely to be prohibitively slow in indoor environments, other reaction pathways for organic compounds involving ozone induced production of the hydroxyl radical have been demonstrated to be not only feasible but potentially significant (Weschler and Shields, 1996, 1997, 1998). Ozone reacts in air with alkenes to produce oxidized compounds such as aldehydes, ketones,

alcohols, and carboxylic acids (Atkinson and Carter, 1984) These reactions also generate the hydroxyl (OH) radical which is an important sink for many organic compounds, including airborne particle-sorbed pesticides (Palm *et al.* 1997) and polychlorinated biphenyls (Anderson and Hites, 1996), in the atmosphere.

Recent studies of chemical sources and sinks for organic compounds in indoor air have demonstrated that indoor hydroxyl radical concentrations can, under some conditions, be comparable to those encountered outdoors because of reactions of ozone with alkenes. Indoor concentrations of alkenes are generally greater than those outdoors because of indoor emission sources. Due to infiltration of outdoor air, indoor ozone concentrations often exceed 20 ppb or even 30 ppb in summer in middle latitude urban areas. Indoor concentrations exceeding 1 ppb are typical in northern mid-latitudes even during winter. Depending on the indoor concentrations of alkenes, these conditions could generate OH radical concentrations of 10^{-6} to 10^{-5} ppb in indoor air. These concentrations are two orders of magnitude lower than typical summer noontime levels in mid latitudes (Atkinson *et al.*, 1995; Weschler and Shields, 1996). Thus, degradation rates for organic compounds in indoor air due to oxidation by OH radical are likely to be at least 10 to 100 times slower than they are in outdoor air. These low reaction rates indicate that homogeneous reaction with radicals is unlikely to contribute significantly as a sink for most indoor SVOCs. However, inclusion of these processes in indoor air quality models is merited because organic compound reactions with the hydroxyl radical typically generate products such as carbonyls, organic acids, and other oxidized organics which are more toxic or irritating than the original reactants. Additionally, ozone chemistry may be an important indoor removal mechanism for SVOCs with conjugated double or triple bonds, such as α-pinene or α-limonene, whose ozone reaction rates are relatively fast (Weschler and Shields, 1996).

MODELING FRAMEWORK

Generalized Governing Equation for Gas Phase SVOCs. Simulation of indoor SVOC concentrations requires simultaneous solution of several coupled differential equations. The first of these equations is the mass balance for a single gas-phase contaminant compound in a well-mixed indoor environment:

$$\frac{dC_g}{dt} = \frac{E_g(t)}{V} + \lambda_v\left(C_{go} - C_g\right) + \sum_{h=r,p,s,d}\left(\frac{dC_g}{dt}\right)_h \tag{5.6}$$

where t is time (h); $E_g(t)$ is the time dependent rate of primary (not reemission of previously sorbed mass) gas-phase SVOC indoor emissions (mg h^{-1}); V is the indoor volume (m^3); λ_v is the building air exchange rate (h^{-1}); C_{go} and C_g are the outdoor and indoor gas-phase SVOC concentrations, respectively (mg m^{-3}); and the four differential term subscripts r, p, s, and d refer to the net rate of mass loss from the gas phase due to chemical reactions, sorption on airborne particles, sorption on surface materials, and sorption on deposited particles, respectively (mg m^{-3} h^{-1}). The emission term is generalized to permit consideration of contaminants, such as environmental tobacco smoke components and cooking or cleaning product emissions, whose emission rates vary with time.

In the model described here, all chemical reactions affecting the concentration of the compound of interest are assumed to be represented by a single pseudo-first order rate constant, k_{rg} (h^{-1}). Thus, the reaction (r) term in equation 5.6 is

$$\left(\frac{dC_g}{dt}\right)_r = -k_{rg}C_g \tag{5.7}$$

This assumption is justified by the relatively minor influence that gas-phase radical chemistry has as a sink for SVOCs. Because of their high reactivity, the concentrations of hydroxyl and other radicals are often assumed to very rapidly achieve a pseudo-steady state based on radical production rates at a given time. Reaction conditions tend to vary

over a diurnal cycle, so k_{rg} represents an effective average rate constant. A more accurate, but significantly more computationally intensive, approach would be to couple the model described in this study to a more complete indoor chemistry model capable of predicting time dependent indoor radical concentrations. The mathematical expressions for the gas-airborne particle (p), gas-surface (s), and gas-deposited particle (d) sorption terms in equation 5.6 are similar. In each case, a separate mass balance equation is required for the sorbed phase. The indoor surface sorbed and deposited particle sorbed phases are immobile with no sources or sinks other than dynamic exchange with the gas phase, heterogeneous decay analogous to equation 5.7, and deposition of particles containing SVOC (deposited particle phase only). The particle-sorbed phase is removed by ventilation, deposition of particles, and heterogeneous decay and replenished by infiltration of potentially contaminated outdoor particles in addition to dynamic gas-particle partitioning. The following three subsections detail model treatments for these indoor sorbed phases. Representative ranges for each of the model parameters discussed in this section are given in Table 5.1 along with justification for selection of the given values.

Particle Phase Mass Balance. The gas-particle partitioning term in equation 5.6 can take a variety of mathematical forms. A simple model in which the adsorption rate on particle surfaces is first order in the gas-phase concentration, and the desorption rate is first order in the mass sorbed is described by

$$\left(\frac{dC_g}{dt}\right)_p = -\sum_{i=1}^{\omega}\left(A_{p_i}C_{pm_i}k_{ag-p_i}C_g - k_{dg-p_i}C_{p_i}\right) \tag{5.8}$$

where k_{ag-p_i} and k_{dg-p_i} are the gas-particle adsorption (m h^{-1}) and desorption (h^{-1}) rate constants, respectively, for particles of aerodynamic diameter d_{p_i}, and ω is the total number of discrete particle diameters considered in the analysis. These adsorption and

desorption rate constants are related through the equilibrium constant K_p' by the following equation:

$$K_p' = {k_{ag-p_i}}/{k_{dg-p_i}} \tag{5.9}$$

where K_p' is the equilibrium partitioning constant (m) from equation 5.3. As noted in a preceding section, no definitive information on gas-particle partitioning kinetics is available in the literature. However, an estimate of the adsorption rate constant, k_{ag-p_i} can be derived from kinetic theory for mass and heat transfer to aerosol particles (Seinfeld, 1986, §8.3) and reactive gas deposition on indoor surfaces (Cano-Ruiz *et al.*, 1993). The diffusive flux, J_{D_i} (mg m^{-2} h^{-1}), to the surface of a single particle whose diameter, d_{p_i}, is much greater than the mean free path (λ_p) of its surrounding air molecules is (Seinfeld, 1986, equation 8.93)

$$J_{D_i} = \frac{2}{d_{p_i}} D_g \left(C_{g\infty} - C_{gS} \right) \tag{5.10}$$

where D_g is the diffusion coefficient for sorbate molecules in air (m^2 h^{-1}); and $C_{g\infty}$ and C_{gS} (mg m^{-3}) are the gas phase sorbate concentration far from the particle and at the particle surface, respectively. The diffusion coefficient of a compound in a binary mixture of gases in which 1) the compound's concentration is very small relative to the concentration of the other component and 2) molecules are assumed to be hard spheres can be calculated from the Chapman-Enskog theory for binary diffusivity (Seinfeld, 1986, §8.1.1). To a first approximation, low concentrations of a sorbate in air can be modeled in this manner. Combining Seinfeld's equations 8.5 and 8.9 produces the following expression for D_g:

$$D_g = \frac{3}{32} \frac{\langle v \rangle \sqrt{1 + {m_s}/{m_a}}}{\sigma_{a-s}^2} \frac{kT}{P} \tag{5.11}$$

where m_s and m_{air} are the molecular weights of a single sorbate and "average" air molecule (m_{air} = 4.8 × 10^{-26} kg at 50% RH), respectively (kg); k is the Boltzmann constant (1.38 × 10^{-23} J K^{-1} = 1.79 × 10^{-10} mg m^2 h^{-2} K^{-1}); P is the air pressure (Pa), $\sigma_{a\text{-}s}$ is the collision diameter for binary collisions between sorbate and air molecules (m), and $\langle v \rangle$ is the mean molecular speed of sorbate molecules in air (m h^{-1}) given by

$$\langle v \rangle = \sqrt{\frac{8kT}{\pi m_s}}. \tag{5.12}$$

For sorbate species that are rapidly adsorbed at the particle surface, the total flux to the particle is given by equation 5.10 with $C_{gS} = 0$. If this simplification is not justified then a correction factor, known as the sticking or accommodation coefficient, γ (no units), is incorporated. This coefficient is the fraction of molecules striking the particle surface that adhere without rebounding. The adsorptive flux at the particle surface, J_{S_i} (mg m^2 h^{-1}) is (Cano-Ruiz *et al.*, 1993)

$$J_{S_i} = \frac{\gamma \langle v \rangle C_{gS}}{4} \tag{5.13}$$

From mass balance, $J_{D_i} = J_{S_i} = J_{p_i}$, the net adsorptive mass flux to the particle surface. The flux to a surface is related to the deposition velocity or adsorption rate coefficient, k_{ag-p_i} by (Nazaroff and Cass, 1989)

$$J_{p_i} = k_{ag-p_i} C_{g\infty}. \tag{5.14}$$

The following expression for k_{ag-p_i} is obtained by combining equations 5.10 and 5.13, solving for J_{p_i}, and substituting equation 5.14 to eliminate $C_{g\infty}$:

$$k_{ag-p_i} = \frac{2}{d_{p_i}} D_g \left[1 + \frac{8D_g}{\gamma \langle v \rangle d_{p_i}} \right]^{-1}. \tag{5.15}$$

Inherent in the derivations of equations 5.10, 5.13, and the resulting equation 5.15 is the assumption that the gas surrounding the particle behaves as a continuum fluid. Mass transport to the particle surface due to random molecular motion can be simulated using

the diffusion equation. However, when the size of the particle approaches the scale of the mean free path of the gas molecules with which it interacts, this approximation begins to fail. The Knudsen number, Kn_i, has been defined to characterize the graininess of the gas relative to the particle diameter as follows (Seinfeld, 1986 §8.1):

$$Kn_i = {2\lambda_p}/{d_{p_i}} \tag{5.16}$$

where λ_p is the mean free path of the gas molecules (0.065 μm for air at 298 K and 1 atmosphere). If $Kn_i << 1$, the continuum approximation is valid and the diffusion equation can be used to predict gas-particle partitioning kinetics. If Kn_i is greater than or approximately equal to 1, gas-particle dynamics are best described using an interpolation equation such as that of Fuchs and Sutugin (Seinfeld, 1986 §8.7) which provides a multiplicative correction factor, f_i, to the gas-particle adsorption coefficient calculated in equation 5.15:

$$f_i = \frac{1 + Kn_i}{1 + 1.71Kn_i + 1.333Kn_i^2}. \tag{5.17}$$

For d_{p_i} = 0.05 μm, the smallest particles considered in this analysis, f_i = 0.25. As the particle size increases, f_i approaches unity — f_i (0.3 μm) = 0.72 and f_i(3 μm) = 0.97.

Figure 5.1 illustrates the effects of varying particle size, accommodation coefficient (γ), and SVOC molecular weight (MW) on the gas-particle deposition velocity for particles of diameter d_{p_i} (k_{ag-p_i}). Changes in γ and d_{p_i} have a significant effect on k_{ag-p_i} while a threefold increase in MW has a small impact on all but the largest particles. The model simulations described in the next section were obtained using values of k_{ag-p_i} from Figure 5.1 (calculated with equations 5.11, 5.15, and 5.17). Gas-particle desorption rate constants were obtained using literature values for the partitioning equilibrium constant (K_p') and equation 5.9, which relates k_{ag-p_i} and k_{dg-p_i}. In this analysis, K_p' is assumed to be independent of d_{p_i}. The adsorption and desorption rate constants do vary with particle size, but their ratio is a constant for any given SVOC. This method is

adequate for compounds present at low concentrations whose equilibrium partitioning is well described by equation 5.3. Additional model complexity would be required to account for partitioning processes that are kinetically limited by transport through the bulk of a particle rather than by particle surface processes or those in which partitioning equilibrium is described by a nonlinear isotherm. For mass balance closure, the arithmetic inverse of this expression must appear in the equation for the airborne concentration of particle-sorbed SVOC:

$$\frac{dC_{p_i}}{dt} = \frac{E_{p_i}(t)}{V} + \lambda_v\left(C_{p_i o} - C_{p_i}\right) - \left(k_{rp} + \frac{k_{dpm_i} S_T}{V}\right) C_{p_i} + \left(A_{p_i} C_{pm_i} k_{ag-p_i} C_g - k_{dg-p_i} C_{p_i}\right) \tag{5.18}$$

where $E_{p_i}(t)$ is the time dependent rate of primary particle-phase SVOC indoor emissions (mg h^{-1}), k_{rp} is the pseudo-first order rate constant for degradation of particle phase SVOCs (h^{-1}), k_{dpm_i} is the particulate matter deposition velocity (m h^{-1}) for particles of diameter d_{p_i}, S_T is the total indoor surface area available for particle deposition (m^2), and $C_{p_i o}$ is the outdoor particle-phase SVOC concentration for particles of diameter d_{p_i} (mg m^{-3}). The pseudo-first order reaction rate constant accounts for heterogeneous reactions of particle-phase SVOCs with gas-phase oxidants such as the OH radical. Particle-phase SVOCs are also removed from indoor air by deposition of the particles with which they are associated onto indoor surfaces. Equation 5.18 does not account for variations in gas-particle sorption dynamics which might result from interparticle differences in chemical composition.

Because the mass concentration of indoor airborne particles may vary independently from gas-phase and particle-phase SVOC concentrations, a mass balance on particle mass must be considered as well:

$$\frac{dC_{pm_i}}{dt} = \frac{E_{pm_i}(t)}{V} + \lambda_v\left(C_{pm_i o} - C_{pm_i}\right) - k_{dpm_i} \frac{S_T}{V} C_{pm_i} \tag{5.19}$$

where $E_{pm_i(t)}$ is the time dependent rate of primary particulate matter indoor emissions (mg h^{-1}) and $C_{pm_i o}$ is the outdoor particulate matter concentration (mg m^{-3}) for particles with aerodynamic diameter d_{p_i}. Equation 5.19 assumes the effects of coagulation on the concentration of particles in each size fraction *i* is negligible.

Sorbed Phase Mass Balance. Airborne SVOCs accumulate on indoor surfaces through two different mechanisms: reversible adsorption from the gas phase and deposition of airborne particle-associated SVOCs. If the gas-surface sorption kinetics are described by a linear model, the gas-surface sorption partitioning term in equation 5.6 is related to the change of sorbed mass in a manner similar to equation 5.8:

$$\left(\frac{dC_g}{dt}\right)_s = -\frac{1}{V}\sum_{j=c,w} S_{s_j}\left(k_{ag-s_j}C_g - k_{dg-s_j}M_{s_j}\right) \tag{5.20}$$

where k_{ag-s_j} and k_{dg-s_j} are the adsorption (m h^{-1}) and desorption (h^{-1}) rate constants, respectively, describing gas-phase sorption kinetics and M_{s_j} is the SVOC mass reversibly sorbed at the air-sorbent interface of indoor surface material *j* (mg m^{-2}). The major difference between equations 5.8 and 5.20 lies in the treatment of the "surface area concentration" which was expressed as the product of the area per particle mass and the particle mass concentration in equation 5.8. For indoor surfaces, this value is better expressed as the ratio of the total available surface area for sorption on surface *j*, S_{s_j} (m^2), and the indoor volume, V (m^3).

Several models of gas-surface interactions are available to predict rates of adsorption and desorption of a reversibly sorbing compound. One of the earliest is that originally described by Dunn and Tichenor (1988) to predict the uptake and release of VOCs by materials in an emission test chamber and later applied by Tichenor *et al.* (1991) to VOC sorption on indoor sinks such as carpet, wallboard, ceiling tile, window glass, and upholstery. Three key assumptions in this model are (1) sorption occurs only on the surface of the sorbent, (2) equilibrium partitioning between the gas and sorbed

phases is best described by the Langmuir adsorption isotherm, and (3) the partial pressure of the sorbate remains significantly below its saturation vapor pressure. The second and third assumptions permit simplification of the Langmuir isotherm to a linear partitioning relationship in which the sorbed mass density is proportional to the gas-phase concentration. Other potential dynamic models for gas-surface partitioning have been reported for nicotine on stainless steel (Chapter 2) and VOCs and SVOCs on porous materials such as carpet and wallboard (Chapter 3; Dunn and Chen, 1993; Little and Hodgson, 1996). The model formulation for the linear partitioning surface sorption model described by Tichenor *et al.* (1991) is shown in equation 5.20 above and completed in the following equation with a term accounting for heterogeneous chemical decay of surface sorbed SVOCs:

$$\frac{dM_{s_j}}{dt} = k_{ag-s_j} C_g - k_{dg-s_j} M_{s_j} - k_{rs_j} M_{s_j} \tag{5.21}$$

where k_{rs_j} is the pseudo-first order heterogeneous chemical decay rate for SVOCs sorbed at the air-sorbent interface of material j (h^{-1}). For porous sorbents such as carpet and wallboard, an additional term accounting for diffusion into the sorbent bulk must also be included in the mass balance equation for the air-sorbent interface:

$$\frac{\partial M_{s_j}}{\partial t} = k_{ag-s_j} C_g - k_{dg-s_j} M_{s_j} + D_{b_j} \left(\frac{\partial C_{b_j}(t,z)}{\partial z} \right)_{z=0} - k_{rs_j} M_{s_j} \tag{5.22}$$

where D_{b_j} is the SVOC diffusion coefficient in the bulk of porous sorbent j ($m^2\ h^{-1}$), $C_{b_j}(t,z)$ is the instantaneous sorbent bulk-phase SVOC concentration at a distance z away from the air-sorbent interface (mg m^{-3}), and z is the distance into the bulk of the sorbent material, with $z = 0$ at the sorbent surface (m). The SVOC mass balance in the sorbent bulk reflects only diffusive transport:

$$\left(\frac{\partial C_{b_j}(t,z)}{\partial t} \right) = D_{b_j} \left(\frac{\partial^2 C_{b_j}(t,z)}{\partial z^2} \right). \tag{5.23}$$

No term for SVOC reaction in the bulk of the sorbent is included in equation 5.22 because chemical decay of SVOCs is assumed to occur by reaction with gas-phase oxidants such as hydroxyl radical and ozone whose lifetimes due to chemical reaction are much shorter than the time necessary to diffuse any significant distance into the bulk of a sorbent.

Surface-Deposited Particle Phase SVOC Mass Balance. Deposition of airborne particles onto indoor surfaces is treated similarly to equation 5.20 with the exception that particles are assumed not to be resuspendable. In this analysis, the deposition velocity for a given particle aerodynamic diameter, k_{dpm_i} (m h^{-1}), is the effective average over all surfaces for particle deposition on indoor surface materials. The term in equation 5.6 accounting for partitioning between the gas phase and deposited particles is

$$\left(\frac{dC_g}{dt}\right)_d = -\frac{1}{V}\sum_{j=c,w}\left[\sum_{i=1}^{\omega}\left(A_{p_i} M_{pm_{ij}} k_{ag-dp_{ij}} C_g - k_{dg-dp_{ij}} M_{p_{ij}}\right)\right] \qquad (5.24)$$

where $M_{pm_{ij}}$ is the deposited particle mass of particles of diameter d_{p_i} per unit area of indoor surface material j (mg m^{-2}); $M_{p_{ij}}$ is the SVOC mass associated with these particles deposited per unit area of surface j (mg m^{-2}); and $k_{ag-dp_{ij}}$ and $k_{dg-dp_{ij}}$ are the adsorption and desorption rate constants, respectively, for sorption of gas-phase SVOCs on particles of diameter d_{p_i} deposited on surface j. These sorption rate constants are represented distinctly from those for sorption on airborne particles because the concentration gradient near a sorbing surface material is likely to differ from that in the mixed core of the room air. The maximum value of $k_{ag-dp_{ij}}$ is limited by k_{ag-s_j}, the adsorption constant for gas-phase SVOCs on surface j, and $k_{dg-dp_{ij}}$ is obtained from equation 5.9 using $k_{ag-dp_{ij}}$ in place of k_{ag-p_i}. The overall mass balance equation for particle associated SVOCs deposited on indoor surfaces also includes deposition of SVOCs associated with freshly deposited airborne particles and heterogeneous chemical decay of deposited particle-associated SVOCs:

$$\frac{dM_{p_{ij}}}{dt} = k_{dpm_i}\frac{S_j}{S_T}C_{p_i} + A_{p_i}M_{pm_{ij}}k_{ag-dp_{ij}}C_g - k_{dg-dp_{ij}}M_{p_{ij}} - k_{rp_{ij}}M_{p_{ij}}. \quad (5.25)$$

One additional equation is necessary to keep track of deposited particle mass:

$$\frac{dM_{pm_{ij}}}{dt} = k_{dpm_i}\frac{S_j}{S_T}C_{pmi}. \quad (5.26)$$

Equations 5.25 and 5.26 assume that particle mass accumulates on surfaces through deposition from indoor air only. No removal mechanisms for deposited particle mass are included. Thus, tracking of dirt indoors and resuspension by vacuuming or other cleaning activities is not considered. However, as particulate mass accumulates on the surfaces, the deposited particles do continue to exchange SVOC mass with the gas phase with the same adsorption and desorption rate constants used for airborne particles.

Gas Phase Mass Balance and Model Implementation Methodology. Substituting the terms described in the preceding sections to account for pseudo-first order chemical decay (equation 5.7) and gas-airborne particle (5.8), gas-surface (5.20), and gas-deposited particle (5.24) partitioning into equation 5.6 yields the complete mass balance for gas phase SVOCs:

$$\begin{aligned}\frac{dC_g}{dt} = \frac{E_g(t)}{V} + \lambda_v\left(C_{go} - C_g\right) - k_{rg}C_g - \sum_{i=1}^{h}\left(A_{p_i}C_{pm_i}k_{ag-p_i}C_g - k_{dg-p_i}C_{p_i}\right) \\ -\frac{1}{V}\sum_{j=c,w} S_{s_j}\left(k_{ag-s_j}C_g - k_{dg-s_j}M_{s_j}\right) \\ -\frac{1}{V}\sum_{i=1}^{h}\left(A_{p_i}M_{pm_i}k_{ag-p_i}C_g - k_{dg-p_i}M_{p_i}\right) \quad (5.27)\end{aligned}$$

Model predictions for the scenarios summarized in Tables 5.2 and 5.3 were calculated by simultaneously integrating the coupled ordinary and partial differential equations describing the mass balances for SVOCs in the gas phase (equation 5.27) and airborne particle-sorbed phase (5.18), SVOCs sorbed at the air-sorbent interface (5.22) and in the bulk (5.23) of indoor surface materials, SVOCs associated with deposited particles (5.25), and airborne (5.19) and surface-deposited (5.26) particles. Integration of a system of

coupled ordinary differential equations can be accomplished by Runge-Kutta integration (Press *et al.*, 1992). However, equations 5.22 and 5.23 are partial differential equations which are not integrable by this method. To overcome this problem, the diffusion equation (5.22) was converted into a set of coupled ordinary differential equations by the finite difference method. The thickness of each sorbent in the z direction (normal to the air-sorbent interface plane) was discretized into 10 equal length nodes with boundary conditions given by equation 5.22 for the air-sorbent interface node and a no-flux condition at the node farthest from the interface. A total of 39 coupled ordinary differential equations are solved simultaneously for each time step in the simulations described in the following section. These include 10 finite difference equations for surface sorption and bulk-phase SVOC transport in the two stationary sorbents (10 equations each for carpet and wallboard), the gas-phase mass balance (1 equation), one equation each for airborne particle associated SVOCs and airborne particle mass in each of the three particle aerodynamic diameters listed in Table 5.1 (6 equations), and one equation each for deposited particle-associated SVOCs and deposited particle mass for each of the three particle diameters on each of the two sorbents (12 equations).

DEFINITIONS OF MODELED SCENARIOS

Indoor gas-, airborne particle-, surface sorbed-, and deposited particle-phase SVOC concentrations were simulated for five model scenarios using the Microsoft Visual Basic for Applications macro program listed and described in Appendix D. In each scenario, a 2000 day period is simulated. An initially clean 500 m^3 house containing 200 m^2 of the carpet and 1000 m^2 of the painted wallboard tested in Chapter 3 is exposed to gas- and particle-sorbed phase SVOCs from outdoor air and an indoor source. This house is assumed to have a constant AER of 0.6 h^{-1} which is comparable to the average value reported by Murray and Burmaster (1995) for the U.S. housing stock. The same outdoor concentrations and indoor source strengths are used in all four scenarios and are listed in

Table 5.2. These values are held constant for 1000 days, after which the outdoor particle concentrations remain at the values given in Table 5.2 and the indoor source is eliminated. The model is run for an additional 1000 days to simulate reemission of sorbed and deposited SVOCs.

The outdoor particle values in Table 5.2 correspond to a 60 $\mu g\ m^{-3}$ total concentration with 45% of the particle mass in each of the larger two particle sizes and 10% in the smallest. This particle concentration and size distribution are reasonably representative of polluted urban areas whose daily average particle concentrations are below the federal standard of 150 $\mu g\ m^{-3}$ for PM_{10} (airborne concentration of particles with diameters smaller than 10 μm) but whose annual average exceeds the standard of 50 $\mu g\ m^{-3}$. Recent measurements of ambient particulate matter concentrations in the United States have indicated that approximately 60% of the mass of airborne particles with diameters smaller than 10 μm is attributable to particles with diameters smaller than 2.5 μm (Falke and Husar, 1998). The simulated distribution is an attempt to capture these features of urban aerosols.

The indoor emission rates approximate the particle mass that would be generated by smoking 30 cigarettes per day in the absence of any other particle sources. Because other indoor sources of particulate matter such as shedding of skin and dander from human and animal occupants and other combustion activities such as cooking or heating also generate particles, the listed values could result from a lower smoking rate. The SVOC emission rates correspond approximately to the nicotine emissions that would result from smoking 15 cigarettes per day in the house. Nicotine has the largest emission rate of any SVOC in ETS (Daisey *et al.*, 1994, 1998). This SVOC emission rate would also be approached with lower smoking rates if all compounds in a given class (such as PAHs) or with similar indoor air behavior were lumped. Model scenarios 5B and 5E compare the impacts on indoor concentrations and persistence of using the different

carpet and wallboard sorption kinetics parameters measured in Chapter 3 for nicotine and phenanthrene.

Table 5.3 gives the specific sorption kinetics parameters for gas-surface and gas-particle partitioning in each scenario. All scenarios except 5E use the phenanthrene sorption data obtained in Chapter 3. Run 5E uses nicotine sorption data for surfaces. In Runs 5A, 5B, and 5C, the gas-particle equilibrium partitioning constant is the same. These three model runs allow comparison of the effects of different gas-particle partitioning kinetics. Run 5B (phenanthrene, medium gas-particle kinetics, low gas-particle equilibrium coefficient) is identical to run 5A (phenanthrene, slow gas-particle kinetics, low gas-particle equilibrium coefficient) except the accommodation coefficient, γ, is increased by one order of magnitude to simulate faster gas particle adsorption kinetics. In Run 5C (phenanthrene, fast gas-particle kinetics, low gas-particle equilibrium coefficient), γ, is increased by an additional order of magnitude to simulate faster sorption kinetics. Run 5D (phenanthrene, medium gas-particle kinetics, high gas-particle equilibrium coefficient) uses the same value of γ as 5B so the gas-particle partitioning kinetics are the same in the two runs, but the gas-particle equilibrium constant is 10 times larger in Run 5D to simulate greater particle phase sorption capacity. Because the gas-particle adsorption coefficient k_{ag-p_i} is determined independently of the partitioning coefficient by kinetic theory using equation 5.15 corrected by the continuum approximation correction factor, f, from equation 5.17, increasing the equilibrium constant decreases the gas-particle desorption coefficient k_{dg-p_i} by the same factor as shown in equation 5.9. Run 5E (nicotine, medium gas-particle kinetics, low gas-particle equilibrium coefficient) uses the particle dynamics parameters from Run 5B with the carpet and wallboard sorption constants obtained in Chapter 3 for nicotine. The following section presents the results of these five model simulations. Intercomparisons are made between Runs 5A, 5B, and 5C to examine the effects of changes in gas-particle sorption kinetics; between Runs 5B and 5D to investigate the impact of an order of

magnitude change in the gas-particle partitioning coefficient; and between Runs 5B and 5E to explore the differences in the behavior of nicotine and phenanthrene in indoor air.

RESULTS AND DISCUSSION

Table 5.1 describes the likely ranges of values for the various model parameters considered in this study and the justification for these ranges. In general, for SVOCs such as PAHs and PCBs that have low reaction rates with hydroxyl radical and ozone, indoor chemistry is not likely to have a significant effect on daily airborne concentrations. However, because deposited SVOCs may persist in the indoor environment for many years, even relatively slow rate constants for heterogeneous decay of SVOCs should not be neglected. Despite their small impact on human exposures on any given day, these reactions can have a significant effect on the long-term persistence of indoor SVOCs. Furthermore, as noted earlier, some unsaturated hydrocarbon SVOCs with conjugated double bonds may react rapidly enough with ozone or the hydroxyl radical for this process to be a significant indoor sink.

Indoor reactions of organic contaminants with ozone and oxidizing radicals must be included in comprehensive indoor IAQ models as a potential secondary source of irritating pollutants even if their effects as an SVOC sink are minimal. Weschler and Shields (1996) note that this process has a mostly beneficial effect in the outdoor atmosphere because it increases the water solubility of organic air contaminants and consequently increases their rate of removal by wet deposition. Wet deposition is not an important SVOC removal mechanism in indoor environments. In contrast, oxidation of SVOCs in indoor air may produce more irritating and corrosive contaminants. Recent assessments of irritant characteristics of indoor air (Sundell *et al.*, 1993; Ten Brinke, 1995) have demonstrated that increases in levels of polar (partially oxidized) VOCs in indoor air lead to more frequent complaints from building occupants even when these increases are more than offset by decreases in nonpolar VOC concentrations. Another

potential impact of organic compounds reactions with oxidants indoors was recently described by Weschler and Shields (1998). These investigators showed significant increases in fine mode particulate matter in indoor environments containing terpene and ozone.

Qualitatively, all of the simulations yield similar results. The gas phase concentration slowly increases during the 1000 day period while the source is present, but fails to achieve a steady state during this period. In contrast, the airborne particle phases reach steady state almost immediately because their dominant removal mechanism, ventilation, has a characteristic time of less than 2 hours. The dominant sink for gas phase species is sorption on indoor surface materials. The uptake rate on these materials slows over time as they become loaded. However, as the "B" panels in Figures 5.2 – 5.6 show, the carpet and wallboard sorbed-phase mass curves have clearly positive slopes even after 1000 days of exposure to an indoor source. Once the near-surface layers of the sorbent materials approach saturation, the uptake and release rate of SVOCs from the material is determined by the rate at which the sorbate diffuses between the air-sorbent interface and the sorbent bulk.

The results presented in Figures 5.2 – 5.6 support the commonly accepted paradigm that particle phase SVOCs are a less significant concern in indoor air than is sorption to fixed surfaces. As discussed above, the airborne particle-phase SVOC concentrations in all five scenarios reach an almost immediate plateau during the indoor source phase of each simulation and then decrease to a negligible level almost immediately after it is turned off. The SVOC mass sorbed to indoor surface materials is more than 3 orders of magnitude larger than that of SVOC sorbed to deposited particles — several milligrams on particles compared to tens of grams of surface-sorbed SVOC. Furthermore, the particle sorbed mass on the surfaces is significantly more labile as shown in Figures 5.2 – 5.6. The surface-sorbed phase SVOC mass increases markedly over time while the indoor source is present and decreases fairly slowly, remaining at a significant level even

1000 days after elimination of the source in each scenario. The deposited particle-SVOC mass increases in a nearly linear fashion while the source is on and the decays exponentially after its removal This indicates that the dominant mechanism for increasing the deposited-particle-sorbed SVOC mass is deposition of particles containing sorbed SVOC. The main pathway for elimination of this surface phase is desorption of the particle-phase SVOCs.

In scenarios 5A, 5B, and 5C, the fixed sorbent sorption parameters are identical, but the gas-particle accommodation coefficient γ increases by a factor of 10 from 5A to 5B and from 5B to 5C while the gas-particle equilibrium constant remains the same. As Figures 5.2 – 5.4 show, each order of magnitude increase in γ increases the gas-phase concentration by approximately 5% to 10%. In contrast, the airborne particle-phase SVOC concentrations drop significantly as γ increases. These results are explained mainly by the coupling of the adsorption and desorption rate coefficients (k_{ag-p_i} and k_{dg-p_i}) through the gas-particle equilibrium constant in equation 5.9. A decrease in k_{ag-p_i} also reduces k_{dg-p_i}. Because the indoor source emits SVOCs in the particle phase, this reduction in k_{dg-p_i} leads to an increased particle phase concentration. Similar effects are observed in the surface-deposited phases (sorbed to surface materials and sorbed to deposited particles), but the changes are smaller relative to the sorbed mass. The carpet and wallboard sorbed SVOC mass increases as γ increases because of the increase in the gas-phase concentration while the source is on. Because reemission of SVOC molecules sorbed to these materials is largely dependent on the rate at which they diffuse to the air-sorbent interface from within the sorbent bulk during periods of lowered concentration, the increased mass uptake by the carpet and wallboard during the source on phase results in a larger final sorbed mass at the end of the simulation. The SVOC mass sorbed to deposited particles also increases as γ gets larger. The reason for this small increase is not obvious, but it may result from the combination of an increase in gas-

phase concentration and the faster equilibration between the gas phase and surface deposited particles.

Scenario 5D has identical surface sorption parameters to scenarios 5A – 5C. The accommodation coefficient in scenario 5D is the same as that in scenario 5B, but the gas-particle equilibrium constant K_p'/A_{p_i} is 10 times greater in scenario 5D. This change has a similar effect to decreasing γ and k_{dg-p_i}: the airborne particle-associated SVOC concentrations increase with an increase in the partitioning coefficient and the gas-phase concentration decreases slightly. The reasons for these changes are similar to those discussed in the preceding paragraph. A greater K_p'/A_{p_i} causes the affinity of SVOCs for the particle phase to increase. For a given k_{dg-p_i} (which is constant between the two scenarios because γ is fixed), equation 5.9 mandates that k_{dg-p_i} decrease as K_p'/A_{p_i} increases. The decreases in the modeled sorbed-phase concentrations between Figures 5.3 and 5.5 result from the decreased gas-phase concentration during the period while the indoor source is on

The final comparison that can be made based on the model simulations is between scenarios 5B and 5E which differ only in the fixed-surface sorption parameters. Scenario 5B uses phenanthrene parameters obtained in Chapter 3 and 5E uses nicotine data. Both carpet and wallboard have a greater equilibrium capacity for nicotine than for phenanthrene as indicated by the larger ratio of k_{ag-s_i} to k_{dg-s_i} (using an analog to equation 5.9). Because of this, the gas-phase concentration in Figure 5.6 approaches a significantly smaller steady state value than in Figure 5.3. Additionally, phenanthrene's surface-adsorption rate coefficients (k_{ag-s_i}) for carpet and wallboard are comparable while nicotine's carpet adsorption coefficient is 4 times greater than that for wallboard sorption (see Table 5.3). Furthermore, the diffusion coefficient for phenanthrene in wallboard is two orders of magnitude faster than that for phenanthrene in carpet. These factors lead to a significantly greater relative uptake of nicotine by carpet than by wallboard compared to the predictions for phenanthrene. Also, the smaller diffusion

constant for nicotine in wallboard and the greater sorption capacity of the carpet cause a much slower rate of decay of the wallboard and carpet sorbed mass in Figure 5.6. After 1000 days with the indoor source off, the fixed surface-sorbed masses decrease by less than 15% from their peak values at 1000 days. The results of all of the scenario simulations also demonstrate one additional point: carpet appears to be a much more significant sorbent than wallboard in indoor environments despite the typically much larger presented surface area of wallboard.

CONCLUSIONS

The results of the analyses presented in this chapter have several important implications for study of the dynamic behavior of semivolatile organic compounds and other reversibly sorbing air contaminants in indoor air. The common generalization that particle-phase organic compound dynamics are relatively unimportant in indoor environments is supported by the results presented here. Of much greater importance are the effects of reversible sorption on indoor surface materials such as carpet and wallboard. Carpet appears to be the dominant indoor sorbent for the two relatively chemically dissimilar SVOCs considered in this study.

Estimates of gas phase and heterogeneous rate constants for reactions of SVOCs in indoor air with hydroxyl radical and other oxidants were included in the model simulations. However, the effects of varying these parameters were not considered. This sink for indoor SVOCs is potentially important as a source for partially oxidized organic compounds such as carbonyls and organic acids which can be highly irritating and/or toxic to human building occupants. Additional experimental investigations of indoor chemistry and sorption kinetics for a wider suite of sorbates and indoor sorbents are necessary to more thoroughly simulate indoor concentrations and overall human exposures to these contaminants.

FIGURES

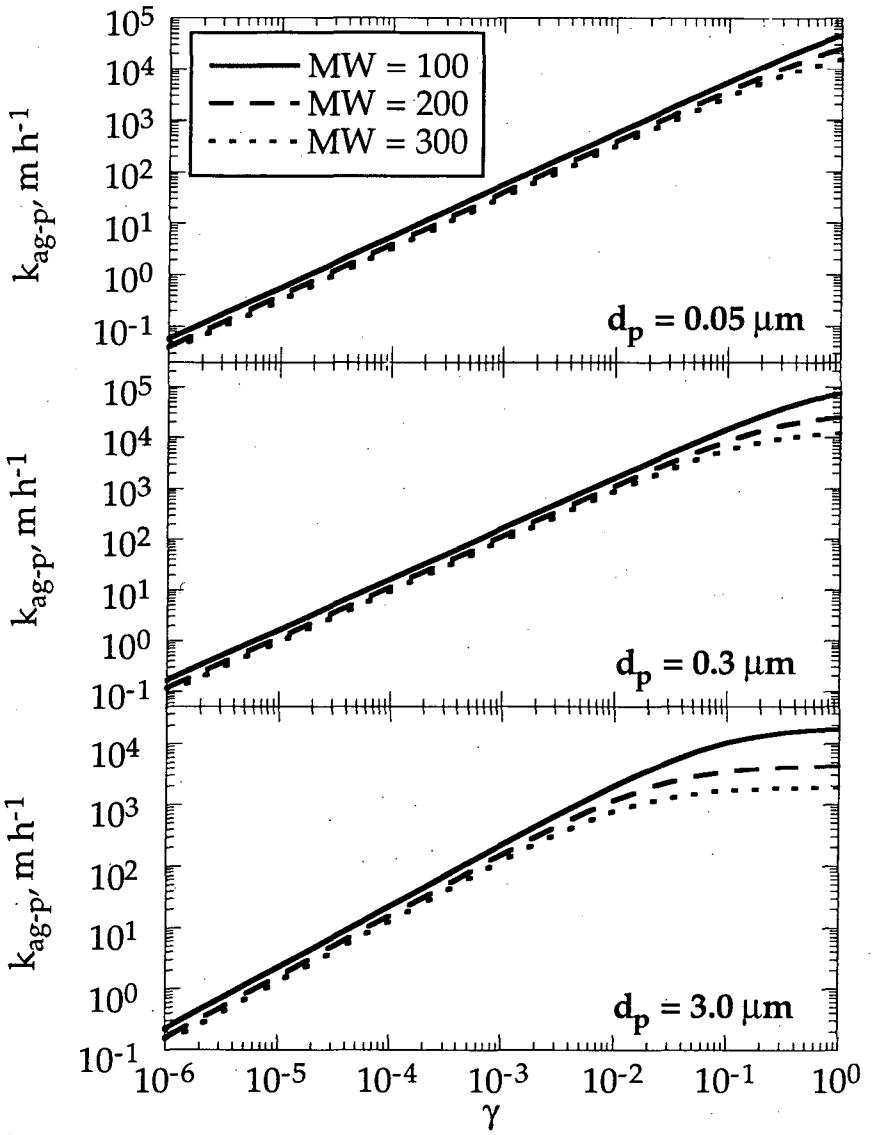

Figure 5.1 Gas-particle adsorption rate constants (k_{ag-p_i}) as a function of accommodation coefficient (γ) and SVOC molecular weight (MW) for different particle diameters, d_{p_i}: 0.05 μm, 0.3 μm, and 3.0 μm. The curves were generated using equation 5.15 and the non-continuum correction factor from equation 5.17.

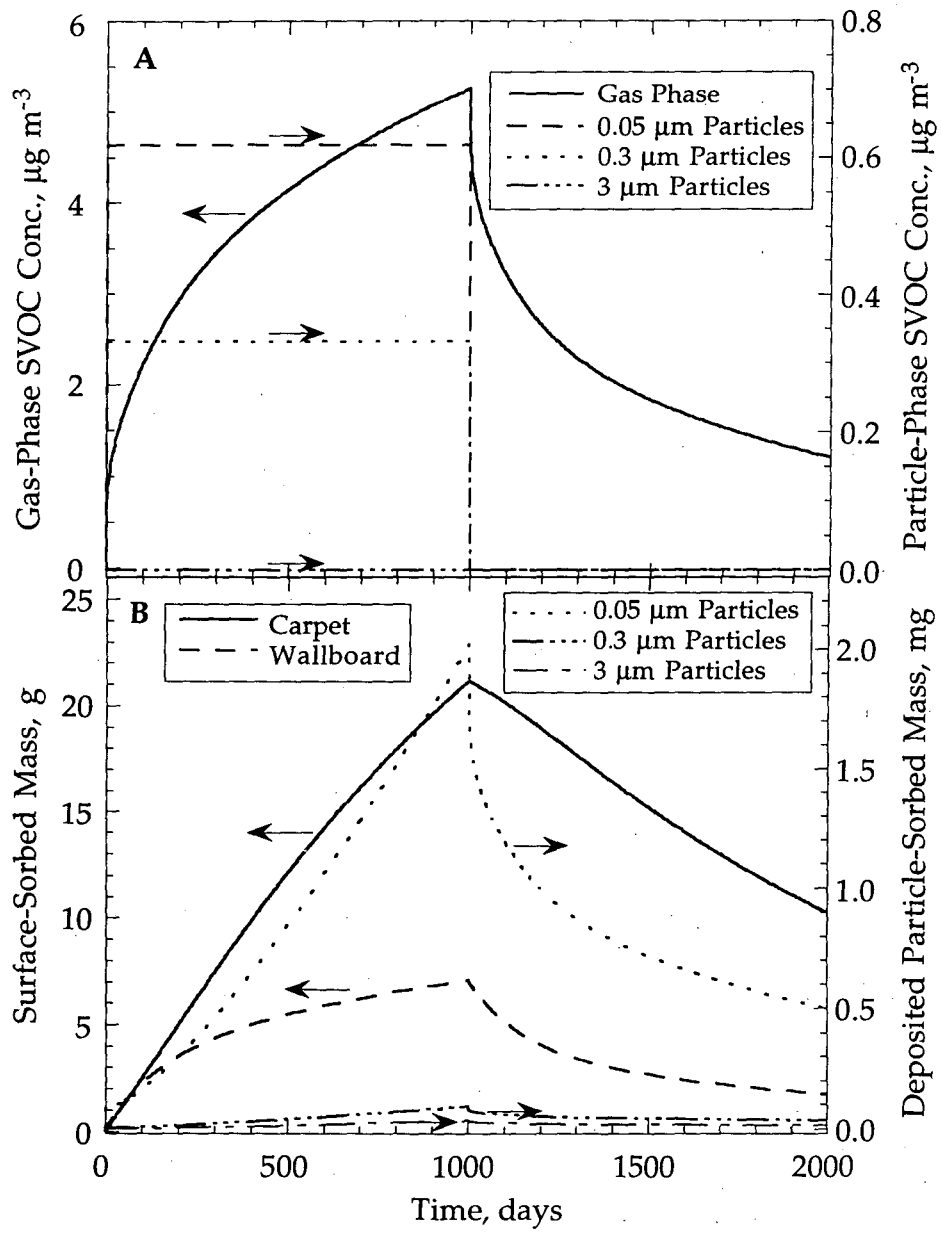

Figure 5.2 Predicted gas and airborne particle phase (**A**) and sorbed and deposited particle phase (**B**) SVOC mass balance for simulation 5A (phenanthrene, slow gas-particle kinetics, low gas-particle equilibrium coefficient).

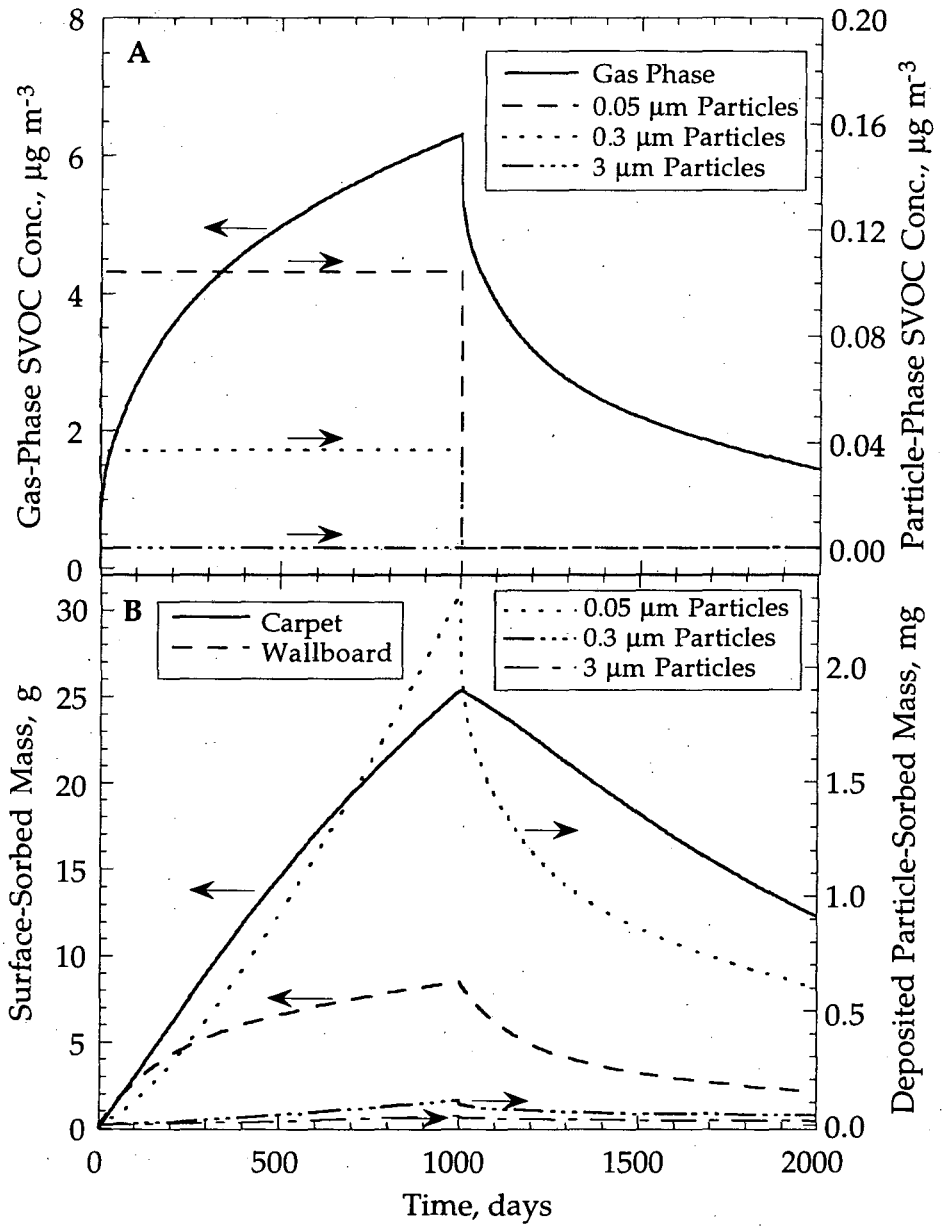

Figure 5.3 Predicted gas and airborne particle phase (**A**) and sorbed and deposited particle phase (**B**) SVOC mass balance for simulation 5B (phenanthrene, medium gas-particle kinetics, low gas-particle equilibrium coefficient).

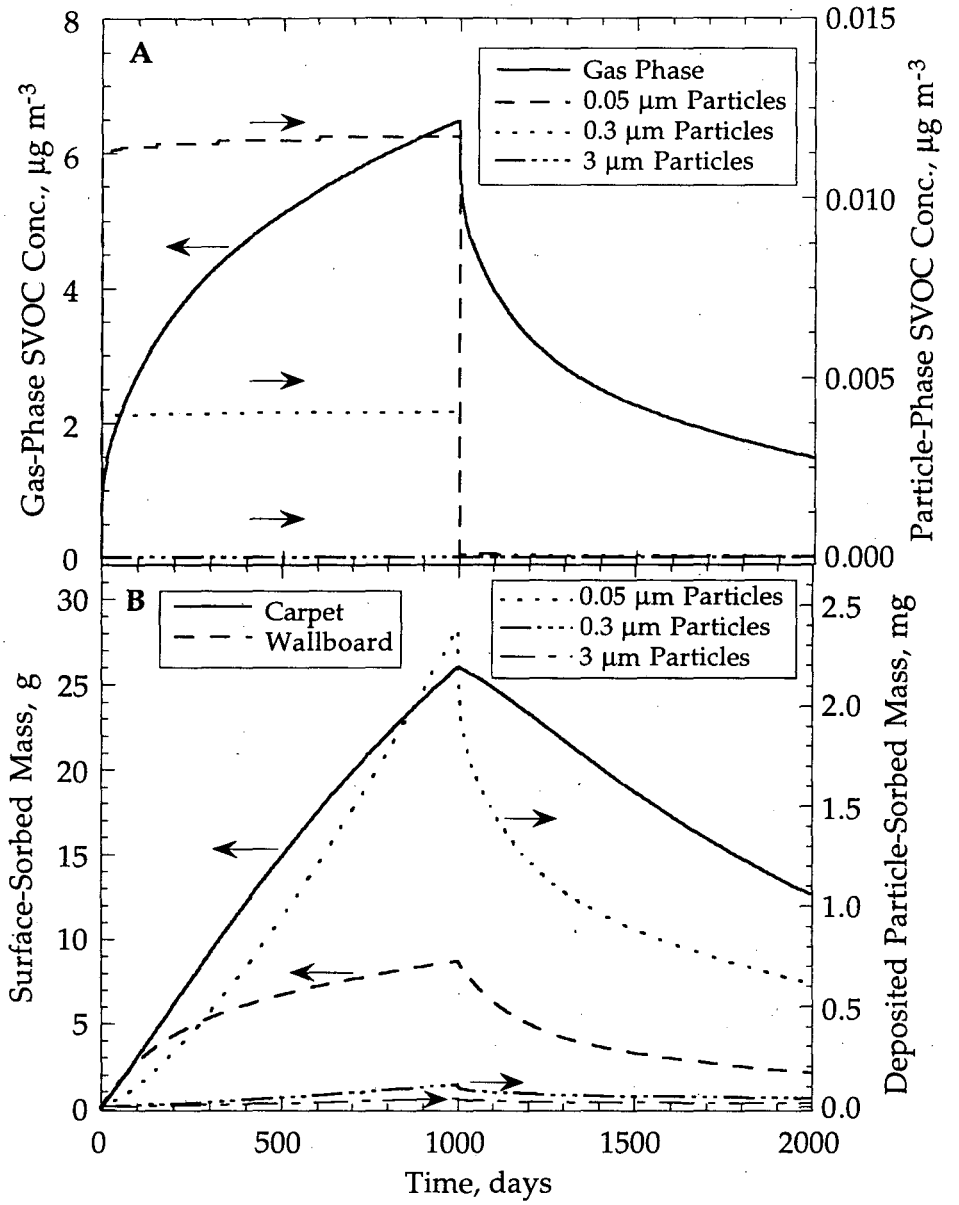

Figure 5.4 Predicted gas and airborne particle phase (**A**) and sorbed and deposited particle phase (**B**) SVOC mass balance for simulation 5C (phenanthrene, fast gas-particle kinetics, low gas-particle equilibrium coefficient).

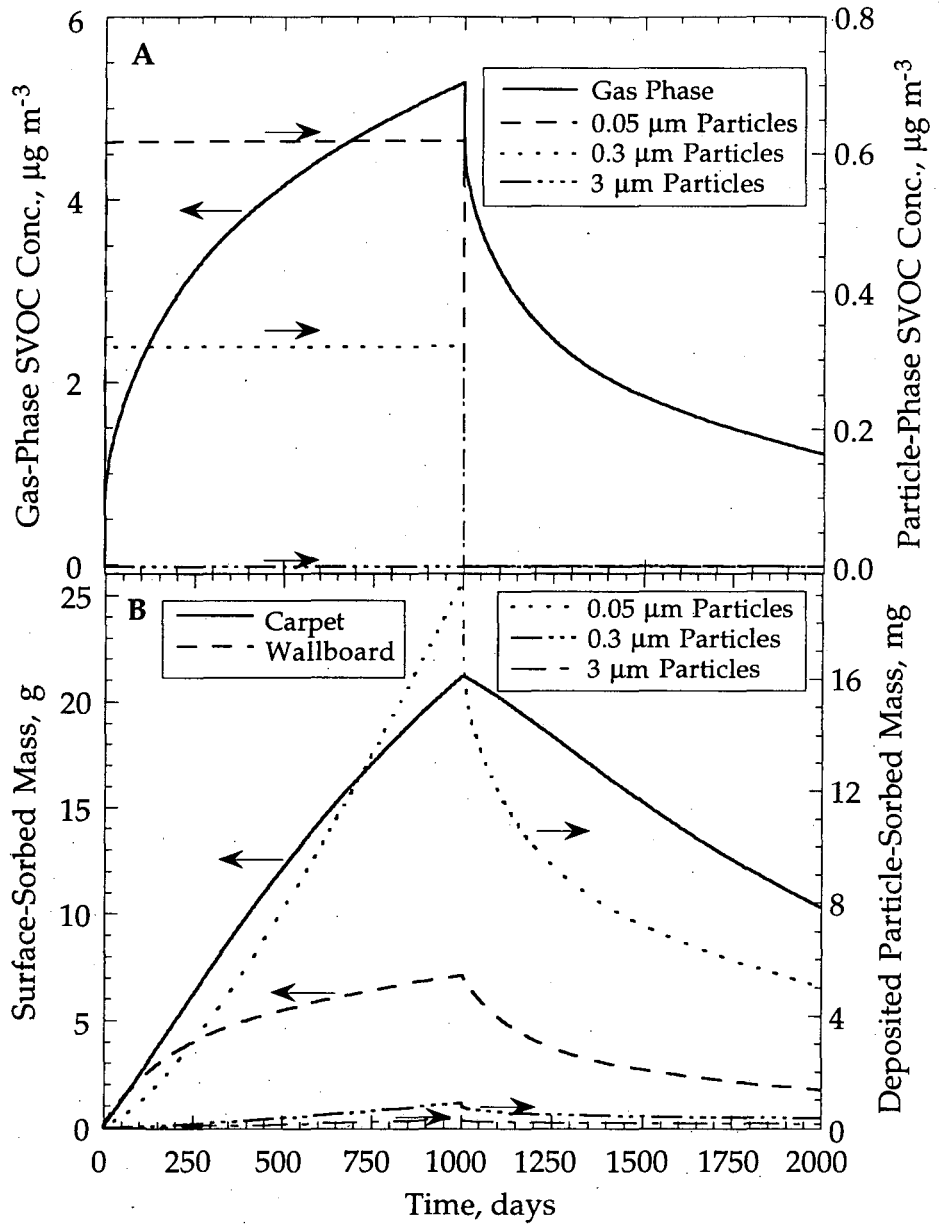

Figure 5.5 Predicted gas and airborne particle phase (**A**) and sorbed and deposited particle phase (**B**) SVOC mass balance for simulation 5D (phenanthrene, medium gas-particle kinetics, high gas-particle equilibrium coefficient).

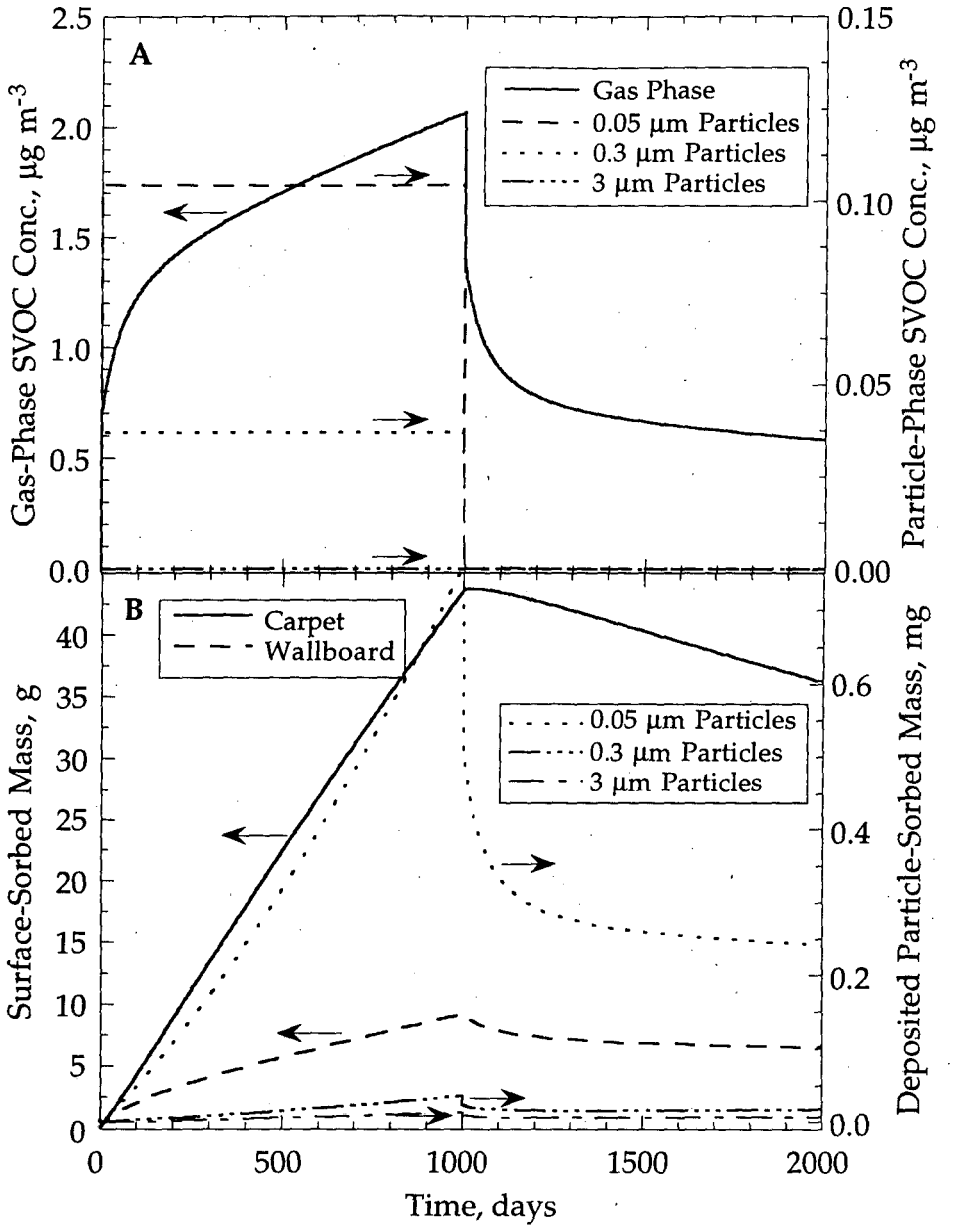

Figure 5.6 Predicted gas and airborne particle phase (**A**) and sorbed and deposited particle phase (**B**) SVOC mass balance for simulation 5E (nicotine, medium gas-particle kinetics, low gas-particle equilibrium coefficient).

TABLES

Table 5.1. Representative values (or ranges of values) and justifications for parameters used in the indoor SVOC dynamics model described in this chapter.

Parameter	Value/Range	Justification
λ_v	0.3 to 1.2 h^{-1}	The geometric mean of air exchange rates for U.S. housing stock is approximately 0.6 h^{-1} with a geometric standard deviation of about 2 (Murray and Burmaster, 1995). This range encompasses one GSD above and below the geometric mean.
d_p	0.05 μm, 0.3 μm, and 3.0 μm	The airborne particle size distribution was assumed to be tridisperse with the given particle diameters. The smallest diameter accounts for 10% of the ambient particle mass concentration while each of the two larger diameters accounts for 45%. This particle size distribution assumes that 60% (by mass) of the airborne particles are smaller than 2.5 μm (Falke and Husar, 1998).
K_p'/A_p	0.03 to 100 $m^3\ mg^{-1}$	The low value is that calculated using equation 5.5 and constants linear regression constants reported by Pankow *et al.* (1993) for phenanthrene at 298 K and $RH = 50\%$. The high value is for benzo[a]pyrene at the same T and RH conditions.
γ	1×10^{-8} to 0.1	The maximum value represents the accommodation coefficient for a highly reactive gases such as nitric acid. The low end of the range is two orders of magnitude lower than the smallest values shown in Figure 5.1. A range of 1×10^{-6} to 1×10^{-4} for γ is considered in this study.
MW	100 or 300 g mol^{-1}	100 g mol^{-1} is an approximate lower limit for compounds that could be classified as SVOCs. 300 g mol^{-1} is the molecular weight of coronene, a 6-ring PAH with whose vapor pressure at ambient temperatures is less than 10^{-5} Pa (Jordan, 1954).

Table 5.1 Continued

Parameter	Value/Range	Justification
D_g	0.01 - 0.06 $m^2\ h^{-1}$	The lower limit corresponds to the diffusivity of ultrafine particles (d_p = 0.001 μm) and is representative of molecules with *MW* of about 300 g mol^{-1}. The upper limit is the diffusivity of ammonia, a very low molecular weight compound (17 g mol^{-1}) in air.
k_{dpm}	0.2, 0.04, or 1 m h^{-1}	The three values correspond to the approximate indoor deposition velocities for 0.05 μm, 0.3 μm, and 3 μm diameter particles calculated using a homogeneous turbulence deposition model (Nazaroff and Cass, 1989).
$k_{ag\text{-}s}$	0.5 to 8 m h^{-1}	The low end of the range is approximately one third of that calculated for nicotine adsorption on wallboard in Chapter 3 and twice that reported for tetrachloroethylene adsorption on carpet by Tichenor *et al.* (1991) using a surface-sorption model. The high end of the range was calculated in Chapter 3 for nicotine adsorption on carpet. This value exceeded the mass-transport limited deposition velocity for a flat plate by a factor of 2.
$k_{dg\text{-}s}$	1×10^{-5} to 0.01 h^{-1}	These values range from an order of magnitude less than the reemission rate constant for nicotine on carpet (Chapter 3) to the value for tetrachloroethylene reemission from carpet reported by Tichenor *et al.* (1991). This range should encompass most SVOC (and probably even VOC) sorbate sorbent pairs encountered in indoor environments.
D_b	3×10^{-12} to 3×10^{-8} $m^2\ h^{-1}$	The high value is that calculated for phenanthrene diffusion in wallboard in Chapter 3. The low value is an order of magnitude smaller than the diffusion coefficient calculated for nicotine diffusion in carpet in Chapter 3 and that reported for 4-phenylcyclohexene (*MW* = 158 g mol^{-1}) in carpet (Little and Hodgson, 1996). It is similar to the value reported by Little *et al.* (1994) for 2-ethyl-1-hexanol in carpet.

Table 5.1 Continued

Parameter	Value/Range	Justification
k_{rg}	0.00001 to 0.01 h^{-1}	This range for the homogeneous decay pseudo-first order rate constant is based on literature values for organic compound decay rate data and an indoor hydroxyl radical concentration of 10^{-6} ppb (Weschler and Shields, 1996, 1997). The high value is for indole's reaction with OH radical (Atkinson *et al.*, 1995), and the low value is an order of magnitude lower than the extrapolated rate constant for 4,4'-dichlorobiphenyl at 298K (Anderson and Hites, 1996).
$k_{r_{sj}}$ $k_{r_{pi}}$	0.0000001 to 0.01 h^{-1}	Surface sorbed SVOCs may decay by reaction with gas-phase oxidants which diffuse to the sorbent surface. Assuming that the rates of these reactions are not large enough to impose a mass transport limitation on the decay process and that the oxidants do not react appreciably with the sorbent itself or other material deposited on the sorbent, the surface-sorbed and particle-sorbed SVOC pseudo-first order reaction rate constants should be equal to the homogeneous rate constant. However, hydroxyl radical and ozone react readily with many common indoor materials, so the actual surface decay rate may be several orders of magnitude smaller than the homogeneous rate. The lower value given here includes the assumption that other reactions at the surface decrease the available oxidant concentration at the surface to 1% of the concentration in the mixed core of the room. Few data on these phenomena are available, so these approximations may not be accurate.
V	500 m^3	The modeled house was chosen to have a floor area of 200 m^2 covered by carpet and a total surface area to volume ratio of 2.1 m^{-1}. The walls and ceilings are covered with painted wallboard. The diffusion thickness for carpet was 2.5 mm which reflects the thickness of the backing layer and for wallboard was 1 cm.
S_c	200 m^2	
L_c	0.0025 m	
S_w	1000 m^2	
L_w	0.01 m	

Table 5.2. SVOC emission rates and outdoor concentrations used in all modeled scenarios.

Indoor Emission Rates[a]	Value	Outdoor Concentrations[b]	Value
E_g, mg h^{-1}	1.5	C_{go}, mg m^{-3}	0.0
E_p(0.05 μm), mg h^{-1}	0.75	C_{po}(0.05 μm), mg m^{-3}	0.0
E_p(0.3 μm), mg h^{-1}	0.75	C_{po}(0.3 μm), mg m^{-3}	0.0
E_p(3.0 μm), mg h^{-1}	0.0	C_{po}(3.0 μm), mg m^{-3}	0.0
E_{pm}(0.05 μm), mg h^{-1}	4.0	C_{pmo}(0.05 μm), mg m^{-3}	0.06
E_{pm}(0.3 μm), mg h^{-1}	12.0	C_{pmo}(0.3 μm), mg m^{-3}	0.27
E_{pm}(3.0 μm), mg h^{-1}	0.0	C_{pmo}(3.0 μm), mg m^{-3}	0.27

a As noted in the text, these emission rates represent the daily emissions of nicotine from 15 cigarettes per day averaged over 24 hours (Daisey, *et al.* 1994, 1998; Martin *et al.*, 1997) . Other single compounds are not emitted from cigarettes at rates as high as nicotine's. However, the sum of the emission rates of a range of high molecular weight compounds whose dynamic behavior is represented by phenanthrene may approach the given emission rates at sufficiently high smoking rates. The source is assumed to emit 50% of the SVOC mass in the gas phase and 50% as particle phase species with the particulate SVOC split evenly between the 0.05 μm and 0.3 μm particles.

b The outdoor particle concentrations represent a polluted urban environment meeting the USEPA daily average PM_{10} standard of 150 μg m^{-3} but exceeding the annual average of 50 μg m^{-3}

Table 5.3. Building operation and sorption dynamics parameters for modeled scenarios.

Scenario/Compound:	**5A/Phen**	**5B/Phen**	**5C/Phen**	**5D/Phen**	**5E/Nic**
Gas-Particle Kinetics:	Slow	Medium	Fast	Medium	Medium
Gas-Particle Equil.:	Low	Low	Low	High	Low
Ventilation:					
λ_v, h^{-1}	0.6	0.6	0.6	0.6	0.6
Particle Sorption:					
γ, no units	1×10^{-6}	1×10^{-5}	1×10^{-4}	1×10^{-5}	1×10^{-5}
K_p' / A_p, m^3 mg^{-1}	0.03	0.03	0.03	0.3	0.03
$k_{ag-p0.05\mu m}$, m h^{-1}	0.04	0.4	4.0	0.4	0.4
$k_{dg-p0.05\mu m}$, h^{-1}	1.3	13.3	132.6	13.3	13.3
$k_{ag-p0.3\mu m}$, m h^{-1}	0.12	1.2	11.5	1.2	1.2
$k_{dg-p0.3\mu m}$, h^{-1}	3.8	38.3	383.3	38.3	38.3
$k_{ag-p3.0\mu m}$, m h^{-1}	0.15	1.5	15.4	1.5	1.5
$k_{dg-p3.0\mu m}$, h^{-1}	5.2	51.6	514.5	51.6	51.6
Surface Sorption:					
k_{ag-s_c}, m h^{-1}	5.0	5.0	8.0	5.0	8.0
k_{dg-s_c}, h^{-1}	0.0023	0.0023	0.0004	0.0023	0.0004
D_{b_c}, m^2 h^{-1}	2.7×10^{-10}	2.7×10^{-10}	2.5×10^{-10}	2.7×10^{-10}	2.5×10^{-10}
k_{ag-s_w}, m h^{-1}	3.7	3.7	2.0	3.7	2.0
k_{dg-s_w}, h^{-1}	0.027	0.027	0.0013	0.027	0.0013
D_{b_w}, m^2 h^{-1}	3.0×10^{-8}	3.0×10^{-8}	2.9×10^{-10}	3.0×10^{-8}	2.9×10^{-10}
Reaction Parameters:					
k_{rg}, h^{-1}	0.0004	0.0004	00004	0.0004	0.0004
$k_{r_{pi}} = k_{r_{sj}}$, h^{-1}	0.00004	0.00004	0.00004	0.00004	0.00004

Chapter 6. Conclusions

SUMMARY

This dissertation investigated the dynamics of gas-surface interactions of two chemically dissimilar SVOCs with stainless steel and with two sorbent materials commonly encountered in indoor environments. In most buildings and other indoor environments, carpet and painted wallboard are two sorbents likely to have the largest available surface area. Because sorption is a surface phenomenon, these materials are likely to dominate the sorptive interactions of many air pollutants in indoor air. Stainless steel is less important as a sorbent in most real buildings. However, it is commonly used in construction of laboratory chambers and analytical devices with which gas-phase SVOCs may come into contact. Improved understanding of SVOC interactions with the these sorbents will assist in design of future experiments and allow more accurate predictions of indoor concentrations and human exposures to these pollutants.

The investigation of nicotine in the empty stainless steel chamber presented in Chapter 2 was originally intended to provide baseline data for the experiments described in Chapter 3. However, the nicotine-stainless steel data did not match predictions generated with the linear partitioning-surface sorption model (Tichenor *et al.*, 1991). Additionally, extraction of nicotine from the chamber walls with ethyl acetate at the end of each kinetic experiment failed to give reasonable mass balance closure — less than 20% of the emitted mass was accounted for in the gas and stainless steel-sorbed phases. Based on these initial results, this sorbate-sorbent system was investigated in greater detail than was originally planned. Equilibrium partitioning was measured and found to be better modeled by the Freundlich isotherm (equation 1.3) than the linear isotherm (equation 1.2). Additionally, thermal desorption of stainless steel samples mounted on the chamber walls during later experiments recovered significantly more nicotine than the originally employed solvent extraction method. This improved sorbed-phase recovery yielded a

mass balance closure of approximately 85% of the emitted nicotine mass. Gas-phase nicotine concentrations measured in the three kinetic experiments described in this chapter were more closely simulated using the nonlinear reversible surface-sorption model defined by equations 2.4 and 2.5. Some model-measurement disagreement persisted during the periods of higher chamber air-exchange rate in experiments 2A – 2C. However, the gas-phase concentrations during these periods were low, so although the fractional disagreement was large the absolute model–measurement discrepancies were small.

Chapter 3 builds on the findings reported in Chapter 2. A similar approach was applied to investigate the interactions of gas phase nicotine and phenanthrene with carpet and wallboard samples in the stainless steel chamber used in Chapter 2. In this study, sorption of both compounds on the two sorbents was effectively simulated using a dynamic model incorporating gas-phase sorption at the air-sorbent interface plus bulk-phase diffusion of the sorbate through the sorbent away from the interface. As in Chapter 2, the model fits the experimental data closely during the higher concentration, low air-exchange rate phases of the experiment. During high air-exchange rate phases, the modeled gas-phase concentration drops to near or below the analytical limits of detection and the model-measurement agreement is less robust. The model parameters derived from best model fits to the data for the four sorbate-sorbent pairs are informative. Despite the different chemical properties of the sorbents and sorbates, the surface deposition rate constants reported in Table 3.3 for carpet and wallboard vary by less than a factor of four. The strength of the sorbate-sorbent interaction has a much greater effect on the surface reemission rate constant which varies by almost two orders of magnitude for the tested sorbents and sorbates. The bulk-phase diffusion coefficients for three of the four sorbate-sorbent pairs are almost identical. Diffusion of phenanthrene through painted wallboard is substantially faster than for any of the other sorption systems, possibly because of the chemical incompatibility of the nonpolar PAH molecule with the more

polar hydrated wallboard core. Wallboard's low sorption capacity for phenanthrene is also likely due to this polarity difference.

Chapter 4 applies the results of Chapters 2 and 3 to examine the effectiveness of nicotine as a marker for human exposures to environmental tobacco smoke components in indoor air. Reversible sorption of nicotine on indoor surfaces was simulated over time using the models developed and validated in Chapter 3 with data from Chapters 2 and 3. Simulations were computed for two indoor environments: a prototypical residence where smoking occurs with a regular pattern and a stainless steel chamber whose walls are free of nicotine prior to lighting of the first cigarette. These simulations were used to demonstrate that previous seemingly contradictory observations of nicotine's dynamic behavior in indoor environments may be reconciled by incorporating the effects that reversible sorption has on the gas phase concentration of nicotine under nonsteady emission conditions. The results of this analysis indicate that measurement of nicotine concentrations is an acceptable method for estimating human exposures to ETS components over periods greater than a few hours in indoor environments in which smoking occurs habitually. Nicotine is significantly less effective as an ETS marker at finer temporal resolutions or in environments where smoking occurs with less regularity.

Chapter 5 also applies the models developed in Chapter 3 to simulate the effects of reversible sorption on SVOC concentrations in a prototypical indoor environment. This analysis includes a review of the literature on reversible sorption of organic compounds to airborne particles and indoor surfaces and chemical decay due to reactions with gas-phase radicals. The model developed in Chapter 5 incorporates these processes, along with airborne particle deposition and accumulation on indoor surfaces, to generate a mass balance based simulation of SVOC dynamics in indoor environments. This model was used to examine the impacts of varying the different empirically determined parameters on the concentrations and persistence of SVOCs in indoor environments. Based on the results of the analysis, the dominant process is reversible sorption on indoor

surfaces. Radical chemistry may play a small role in degrading sorbed or particle-deposited SVOCs, but available evidence suggests that this process is more important as a generation mechanism for carbonyls and other potentially irritating oxidized organic species in indoor air than as a sink for SVOCs.

IMPLICATIONS AND DIRECTIONS FOR FUTURE RESEARCH

The results of this research indicate that reversible sorption of semivolatile organic compounds on building materials can have a substantial impact on indoor air quality. A significant body of research focusing on gas-surface interactions of VOCs has been published recently in the literature. Because of their lower vapor pressures and higher affinities for condensed phases, SVOCs are likely to be more substantially impacted by reversible sorption on indoor surface materials. However, few studies have investigated this important class of indoor air pollutants. This dissertation addresses one key aspect of SVOC dynamics in indoor air and identifies several others that merit future research attention.

The research discussed in this dissertation should serve as a starting point for future investigations of other SVOCs in the indoor environment. Nicotine and phenanthrene are representative of two classes of SVOCs. However, there are several potentially important compound classes whose behavior in buildings may differ markedly from that of the tested sorbates. For instance, oxidized compounds such as carbonyls and carboxylic acids may participate in stronger chemical interactions with polar sorbents such as wallboard. The results of a recent study by Chang *et al.* (1998) indicate that sorption of polar VOCs such as glycols and alcohols on wallboard may be irreversible to some extent. This phenomenon merits further study in experiments of greater duration than the 1 week exposure and reemission periods used by Chang *et al.* In addition to the study of other SVOCs, investigations of the impacts of other sorbents present in indoor environments is also warranted. Carpet and wallboard may account for the majority of

the exposed surface area in many buildings. However, other sorbents, such as upholstery, furniture stuffing, wood, or synthetic floor and counter coverings may contribute significantly to the overall sorption capacity in an indoor environment and may behave in a different manner than the sorbents tested in this research.

The results presented in Chapter 4 indicate that while nicotine is a suitable marker for estimating long-term ETS exposure under the proper conditions, it may not be an acceptable tracer for shorter exposure times. Many of the compounds emitted in ETS are acute irritants. Thus, additional research is necessary to either improve our understanding of the relative differences in the dynamic behavior of nicotine and other ETS constituents in indoor air or to identify more suitable species to use as ETS markers under more variable smoking conditions. Several alternative candidates for ETS markers are already being evaluated, and some, such as 3-ethenylpyridine, look promising.

Chapter 5 also identifies several potential future research topics. As stated in the discussion of the modeling results, indoor radical chemistry is a potentially important source of irritating and toxic oxidized SVOCs. Weschler and Shields (1996, 1997, 1998) have investigated these phenomena in some detail. Because the potential impacts of these processes on indoor air quality are significant, additional research is merited. Likewise, additional research is required on the interactions of the gas and particle-sorbed phases both in indoor and outdoor air. Airborne particles behave very differently than gas molecules both in indoor air and in the human respiratory system. However, little is known about the rates of gas-particle partitioning either indoors or outdoors. Part of this difficulty lies in the extremely heterogeneous nature of typical urban aerosols and the huge differences in aerodynamic and sorptive behavior over the range of typically encountered particle sizes. Although the results presented in Chapter 5 indicate that gas-particle sorption dynamics are significantly less important than gas-fixed surface sorption under the modeled conditions, particles may still play an important role because their

different respiratory tract deposition patterns differ markedly from those of gas molecules.

An additional extension of the model framework in Chapter 5 is source apportionment of indoor air pollutants. It is widely known that indoor and outdoor concentrations of air pollutants are not well coupled for many indoor environments. Quantification of the impacts of outdoor pollution sources on exposures occurring indoors could be significantly improved by studies which couple indoor measurements of gas and particle phase contamination with outdoor source emission profiles using a comprehensive indoor contaminant dynamics model based on that developed in Chapter 5. Identification of those sources with the greatest impacts on indoor exposures will facilitate more effective use of the resources available to protect human health.

CLOSING THOUGHTS

The work presented in this dissertation has significant implications for human exposures to semivolatile organic compounds. Because people spend so much of their time indoors, a thorough understanding of the processes affecting pollutant concentrations and persistence in this microenvironment is essential for accurate exposure calculations and risk assessments. Because the most commonly available measurements of airborne contaminants are those collected at outdoor air quality monitoring stations, extrapolation to indoor exposures through mathematical modeling of pollutant dynamics is often necessary. While modeling is not an acceptable substitute for accurate personal exposure sampling, when applied judiciously with full understanding of the assumptions and limitations inherent in the model to be used, it can be a powerful research and exposure assessment tool. In addition, models such as those developed in this dissertation are very valuable in parameterizing a problem to be studied and identifying where and how to apply expensive experimental resources.

References

Adamson, A.W. *Physical Chemistry of Surfaces*, 5th Edition; John Wiley and Sons: New York, **1990**.

Allen, J.O.; Dookeran, N.M.; Smith, K.A.; Sarofim, A.F. Measurement of polycyclic aromatic hydrocarbons associated with size-segregated atmospheric aerosols in Massachusetts, *Environmental Science and Technology* **1996**, *30*, 1023-1031.

Allen, J.O.; Dookeran, N.M.; Taghizadeh, K.; Lafleur, A.L.; Smith, K.A.; Sarofim, A.F. Measurement of oxygenated polycyclic aromatic hydrocarbons associated with a size-segregated urban aerosol, *Environmental Science and Technology* **1997**, *31*, 2064-2070.

Anderson, P.N.; Hites, R.A. System to measure relative rate constants of semivolatile organic compounds with hydroxyl radicals, *Environmental Science and Technology* **1996**, *30*, 301-306.

Atkinson, R.; Carter, W.P.L. Kinetics and mechanisms of the gas-phase reactions of ozone with organic compounds under atmospheric conditions, *Chemical Reviews* **1984**, *84*, 437-470.

Atkinson, R.; Tuazon, E.C.; Arey, J.; Aschmann, S.M. Atmospheric and indoor chemistry of gas-phase indole, quinoline, and isoquinoline, *Atmospheric Environment* **1995**, *29*, 3423-3432.

Aviado, D.M. Health effects of 50 selected constituents of environmental tobacco smoke, in *Indoor Air Quality*; Kasuga, H., Ed.; Springer-Verlag: Berlin, **1990**; pp. 383-389.

Axley, J.W. Adsorption modelling for building contaminant dispersal analysis, *Indoor Air* **1991**, *2*, 147-171.

Axley, J.W.; Lorenzetti, D. Sorption transport models for indoor air quality analysis, in *Modeling of Indoor Air Quality and Exposure*, ASTM STP 1287; Nagda, N.L., Ed.; American Society for Testing and Materials: Philadelphia, **1993**; pp. 105-127.

Baker, R.R.; Case, P.D.; Warren, N.D. The build-up and decay of ETS constituents as a function of room conditions, in *Indoor Air and Ambient Air Quality*, Perry, R.; Kirk, P.W., Eds., Selper: London, **1988**; pp. 121-130.

Baker, R.R.; Proctor, C.J. The origins and properties of environmental tobacco smoke, *Environment International* **1990**, *16*, 231-245.

Baker, R.R. Product formation mechanisms inside a cigarette, *Progress in Energy and Combustion Science* **1981**, *7*, 135-153.

Bidleman, T.F. Atmospheric processes: Wet and dry deposition of organic compounds are controlled by their vapor particle partitioning, *Environmental Science and Technology* **1988**, *22*, 361-367.

Borrazzo, J.E.; Davidson, C.I.; Andelman, J.B. Sorption of organic vapors to indoor surfaces of synthetic and natural fibrous materials, in *Indoor Air '90, Proceedings of the 5th International Conference on Indoor Air Quality and Climate — Vol. 3*; International Society for Indoor Air Quality: Toronto, **1990**; pp. 617-622.

Borrazzo, J.E.; Davidson, C.I.; Andelmann, J.B. Small closed-chamber measurements for the uptake of trichloroethylene and ethanol vapor by fibrous surfaces, in *Modeling of Indoor Air Quality and Exposure,* ASTM STP 1205; Nagda, N.L., Ed.; American Society for Testing and Materials: Philadelphia, **1993**; pp. 25-41.

Brown, S.K.; Sim, M.R.; Abramson, M.J.; Gray, C.N. Concentrations of volatile organic compounds in indoor air — A review, *Indoor Air* **1994**, *4*, 123-134.

Caka, F.M.; Eatough, D.J.; Lewis, E.A.; Tang, H.; Hammond, S.K.; Leaderer, B.P.; Koutrakis, P.; Spengler, J.D.; Fasano, A.; McCarthy, J.; Ogden, M.W.; Lewtas, J. An intercomparison of sampling methods for nicotine in indoor environments, *Environmental Science and Technology* **1990**, *24*, 1196-1203.

California EPA Office of Environmental Health Hazard Assessment. *Health Effects of Exposure to Environmental Tobacco Smoke*, California Environmental Protection Agency: Sacramento, **1997**.

Cano-Ruiz, J.A.; Kong, D.; Balas, R.B.; Nazaroff, W.W. Removal of reactive gases at indoor surfaces: Combining mass transport and surface kinetics, *Atmospheric Environment* **1993**, *27A*, 2039-2050.

Chang, C.S.; Sparks, L.E.; Guo, Z.; Fortmann, R. Evaluation of sink effects on VOCs from a latex paint, *Journal of the Air and Waste Management Association* **1998**, *48*, 953-958.

Colombo, A.; De Bortoli, M.; Knöppel, H.; Pecchio, E.; Vissers, H. Adsorption of selected volatile organic compounds on a carpet, a wall coating, and a gypsum board in a test chamber, *Indoor Air* **1993**, *3*, 276-282.

Cooney, D.O. On the basis for the Freundlich isotherm, *Chemical Engineering Communications* **1990**, *94*, 27-34.

Coultas, D.B.; Samet, J.M.; McCarthy, J.F.; Spengler, J.D. Variability of measures of exposure to environmental tobacco smoke in the home, *American Review of Respiratory Diseases* **1990**, *142*, 602-606.

Daisey, J.M.; Mahanama, K.R.R.; Hodgson, A.T. *Toxic Volatile Organic Compounds in Environmental Tobacco Smoke: Emission Factors for Modeling Exposures of California Populations*; Lawrence Berkeley Laboratory: Berkeley, **1994**; LBNL-36379.

Daisey, J.M.; Mahanama, K.R.R; Hodgson, A.T. Toxic volatile organic compounds in simulated environmental tobacco smoke: Emission factors for exposure assessment, *Journal of Exposure Analysis and Environmental Epidemiology* **1998**, *8*, 313-334

De Bortoli, M.; Knöppel, H.; Colombo, A.; Kefalopoulos, S. Attempting to characterize the sink effect in a small stainless steel test chamber, in *Characterizing Sources of Indoor Air Pollution and Related Sink Effects*, ASTM STP 1287; Tichenor, B.A., Ed.; American Society for Testing and Materials: Philadelphia, **1996**; pp. 307-320.

Dunn, J.E.; Chen, T. Critical evaluation of the diffusion hypothesis in the theory of porous media volatile organic compound (VOC) sources and sinks, in *Modeling of Indoor Air Quality and Exposure,* ASTM STP 1205; Nagda, N.L., Ed.; American Society for Testing and Materials: Philadelphia, **1993**; pp. 64-80.

Dunn, J.E.; Tichenor, B.A. Compensating for sink effects in emissions test chambers by mathematical modeling, *Atmospheric Environment* **1988**, *22*, 885-894.

Eatough, D.J. Assessing exposure to environmental tobacco smoke, in *Modeling of Indoor Air Quality and Exposure,* ASTM STP 1205; Nagda, N.L., Ed.; American Society for Testing and Materials: Philadelphia, **1993**; pp. 42-63.

Eatough, D.J.; Hansen, L.D.; Lewis, E.A. The chemical characterization of environmental tobacco smoke, in *Environmental Tobacco Smoke: Proceedings of the International Symposium at McGill University*; Ecobichon, D.J., Wu, J.M., Eds.; D.C. Heath and Company: Lexington, Massachusetts, **1989a**; pp. 3-39.

Eatough, D.J.; Benner, C.L.; Bayona, J.M.; Richards, G.; Lamb, J.D; Lee, M.L.; Lewis, E.A.; Hansen, L.D. Chemical composition of environmental tobacco smoke. 1. Gas-phase acids and bases, *Environmental Science and Technology* **1989b**, *23*, 679-687.

Eatough, D.J.; Benner, C.L.; Tang, H.; Landon, V.; Richards, G.; Caka, F.M.; Crawford, J.; Lewis, E.A.; Hansen, L.D. The chemical composition of environmental tobacco smoke III. Identification of conservative tracers of environmental tobacco smoke, *Environment International* **1989c**, *15*, 19-28.

Falconer, R.L.; Bidleman, T.F. Vapor pressures and predicted particle/gas distributions of polychlorinated biphenyl congeners as functions of temperature and ortho-chlorine substitution, *Atmospheric Environment* **1994**, *28*, 547-554.

Falke, S.R., Husar, R.B. Maps of $PM_{2.5}$ over the U.S. derived from regional $PM_{2.5}$ and surrogate visibility and PM_{10} monitoring data, in *Proceedings of the Air and Waste Management Association 91st Annual Meeting,* Air and Waste Management Association: San Diego, **1998**; pp. 98-MA1.04

Foreman, W.T.; Bidleman, T.F. Semivolatile organic compounds in the ambient air of Denver, Colorado, *Atmospheric Environment* **1990**, *24*, 2405-2416.

Gebefugi, I.; Korte, F. Pathways and behaviour of semi-volatile chemicals in enclosed spaces, in *Indoor and Ambient Air Quality*; Perry, R.; and Kirk, P.W., Eds.; Selper Ltd.: London, **1988**; pp. 393-398.

Glantz, S.A.; Parmley, W.W. Passive smoking and heart disease: mechanisms and risk, *J. Amer. Med. Association* **1995**, *273*, 1047-1053.

Gold, D.R. Indoor air pollution, *Clinics in Chest Medicine* **1992**, *13*, 215-229.

Goss, K.-U.; Eisenreich, S.J. Adsorption of VOCs from the gas phase to different minerals and a mineral mixture, *Environmental Science and Technology* **1996**, *30*, 2135-2142.

Gundel, L.A.; Lee, V.C.; Mahanama, K.R.R.; Stevens, R.K.; Daisey, J.M. Direct determination of the phase distributions of semi-volatile polycyclic aromatic hydrocarbons using annular denuders, *Atmospheric Environment* **1995**, *29*, 1719-1733.

Guo, Z. On validation of source and sink models: problems and possible solutions, in *Modeling of Indoor Air Quality and Exposure,* ASTM STP 1205; Nagda, N.L., Ed.; American Society for Testing and Materials: Philadelphia, **1993**; pp. 131-144.

Guo, Z.; Dunn, J.E.; Tichenor, B.A.; Mason, M.A.; Krebs, K.A. On representing reversible sinks in indoor air quality models, in *Indoor Air '90, Proceedings of the 5th International Conference on Indoor Air Quality and Climate — Vol. 2*, International Society for Indoor Air Quality: Toronto, **1990**; pp. 177-182.

Gustafson, K.E.; Dickhut, R.M. Particle/gas concentrations and distributions of PAHs in the atmosphere of southern Chesapeake Bay, *Environmental Science and Technology* **1997**, *31*, 140-147.

Hammond, S.K.; Leaderer, B.P.; Roche, A.C.; Schenker, M. Collection and analysis of nicotine as a marker for environmental tobacco smoke, *Atmospheric Environment* **1987**, *21*, 457-462.

Hammond, S.K.; Sorensen, G.; Youngstrom, R.; Ockene, J.K. Occupational exposure to environmental tobacco smoke, *Journal of the American Medical Association* **1995**, *274*, 956-960.

Hammond, S.K. Occupational exposure to environmental tobacco smoke — reply to letter to the editor, *Journal of the American Medical Association* **1996**, *275*, 442.

Hodgson, A.T.; Girman, J.R. Application of a multisorbent sampling technique for investigation of volatile organic compounds in buildings, in *Design and Protocol for Monitoring Indoor Air Quality*, ASTM STP 1002, Nagda, N.L.; Harper, J.P., Eds.; American Society for Testing and Materials: Philadelphia, **1989**; pp. 244-256 .

Hornbuckle, K.C.; Eisenreich, S.J. Dynamics of gaseous semivolatile organic compounds in a terrestrial ecosystem — effects of diurnal and seasonal climate variations, *Atmospheric Environment* **1996**, *30*, 3935-3945.

International Agency for Research on Cancer. Chemistry and analysis of environmental tobacco smoke, in *IARC Monographs on the Evaluation of the Carcinogenic Risk of Chemicals to Humans: Tobacco Smoking, Volume 38*; World Health Organization: Switzerland, **1985**; pp. 83-126.

Jang, M.; Kamens, R.M.; Leach, K.B.; Strommen, M.R. A thermodynamic approach using group contribution methods to model the partitioning of semivolatile organic compounds on atmospheric particulate matter, *Environmental Science and Technology* **1997**, *31*, 2805-2811.

Jenkins, B.M.; Jones, A.D.; Turn, S.Q.; Williams, R.B. Particle concentrations, gas-particle partitioning, and species intercorrelations for polycyclic aromatic hydrocarbons (PAH) emitted during biomass burning, *Atmospheric Environment* **1996a**, *30*, 3825-3835.

Jenkins, R.A.; Palausky, A.; Counts, R.W.; Bayne, C.K.; Dindal, A.B.; Guerin, M.R. Exposure to environmental tobacco smoke in sixteen cities in the United States as determined by personal breathing zone air sampling, *J. Exposure Analysis and Environmental Epidemiology* **1996b**, *6*, 473-502.

Jordan, T.E. *Vapor Pressure of Organic Compounds*; Interscience Publishers: New York, **1954**.

Jørgensen, R.B.; Knudsen, H.N.; Fanger, P.O. The influence on indoor air quality of adsorption and desorption of organic compounds on materials, in *Indoor Air '93, Proceedings of the 5th International Conference on Indoor Air Quality and Climate — Vol. 2*; International Society for Indoor Air Quality: Helsinki, **1993**; pp. 383-388.

Kamens, R.; Odum, J.; Fan, Z.-H. Some observations on times to equilibrium for semivolatile polycyclic aromatic hydrocarbons, *Environmental Science and Technology* **1995**, *29*, 43-50.

Kaupp, H.; Towara, J.; McLachlan, M.S. Distribution of polychlorinated dibenzo-p-dioxins and dibenzofurans in atmospheric particulate matter with respect to particle size, *Atmospheric Environment* **1994**, *28*, 585-593.

Kaupp, H.; Umlauf, G. Atmospheric gas-particle partitioning of organic compounds: comparison of sampling methods, *Atmospheric Environment* **1992**, *26A*, 2259-2267.

Kjaer, U.D.; Nielsen, P.A.; Vejrup, K.V.; Wolkoff, P. A method for determination of the sink effect of VOCs from building materials, in *Characterizing Sources of Indoor Air Pollution and Related Sink Effects*, ASTM STP 1287; Tichenor, B.A., Ed.; American Society for Testing and Materials: Philadelphia, **1996**; pp. 123-133.

Leaderer, B.P.; Hammond, S.K. Evaluation of vapor-phase nicotine and respirable suspended particle mass as markers for environmental tobacco smoke, *Environmental Science and Technology* **1991**, *25*, 770-777.

Lee, D.S.; Nicholson, K.W. The measurement of atmospheric concentrations and deposition of semi-volatile organic compounds, *Environmental Monitoring and Assessment* **1994**, *32*, 59-91.

Lee, W.M.G.; Tsay, L.Y. The partitioning model of polycyclic aromatic hydrocarbon between gaseous and particulate (PM10μ) phases in urban atmosphere with high humidity, *Science of the Total Environmental* **1994**, *145*, 163-171.

Lencka, M.; Szafranski, A.; Maczynski, A. *Verified Vapor Pressure Data — Vol. 1: Organic Compounds Containing Nitrogen*; PWN-Polish Scientific Publishers: Warsaw, **1984**.

Lewtas, J. Human exposure to complex mixtures of air pollutants, *Toxicology Letters* **1994**, *72*, 163-169.

Liang, C.; Pankow, J.F. Gas/particle partitioning of organic compounds to environmental tobacco smoke: partition coefficient measurements by desorption and comparison to urban particulate material, *Environmental Science and Technology* **1996**, *30*, 2800-2805.

Liang, C.; Pankow, J.F.; Odum, J.R.; Seinfeld, J.H. Gas/particle partitioning of semivolatile organic compounds to model inorganic, organic, and ambient smog aerosols, *Environmental Science and Technology* **1997**, *31*, 3086-3092.

Lin, T.-F. *Transport and Sorption of Volatile Organic Compounds and Water Vapor in Porous Media*, Ph.D. Dissertation, University of California: Berkeley, **1995**.

Lin, T.-F.; Van Loy, M.D.; Nazaroff, W.W. Gas-phase transport and sorption of benzene in soil columns, *Environmental Science and Technology*, **1996**, *30*, 2178-2186.

Little, J.C.; Hodgson, A.T. A strategy for characterizing homogeneous, diffusion-controlled indoor sources and sinks, in *Characterizing Sources of Indoor Air Pollution and Related Sink Effects*, ASTM STP 1287; Tichenor, B.A., Ed.; American Society for Testing and Materials: Philadelphia, **1996**; pp. 294-304.

Little, J.C.; Hodgson, A.T.; Gadgil, A.J. Modeling emissions of volatile organic compounds from new carpet, *Atmospheric Environment* **1994**, *28*, 227-234.

Löfroth, G. Environmental tobacco smoke: multicomponent analysis and room-to-room distribution in homes, *Tobacco Control* **1993**, *2*, 222-225.

Löfroth, G.; Burton, R.M.; Forehand, L.; Hammond, S.K.; Sella, R.L.; Zweldinger, R.B.; Lewtas, J. Characterization of environmental tobacco smoke, *Environmental Science and Technology* **1989**, *23*, 610-614.

Martin, P.; Heavner, D.L.; Nelson, P.R.; Maiolo, K.C.; Risner, C.H.; Simmons, P.S.; Morgan, W.T.; Ogden, M.W. Environmental tobacco smoke (ETS): A market cigarette study, *Environment International* **1997**, *23*, 75-90.

Matthews, T.G.; Hawthorne, A.R.; Thompson, C.V. Formaldehyde sorption and desorption characteristics of gypsum wallboard, *Environmental Science and Technology* **1987**, *21*, 629-634.

Mendell, M.J. Non-specific symptoms in office workers — a review and summary of the epidemiologic literature, *Indoor Air* **1994**, *3*, 227-236.

Miesner, E.A.; Rudnick, S.N.; Hu, F.-C.; Spengler, J.D.; Preller, L. Particulate and nicotine sampling in public facilities and offices, *Journal of the Air Pollution Control Association* **1989**, *39*, 1577-1582.

Mølhave, L.; Bach, B.; Pedersen, O.F. Human reactions to low concentrations of volatile organic compounds, *Environment International* **1986**, *12*, 167-175.

Morrow, L.A. Sick building syndrome and related workplace disorders, *Otolaryngology and Head and Neck Surgery* **1992**, *106*, 649-654.

Murray, D.M.; Burmaster, D.E. Residential air exchange rates in the United States — empirical and estimated parametric distributions by season and climatic region, *Risk Analysis* **1995**, *15*, 459-465.

National Research Council, *Environmental Tobacco Smoke: Measuring Exposure and Assessing Health Effects*; National Academy Press: Washington, D.C., **1986**.

Nazaroff, W.W.; Cass, G.R. Mathematical modeling of chemically reactive pollutants in indoor air, *Environmental Science and Technology* **1986**, *20*, 924-934.

Nazaroff, W.W.; Cass, G.R. Mass-transport aspects of pollutant removal at indoor surfaces, *Environment International* **1989**, *15*, 567-584.

Nazaroff, W.W.; Gadgil, A.J.; Weschler, C.J. Critique of the use of deposition velocity in modeling indoor air quality, in *Modeling of Indoor Air Quality and Exposure,* ASTM STP 1205; N.L. Nagda, Ed., American Society for Testing & Materials: Philadelphia; **1993a**, pp. 81-104.

Nazaroff, W.W.; Hung, W.-Y.; Sasse, A.G.B.M.; Gadgil A.J. Predicting regional lung deposition of environmental tobacco smoke particles, *Aerosol Science and Technology* **1993b**, *19*, 243-254.

Nelson, P.R. and Conrad, F.W. Interaction of environmental tobacco smoke components with a ventilation system, *Tobacco Science* **1997**, *41*, 45-52.

Nelson, P.R.; Heavner, D.L.; Collie, B.B.; Maiolo, K.C.; Ogden, M.W.; Effect of ventilation and sampling time on environmental tobacco smoke component ratios, *Environmental Science and Technology* **1992**, *26*, 1909-1915.

Nelson, P.R.; Ogden, M.W.; Maiolo, K.C.; Heavner, D.L.; Collie, B.B. Predictive value of nicotine as an environmental tobacco smoke marker, in *Indoor Air '90, Proceedings of the 5th International Conference on Indoor Air Quality and Climate*; International Society for Indoor Air Quality: Toronto, **1990**; Vol. 2, pp. 367-373.

Neretnieks, I.; Christiansson, J.; Romero, L.; Dagerholt, L.; Yu, J.-W. Modeling of emission and re-emission of volatile organic compounds from building materials with indoor air applications, *Indoor Air* **1993**, *3*, 2-11.

Odum, J.R.; Hoffman, T.; Bowman, F.; Collins, D.; Flagan, R.C.; Seinfeld, J.H. Gas/particle partitioning and secondary organic aerosol yields, *Environmental Science and Technology* **1996**, *30*, 2580-2585.

Odum, J.R.; Yu, J.; Kamens, R.M. Modeling the mass transfer of semivolatile organics in combustion aerosols, *Environmental Science and Technology* **1994**, *28*, 2278-2285.

Ogden, M.W. Occupational exposure to environmental tobacco smoke — letter to the editor, *Journal of the American Medical Association* **1996**, *275*, 441-441.

Ogden, M.W.; Eudy, L.W.; Heavner, D.L.; Conrad Jr., F.W.; Green, C.R. Improved gas chromatographic determination of nicotine in environmental tobacco smoke, *Analyst* **1989**, *114*, 1005-1008.

Palm, W.-U.; Elend, M.; Krueger, H.-U.; Zetzsch, C. OH radical reactivity of airborne terbutylazine adsorbed on inert aerosol, *Environmental Science and Technology* **1997**, *31*, 3389-3396.

Pankow, J.F. Review and comparative analysis of the theories on partitioning between the gas and aerosol particulate phases in the atmosphere, *Atmospheric Environment* **1987**, *21*, 2275-2283.

Pankow, J.F. An absorption model of gas/particle partitioning of organic compounds in the atmosphere, *Atmospheric Environment* **1994**, *28*, 185-188.

Pankow, J.F.; Bidleman, T.F. Interdependence of the slopes and intercepts from log-log correlations of measured gas-particle partitioning and vapor pressure — I. Theory and analysis of available data, *Atmospheric Environment* **1992**, *26A*, 1071-1080.

Pankow, J.F.; Storey, J.M.E.; Yamasaki, H. Effects of relative humidity on gas/particle partitioning of semivolatile organic compounds to urban particulate matter, *Environmental Science and Technology* **1993**, *27*, 2220-2226.

Press, W.H.; Teukolsky, S.A.; Vetterling. W.T.; Flannery, B.P. *Numerical Recipes in FORTRAN*; Cambridge University Press: New York, **1992**.

Pritchard, J.N.; Black, A.; McAughey, J.J. The physical behavior of sidestream tobacco smoke under ambient conditions, in *Indoor and Ambient Air Quality*, Perry, R.; Kirk, P.W., Eds.; Selper Ltd.: London, **1988**; pp. 49-56.

Rothweiler, H.; Schlatter, C. Human exposure to volatile organic compounds in indoor air — a health risk? *Toxicological and. Environmental Chemistry* **1993**, *40*, 93-102.

Seifert, B.; Schmahl, H. Quantification of sorption effects for selected organic substances present in indoor air, in *Indoor Air '87, Proceedings of the 4th International Conference on Indoor Air Quality and Climate -- Vol. 1*, Institute for Water, Soil, and Air Hygiene: Berlin, **1997**; pp. 383-388.

Seinfeld, J.H. *Atmospheric Chemistry and Physics of Air Pollution*; John Wiley and Sons: New York, **1986**.

Simonich, S. L.; Hites, R. A. Vegetation-atmosphere partitioning of polycyclic aromatic hydrocarbons, *Environmental Science and Technology* **1994**, *28*, 939-943.

Sollinger, S.; Levsen, K.; Wunsch, G. Indoor air pollution by organic emissions from textile floor coverings. Climate chamber studies under dynamic conditions, *Atmospheric Environment* **1993**, *27B*, 183-192.

Sollinger, S.; Levsen, K; Wunsch, G. Indoor pollution by organic emissions from textile floor coverings: climate test chamber studies under static conditions, *Atmospheric Environment* **1994**, *28*, 2369-2378.

Sparks, L.E.; Tichenor, B.A.; Chang, J.; Guo, Z. Gas-phase mass transfer model for predicting volatile organic compound (VOC) emission rates from indoor pollutant sources, *Indoor Air* **1996**, *6*, 31-40.

Sparks, L.E.; Tichenor, B.A.; White, J.B. Modeling individual exposure from indoor sources, in *Modeling of Indoor Air Quality and Exposure,* ASTM STP 1287; Nagda, N. L., Ed.; American Society for Testing and Materials: Philadelphia, **1993**; pp. 245-256.

Steenland, K. Passive smoking and the risk of heart disease, *Journal of the American Medical Association* **1992**, *267*, 94-99.

Storey, J.M.E.; Luo, W.; Isabelle, L.M.; Pankow, J.F. Gas solid partitioning of semivolatile organic compounds to model atmospheric solid surfaces as a function of relative humidity 1. Clean quartz, *Environmental Science and Technology* **1995**, *29*, 2420-2428.

Subramanyam, V.; Valsaraj, K.T.; Thibodeaux, L.J.; Reible, D.D. Gas-to-particle partitioning of polycyclic aromatic hydrocarbons in an urban atmosphere, *Atmospheric Environment* **1994**, *28*, 3083-3091.

Sundell, J.; Andersson, B.; Andersson, K.; Lindvall, T. Volatile organic compounds in ventilating air in buildings at different sampling points in the buildings and their relationship with the prevalence of occupant symptoms, *Indoor Air* **1993**, *3*, 82-93.

TenBrinke, J.; Selvin, S.; Hodgson, A.T.; Fisk, W.J.; Mendell, M.J.; Koshland, C.P.; Daisey, J.M. Development of new volatile organic compound (VOC) exposure metrics and their relationship to "sick building syndrome" symptoms, *Indoor Air* **1998**, *8*, 140-152.

Ten Brinke, J. *Development of New VOC Exposure Metrics and Their Relationship to "Sick Building Syndrome" Symptoms*, Ph.D. Dissertation, University of California: Berkeley, **1995**.

Thibodeaux, L.J.; Nadler, K.C.; Valsaraj, K.T.; Reible, D.D. The effect of moisture on volatile organic chemical gas-to-particle partitioning with atmospheric aerosols — competitive adsorption theory predictions, *Atmospheric Environment* **1991**, *25A*, 1649-1656.

Thompson, C.V.; Jenkins, R.A.; Higgins, C.E. A thermal desorption method for the determination of nicotine in indoor environments, *Environmental Science and Technology* **1989**, *23*, 429-435.

Tichenor, B.A.; Guo, Z.; Dunn, J.E.; Sparks, L.E.; Mason, M.A. The interaction of vapour phase organic compounds with indoor sinks, *Indoor Air* **1991**, *1*, 23-35.

Turner, S.; Cyr, L.; Gross, A.J. The measurement of environmental tobacco smoke in 585 office environments, *Environment International* **1992**, *18*, 19-28.

USEPA, *Respiratory Health Effects of Passive Smoking: Lung Cancer and Other Disorders*; United States Environmental Protection Agency: Washington, D.C., **1992**; EPA/600/6-90/006F.

Umlauf, G.; Hauk, H.; Reissinger, M. The distribution of semivolatile organic compounds in conifer needles following gas phase contamination, *Chemosphere* **1994**, *28*, 1689-1699.

Van Loy, M.D.; Nazaroff, W.W.; Lee, V.C.; Gundel, L.A.; Sextro, R.G.; Daisey, J.M. Investigation of the fate of nicotine in a stainless-steel chamber, in *Proceedings of the Air and Waste Management Association 89th Annual Meeting,* Air and Waste Management Association: Nashville, **1996**; pp. 96-WA61.04.

Van Loy, M.D., Nazaroff, W.W., Daisey, J.M. Sorptive interactions of gas-phase environmental tobacco smoke components with carpet, in *Proceedings of the Air and Waste Management Association 90th Annual Meeting,* Air and Waste Management Association: Toronto, **1997a**; pp. 97-MP3.05.

Van Loy, M.D., Nazaroff, W.W., and Daisey, J.M. Implications of nicotine interactions with indoor surfaces on its use as a marker for environmental tobacco smoke, in *Proceedings of the Air and Waste Management Association/Environmental Protection Agency Symposium on Engineering Solutions to Indoor Air Quality Problems*, Research Triangle Park, North Carolina, **1997b**.

Vorhees, D.J.; Cullen, A.C.; Altshul, L.M. Exposure to polychlorinated biphenyls in residential indoor air and outdoor air near a Superfund site, *Environmental Science and Technology* **1997**, *31*, 3612-3618.

Weschler, C.J.; Shields, H.C. Production of the hydroxyl radical in indoor air, *Environmental Science and Technology* **1996**, *30*, 3250-3258.

Weschler, C.J.; Shields, H.C. Measurements of the hydroxyl radical in a manipulated but realistic indoor environment, *Environmental Science and Technology* **1997**, *31*, 3719-3722.

Weschler, C.J.; Shields, H.C. Indoor ozone/terpene reactions as a source of indoor particles, in *Proceedings of the Air and Waste Management Association 91st Annual Meeting,* Air and Waste Management Association: San Diego, **1998**; pp. 98-TP48.01.

Westerholm, R.N.; Almén, J.; Li, H.; Rannug, J.U.; Egebäck, K.-E.; Grägg, K. Chemical and biological characterization of particulate-, semivolatile-, and gas-phase-associated compounds in diluted heavy-duty diesel exhausts: a comparison of three different semivolatile-phase samplers, *Environmental Science and Technology* **1991**, *25*, 332-338.

Wiley, J.A.; Robinson, J.P.; Piazza, T.; Garrett, K.; Cirksena, K.; Cheng, Y.-T.; Martin, G. *Activity Patterns of California Residents*. Final Report, Contract No. A6-177-33, California Air Resources Board, Research Division: Sacramento, **1991**.

Wynder, E.L.; Kabat, G.C. Environmental tobacco smoke and lung cancer: a critical assessment, in *Indoor Air Quality*, H. Kasuga, Ed., Springer-Verlag, Berlin, **1990**, pp. 5-15.

Xu, M.; Nematollahi, M.; Sextro, R.G.; Gadgil, A.J.; Nazaroff, W.W. Deposition of tobacco smoke particles in a low ventilation room, *Aerosol Science and Technology* **1994**, *20*, 194-206.

Zhang, J.S.; Kanabus-Kaminska, J.M.; Shaw, C.Y. A full-scale test chamber for material emission studies and indoor air quality modeling, in *Characterizing Sources of Indoor Air Pollution and Related Sink Effects*, ASTM STP 1287; Tichenor, B.A., Ed.; American Society for Testing and Materials: Philadelphia, **1996**; pp. 58-66.

Appendices

APPENDIX A: NON-POROUS SORBENT DATA ANALYSIS PROGRAM

This program compares experimental gas-phase concentration data from a user specified input file with modeled concentrations based on stainless steel sorption parameters provided by the user. From the inputted sorption parameters k_{as} and n_{as} (the adsorption rate constant and exponential coefficient, respectively) and the isotherm parameters given in the data file (K_s and n_s) the program calculates k_{ds} and n_{ds} (the desorption rate constant and exponential coefficient, respectively). Then, the code discretizes the experimental period into time steps whose lengths are determined by the time elapsed since the start of each individual phase of the experiment. At longer times after a change in experimental conditions (for instance, addition of more gas-phase sorbate through flash evaporation or an increase of decrease in the chamber air-exchange rate), the time steps increase in length. The coupled differential equations describing the gas-phase and sorbed phase mass balances (equations 2.4 and 2.5) are solved by 4th order Runge-Kutta integration (Press *et al.*, 1992). This program was used to analyze nicotine-stainless steel sorption data collected in experiments 2A – 2C and phenanthrene-stainless steel data from experiment 3C. For nicotine, whose sorption isotherm is nonlinear, n_{as} and n_{ds} were not equal to one. Phenanthrene's isotherm was found to be linear, so one was used for the values of n_{as} and n_{ds}.

```
      Program  sorbdf
      integer h, i, j, nmeas, nrun, runnum(150), outqs
      integer runknt, samknt, stpknt, samtrg, nguess, outstp
      real kas, kds, nas, nds, Ss, Ks, ns
      real U, Q, Me(15), temit(15), ach(15), dtmin
      real kMs(4), kCg(4)
      real Cg, Cgi, Ms, Msi, t, dt
      real ts(150), te(150), Cm(150), Ce(150)
      real chisqr, cher(150)
      real olkas(100), olkds(100), olnas(100), olnds(100), olchi(100)

c  ******************************************************************
c Convergence tolerance, data file names and numbers, & time counters
c t = cumulative time since start of model run (min)
c dt = time step (min)
```

```
c  filsuf = input data file suffix (sorbate, sorbent, run #)
      character*6  filsuf, quest
      character*14  filnam

c  ***********************************************************************
c  Chamber operation and stainless steel sorption parameters
c  U = chamber air volume [m3]
c  Ss = surface area of stainless steel [m2]
c  kas = deposition velocity for stainless steel [m/min]
c  kds = desorption coefficient for stainless steel [m/min]
c  nas = adsorption exponential coefficient for stainless steel [-]
c  nas = desorption exponential coefficient for stainless steel [-]
      U  = 20
      Ss = 45.2


c  ***********************************************************************
c  Read in the experimental data from the data file
c  File must be named "Exdata-??????"
      print*, 'Please give input file suffix (??????)'
       read*, filsuf
        filnam = 'Exdata-'//filsuf
         open (unit=10,file=filnam,status='old')

       print*, ' '
        print*, 'Please give descriptor for output file (??????)'
       read*, filsuf
        filnam =filsuf // '-sum.out'
         open (unit=20,file=filnam,status='new')

      write(20,450)

c           First line of input file contains number of runs
c           including ventilation and reemission phases,total
c           number of measurements during experiment, and frequency
c           at which to store result values in output file
      read (10,*) nrun, nmeas, outstp

c           Second line of input file gives equilibrium partitioning
c           coefficient (K) and exponent (n) for gas-sorbent sorption
      read (10,*) Ks, ns

c     Now, read in each run's parameters
      do 20 i=1,nrun
c             Third and following lines of input file contain emitted
c             mass [mg], time of start of run (SVOC emission or change
c             in other chamber parameters) [min], and chamber
c             ventilation rate [ach] during run.
              read (10,*) Me(i), temit(i), ach(i)
   20 continue

c               Each remaining line contains run number, start t [min],
c             finish t [min], and each measured C [mg m^-3].  Each
sample's
c             start and finish times are measured from the start of the
c             individual run.  We adjust these values after reading
c             them in so that all times are from the start of the
c             experiment.
      do 30 j=1,nmeas
            read (10,*) runnum(j),ts(j),te(j),Ce(j)
            ts(j) = ts(j) + temit(runnum(j))
            te(j) = te(j) + temit(runnum(j))
            write(6,330) runnum(j),ts(j),te(j),Ce(j)
   30 continue
```

```
      temit(nrun+1)  =  te(nmeas)
      nguess = 0

c  ***********************************************************************

c Get initial sorption parameter values
  40  dtmin = 0.01
      print*, 'Please give kas and nas in m, min, mg units.'
      read*, kas, nas

c Calculate remaining values using inputted values and isotherm
paramters
c from data file
       nds = nas*ns
       kds = kas/Ks**nds

       print*, ' '
        print*, 'Output concentration and sorbed mass time series'
        print*, 'for these parameters values? (enter "1" if yes)'
       read*, outqs

      write(6,320)

c  ***********************************************************************

c Set initial conditions -- gas-phase and SS are clean at run start
      Cg = 0
      Ms = 0

c Initialize start time
      t = 0

c  ***********************************************************************
c Initialize counters for run number and time step number
      stpknt = outstp
c  ***********************************************************************
c Initialize counters: run number, sample number, time step number,
c and sample ave.
      runknt = 1
      samknt = 1
      samave = 0
      samtrg = 0

c  ***********************************************************************

c Check whether we've done the last sample
  70  if (samknt.ge.nmeas) then
c           Done.   Now calculate chisqr
            write (6,*) samknt
            goto 290
      end if


      Cgs = Cg

c Figure out proper timestep sizes

c Set dt for the next time step.  Smaller timesteps immediately
c after SVOC emission then growing larger with time
      if (t.eq.0) then
            dt = dtmin
      else if ((t-temit(runknt-1)).lt.10) then
```

```
            dt = dtmin
      else  if  ((t-temit(runknt-1)).lt.30)  then
            dt = 2*dtmin
      else  if  ((t-temit(runknt-1)).lt.100)  then
            dt = 5*dtmin
      else  if  ((t-temit(runknt-1)).lt.300)  then
            dt = 10*dtmin
      else  if  ((t-temit(runknt-1)).lt.1000)  then
            dt = 20*dtmin
      else  if  ((t-temit(runknt-1)).lt.2000)  then
            dt = 20*dtmin
      else  if  ((t-temit(runknt-1)).lt.4000)  then
            dt = 50*dtmin
      else
            dt = 100*dtmin
      end if

c Find the start of the next run
c If it's time for the start of the next run, increase Cg by the
c appropriate amount and change Q to reflect new conditions.
      if  ((t+dt).ge.temit(runknt))  then
            if  (t.eq.temit(runknt))  then
                  Cg = Me(runknt)/V + Cg
                  Q = ach(runknt)*V/60
                  runknt = runknt + 1
                  stpknt=outstp
                  dt = dtmin
            else
                  dt = temit(runknt) - t
            end if
      end if


c Now find the start and ends of the samples

      if  ((t+dt).gt.ts(samknt))  then

            if  (samtrg.eq.0)  then
                  if  (t.lt.ts(samknt))  then
c                    We're going to overshoot the beginning of the next
c                    with this dt -- set dt to start the next timestep
c                    exactly at the beginning of the sample
                        dt = ts(samknt) - t
                  else  if  (t.eq.ts(samknt))  then
                        samtrg = 1
                  else
                        print*, 'Something is wrong with t and ts!'
                        read*, quest
                  end if
            else  if  (samtrg.eq.1)  then
c              We're in the middle of a sample!
c              Check if the sample is finished yet
                  if  ((t+dt).gt.te(samknt))  then
c                        We're at the end of a sample -- set dt so we
c                        end exactly at the end of the sample period
                        dt = te(samknt) - t
                  end if

            else
                  print*, 'Improper value in samtrg'
            end if
      end if
```

```
c  ***********************************************************************

c  Initialize intermediate values of Ms, and Cg
            Cgi = Cg
            Msi = Ms

      t = t + dt

c  Cycle through all k values (1-4 for Cg and Ms)

            do 200 j=1,4
c                   Gas phase mass balance
                  kCg(j) = dt*(-Q*Cgi
     +                  -(kas*Cgi**nas-kds*Msi**nds)*Ss)/V

c                   Stainless Steel sorbed phase mass balance
                  kMs(j) = dt*(kas*Cgi**nas - kds*Msi**nds)


                  if (j.eq.3) then
                        Cgi = Cg + kCg(j)
                        Msi = Ms + kMs(j)

                  else
                        Cgi = Cg + kCg(j)/2
                        Msi = Ms + kMs(j)/2
                  endif


  200       continue


c  Step forward in time by dt.
c  Add (k1)/6 + (k2)/3 + (k3)/3 + (k4)/6 to old values to get new ones

            Cg = Cg + (kCg(1) + kCg(4))/6 + (kCg(3) + kCg(2))/3
            Ms = Ms + (kMs(1) + kMs(4))/6 + (kMs(3) + kMs(2))/3

  210 continue


c  ***********************************************************************

c  Sample average calculations
c  If we're in the middle of a sample, add C*dt to samave
      if (t.gt.ts(samknt)) then
            if (t.le.te(samknt)) then
                  samave = samave + (Cg + Cgs)*dt/2
            end if
      end if

c  When sample is finished, calculate Cm and terminate integration
      if (t.eq.te(samknt)) then
            h = samknt
            Cm(h) = samave/(te(h) - ts(h))
            cher(h) = abs(Cm(h)-Ce(h))/Ce(h)

            write(6,330) runnum(h),ts(h),te(h),Ce(h),Cm(h),cher(h)


c             Check whether the next sample overlapped this one
            if (ts(samknt).eq.ts(samknt+1)) then
```

```
                    if  (te(samknt).eq.te(samknt+1))  then
c                         We've got identical sample periods
c                         Enter modeled average C for next sample also
                        h = samknt+1
                        Cm(h) = Cm(samknt)
                        cher(h) = abs(Cm(h)-Ce(h))/Ce(h)
                        write(6,330)  runnum(h),ts(h),te(h),Ce(h),
     +                        Cm(h),cher(h)

c                        Jump two samples
                        samknt = samknt + 2
                        samave = 0
                        samtrg = 0
                        goto 70

                    else if (te(samknt).lt.te(samknt+1))  then
c                         Next sample is longer.  We need to keep
c                         integrating to get Cm(samknt+1)
                        samknt = samknt + 1
                        goto 70
                    else
c                       Print*,'Oops.   Samples are ordered wrong!'
                    end if

              else
c               Next sample period doesn't overlap this one.
c               Calculate next sample's samave.
                    samknt = samknt + 1
                    samave = 0
                    samtrg = 0
                    goto 70
              end if

      else
c        Keep on stepping through time, storing output at desired
c        intervals
                    if (stpknt.eq.outstp)  then
                        stpknt = 0
                        write(20,500)  t/60,Cg*1000,Ms*1000
                    else
                        stpknt = stpknt + 1
                        goto 70
                    end if
              goto 70
      end if


c  ***********************************************************************

  290 chisqr = 0
      do 300 i=1,nmeas
            chisqr = chisqr + cher(i)
  300 continue

      nguess = nguess + 1
      olkas(nguess) = kas
      olkds(nguess) = kds
      olnas(nguess) = nas
      olnds(nguess) = nds
      olchi(nguess) = chisqr

      write(6,*) ' '
      do 310 i=1,nguess
```

```
          write(6,350)  olkas(i),olkds(i),olnas(i),olnds(i),olchi(i)

310 continue
          write(6,*)  ' '

    goto  40


320 format(1x,'num',2x,'     ts,  min',3x,'     te,  min',4x,
    +   'Cexp,  mg/m3',5x,'Cmod,  mg/m3',6x,'           err')
330 format(1x,I3,2x,f10.2,3x,f10.2,4x,E11.4,5x,E11.4,6x,E11.4)
340 format(1x,'ka  =',E11.4,',  kd  =',E11.4,',  na  =',E11.4,
   +        ',  nd  =',E11.4,  'chi^2  ='E11.4)
345 format(1x,'           kas',2x,'           kds',3x,
   +        '           nas',4x,'           nas',5x,'        chi^2')
350 format(1x,f11.7,2x,f11.7,3x,f6.4,4x,f6.4,5x,f11.7)
 360  format(1x,E11.4,2x,E11.4)
 450  format(1x,'t,hours',2x,'Cg,µg/m3',3x,'Ms,µg/m2')
500 format(1x,f10.5,2x,e11.4,3x,e11.4)

    end
```

APPENDIX B: POROUS SORBENT DATA ANALYSIS PROGRAM

This program was used to analyze the experimental data collected in experiments 3A, 3B, 3D, and 3E to obtain sorption kinetics parameters for nicotine and phenanthrene on carpet and painted wallboard. As in the program presented in Appendix A, this routine reads experimental data values from a user specified input file and then requests guesses for the adsorption and desorption rate constants and the diffusion coefficient in the bulk of the tested sorbent (k_{ab}, k_{db}, and D_b, respectively). The coupled differential equations describing the gas-phase mass balance, sorption on the sorbent surface, and diffusive transport of the sorbate through the sorbent bulk (equations 3.3 – 3.6) are solved by a modified Runge-Kutta integration scheme. The Runge-Kutta method is designed to integrate coupled ordinary differential equations. Because equations 3.3 and 3.4 are partial differential equations, they are first discretized into sets of coupled ordinary differential equations by the finite difference method. Then. the complete set of equations describing gas-phase mass balance (equation 3.5), sorption on the walls of the stainless steel chamber (3.6), sorption at the air-sorbent interface (3.3), and bulk-phase diffusion (finite difference approximation to equation 3.4) are solved by the standard Runge-Kutta method employed in Appendix A.

```
      Program  sorbdf
      integer  ques,  h,  i,  j,  nmeas,  nrun,  runnum(150),  stpknt,  outstp
      integer  nodes,  runknt,  samknt,  samtrg,  nguess
      real  kab,  kdb,  Db,  Sb,  Lb,  dzb,  kas,  kds,  nas,  nds,  Ss
      real  U,  Q,  Me(15),  temit(15),  ach(15),  dtmin
      real  kCb(4,15),  kMs(4),  kCg(4)
      real  Cg,  Cgi,  Cgs,  Ms,  Msi,  Mb,  t,  dt
      real  Cb(50),  Cbi(50)
      real  ts(150),  te(150),  Cm(150),  Ce(150)
      real  chisqr,  cher(150)
      real  olkab(100),  olkdb(100),  olDb(100),  olchi(100)

c  ***********************************************************************
c  Convergence tolerance, data file names and numbers, & time counters
c  t = cumulative time since start of model run (min)
c  dt = time step (min)
c  filsuf = suffix for input file (sorbate, sorbent, run number)
      character*6  filsuf,  quest
```

```
      character*14  filnam

c  ***********************************************************************
c Porous sorbent paramters (provided by input file or model
c   fitting below)
c Sb = presented surface area of porous sorbent [m2]
c Lb = thickness of porous sorbent [m]
c Db = diffusion coefficient in porous sorbent [m2/min]
c kab = adsorption coefficient for porous sorbent [m/min]
c kdb = desorption coefficient for porous sorbent [m/min]

c  ***********************************************************************
c Chamber operation and stainless steel sorption parameters
c U = chamber air volume [m3]
c Ss = surface area of stainless steel [m2]
c kas = deposition velocity for stainless steel [m/min]
c kds = desorption coefficient for stainless steel [m/min]
c nas = adsorption exponential coefficient for stainless steel [-]
c nas = desorption exponential coefficient for stainless steel [-]
      U  = 20
      Ss = 45.2


c  ***********************************************************************
c Read in the experimental data from the data file
c File must be named "Exdata-??????"
      print*, 'Please give input file suffix (??????)'
       read*, filsuf
        filnam = 'Exdata-'//filsuf
         open (unit=10,file=filnam,status='old')
       print*, ' '
        print*, 'Please give descriptor for output file (??????)'
       read*, filsuf
        filnam =filsuf // '-sum.out'
         open (unit=20,file=filnam,status='new')

        filnam =filsuf // '-sor.out'
         open (unit=25,file=filnam,status='new')

      write(20,450)
      write(25,460)


c           First line of input file contains nas, nds, kas, kds
c           (sorption parameters for stainless steel chamber surfaces)
      read (10,*) nas, nds, kas, kds

c           Second line of input file contains Sb [m2] and Lb [m]
      read (10,*) Sb, Lb

c           Third line of input file contains number of runs
c           including ventilation and reemission phases, total
c           number of measurements during experiment , and frequency
c           at which to store result values in output file

      read (10,*) nrun, nmeas, outstp

c     Now, read in run-specific parameters for each run
      do 20 i=1,nrun
c             Fourth and following lines of input file contain emitted
c             mass [mg], time of start of run (SVOC emission or change
c             in other chamber paramters) [min], and chamber
c             ventilation rate [ach] during run.
              read (10,*) Me(i), temit(i), ach(i)
```

```
   20  continue

c                Each remaining line contains run number, start t [min],
c              final t [min], and measured C [mg m^-3] for each
c              gas-phase measurement.  The start and finish times for
c              each sample are measured from the start of the
c              individual run.  We adjust these values after reading
c              them in so that all times are from the start of the
c              experiment.
       do 30 j=1,nmeas
             read (10,*) runnum(j),ts(j),te(j),Ce(j)
             ts(j) = ts(j) + temit(runnum(j))
             te(j) = te(j) + temit(runnum(j))
             write(6,330) runnum(j),ts(j),te(j),Ce(j)
   30  continue

       temit(nrun+1) = te(nmeas)
       nguess = 0

c  ***********************************************************************

c Ask for desired number of nodes, sorption parameter values, and
c smallest time step
   40  nodes = 10
       dtmin = 0.1
       print*, 'Values for kab (m/min), kdb (/min), and Db (m2/min)? '
       read*, kab, kdb, Db

        print*, ' '
       write(6,320)


c discretize porous sorbent thickness into nodes.
c dzb = node thickness [m]
       dzb = Lb/nodes


c  ***********************************************************************

c Set initial conditions -- chamber and sorbents are clean at run start
       Cg = 0
       Ms = 0
       do 60 i=1,nodes
             Cb(i) = 0
    60 continue

c Initialize t to 0
       t = 0

c  ***********************************************************************

c Initialize counters for run number, sample number, time step number,
c and sample ave.
       runknt = 1
       samknt = 1
       samtrg = 0
       stpknt = outstp
       samave = 0
c  ***********************************************************************
c Check whether we've done the last sample
   70  if (samknt.ge.nmeas) goto 290
c            Done. Now calculate chisqr
```

```
      Cgs = Cg

c Figure out proper timestep sizes

c Set dt for the next time step.  Smaller timesteps immediately
c after SVOC emission then growing larger with time
      if (t.eq.0) then
            dt = dtmin
      else if ((t-temit(runknt-1)).lt.10) then
            dt = dtmin
      else if ((t-temit(runknt-1)).lt.30) then
            dt = 2*dtmin
      else if ((t-temit(runknt-1)).lt.100) then
            dt = 5*dtmin
      else if ((t-temit(runknt-1)).lt.300) then
            dt = 10*dtmin
      else if ((t-temit(runknt-1)).lt.1000) then
            dt = 20*dtmin
      else if ((t-temit(runknt-1)).lt.2000) then
            dt = 20*dtmin
      else if ((t-temit(runknt-1)).lt.4000) then
            dt = 50*dtmin
      else
            dt = 100*dtmin
      end if

c Find the start of the next run
c If it's time to start the next run, increase Cg by the
c appropriate amount and change Q to reflect new conditions.
      if ((t+dt).ge.temit(runknt)) then
            if (t.eq.temit(runknt)) then
                  Cg = Me(runknt)/V
                  Q = ach(runknt)*V/60
                  runknt = runknt + 1
                  stpknt = outstp
                  dt = dtmin
            else
                  dt = temit(runknt) - t
            end if
      end if


c Now find the start and ends of the samples

      if ((t+dt).gt.ts(samknt)) then

            if (samtrg.eq.0) then
                  if (t.lt.ts(samknt)) then
c                    We're going to overshoot the beginning of the next
c                    with this dt -- set dt to start the next timestep
c                    exactly at the beginning of the sample
                        dt = ts(samknt) - t
                  else if (t.eq.ts(samknt)) then
                        samtrg = 1
                  else
                        print*, 'Something is wrong with t and ts!'
                        read*, quest
                  end if
            else if (samtrg.eq.1) then
c              We're in the middle of a sample, you putz!
c              Check if the sample is finished yet
                  if ((t+dt).gt.te(samknt)) then
```

```
c                         We're at the end of a sample -- set dt so we
c                         end exactly at the end of the sample period
                        dt = te(samknt) - t
                  end if

            else
                  print*, 'Improper value in samtrg'
            end if
      end if


c  ******************************************************************

c Initialize intermediate value matrices for Cb, Ms, and Cg
            Cgi = Cg
            Msi = Ms
            do 90 i=1,nodes
                  Cbi(i) = Cb(i)
   90       continue

      t = t + dt

c Cycle through all k values (1-4 for each data point: Cg, Ms and nodes
c for Cb)

            do 200 j=1,4
c                   Gas phase mass balance
                  kCg(j) = dt*(-Q*Cgi
     +                  -(kab*Cgi-kdb*Cbi(1)*dzb)*Sb
     +                  -(kas*Cgi**nas-kds*Msi**nds)*Ss)/U

c                   Stainless Steel sorbed phase mass balance
                  kMs(j) = dt*(kas*Cgi**nas - kds*Msi**nds)

c                   Mass balance for porous sorbent surface
                  kCb(j,1) = dt*((kab*Cgi/dzb - kdb*Cbi(1)) +
     +                  Db/dzb/dzb*(Cbi(2) - Cbi(1)))

c                   Mass balances for porous sorbent bulk nodes
                  do 100 i=2,(nodes-1)
                        kCb(j,i) = dt*Db/dzb/dzb*(Cbi(i-1)+
     +                        Cbi(i+1)-2*Cbi(i))
  100             continue
                  kCb(j,nodes) =dt*Db/dzb/dzb*(Cbi(nodes-1)-Cbi(nodes))

                  if (j.eq.3) then
                        Cgi = Cg + kCg(j)
                        Msi = Ms + kMs(j)
                        do 110 i=1,nodes
                              Cbi(i) = Cb(i) + kCb(j,i)
  110                   continue

                  else
                        Cgi = Cg + kCg(j)/2
                        Msi = Ms + kMs(j)/2
                        do 120 i=1,nodes
                              Cbi(i) = Cb(i) + kCb(j,i)/2
  120                   continue
                  endif


  200       continue
```

```
c Step forward in time by dt.
c Add (k1)/6 + (k2)/3 + (k3)/3 + (k4)/6 to old values to get new ones

            Cg = Cg + (kCg(1) + kCg(4))/6 + (kCg(3) + kCg(2))/3
            Ms = Ms + (kMs(1) + kMs(4))/6 + (kMs(3) + kMs(2))/3
            do 210 i=1,nodes
                  Cb(i) = Cb(i)+(kCb(1,i) + kCb(4,i))/6 +
     +                  (kCb(3,i) + kCb(2,i))/3

  210       continue


c  ******************************************************************

c Sample average calculations
c If we're in the middle of a sample, add C*dt to samave
      if (t.gt.ts(samknt)) then
            if (t.le.te(samknt)) then
                  samave = samave + (Cg + Cgs)*dt/2
            end if
      end if

c If we're at the end of a sample, calculate Cm and end integration
      if (t.eq.te(samknt)) then
            h = samknt
            Cm(h) = samave/(te(h) - ts(h))
            cher(h) = abs(Cm(h)-Ce(h))/Ce(h)

            write(6,330) h,ts(h),te(h),Ce(h),Cm(h),cher(h)


c             Check whether the next sample overlapped this one
            if (ts(samknt).eq.ts(samknt+1)) then

                  if (te(samknt).eq.te(samknt+1)) then
c                        We've got identical sample periods
c                        Enter modeled average C for next sample also
                        h = samknt+1
                        Cm(h) = Cm(samknt)
                        cher(h) = abs(Cm(h)-Ce(h))/Ce(h)
                        write(6,330) h,ts(h),te(h),Ce(h),Cm(h),cher(h)

c                        Jump two samples
                        samknt = samknt + 2
                        samave = 0
                        samtrg = 0
                        goto 70

                  else if (te(samknt).lt.te(samknt+1)) then
c                        Next sample is longer.  We need to keep
c                        integrating to get Cm(samknt+1)
                        samknt = samknt + 1
                        goto 70
                  else
c                       Print*,'Oops.  Samples are ordered wrong!'
                  end if

            else
c             Next sample period doesn't overlap this one.
c             Prepare for calculation of samave for next sample.
                  samknt = samknt + 1
                  samave = 0
                  samtrg = 0
```

```
                goto 70
            end if

        else
c           Keep on stepping through time, storing output at desired
c           intervals
            if (stpknt.eq.outstp) then
                Mb = 0
                do 280 i=1,nodes
                    Mb = Mb + Cb(i)*dzb
280             continue
                stpknt = 0
                write(20,500)  t/60,Cg*1000,Ms*1000,Mb*1000
                write(25,510)  t/60,Cb(1)*1000,Cb(3)*1000,
     +                  Cb(5)*1000,Cb(7)*1000,Cb(10)*1000
            else
                stpknt = stpknt + 1
                goto 70
            end if
            goto 70
        end if

c  ***********************************************************************

290 chisqr = 0
    do 300 i=1,nmeas
        chisqr = chisqr + cher(i)
300 continue

    nguess = nguess + 1
    olkab(nguess) = kab
    olkdb(nguess) = kdb
    olDb(nguess)  = Db
    olchi(nguess) = chisqr

    write(6,*) ' '
    do 310 i=1,nguess
        write(6,350)  olkab(i),olkdb(i),olDb(i),olchi(i)
310 continue
        write(6,*) ' '

    goto 40


320 format(1x,' #',2x,'      ts, min',3x,'     te, min',4x,
    +  'Cexp, mg/m3',5x,'Cmod, mg/m3',6x,'          err')
330 format(1x,I3,2x,f10.2,3x,f10.2,4x,E11.4,5x,E11.4,6x,E11.4)
340 format(1x,'ka =',E11.4,',  kd =',E11.4,',  Db =',E11.4,
   +       'chi^2 =' f11.7)
345 format(1x,'          kab',2x,'          kdb',3x,
   +       '          Db',4x,'       chi^2')
350 format(1x,f11.7,2x,f11.9,3x,E11.4,4x,f11.7)
 360  format(1x,E11.4,2x,E11.4)

 450  format(1x,'t,hours',2x,'Cg,µg/m3',3x,'Ms,µg/m2',4x,'Mb,µg/m2')
460 format(1x,'t,hours',2x,'  Cb1,µg/m3',3x,'  Cb3,µg/m2',4x,
   +       '  Cb5,µg/m2',5x,'  Cb7,µg/m2',6x,'  Cb10,µg/m2')
500 format(1x,f10.5,2x,e11.4,3x,e11.4,4x,e11.4)
510 format(1x,f10.5,2x,e11.4,3x,e11.4,4x,e11.4,5x,e11.4,6x,e11.4)
    end
```

APPENDIX C: ETS NICOTINE/RSP PREDICTOR PROGRAM

This program was used in Chapter 4 to simulate gas-phase nicotine and respirable suspended particle (RSP) concentrations in an experimental chamber (or house) based on the number and frequency of cigarettes smoked in the indoor environment. The user specified data file contains information about the nicotine sorption parameters for the various sorbents in the volume to be tested and about the RSP deposition parameters. The program allows for one non-porous sorbent (for instance stainless steel), and up to two porous sorbents (for instance carpet and painted wallboard). The input file also gives emission rates for RSP and nicotine on a per-cigarette basis. Then, the user is prompted for the number of finite difference nodes into which to discretize the thickness of each porous sorbent, the smallest desired Runge-Kutta time step, and the frequency with which to output model data to a file.

```
      Program  expsim

c  This program calculates Cn(t) and Cr(t) for a user defined chamber
c  experiment.   The input file 'Exp-sim-data-??????' must contain info
c  regarding chamber operation and sorption dynamics and surface area
c  It must also contain information about the time series of smoking
c  in the chamber.  Detailed intructions for the data file start on
c  line 43.


      integer i, j, nphase, nodes
      integer runknt, stpknt, outstp

c  General chamber and phase parameters
      real V, Q, ach(100), dtmin, t, dt
      real dur(100), ncig(100), tstart(100)

c  RSP parameters, etc.
      real Cr, kdr, Er

c  Gas-phase nicotine parameters, storage arrays, etc.
      real Cg, Cgi, kCg(4), En

c  Wallboard parameters, storage arrays, etc.
      real kaw, kdw, Dw, Sw, Lw, dzw
      real Cw(25), Cwi(25), kCw(4,25), Mw

c  Carpet parameters, storage arrays, etc.
      real kac, kdc, Dc, Sc, Lc, dzc
      real Cc(25), Cci(25), kCc(4,25), Mc
```

```
c  Stainless steel parameters, storage arrays, etc.
      real kas, kds, nas, nds, Ss
      real Ms, Msi, kMs(4)


c  filsuf = suffix for input data file (sorbate, sorbent, run #, etc.)
c  filnam = full file name for input parameter file
      character*6  filsuf, quest
      character*20  filnam


c  ***********************************************************************
c  Read in experimental data from the data file
c  File must be named "Exp-sim-data-??????"
      print*, 'Please give input file suffix (??????)'
       read*, filsuf
        filnam = 'Exp-sim-data-'//filsuf
        open (unit=10,file=filnam,status='old')

c            First line of data file contains chamber volume
c            and per cigarette nic & RSP mass emissions
      read (10,*) V, En, Er

c            Second line of data file contains sorption parameters for
c            stainless steel chamber surfaces (kas, kds, nas, & nds, Ss)
      read (10,*) nas, nds, kas, kds, Ss

c            Third line of data file contains sorption parameters for
c            wallboard surfaces (kaw, kdw, Dw, Sw, Lw)
      read (10,*) kaw, kdw, Dw, Sw, Lw

c            Fourth line of data file contains sorption parameters for
c            carpet surfaces (kac, kdc, Dc, Sc, Lc)
      read (10,*) kac, kdc, Dc, Sc, Lc

c            Fifth line of data file contains depositin parameters for
c            airborne RSP
      read (10,*) kdr

c            Sixth line of data file contains number of different
c            chamber parameter "phases."  Use a new "phase" for each
c            change in the ventilation rate and each cigarette event.
      read (10,*) nphase

c     Now, read in parameters for each run
c            Sixth and following lines of data file contain duration
c            of phase, number of cigarettes smoked, and chamber
c            ventilation rate [ach] for each phase.
      read (10,*) dur(1), ncig(1), ach(1)
      tstart(1) = 0
      do 20 i=2,nphase
            read (10,*) dur(i), ncig(i), ach(i)
            tstart(i) = dur(i-1) + tstart(i-1)
   20 continue
      tstart(nphase+1) = dur(nphase) + tstart(nphase)


c  ***********************************************************************
c  Open data file and prep it for concentration and sorbed mass data

      open (unit=20,file='ETS-chamber-sim.out',status='new')

      write(20,25)
   25 format(1x,'        t, h',2x,' Cn, µg/m3',3x,' Cr, µg/m3',
```

```
     +       4x,'Mn-s,  µg/m2',5x,'Mn-c,  µg/m2',6x,'Mn-w,  µg/m2')


c  ******************************************************************

c Ask for desired number of nodes and smallest time step
      print*, 'Input the desired number of finite difference nodes '
       read*, nodes
      print*, 'Input the desired smallest time step (min) '
       read*, dtmin
      print*, 'Input X (every Xth timestep is sent to output file)'
       read*, outstp


c discretize carpet and wallboard thicknesses into nodes.
c dz* = node thickness [m] for sorbent *
      dzw = Lw/nodes
      dzc = Lc/nodes



c  ******************************************************************

c Set initial conditions -- chamber and sorbents are clean at start of
c first cigarette
      Cr = 0
      Cg = 0
      Ms = 0
      do 60 i=1,nodes
            Cw(i) = 0
            Cc(i) = 0
   60 continue

c Initialize t to 0
      t = 0

      write(20,250)  (t-27996.75)/60,Cg*1000,Cr*1000,Ms*1000,
     +        Mc*1000,Mw*1000

c  ******************************************************************

c Initialize counters for run # and time step #
      runknt = 1
      stpknt = outstp


  70  if (t.ge.(tstart(nphase) + dur(nphase))) then
c  We're done.
            Stop
      end if


c Figure out proper size for next timestep

c Set dt for the next time step.  Samller timesteps immediately
c after SVOc emission then growing larger with time
      if (t.eq.0) then
            dt = dtmin
      else if ((t-tstart(runknt-1)).lt.10) then
            dt = dtmin
      else if ((t-tstart(runknt-1)).lt.30) then
            dt = 2*dtmin
```

```
      else  if  ((t-tstart(runknt-1)).lt.100)  then
            dt  =  5*dtmin
      else  if  ((t-tstart(runknt-1)).lt.300)  then
            dt  =  10*dtmin
      else  if  ((t-tstart(runknt-1)).lt.1000)  then
            dt  =  20*dtmin
      else  if  ((t-tstart(runknt-1)).lt.2000)  then
            dt  =  20*dtmin
      else  if  ((t-tstart(runknt-1)).lt.4000)  then
            dt  =  50*dtmin
      else
            dt  =  100*dtmin
      end  if

c Find the start of the next run.  If it's time to start the next run,
c change Q, Er, and En to reflect new conditions.
      if  ((t+dt).ge.tstart(runknt))  then
            if  (t.eq.tstart(runknt))  then
                  Ercurr  =  ncig(runknt)/dur(runknt)*Er
                  Encurr  =  ncig(runknt)/dur(runknt)*En
                  Q  =  ach(runknt)*U/60


                  runknt  =  runknt  +  1
                  dt  =  dtmin
            else
                  dt  =  tstart(runknt)  -  t
            end  if
      end  if



c  ***********************************************************************

c Initialize intermediate value matrices for Cw(i),Cc(i),  Ms,  and  Cg
            Cgi  =  Cg
            Msi  =  Ms
            do  90  i=1,nodes
                  Cwi(i)  =  Cw(i)
                  Cci(i)  =  Cc(i)
   90       continue

      t  =  t  +  dt


c Cycle through all k values (1-4 for each data point: Cg, Ms and nodes
c for Cw and Cc)

            do  200  j=1,4

c                   Gas phase mass balance
                  kCg(j)  =  dt*(Encurr  -Q*Cgi
     +                  -(kaw*Cgi-kdw*Cwi(1)*dzw)*Sw
     +                  -(kac*Cgi-kdc*Cci(1)*dzc)*Sc
     +                  -(kas*Cgi**nas-kds*Msi**nds)*Ss)/U


c                   Stainless Steel  sorbed phase mass balance
                  kMs(j)  =  dt*(kas*Cgi**nas  -  kds*Msi**nds)


c                   Mass balance for wallboard surface
                  kCw(j,1)  =  dt*((kaw*Cgi/dzw  -  kdw*Cwi(1))  +
```

```
     +                    Dw/dzw/dzw*(Cwi(2)  -  Cwi(1)))

c                     Mass balances for wallboard bulk nodes
                    do  100  i=2,(nodes-1)
                          kCw(j,i)  =  dt*Dw/dzw/dzw*(Cwi(i-1)+
     +                          Cwi(i+1)-2*Cwi(i))
 100                continue
                    kCw(j,nodes)  =dt*Dw/dzw/dzw*(Cwi(nodes-1)-Cwi(nodes))


c                     Mass balance for carpet surface
                    kCc(j,1)  =  dt*((kac*Cgi/dzc  -  kdc*Cci(1))  +
     +                    Dc/dzc/dzc*(Cci(2)  -  Cci(1)))

c                     Mass balances for carpet bulk nodes
                    do  105  i=2,(nodes-1)
                          kCc(j,i)  =  dt*Dc/dzc/dzc*(Cci(i-1)+
     +                          Cci(i+1)-2*Cci(i))
 105                continue
                    kCc(j,nodes)  =dt*Dc/dzc/dzc*(Cci(nodes-1)-Cci(nodes))



                    if  (j.eq.3)  then
                          Cgi  =  Cg  +  kCg(j)
                          Msi  =  Ms  +  kMs(j)
                          do  110  i=1,nodes
                                Cwi(i)  =  Cw(i)  +  kCw(j,i)
                                Cci(i)  =  Cc(i)  +  kCc(j,i)
 110                      continue

                    else
                          Cgi  =  Cg  +  kCg(j)/2
                          Msi  =  Ms  +  kMs(j)/2
                          do  120  i=1,nodes
                                Cwi(i)  =  Cw(i)  +  kCw(j,i)/2
                                Cci(i)  =  Cc(i)  +  kCc(j,i)/2
 120                      continue
                    endif


  200       continue

c  ***********************************************************************

c Step forward in time by dt.
c Add (k1)/6 + (k2)/3 + (k3)/3 + (k4)/6 to old values to get new ones

c  Calculate particle concentration
      Cr  =  Ercurr/(Q  +  kdr*(Ss+Sc+Sw))  *
     +       (1-exp(-(Q  +  kdr*(Ss+Sc+Sw))*dt/U))  +
     +       Cr*exp(-(Q  +  kdr*(Ss+Sc+Sw))*dt/U)

c  Calculate gas-phase concentration
      Cg  =  Cg  +  (kCg(1)  +  kCg(4))/6  +  (kCg(3)  +  kCg(2))/3

c  Calculate stainless steel sorbed mass density
      Ms  =  Ms  +  (kMs(1)  +  kMs(4))/6  +  (kMs(3)  +  kMs(2))/3

c  Calculate bulk concentrations in wallboard and carpet
      do  210  i=1,nodes
            Cw(i)  =  Cw(i)+(kCw(1,i)  +  kCw(4,i))/6  +
     +                    (kCw(3,i)  +  kCw(2,i))/3
            Cc(i)  =  Cc(i)+(kCc(1,i)  +  kCc(4,i))/6  +
```

```
     +                    (kCc(3,i) + kCc(2,i))/3
  210 continue


      if (stpknt.eq.outstp) then
c Store information for this timestep in output file

            Mw = 0
            Mc = 0
            do 220 i=1,nodes
                  Mw = Mw + dzw*Cw(i)
                  Mc = Mc + dzc*Cc(i)
  220       continue
                  write(20,250) (t-27996.75)/60,Cg*1000,Cr*1000,
     +                  Ms*1000,Mc*1000,Mw*1000

            stpknt = 0
            goto 70
      else
            stpknt = stpknt + 1
            goto 70
      end if


  250 format(1x,f10.3,2x,E11.4,3x,E11.4,4x,E11.4,5x,E11.4,6x,E11.4)


      end
```

APPENDIX D: SVOC GAS-PARTICLE-SORPTION PROGRAM

This program was used in Chapter 5 to predict the mass of an SVOC in indoor air in each of the gas, airborne particle-sorbed, deposited particle-sorbed, and surface-sorbed phases. The code is used with a Microsoft Excel (version 6.0/95 or higher) workbook containing a worksheet labeled "Input Params" that lists the the gas-sorbent and gas-particle sorption parameters; the outdoor particle and particle-phase and gas-phase SVOC concentrations; the building air-exchange rate; the initial gas phase, particle phase and sorbed phase conditions; and the indoor emission rates of particle mass and SVOCs in the gas and airborne particle-sorbed phases as specified in the code. Using these parameters, equations 5.8, 5.18, 5.19, 5.22, 5.23, 5.25, 5.26, and 5.27 are integrated simultaneously using the modified Runge-Kutta approach described in Appendix B to simulate the behavior of the SVOC of interest in indoor air. Data are outputted at specified intervals to a sheet labeled "Plot Data." The final value of each time dependent value is listed on the "Final Values" worksheet at the end of the simulation period.

```
Option Explicit

'Initialize variables
'*********************************************************************
'Counter variables
Public i As Integer
Public j As Integer
Public counter As Integer
Public allcounter As Integer

'Number of sorbent nodes/number of particle size bins
Public n1 As Integer
Public n2 As Integer
Public bins As Integer

'Diagnostic output of all time steps indicator
Public allout As String

'  *********************************************************************
'Concentration variables and intermediate storage registers
'and Runge-Kutta "k" matrices for variables
'Cg = gas-phase SVOC concentration (mg m-3)
'Cgo = outdoor gas-phase SVOC concentration (mg m-3)

'Cb1 = SVOC surface concentration on fixed sorbent 1 (mg m-2)
'Cb2 = SVOC surface concentration on fixed sorbent 2 (mg m-2)

'Cp(i) = indoor particle-phase SVOC concentration in bin i (mg m-3)
```

```
'Cpo(i) = outdoor particle-phase SVOC concentration in bin i (mg m-3)
'Cpm(i) = indoor particulate matter concentration in bin i (mg m-3)
'Cpmo(i) = outdoor particulate matter concentration in bin i (mg m-3)
Public Cg As Double
Public Cgi As Double
Public Cgo As Double
Public kCg(4) As Double
Public Cb1(25) As Double
Public Cb1i(25) As Double
Public kCb1(4, 25) As Double
Public Mb1 As Double
Public Mb2 As Double

Public Cb2(25) As Double
Public Cb2i(25) As Double
Public kCb2(4, 25) As Double

Public Cp(5) As Double
Public Cpi(5) As Double
Public Cpo(5) As Double
Public kCp(5, 4) As Double

Public Cpm(5) As Double
Public Cpmi(5) As Double
Public Cpmo(5) As Double
Public kCpm(5, 4) As Double

Public div
'*********************************************************************
'General building parameters
'lv = building air exchange rate (h-1)
'V = volume(m3)
'Q = building ventilation flow rate (m3 h-1)
Public lv As Double
Public V As Double
Public Q As Double
'*********************************************************************
'Emissions parameters
'Eg = Gas-phase SVOC emission rate (mg h-1)
'Ep(i) = Particle-phase SVOC emission rate in bin i (mg h-1)
'Epm(i)= Particulate mass emission rate in bin 1 (mg h-1)
Public Eg As Double
Public Ep(5) As Double
Public Epm(5) As Double

'*********************************************************************
'Gas-particle reversible sorption kinetic parameters
'kagp(i) = gas-particle adsorption rate constant for bin i (m h-1)
'kdgp(i) = gas-particle desorption rate constant for bin i (h-1)
'kagp1(i) = gas-sorbed particle adsorption rate constant for bin
'           i on surface 1 (m h-1)
'kdgp1(i) = gas-sorbed particle desorption rate constant for bin
'           i on surface 1 (h-1)
'kagp2(i) = gas-sorbed particle adsorption rate constant for bin
'           i on surface 2 (m h-1)
'kdgp2(i) = gas-sorbed particle desorption rate constant for bin
'           i on surface 2 (h-1)
'Kp = gas-particle equilibrium constant for all particle sizes (m)
'Ap(i) = particle surface area per unit mass for bin i (m2 mg-1)
'kdpm(i) = deposition velocity for particles in bin i (m h-1)
'St = total available surface area for particle deposition (m2)
Public kagp(5) As Double
Public kagp1(5) As Double
Public kagp2(5) As Double
```

```
Public kdgp(5) As Double
Public kdgp1(5) As Double
Public kdgp2(5) As Double
Public Ap(5) As Double
Public kdpm(5) As Double

'*********************************************************************
'Deposited particle mass balance parameters
'Mp(i) = Surface-deposited bin 1 particle-phase SVOC mass (mg m-2)
'Mpm(i)= Surface-deposited particle mass in bin i (mg m-2)
Public Mp1(5) As Double
Public Mpm1(5) As Double
Public kMp1(5, 4) As Double
Public kMpm1(5, 4) As Double
Public Mp1i(5) As Double
Public Mpm1i(5) As Double

Public Mp2(5) As Double
Public Mpm2(5) As Double
Public kMp2(5, 4) As Double
Public kMpm2(5, 4) As Double
Public Mp2i(5) As Double
Public Mpm2i(5) As Double

'*********************************************************************
'Gas-surface reversible sorption parameters
'kags = sorbent gas-phase deposition rate constant (m h-1)
'kdgs = sorbent gas-phase re-emission rate constant (h-1)
'Sb = stationary sorbent surface area (m2)
'Db = SVOC diffusion coefficient in porous sorbent bulk (m2 h-1)
'L = Porous sorbent material bulk thickness (m)
'nodes = number of finite difference nodes in sorbent bulk (-)
'dzb = discretization of sorbent thickness (m)
Public kags1 As Double
Public kdgs1 As Double
Public Db1 As Double
Public Lb1 As Double
Public dzb1 As Double
Public Sb1 As Double

Public kags2 As Double
Public kdgs2 As Double
Public Db2 As Double
Public Lb2 As Double
Public dzb2 As Double
Public Sb2 As Double

'*********************************************************************
'Reaction decay parameters
'krg = Gas-phase SVOC 1st order degradation rate constant (h-1)
'krp = Particle-phase SVOC 1st order degradation rate constant (h-1)
'krs = Sorbed-phase SVOC 1st order degradation rate constant (h-1)
Public krg As Double
Public krp As Double
Public krs As Double

'*********************************************************************
'Convergence tolerance, data file names and numbers,
'and time counters / other parameters
'dt = time step (h)
Public t As Double
Public dt As Double
Public tend As Double
Public tstart As Double
```

```
Public dtmin As Double
Public dtmax As Double
Public multip As Double
Public tprev As Double
Public outstp As Double

Sub SVOC()
      Application.Calculation = xlManual

       Worksheets("Plot Data").Rows("2:4000").ClearContents
       Worksheets("Raw Data").Rows("2:8000").ClearContents

      allout = Worksheets("Input Params").Cells(1, 5)

      tstart = Worksheets("Input Params").Cells(9, 5)
      tend = Worksheets("Input Params").Cells(10, 5)
      dtmin = Worksheets("Input Params").Cells(48, 2)
      dtmax = Worksheets("Input Params").Cells(49, 2)
      multip = Worksheets("Input Params").Cells(48, 5)

      'Get model parameters from "Input Params" sheet
      'Number of particle size bins
      bins = Worksheets("Input Params").Cells(15, 2)


      'Emission rates, outdoor concentrations, and area/mass for particles
      Eg = Worksheets("Input Params").Cells(17, 2)
      Cgo = Worksheets("Input Params").Cells(19, 2)
     For i = 1 To bins
            Ep(i) = Worksheets("Input Params").Cells(17, i + 2)
            Epm(i) = Worksheets("Input Params").Cells(18, i + 2)
            Cpo(i) = Worksheets("Input Params").Cells(19, i + 2)
            Cpmo(i) = Worksheets("Input Params").Cells(20, i + 2)
            Ap(i) = Worksheets("Input Params").Cells(16, i + 2)
     Next i

      'Building and sorbent physical parameters
      U = Worksheets("Input Params").Cells(2, 2)
      lu = Worksheets("Input Params").Cells(3, 2)
      Q = Worksheets("Input Params").Cells(4, 2)
      Sb1 = Worksheets("Input Params").Cells(5, 2)
      Lb1 = Worksheets("Input Params").Cells(6, 2)
      n1 = Worksheets("Input Params").Cells(7, 2)
      Sb2 = Worksheets("Input Params").Cells(8, 2)
      Lb2 = Worksheets("Input Params").Cells(9, 2)
      n2 = Worksheets("Input Params").Cells(10, 2)

     dzb1 = Lb1 / n1
     dzb2 = Lb2 / n2

      'Fixed sorbent 1 sorption parameters
      kags1 = Worksheets("Input Params").Cells(28, 2)
      kdgs1 = Worksheets("Input Params").Cells(29, 2)
      Db1 = Worksheets("Input Params").Cells(30, 2)

      'Fixed sorbent 2 sorption parameters
      kags2 = Worksheets("Input Params").Cells(31, 2)
      kdgs2 = Worksheets("Input Params").Cells(32, 2)
      Db2 = Worksheets("Input Params").Cells(33, 2)

      'Gas-particle sorption paramters adsorption & desorption
      'rate constants (m/h) for each bin (airborne and surface-deposited
      'particles)
     For i = 1 To bins
```

```
        kagp(i) = Worksheets("Input Params").Cells(24, i + 2)
        kdgp(i) = Worksheets("Input Params").Cells(25, i + 2)
        kagp1(i) = Worksheets("Input Params").Cells(35, i + 2)
        kdgp1(i) = Worksheets("Input Params").Cells(36, i + 2)
        kagp2(i) = Worksheets("Input Params").Cells(37, i + 2)
        kdgp2(i) = Worksheets("Input Params").Cells(38, i + 2)
        kdpm(i) = Worksheets("Input Params").Cells(40, i + 2)
    Next i

     'Reaction decay parameters
     krg = Worksheets("Input Params").Cells(43, 2)
     krp = Worksheets("Input Params").Cells(44, 2)
     krs = Worksheets("Input Params").Cells(45, 2)


     'Initial conditions
     'Gas-phase concentration IC
     'deposited particle-SVOC mass and deposited particle mass
     Cg = Worksheets("Input Params").Cells(52, 2)
     ' Airborne and surface-deposited particle & particle-phase SVOC ICs
    For i = 1 To bins
        Cp(i) = Worksheets("Input Params").Cells(55, i + 1)
        Cpm(i) = Worksheets("Input Params").Cells(56, i + 1)
        Mp1(i) = Worksheets("Input Params").Cells(57, i + 1)
        Mpm1(i) = Worksheets("Input Params").Cells(58, i + 1)
        Mp2(i) = Worksheets("Input Params").Cells(59, i + 1)
        Mpm2(i) = Worksheets("Input Params").Cells(60, i + 1)
    Next i

     'Fixed sorbent sorbed mass density ICs
    For i = 1 To n1
        Cb1(i) = Worksheets("Input Params").Cells(63, i + 1)
    Next i

    For i = 1 To n2
        Cb2(i) = Worksheets("Input Params").Cells(66, i + 1)
    Next i

'  ***********************************************************************
' Initialize t to 0
    t = 0

     'Record IC data on output sheet
    counter = 2
    Call plotdata
    counter = 3

    If allout = "yes" Then
        'User has specified output of data from all time steps
        allcounter = 2
        Call alldata
        allcounter = 3
    End If

    Do While t < tend * 24
        Call Integrate
    Loop

     'Output final values to "Final Values" worksheet
     'Gas-phase SVOC conc.
     Worksheets("Final Values").Cells(1, 2).Value = Cg
    For i = 1 To bins
        'Airborne particle-phase SVOC conc.
        Worksheets("Final Values").Cells(4, i + 1).Value = Cp(i)
```

```
            'Airborne particle conc.
             Worksheets("Final Values").Cells(5, i + 1).Value = Cpm(i)
             'Carpet-deposited particle-phase SVOC density
             Worksheets("Final Values").Cells(6, i + 1).Value = Mp1(i)
             'Carpet-deposited particle density
             Worksheets("Final Values").Cells(7, i + 1).Value = Mpm1(i)
             'Wallboard-deposited particle-phase SVOC density
             Worksheets("Final Values").Cells(8, i + 1).Value = Mp2(i)
             'Wallboard-deposited particle density
             Worksheets("Final Values").Cells(9, i + 1).Value = Mpm2(i)
     Next i
      'Carpet-sorbed SVOC nodes conc.
     For i = 1 To n1
             Worksheets("Final Values").Cells(11, i + 1).Value = n1
             Worksheets("Final Values").Cells(12, i + 1).Value = Cb1(i)
     Next i
      'Wallboard-sorbed SVOC nodes conc.
     For i = 1 To n2
             Worksheets("Final Values").Cells(14, i + 1).Value = n2
             Worksheets("Final Values").Cells(15, i + 1).Value = Cb2(i)
     Next i

      Application.Calculation = xlAutomatic

End Sub
Sub Integrate()

' Figure out timestep size (increasing at user defined rate over time
' with a cap at user specified dtmax)
  If t = 0 Then
         dt = dtmin
     ElseIf dt * multip < dtmax Then
         dt = dt * multip
     Else
         dt = dtmax
     End If


'*********************************************************************
      'Initialize intermediate value matrices for Cb, Cg, and Cp

     Cgi = Cg
     For i = 1 To bins
          Cpi(i) = Cp(i)
          Cpmi(i) = Cpm(i)
     Next i

     For i = 1 To n1
          Cb1i(i) = Cb1(i)
     Next i

     For i = 1 To n2
          Cb2i(i) = Cb2(i)
     Next i

'*********************************************************************
      'Cycle through all k values (1-4 for each data point: Cg, nodes for
      'Cb, Cp, and Cpm)

     For j = 1 To 4
            'Gas-phase mass balance (effects of ventilation,
            'reaction, and sorbents)
           kCg(j) = dt * (((Eg + Q * (Cgo - Cgi) - (kags1 * Cgi _
                - kdgs1 * Cb1i(1) * dzb1) * Sb1 - (kags2 * Cgi _
```

```
      - kdgs2 * Cb2i(1) * dzb2) * Sb2)) / U - krg * Cgi)

For i = 1 To bins
      'Effects of particles on gas-phase MB
      kCg(j) = kCg(j) - dt * ((kagp(i) * Cgi * Ap(i) * Cpmi(i) _
           - kdgp(i) * Cpi(i)) - (kagp1(i) * Cgi * Ap(i) * Mpm1i(i)

          - kdgp1(i) * Mp1i(i)) * Sb1 / U _
          - (kagp2(i) * Cgi * Ap(i) * Mpm2i(i) _
          - kdgp2(i) * Mp2i(i)) * Sb2 / U)

      'Airborne particle-phase SVOC MB
      kCp(i, j) = dt * (((Ep(i) + Q * (Cpo(i) _
           - Cpi(i)))) / U + kagp(i) * Cgi * Ap(i) * Cpmi(i) _
           - (kdgp(i) + kdpm(i) * (Sb1 + Sb2) / U + krp) * Cpi(i))

      'Airborne Particles MB
      kCpm(i, j) = dt * (Epm(i) + Q * (Cpmo(i) - Cpmi(i)) _
           - kdpm(i) * Cpmi(i) * (Sb1 + Sb2)) / U

      'Carpet-deposited particle-phase SVOC MB
      kMp1(i, j) = dt * (kdpm(i) * Cpi(i) * Sb1 / (Sb1 + Sb2) _
           + Ap(i) * Mpm1i(i) * kagp1(i) * Cgi - (kdgp1(i) + krp) _
          * Mp1i(i))

      'Wallboard-deposited particle-phase SVOC MB
      kMp2(i, j) = dt * (kdpm(i) * Cpi(i) * Sb2 / (Sb1 + Sb2) _
           + Ap(i) * Mpm2i(i) * kagp2(i) * Cgi - (kdgp2(i) + krp) _
          * Mp2i(i))

      'Carpet-deposited particles MB
      kMpm1(i, j) = dt * kdpm(i) * Cpmi(i) * Sb1 / (Sb1 + Sb2)

      'Wallboard-deposited particles MB
      kMpm2(i, j) = dt * kdpm(i) * Cpmi(i) * Sb2 / (Sb1 + Sb2)

Next i

 'MBs for SVOC at surface of each porous sorbent
 'Air-carpet interface node MB
 kCb1(j, 1) = dt * ((kags1 * Cgi / dzb1 - kdgs1 * Cb1i(1)) _
      + Db1 / dzb1 / dzb1 * (Cb1i(2) - Cb1i(1)) - krs * Cb1i(1))
 'Air-wallboard interface node MB
 kCb2(j, 1) = dt * ((kags2 * Cgi / dzb2 - kdgs2 * Cb2i(1)) _
      + Db2 / dzb2 / dzb2 * (Cb2i(2) - Cb2i(1)) - krs * Cb2i(1))

 'MBs for SVOC in the bulk of each porous sorbent
 'Carpet bulk nodes MB
For i = 2 To n1 - 1
      kCb1(j, i) = dt * Db1 / dzb1 / dzb1 * (Cb1i(i - 1) _
           + Cb1i(i + 1) - 2 * Cb1i(i))
Next i

 'Wallboard bulk nodes MB
For i = 2 To n2 - 1
      kCb2(j, i) = dt * Db2 / dzb2 / dzb2 * (Cb2i(i - 1) _
           + Cb2i(i + 1) - 2 * Cb2i(i))
Next i

 'Deepest carpet node SVOC MB
 kCb1(j, n1) = dt * Db1 / dzb1 / dzb1 * (Cb1i(n1 - 1) _
      - Cb1i(n1))

 'Deepest wallboard node SVOC MB
```

```
            kCb2(j, n2) = dt * Db2 / dzb2 / dzb2 * (Cb2i(n2 - 1) _
                - Cb2i(n2))


            'Sum k1, k2, k3, and k4 for each variable and advance a time
step
           If j = 3 Then
               div = 1
           Else
               div = 2
           End If

            'Gas-phase SVOC
           Cgi = Cg + kCg(j) / div
            'Particles & particle-sorbed SVOC: airborne & deposited
           For i = 1 To bins
                Cpi(i) = Cp(i) + kCp(i, j) / div
                Cpmi(i) = Cpm(i) + kCpm(i, j) / div
                Mp1i(i) = Mp1(i) + kMp1(i, j) / div
                Mp2i(i) = Mp2(i) + kMp2(i, j) / div
                Mpm1i(i) = Mpm1(i) + kMpm1(i, j) / div
                Mpm2i(i) = Mpm2(i) + kMpm2(i, j) / div
           Next i
            'Carpet-sorbed SVOC
           For i = 1 To n1
                Cb1i(i) = Cb1(i) + kCb1(j, i) / div
           Next i
            'Wallboard-sorbed SVOC
           For i = 1 To n2

                Cb2i(i) = Cb2(i) + kCb2(j, i) / div
           Next i
       Next j

'  ***********************************************************************
' Step forward in time by dt.
' Add (k1)/6 + (k2)/3 + (k3)/3 + (k4)/6 to old values to get new ones

       Cg = Cg + (kCg(1) + kCg(4)) / 6 + (kCg(3) + kCg(2)) / 3

       For i = 1 To bins
            'Airborne particle-phase SVOC
           Cp(i) = Cp(i) + (kCp(i, 1) + kCp(i, 4)) / 6 + (kCp(i, 3) +
kCp(i, 2)) / 3
           'Airborne particlse
           Cpm(i) = Cpm(i) + (kCpm(i, 1) + kCpm(i, 4)) / 6 _
                + (kCpm(i, 3) + kCpm(i, 2)) / 3
            'Carpet-deposited particle-phase SVOC
           Mp1(i) = Mp1(i) + (kMp1(i, 1) + kMp1(i, 4)) / 6 _
                + (kMp1(i, 3) + kMp1(i, 2)) / 3
            'Wallboard-deposited particle-phase SVOC
           Mp2(i) = Mp2(i) + (kMp2(i, 1) + kMp2(i, 4)) / 6 _
                + (kMp2(i, 3) + kMp2(i, 2)) / 3
            'Carpet-deposited particles
           Mpm1(i) = Mpm1(i) + (kMpm1(i, 1) + kMpm1(i, 4)) / 6 _
                + (kMpm1(i, 3) + kMpm1(i, 2)) / 3
            'Wallboard-deposited particles
           Mpm2(i) = Mpm2(i) + (kMpm2(i, 1) + kMpm2(i, 4)) / 6 _
                + (kMpm2(i, 3) + kMpm2(i, 2)) / 3
       Next i

        'Carpet-sorbed SVOC
       For i = 1 To n1
           Cb1(i) = Cb1(i) + (kCb1(1, i) + kCb1(4, i)) / 6 _
```

```
                + (kCb1(3, i) + kCb1(2, i)) / 3
        Next i
         'Wallboard-sorbed SVOC
        For i = 1 To n2
             Cb2(i) = Cb2(i) + (kCb2(1, i) + kCb2(4, i)) / 6 _
                + (kCb2(3, i) + kCb2(2, i)) / 3
        Next i


        t = t + dt

         'Set intervals at which to record model data
        If t < 1 * 24 Then
            outstp = 1
        ElseIf t < 2 * 24 Then
            outstp = 2
        ElseIf t < 10 * 24 Then
            outstp = 4
        ElseIf t < 50 * 24 Then
            outstp = 12
        ElseIf t < 200 * 24 Then
            outstp = 24
        ElseIf t < 500 * 24 Then
            outstp = 48
        ElseIf t < 1000 * 24 Then
            outstp = 5 * 24
        Else
            outstp = 10 * 24
        End If

         'Record data on output sheet
        If t - tprev >= outstp Then
             Call plotdata
             counter = counter + 1
             tprev = tprev + outstp
        End If

        If allout = "yes" Then
             'User has specified output of data from all time steps -- bombs
away!
             Call alldata
             allcounter = allcounter + 1
        End If

End Sub


Sub alldata()

        Mb1 = 0
        Mb2 = 0
        For i = 1 To n1
             Mb1 = Mb1 + Cb1(i) * dzb1
        Next i
        For i = 1 To n2
             Mb2 = Mb2 + Cb2(i) * dzb2
        Next i

         Worksheets("Raw Data").Cells(allcounter, 1).Value = t + tstart * 24
         Worksheets("Raw Data").Cells(allcounter, 2).Value = Cg * 1000
        For i = 1 To bins
             Worksheets("Raw Data").Cells(allcounter, i + 2).Value = Cp(i) *
1000
```

```
            Worksheets("Raw Data").Cells(allcounter, i + 5).Value = Cpm(i) *
1000
            Worksheets("Raw Data").Cells(allcounter, i + 10).Value = _
                (Mp1(i) * Sb1 + Mp2(i) * Sb2)
            Worksheets("Raw Data").Cells(allcounter, i + 13).Value = _
                (Mpm1(i) * Sb1 + Mpm2(i) * Sb2)
    Next i
     Worksheets("Raw Data").Cells(allcounter, 9).Value = Mb1 * Sb1
     Worksheets("Raw Data").Cells(allcounter, 10).Value = Mb2 * Sb2

End Sub

Sub plotdata()

    Mb1 = 0
    Mb2 = 0
    For i = 1 To n1
         Mb1 = Mb1 + Cb1(i) * dzb1
    Next i
    For i = 1 To n2
         Mb2 = Mb2 + Cb2(i) * dzb2
    Next i

     Worksheets("Plot Data").Cells(counter, 1).Value = t / 24 + tstart
     Worksheets("Plot Data").Cells(counter, 2).Value = Cg * 1000
    For i = 1 To bins
            Worksheets("Plot Data").Cells(counter, i + 2).Value = Cp(i) *
1000
            Worksheets("Plot Data").Cells(counter, i + 5).Value = Cpm(i) *
1000
            Worksheets("Plot Data").Cells(counter, i + 10).Value = _
                (Mp1(i) * Sb1 + Mp2(i) * Sb2) / 1000#
            Worksheets("Plot Data").Cells(counter, i + 13).Value = _
                (Mpm1(i) * Sb1 + Mpm2(i) * Sb2) / 1000#
    Next i
     Worksheets("Plot Data").Cells(counter, 9).Value = Mb1 * Sb1 / 1000#
     Worksheets("Plot Data").Cells(counter, 10).Value = Mb2 * Sb2 / 1000#
     Worksheets("Plot Data").Cells(counter, 17).Value = dt

     ActiveWindow.SmallScroll down:=1
End Sub
```

Ernest Orlando Lawrence Berkeley National Laboratory
One Cyclotron Road | Berkeley, California 94720

Prepared for the U.S. Department of Energy under Contract No. DE-AC03-76SF00098